Forest Service

Technology &
Development
Program

3400–Forest Pest
Management
September 1989
MTDC 89-30

AGDISP Analysis of Vortex Decay from Program WIND Phases I and III *Final Report*

C130

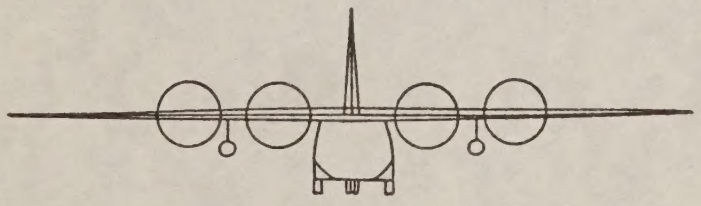

Ag-Husky

Ag-Cat

Bell 206B

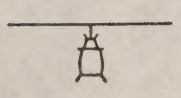

Hiller 12E

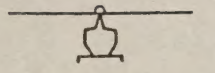

10 meters

AGDISP Analysis of Vortex Decay from Program WIND Phases I and III *Final Report*

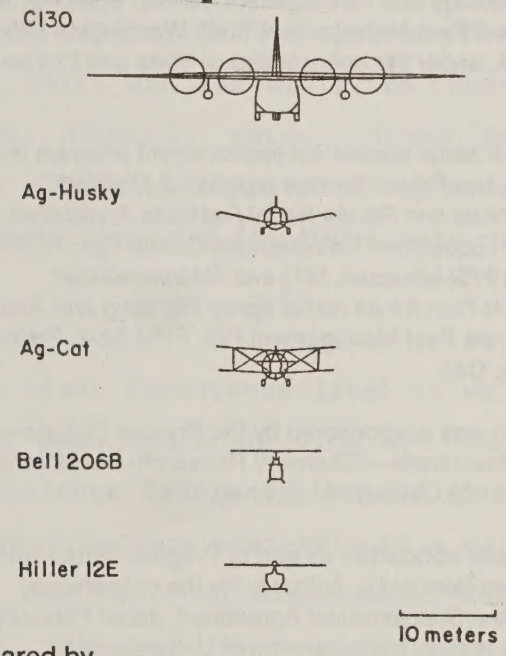

Prepared by
Milton E. Teske

Approved by
Alan J. Bilanin
Continuum Dynamics
P.O. Box 3073
Princeton, NJ 08540

Prepared for
U.S. Department of Agriculture
Forest Service
Technology and Development Center
Missoula, MT 59801

Robert B. Ekblad
Project Leader

(This work was done under contract 53-0343-7-00952)

Pesticide Precautionary Statement

This publication reports research involving pesticides. It does not contain recommendations for their use, nor does it imply that the uses discussed here have been registered. All uses of pesticides must be registered by appropriate State and/or Federal agencies before they can be recommended.

Caution: Pesticides can be injurious to humans, domestic animals, desirable plants, and fish or other wildlife—if they are not handled or applied properly. Use all pesticides selectively and carefully. Follow recommended practices for the disposal of surplus pesticides and pesticide containers.

Foreword

This report is published as a part of the USDA Forest Service program to improve aerial application of pesticides, specifically by using pesticides and delivery systems tailored to the forest environment. The program is conducted jointly by the Technology and Development Center, Missoula, MT, and the Forest Pest Management Staff, Washington Office at Davis, CA, under the sponsorship of State and Private Forestry.

Details of the aerial application improvement program are explained in two Forest Service reports: *A Problem Analysis: Forest and Range Aerial Pesticide Application Technology* (Equipment Development Center Rpt. 7934 2804, July 1979, Missoula, MT) and *Recommended Development Plan for an Aerial Spray Planning and Analysis System* (Forest Pest Management Rpt. FPM 82-2, February 1982, Davis, CA).

The analysis was cosponsored by the Physics Division—Research Directorate—(Chemical Research, Development and Engineering Center)—U.S. Army.

This study was conducted as part of Program WIND (winds in nonuniform domains). Authority for the cooperative program is the Supplemental Agreement, dated Febraury 1985, to the master Memorandum of Understanding Between U.S. Department of Defense and U.S. Department of Agriculture Relative to Cooperation with Respect to Food, Agriculture, and Other Research of Mutual Interest.

EXECUTIVE SUMMARY

Program WIND Phases I and III provide an extensive set of tower anemometer data with which to correlate the AGDISP vortex circulation strength decay model. In this Technical Note a generalized algorithm is used with all available data from test sites at Foresthill, Chico and Red Bluff, to recover vortex circulation time histories from tower velocity data. These data results are then fit by least squares to the AGDISP circulation decay model. Representative atmospheric turbulence levels are recovered for these runs, and the decay coefficient is determined.

The quantity defined by decay coefficient times turbulence level is well-correlated in the 132 final runs to have a mean value of 0.56 m/s and a standard deviation of 0.32 m/s. For the turbulence levels determined at the test sites, the decay coefficient is seen to vary between near-zero to a value of 2.0. This result correlates well with the expected atmospheric decay coefficient level of 0.41.

TABLE OF CONTENTS

1. INTRODUCTION

Program WIND ("Winds in Nonuniform Domains") was performed in phases jointly by the United States Department of Agriculture Forest Service and the United States Army at several sites in northern California. Phase I was conducted from May through July, 1985 at a cleared and forested site (Foresthill Seed Orchard) and an almond orchard (Hennigan Almond Orchard north of Chico); and Phase III, from late April to early May, 1986 at a cleared sloping site in the Sierra Nevada foothills near Red Bluff. In both of these experimental studies, anemometer tower grids recorded the ambient vertical velocity time histories as various aircraft repeatedly traversed normal to the grid. These digitized velocity traces produce an aircraft wake signature that can be used to infer the strength and lateral and vertical motion of the aircraft vortex pairs generating the traces. Two reports (Refs. 1 and 2) summarize the anemometer technique and provide a preliminary assessment of the tower grid approach. This report serves to complete the examination of this data base by using a generalized algorithm to locate the trailed vortex pairs in all available data, and to infer their decay properties in the atmosphere. This decay effect is then quantified as a decay coefficient range for subsequent input in the AGDISP computer code (Ref. 3).

References 1 and 2 detail the data collection procedure; it will be assumed here that the data have been suitably manipulated into its proper units and time history signals. In the first tests (Phase I, Ref. 1) the tower grid included anemometers for both horizontal and vertical velocities, with a total of 32 anemometers available for the analog-to-digital system employed to record the data. This study determined that the horizontal velocity signals would be easily polluted by any crosswind velocity component, giving a decidedly incorrect impression of the vortex positions and strength. Also, the closeness of the tower grid (the towers were spaced 2.7 to 6.1 meters apart with seven towers) meant that no more than 20 - 40 seconds of data would be taken before the vortices would drift off the grid. Thus, in

the second series of tests (Phase III, Ref. 2) the towers contained only vertical velocity anemometers, and were spaced uniformly apart at 6.1 meters (with 10 towers). A longer sampling time was used to track the vortices across this wider tower grid.

The Phase I results suffer somewhat from not having long enough time histories to track the vortex pairs adequately (a crosswind velocity always blew the vortices off the tower grid). The Phase III results corrected the shorter experimental data times but contain decidedly noisier anemometer signals because of ambient downslope/upslope conditions. The local winds at Red Bluff resulted in stronger crosswind velocities, moving the vortices off the tower grid prematurely and in some cases negating the effect of the more widely spaced towers.

All tests conducted at Foresthill, Chico and Red Bluff are summarized in Section 2 of this report. Section 3 reviews the generalized algorithm used to reduce the data, and Section 4 correlates the vortex circulation decay data with the atmospheric decay law formulated in AGDISP. Conclusions are offered in Section 5.

Appendices A, B and C present all reduceable data for Foresthill, Chico and Red Bluff, respectively.

2. SUMMARY OF TESTS CONDUCTED

Tables 2-1, 2-2 and 2-3 present a complete record of the digitized tower data recorded at Foresthill, Chico and Red Bluff, respectively. The dates shown are the dates of the tests. Thus, in Table 2-1, the first ten Foresthill tests were conducted in the morning hours of June 6, 1985. The aircraft characteristics are given in Table 2-4. The "Open Field" location was in a cleared area at Foresthill; the "Forest" location was within the tree line at Foresthill; the "Orchard" location was within the almond orchard at Chico; and the "Downslope" location was at Red Bluff.

The tower grid designations A through I are illustrated in scale in Figure 2-1. The differences between grids F and G are in the signal setup and are not relevant here but are included for completeness. Grid I is the Red Bluff grid with a downslope of 3.8 degrees. The aircraft flying over these grids are shown schematically in the same scale in Figure 2-2, to guide a qualitative impression of the size of the wakes and the positions of their vortex pairs (near the wing tips or the rotor edges). As in the previous reports, once one of the aircraft vortices moves substantially off the tower grid, it becomes difficult for the generalized algorithm (discussed in Section 3) to continue tracking the vortices.

The run numbers shown in Tables 2-1, 2-2 and 2-3 are Continuum Dynamics, Inc. numbers generated to differentiate the runs. The Status notations contain a relevant summary of each run. All runs producing vortex tracking results are plotted in the Appendices. The possibilities are the following:

No data: In these cases a C.D.I. run number was assigned but the data diskettes and test records indicate that no data were recorded.

Tare readings: In these cases the anemometer tower grid recorded a brief period of data (generally less than ten seconds) before the aircraft flyovers

began. These data were used to test the tower grid (typically the first test in the morning) and contain no vortex data (they do contain atmospheric data used in Section 4 of this report to deduce the ambient turbulence level, however).

xx sec of data: The generalized algorithm (discussed in Section 3) applied to this test run was able to track the vortex pair for at least xx seconds. Vortex decay-like behavior appears to be present in the results for xx seconds, even though the generalized algorithm followed the vortices for longer time periods. These data are the data used to infer the decay coefficient in Section 4.

Marginal data: The generalized algorithm was able to follow the vortices for a brief period of time, but the time histories for the vortex pair positions and strength do not seem to be physical.

No solution: The generalized algorithm could not track the vortex pair. Under the best of conditions, a numerical algorithm could not be expected to cover all of the physical possibilities during data collection. Most of the "no solution" results occur in the almond orchard tests, although, as indicated later, canopy effects cannot be considered important, when examining vortex circulation strength decay.

TABLE 2-1. FORESTHILL RUN LOG

Date	Aircraft	Location	Grid	Run #	Status
06/06/85	Bell 206B	Open Field	A	1	no data
				2	no data
				3	no data
				4	no data
				5	20 sec of data
				6	no solution
				7	15 sec of data
				8	19 sec of data
				9	28 sec of data
				10	22 sec of data
06/07/85	Bell 206B	Open Field	A	11	28 sec of data
				12	25 sec of data
				13	no solution
				14	18 sec of data
				15	no data
				16	no data
				17	39 sec of data
				18	59 sec of data
				19	no data
				20	27 sec of data
				21	15 sec of data
				22	16 sec of data
				23	12 sec of data
				24	marginal data
				25	marginal data
06/08/85	AgHusky	Open Field	A	26	tare readings
				27	no data
				28	marginal data
				29	no solution
				30	13 sec of data
				31	marginal data
				32	15 sec of data
				33	no solution
				34	16 sec of data
				35	15 sec of data
				36	marginal data
				37	15 sec of data
				38	15 sec of data
				39	48 sec of data
06/09/85	AgHusky	Open Field	A	40	tare readings
				41	29 sec of data
				42	17 sec of data
				43	12 sec of data
				44	30 sec of data
				45	22 sec of data
				46	44 sec of data
				47	no data
				48	39 sec of data
				49	31 sec of data

TABLE 2-1. (continued)

Date	Aircraft	Location	Grid	Run #	Status
06/09/85	AgHusky	Open Field	A	50	23 sec of data
				51	33 sec of data
				52	19 sec of data
				53	23 sec of data
				54	22 sec of data
				55	no solution
				56	25 sec of data
				57	25 sec of data
				58	33 sec of data
				59	38 sec of data
				60	24 sec of data
06/14/85	Bell 206B	Forest	B	61	tare readings
				62	21 sec of data
				63	21 sec of data
				64	marginal data
				65	27 sec of data
				66	23 sec of data
				67	29 sec of data
			C	68	26 sec of data
				69	37 sec of data
				70	26 sec of data
				71	21 sec of data
				72	26 sec of data
				73	marginal data
				74	20 sec of data
06/15/85	Bell 206B	Forest	E	75	tare readings
				76	32 sec of data
				77	marginal data
				78	marginal data
				79	28 sec of data
				80	no solution
				81	21 sec of data
				82	20 sec of data
			D	83	marginal data
				84	26 sec of data
				85	17 sec of data
				86	23 sec of data
				87	marginal data
				88	14 sec of data
				89	25 sec of data
				90	34 sec of data
				91	32 sec of data
				92	23 sec of data
				93	11 sec of data
				94	no solution
				95	33 sec of data
				96	12 sec of data
				97	26 sec of data
				98	33 sec of data

TABLE 2-1. (continued)

Date	Aircraft	Location	Grid	Run #	Status
06/16/85	AgHusky	Forest	B	99	tare readings
				100	tare readings
				101	marginal data
				102	25 sec of data
				103	marginal data
				104	no solution
			C	105	no solution
				106	marginal data
				107	no solution
				108	marginal data
				109	no solution
				110	marginal data
				111	no solution
				112	13 sec of data
				113	marginal data
				114	25 sec of data
				115	no solution
				116	marginal data
				117	27 sec of data
06/17/85	AgHusky	Forest	E	118	tare readings
				119	48 sec of data
				120	16 sec of data
				121	38 sec of data
				122	25 sec of data
				123	40 sec of data
			D	124	25 sec of data
				125	19 sec of data
				126	25 sec of data
				127	45 sec of data
				128	22 sec of data
				129	marginal data
				130	23 sec of data
				131	26 sec of data
				132	marginal data
				133	15 sec of data
				134	30 sec of data
				135	30 sec of data
				136	25 sec of data

TABLE 2-2. CHICO RUN LOG

Date	Aircraft	Location	Grid	Run #	Status
06/24/85	AgCat	Orchard	F	1	no data
				2	tare readings
				3	no solution
				4	no solution
				5	17 sec of data
				6	marginal data
				7	no solution
				8	34 sec of data
				9	no data
				10	tare readings
				11	no solution
				12	marginal data
				13	marginal data
				14	no solution
				15	no solution
				16	no solution
				17	no data
06/26/85	AgCat	Orchard	F	18	tare readings
				19	38 sec of data
				20	22 sec of data
				21	marginal data
				22	no data
				23	tare readings
				24	no solution
				25	14 sec of data
				26	21 sec of data
				27	30 sec of data
				28	marginal data
				29	no solution
				30	no data
				31	tare readings
				32	32 sec of data
				33	marginal data
				34	28 sec of data
				35	42 sec of data
				36	35 sec of data
				37	39 sec of data
				38	no solution
				39	no data
06/28/85	Hiller 12E	Orchard	F	40	tare readings
				41	no data
				42	tare readings
				43	29 sec of data
				44	tare readings
				45	26 sec of data
				46	27 sec of data
				47	22 sec of data
				48	15 sec of data
				49	12 sec of data

TABLE 2-2. (continued)

Date	Aircraft	Location	Grid	Run #	Status
06/28/85	Hiller 12E	Orchard	F	50	26 sec of data
				51	30 sec of data
				52	no solution
				53	no data
				54	tare readings
				55	marginal data
				56	marginal data
				57	22 sec of data
				58	marginal data
				59	no solution
				60	no solution
				61	29 sec of data
				62	29 sec of data
				63	21 sec of data
				64	no data
07/02/85	Hiller 12E	Orchard	G	65	tare readings
				66	no data
				67	tare readings
				68	no solution
				69	tare readings
				70	15 sec of data
				71	no solution
				72	no solution
				73	no solution
				74	no solution
				75	13 sec of data
				76	12 sec of data
				77	no solution
				78	no solution
				79	no data
			F	80	tare readings
				81	25 sec of data
				82	17 sec of data
				83	no solution
				84	20 sec of data
				85	tare readings
				86	no solution
				87	no solution
				88	marginal data
				89	marginal data
				90	no solution
				91	no solution
				92	no data
07/04/85	Hiller 12E	Orchard	H	93	tare readings
				94	no data
				95	tare readings
				96	32 sec of data
				97	28 sec of data
				98	25 sec of data

TABLE 2-2. (continued)

Date	Aircraft	Location	Grid	Run #	Status
07/04/85	Hiller 12E	Orchard	H	99	tare readings
				100	32 sec of data
				101	27 sec of data
				102	27 sec of data
				103	tare readings
				104	31 sec of data
				105	marginal data
				106	marginal data
				107	tare readings
				108	no solution
				109	no solution
				110	no solution
				111	25 sec of data
				112	38 sec of data
				113	34 sec of data
	AgCat	Orchard	H	114	no data
				115	tare readings
				116	no data
				117	22 sec of data
				118	no solution
				119	no solution
				120	25 sec of data
				121	21 sec of data
				122	no solution
				123	no solution
				124	no data
				125	marginal data
				126	27 sec of data
				127	no data
				128	tare readings
				129	19 sec of data
				130	19 sec of data
				131	24 sec of data
				132	no data
07/06/85	Hiller 12E	Orchard	H	133	tare readings
				134	no data
				135	tare readings
				136	27 sec of data
				137	no solution
				138	marginal data
				139	16 sec of data
				140	15 sec of data
				141	19 sec of data
				142	no solution
				143	no data

TABLE 2-3. RED BLUFF RUN LOG

Date	Aircraft	Location	Grid	Run #	Status
04/27/86	C130	Downslope	I	1	marginal data
				2	no solution
				3	no solution
				4	24 sec of data
04/28/86	Bell 206B	Downslope	I	5	40 sec of data
				6	99 sec of data
				7	marginal data
04/29/86	Bell 206B	Downslope	I	8	marginal data
				9	64 sec of data
				10	31 sec of data
				11	marginal data
				12	marginal data
				13	marginal data
04/30/86	Bell 206B	Downslope	I	14	marginal data
				15	19 sec of data
				16	21 sec of data
				17	15 sec of data
				18	66 sec of data
				19	36 sec of data
05/01/86	Bell 206B	Downslope	I	20	marginal data
05/04/86	Bell 206B	Downslope	I	21	32 sec of data
				22	marginal data
				23	marginal data
				24	46 sec of data
				25	33 sec of data
				26	80 sec of data
				27	marginal data
				28	67 sec of data
				29	45 sec of data
				30	67 sec of data
				31	83 sec of data
				32	59 sec of data
				33	32 sec of data
				34	marginal data
				35	17 sec of data
				36	45 sec of data
				37	16 sec of data
				38	25 sec of data
05/07/86	Bell 206B	Downslope	I	39	26 sec of data
				40	53 sec of data
				41	marginal data
				42	58 sec of data
05/08/86	Bell 206B	Downslope	I	43	marginal data
				44	90 sec of data
				45	marginal data
				46	40 sec of data
				47	marginal data
				48	11 sec of data
				49	14 sec of data

TABLE 2-4. AIRCRAFT SUMMARY

Aircraft	Owner	Location	Number of Runs
Bell 206B	Chuck Jones Flying Service	Foresthill	54
		Red Bluff	45
Cessna Ag Husky	Gilbert Aviation	Foresthill	66
Hiller 12E	Chico Aerial Applicators	Chico	61
Schweizer Ag Cat	Chico Aerial Applicators	Chico	40
C-130	Air National Guard Rickenbacker ANGB	Red Bluff	4

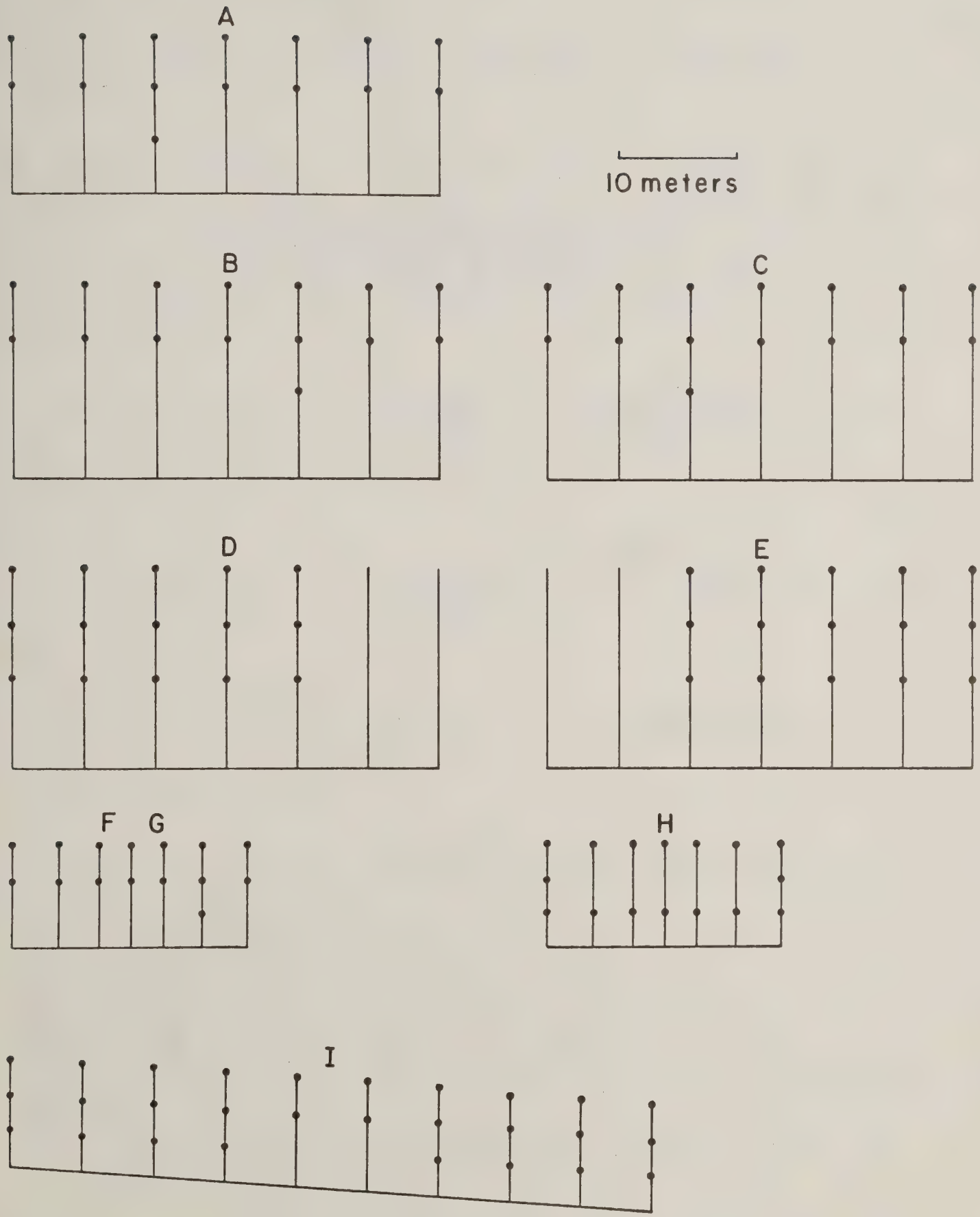

Figure 2-1. Scaled anemometer tower grids for Foresthill (A-E), Chico (F-H) and Red Bluff (I).

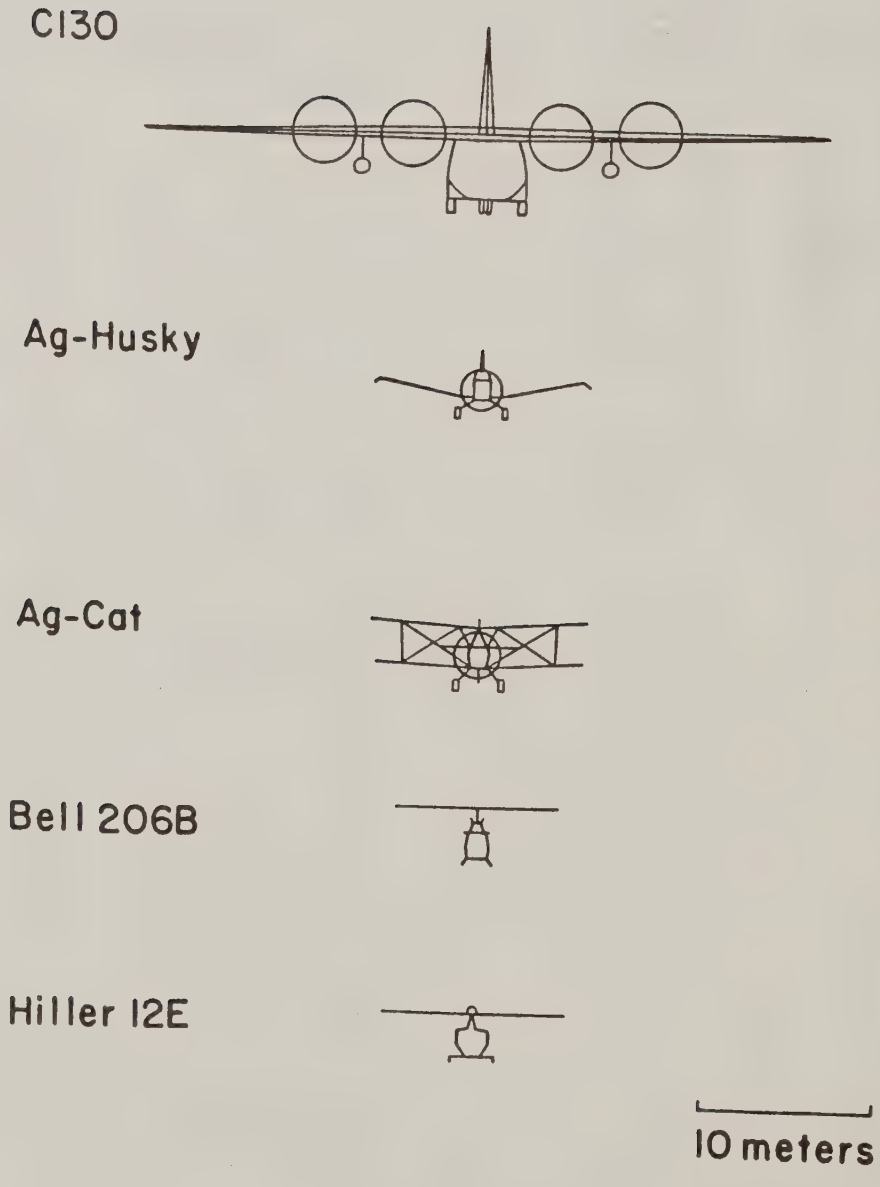

Figure 2-2. Scaled cross-sections of the aircraft operating at Foresthill, Chico and Red Bluff (Table 2-4).

3. GENERALIZED ALGORITHM FOR DETERMINING VORTEX TRAJECTORIES

Reference 1 summarized a preliminary model for inferring the location and strength of the vortex pair traveling through an anemometer tower grid. Reference 2 extended this algorithm to include the slight downslope at Red Bluff. In this section of the report the generalization of this technique to include vortex core effects and analytically determined derivatives is summarized.

An aircraft wake may be represented by a simple vortex pair (with its image pair below the surface, Figure 3-1), each vortex of which may be characterized by a velocity field of the form

$$v = \frac{\Gamma}{2\pi} \frac{R}{(R_c^2 + R^2)} \qquad (3\text{-}1)$$

where

v = velocity magnitude

Γ = vortex circulation strength

R = radius from vortex center

R_c = vortex core radius

The resultant velocity at any point in the flow field (in particular, at an anemometer location) is then the algebraic sum of the velocity contributions from the four vortices acting on the flow. The aircraft vortex pair is located in a coordinate system relative to the tower grid (Figure 3-2). The wake model introduces five unknowns that must be deduced from the data in any run at any time at which data are collected. These unknowns are the vortex circulation strength, the vortex core radius and the three spatial dimensions

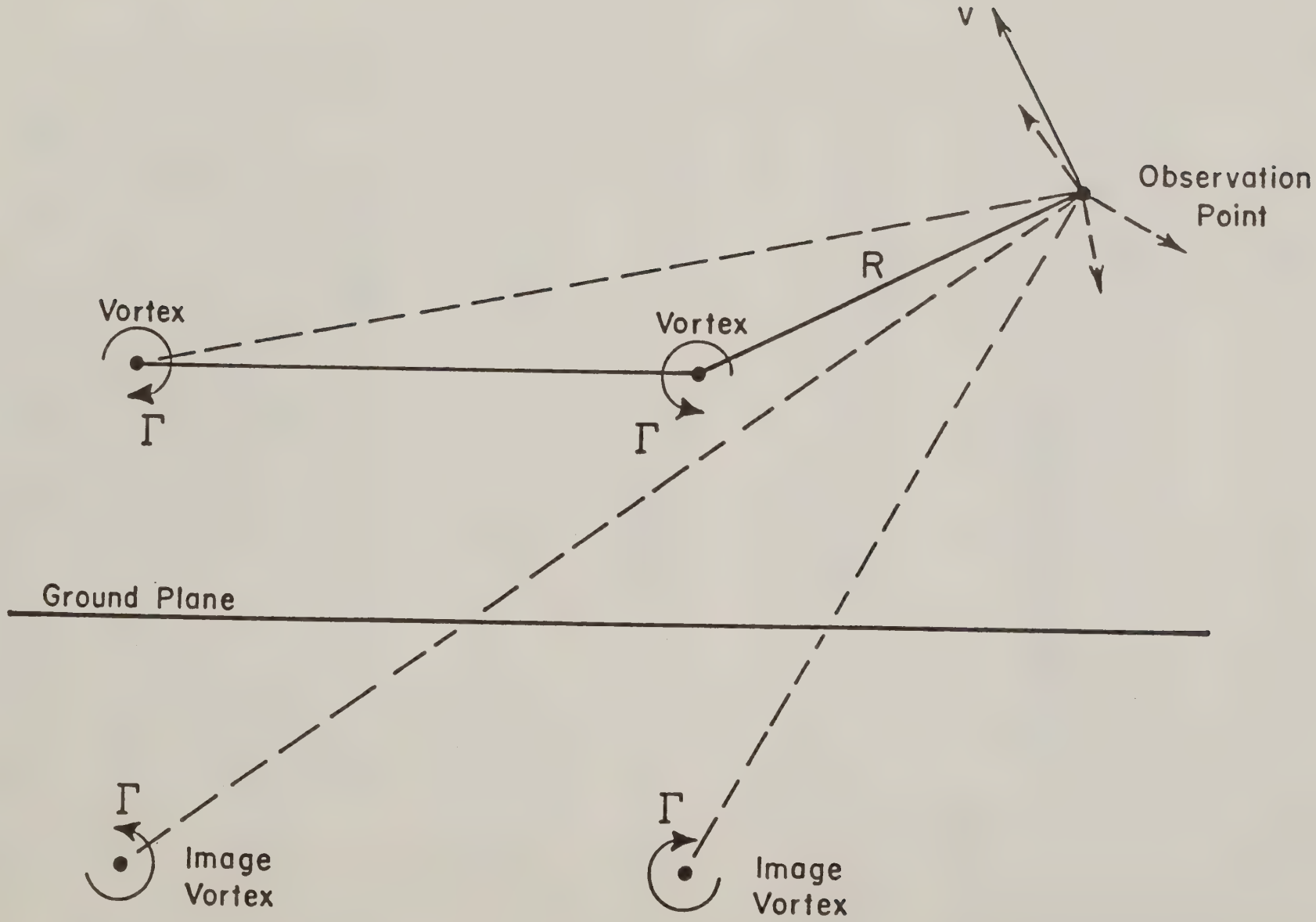

Figure 3-1. The composite velocity vector at an observation point found by summing the contributions of the aircraft vortex pair and its image system below the ground plane.

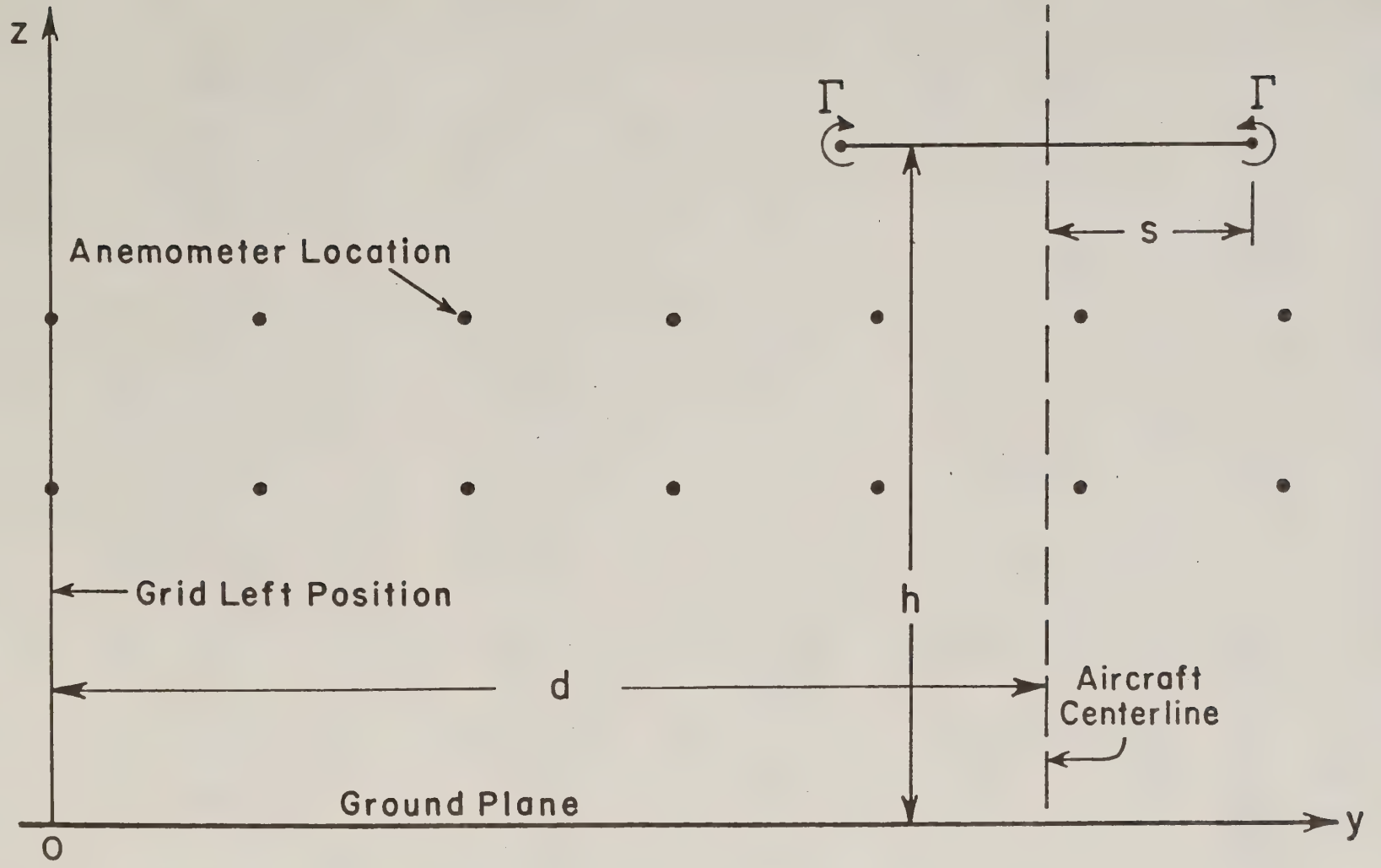

Figure 3-2. The aircraft vortex pair located relative to the anemometer tower grid. The relevant lengths are the height of the vortex pair h , the semispan distance between the vortices s , and the offset d of the aircraft centerline from the grid left position.

h = the height of the vortex pair above the surface

s = the semispan of the vortex pair (the half distance between their centers)

d = the offset distance of the aircraft centerline from the leftmost anemometer tower.

It is realized that the aircraft wake physics are only approximated by the simple velocity law given in Eq. (3-1). Thus, the intent of the generalized analysis is to seek a solution for these five parameters in any run at every time so as to minimize the error in the velocity predictions at all of the anemometer locations. With five unknowns and many more anemometer locations, it seems clear that the problem may be cast into a least squares analysis by defining the error E as

$$E = \sum_{n=1}^{N} \left(w_n - \bar{w}_n\right)^2 \qquad (3\text{-}2)$$

where the overbar denotes the data, and the index n is from 1 to N, the total number of anemometers. The error E is a positive definite quantity. The vertical velocities w are determined by summing the contributions of the four vortices in the model, calculated for specific values of the parameters Γ, R_c, h, s and d. The data $\bar{w}$ are found directly from the test results.

A crucial physical observation is made at this point: if the experimental data were normalized by any positive value, the resulting velocity vectors could still be used to infer the spatial position of the vortex pair in the anemometer field irrespective of the actual vortex circulation strength. This observation implies that locating the vortex pair involves the solution for R_c, h, s and d without regard to the value of Γ.

The approach used here normalizes the vertical velocities in the error equation by their respective root mean square velocities to give

$$E^* = \sum \left[\left(\frac{w_n}{w_{rms}} \right) - \left(\frac{\bar{w}_n}{\bar{w}_{rms}} \right) \right]^2 \qquad (3\text{-}3)$$

where

$$w_{rms} = \sqrt{\frac{1}{N} \sum w_n^2}$$

$$\bar{w}_{rms} = \sqrt{\frac{1}{N} \sum \bar{w}_n^2} \qquad (3\text{-}4)$$

Because the predicted vertical velocities are all linear in vortex circulation strength Γ, this modification to the error removes Γ from the equation for E^* and recasts the problem into one involving the four parameters R_c, h, s and d.

Equation (3-3) for E^* is nonlinear in R_c, h, s and d, but may be analytically differentiated with respect to these unknowns to give

$$F_R = \partial E^* / \partial R_c$$

$$F_h = \partial E^* / \partial h$$

$$F_s = \partial E^* / \partial s \qquad (3\text{-}5)$$

$$F_d = \partial E^* / \partial d$$

Clearly, when all four derivatives in Eq. (3-5) tend to zero, the slopes of E^* also tend to zero and E^* reaches a local minimum. These F functions are nonlinearly related to R_c , h , s and d . At any value set of (R_c,h,s,d), the local values of the F's in Eq. (3-5) may be determined analytically to generate partial derivatives of the form $\partial F/\partial R_c$, $\partial F/\partial h$, $\partial F/\partial s$ and $\partial F/\partial d$ to construct the model equation for F (representing F_R , F_h , F_s and F_d of the form

$$\Delta F = \frac{\partial F}{\partial R_c} \Delta R_c + \frac{\partial F}{\partial h} \Delta h + \frac{\partial F}{\partial s} \Delta s + \frac{\partial F}{\partial d} \Delta d \qquad (3\text{-}6)$$

The partial derivatives in this equation are known as influence coefficients. For any value of (R_c,h,s,d) , the values of the four partial derivatives and F may be generated. Since the solution requires F to tend to zero, the left-hand side of Eq. (3-6) may be specified by

$$\Delta F = - F \qquad (3\text{-}7)$$

The complete system may be seen to be a four-equation system for the values $(\Delta R_c,\Delta h,\Delta s,\Delta d)$ to add to the present values (R_c,h,s,d) to give new values $(R_c+\Delta R_c,h+\Delta h,s+\Delta s,d+\Delta d)$ to recompute E^* and drive the solution to a minimum. This iteration procedure is followed at every time in the test run being analyzed.

Once values for (R_c,h,s,d) have been determined, the original error E may be differentiated to give

$$F_\Gamma = \partial E/\partial \Gamma = 0 \qquad (3\text{-}8)$$

to find the minimum of E and determine Γ. This equation is solved easily because the equation for F is linear in Γ. With the solution in hand for (Γ, R_c, h, s, d), these values are used as initial guesses for the next time in the run being analyzed.

In practice, the vortex core radius parameter could never be adequately quantified from the data. Although the anemometer tower grids were as little as 2.7 meters apart, this distance was still too large to infer the vortex core size. For this reason all results have been computed with a core size of $R_c = 0.15$ meters.

All results are plotted in Appendices A (Foresthill), B (Chico) and C (Red Bluff).

4. DETERMINATION OF DECAY COEFFICIENT

Of the runs shown in the Appendices, 132 were selected as best representing the expected behavior as the vortex pairs approached the ground. These cases include vortex penetration into the almond orchard and Foresthill canopies.

The vortex strength decay model proposed in Ref. 3 is of the form

$$\Gamma(t) = \frac{\Gamma_o}{1 + \frac{bqt}{s}} \tag{4-1}$$

where

Γ = vortex circulation strength as a function of time t

Γ_o = initial vortex circulation strength at $t = 0$

b = decay coefficient

q = turbulence level

s = vortex pair semispan

An alternate form for vortex strength decay is

$$\Gamma(t) = \Gamma_o \exp\left(-\frac{bqt}{s}\right) \tag{4-2}$$

Both of these expressions are suggested as possible models for vortex decay in the atmosphere in Ref. 4. After numerous attempts to implement Eq. (4-1), it was decided to modify the AGDISP model to that of Eq. (4-2).

Again, a least squares approach was used to curve fit the vortex circulation strength data developed by the generalized algorithm. The vortex

circulation strength profiles were fit to Eq. (4-2) by minimizing the logarithmic error

$$E = \sum [G - (A - Bt)]^2 \qquad (4\text{-}3)$$

over all applicable time increments in each run examined, where

G = logarithm of Γ_i

A = logarithm of Γ_o

B = bq/s

Γ_i = vortex circulation strength generalized algorithm values

Equation (4-3) returns the best fit values for Γ_o and B for each run examined. Typical comparisons are shown in Figure 4-1. Since the semispan s of the test aircraft are known, the value of B may be used to infer the product bq for each run examined. The tare readings in Phase I and the U-V-W anemometer data in Phase III are then examined to estimate the turbulence level q for each final run, and from this result, determine the decay coefficient b.

All tare readings and U-V-W anemometer data were subsequently least squares curve fit to a neutral logarithmic profile of the form

$$U = U_o \ln(z/z_o) \qquad (4\text{-}4)$$

where

U = horizontal surface velocity

U_o = reference velocity

z = height

z_o = surface roughness

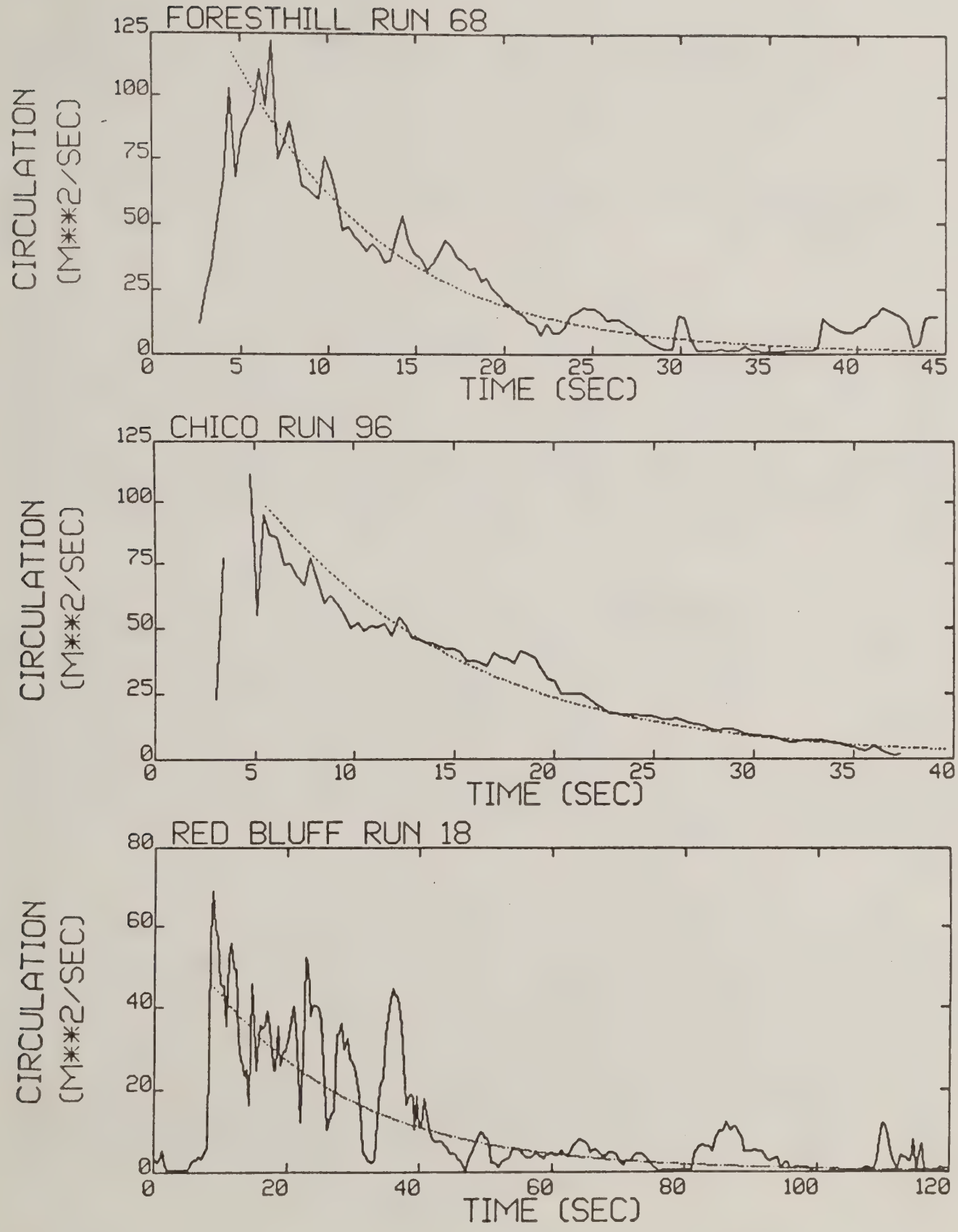

Figure 4-1. Comparison of vortex circulation strength decay (solid curves) with the experimental curve fit of Eq. 4-2 (dotted curves) for three representative Phase I and III test runs.

A consistent turbulence level may be obtained by using an equation found in Ref. 3

$$q^2 = 0.845U_o^2 \qquad (4\text{-}5)$$

Both U_o and z_o in Eq. (4-4) were obtained by examining the velocity data available from the Phase I and III test results. Three tower anemometer heights were available in the Phase I results, although the horizontal velocity component normal to the tower grid had to be scaled from the top row to the other two rows. The Phase III results were straightforward since all three velocity components were available at both the 6.10 and 9.15 meter heights.

With the turbulence level q determined, the product bq may be plotted as shown in Figure 4-2. Here it may be seen that bq is approximated by its average value of 0.56 m/s and standard deviation of 0.32 m/s. The decay coefficient b is plotted against turbulence level in Figure 4-3 with the corresponding mean and standard deviation curves also plotted. The results show a correlation for the varied terrain and canopy conditions, and the algorithm assumptions made in reducing the data.

Reference 4 suggests that a decay coefficient of 0.41 describes decay in the atmosphere away from the ground. The present results suggest that a decay coefficient of near zero to 2.0 may be used as input on card 0075 in AGDISP. The data results scatter across Figures 4-2 and 4-3 for Foresthill, Chico and Red Bluff, and a sense of when to invoke a smaller value of b rather than a larger value of b could not be obtained. It is suggested that the mean curve in Figure 4-3 be used to set the decay coefficient, given the turbulence level assumed in the AGDISP simulation.

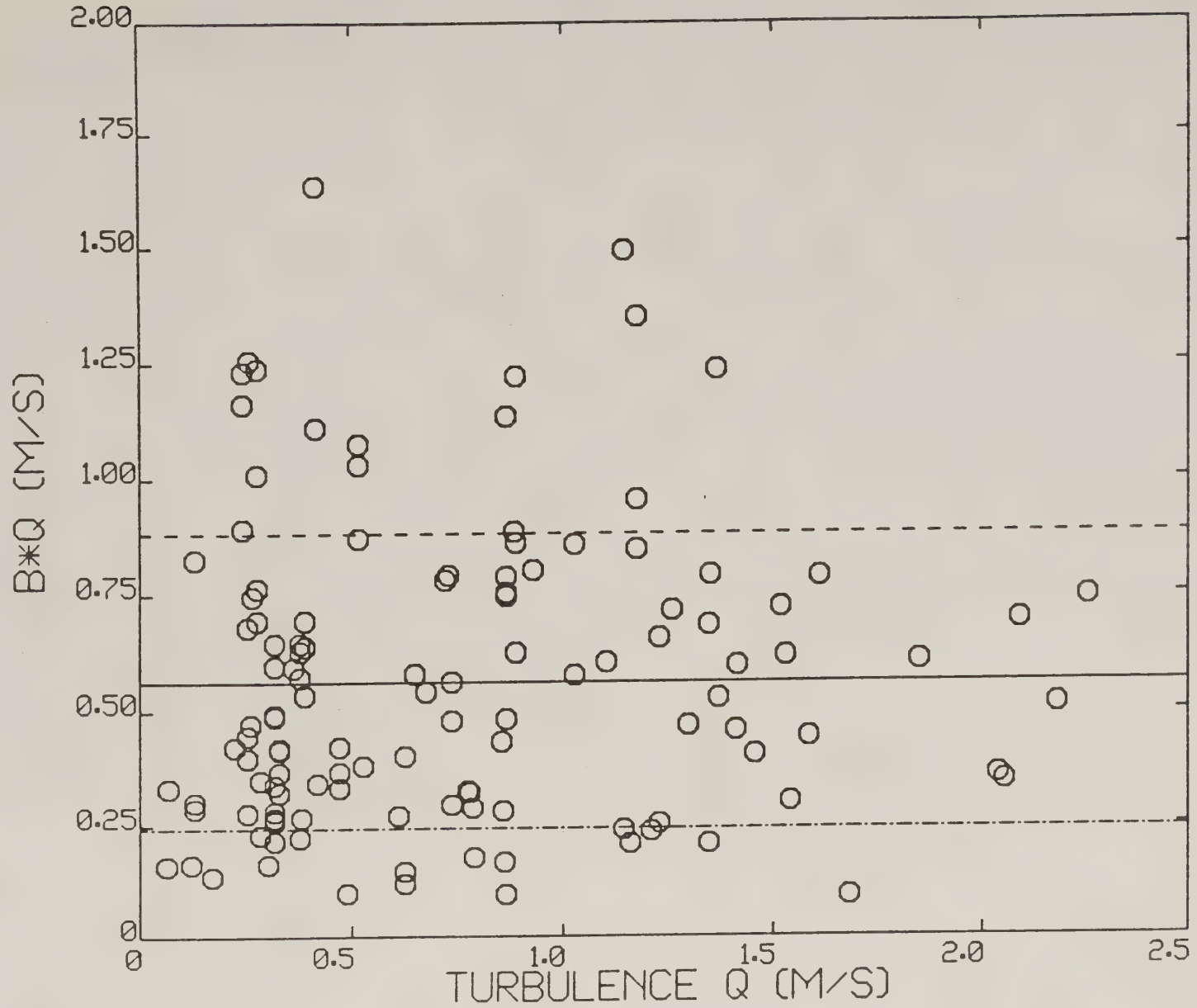

Figure 4-2. The behavior of the product bq (Eq. 4-2) with turbulence level q in the Program WIND Phase I and III data sets. Each circle represents one of the 132 applicable test runs. The solid curve is the mean of the data; the dashed curves represent the standard deviation.

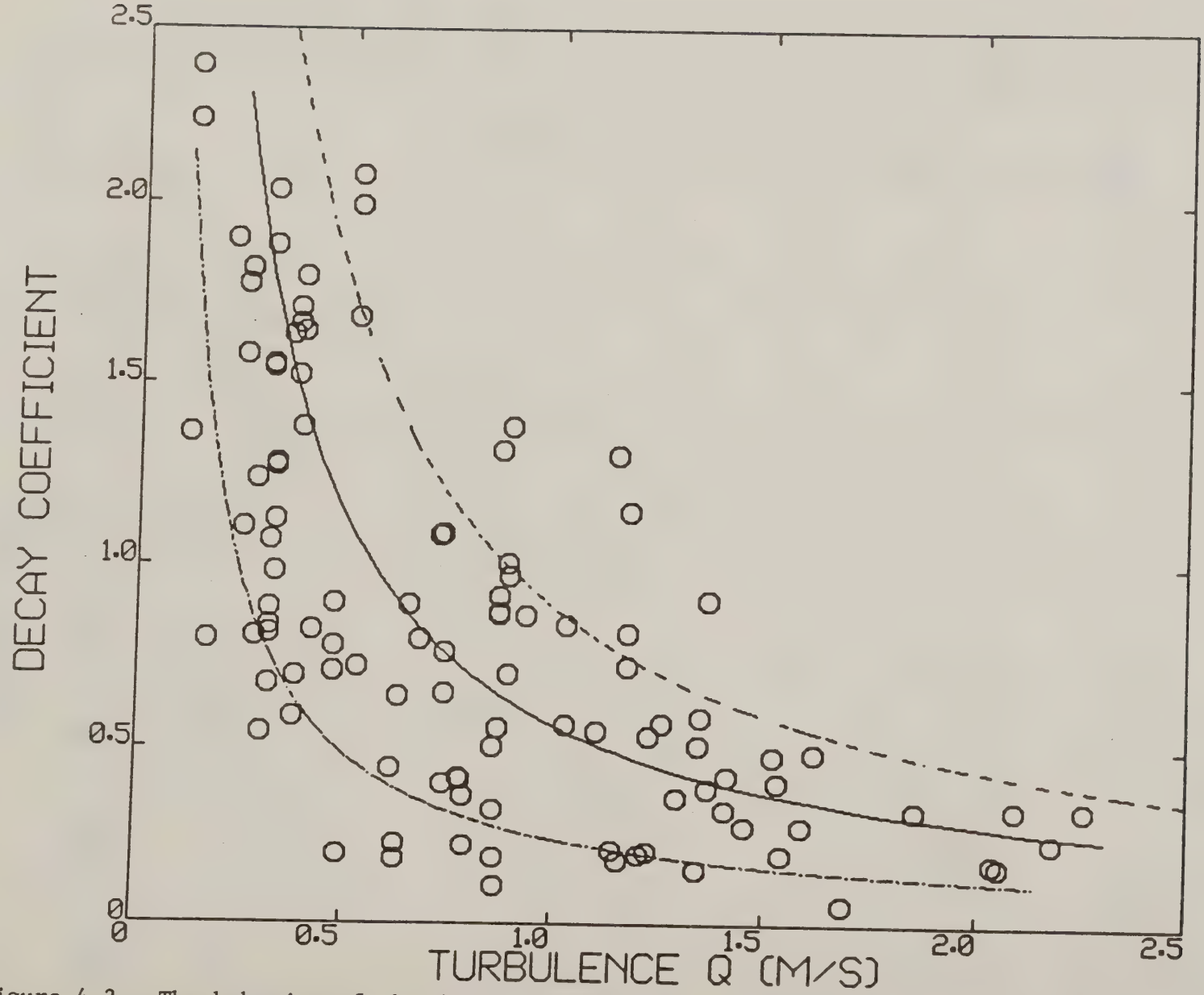

Figure 4-3. The behavior of the decay coefficient b with turbulence level q in the Program WIND Phase I and III data sets. Each circle represents one of the 132 applicable test runs. The solid curve is the mean of the correlated data; the dashed curves represent the standard deviation.

The quantity bq/s may be used to estimate the e-folding time of the decay of the vortex circulation strength. The e-folding time may be seen from Eq. (4-2) to occur when

$$t = s/bq \qquad (4\text{-}6)$$

For typical aircraft used by the USDA Forest Service, and with bq = 0.56 m/s from Figure 4-2, the e-folding time may be computed to be 9 to 12 seconds. In this time period, aircraft wake effects will have deposited, or nearly deposited, all material sizes above 100 microns. Thus, a recommendation of this study is to neglect vortex circulation strength decay except in small material size categories. And, when the material sizes are less than 100 microns, to assume that bq = 0.56 m/s , estimate the turbulence level (guidelines are given in Ref. 3) and use the 0075 card in AGDISP.

The most surprising result is how well the results correlated with each other. The second surprising result is that vortex circulation strength decay seemed to be independent of canopy vegetation. Additional work was performed by examining the vortex scrubbing model in the AGDISP code (Ref. 3) to see whether it could generate circulation strength decays of the magnitude suggested here. For this purpose, an average plant area coverage profile shape was developed from the data in Ref. 5 for the almond orchard. This shape in the vortex scrubbing model resulted in very little change to the vortex circulation strength by the canopy, even with an increase in the assumed drag coefficient to a blunt body value of 1.28. The maximum plant area coverage fraction was 0.22, and appears to have little effect in participating in vortex circulation strength decay in the orchard. The data found in Ref. 6 would also suggest that the canopy will have little effect in reducing vortex circulation strength at Foresthill, since the maximum coverage is less than nine percent for forested areas examined during Program WIND.

5. CONCLUSIONS

Program WIND Phases I and III tower anemometer data sets suggest a vortex circulation strength decay coefficient of 0.0 to 2.0 depending on the ambient turbulence level assumed in the AGDISP simulation. An examination of the anticipated decay time further suggests that only material sizes below 100 microns will be noticeably affected by the decay model.

6. REFERENCES

1. Williamson, G.G., Teske, M.E. and Geyer, R.G.: "Experimental Study of Aircraft Wakes in Forest Canopies," Continuum Dynamics, Inc. Report No. 85-7, September 1985.

2. Teske, M.E.: "Field Study of Interaction of Spray Aircraft Wake with Convective Surface Winds in Hilly Terrain," Continuum Dynamics, Inc. Report No. 86-5, September 1986.

3. Teske, M.E.: "User Manual Extension for the Computer Code AGDISP Mod 4.0," USDA Forest Service Equipment Development Center Report No. 8634 2809, April 1986.

4. Donaldson, C. duP. and Bilanin, A.J.: "Vortex Wakes of Conventional Aircraft," AGARDograph No. 204, May 1975.

5. Newton, W.E., Barnes, R. and Barry, J.W.: "Almond Tree Foliage Characteristics," USDA Forest Service Forest Pest Management Report No. FPM 87-1, February 1987.

6. Bergen, J., Hutchinson, B. and Waite, W.: "Supplement to Preliminary Canopy Structure Estimates for the Forest Site of the Program WIND Study," USDA Forest Service Forest Pest Management Report No. FPM 88-1, October 1987.

APPENDIX A

Foresthill Reduced Plots

The generalized algorithm discussed in Section 3 was applied to all available test data from Program WIND Phase I at Foresthill. The results are plotted on the following pages as three time history traces in the following format.

1. The top figure shows the horizontal location of the vortex pair centerlines during the test run. Here, time is measured relative to when the anemometer data recording began (near aircraft flyover). The leftmost tower is located at a horizontal distance of 0 meters, and the tower grid extends in the positive distance direction. The right vortex trail is denoted by a solid curve; the left vortex trail is a dotted curve.

2. The middle figure shows the vertical location of the vortex pair centerlines during the test run.

3. The bottom figure shows the vortex circulation strength during the test run.

Test runs subsequently selected for vortex circulation strength decay study are denoted in the figure title by an asterisk (*).

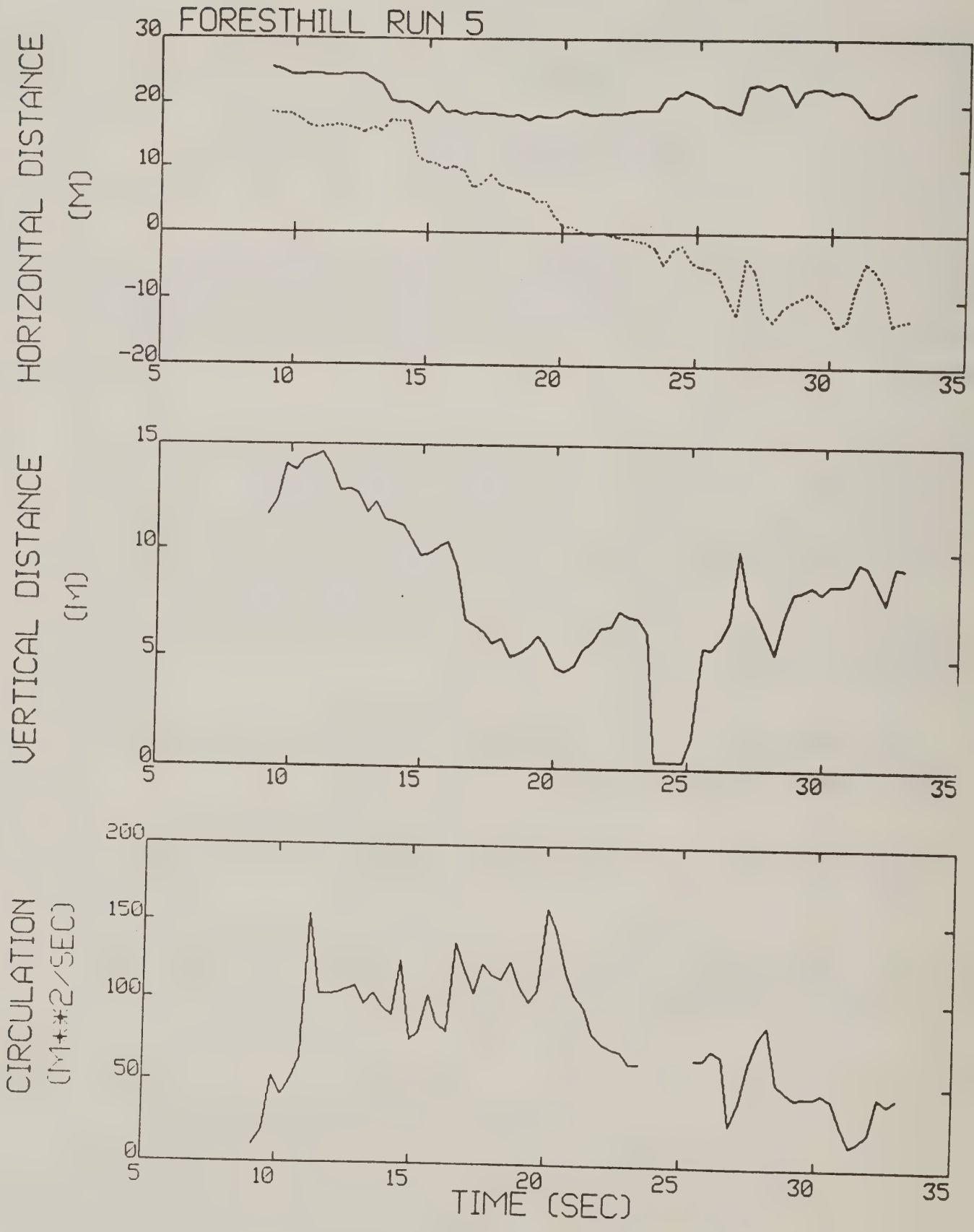

Figure A-1. Foresthill test run 5 generalized algorithm results (*).

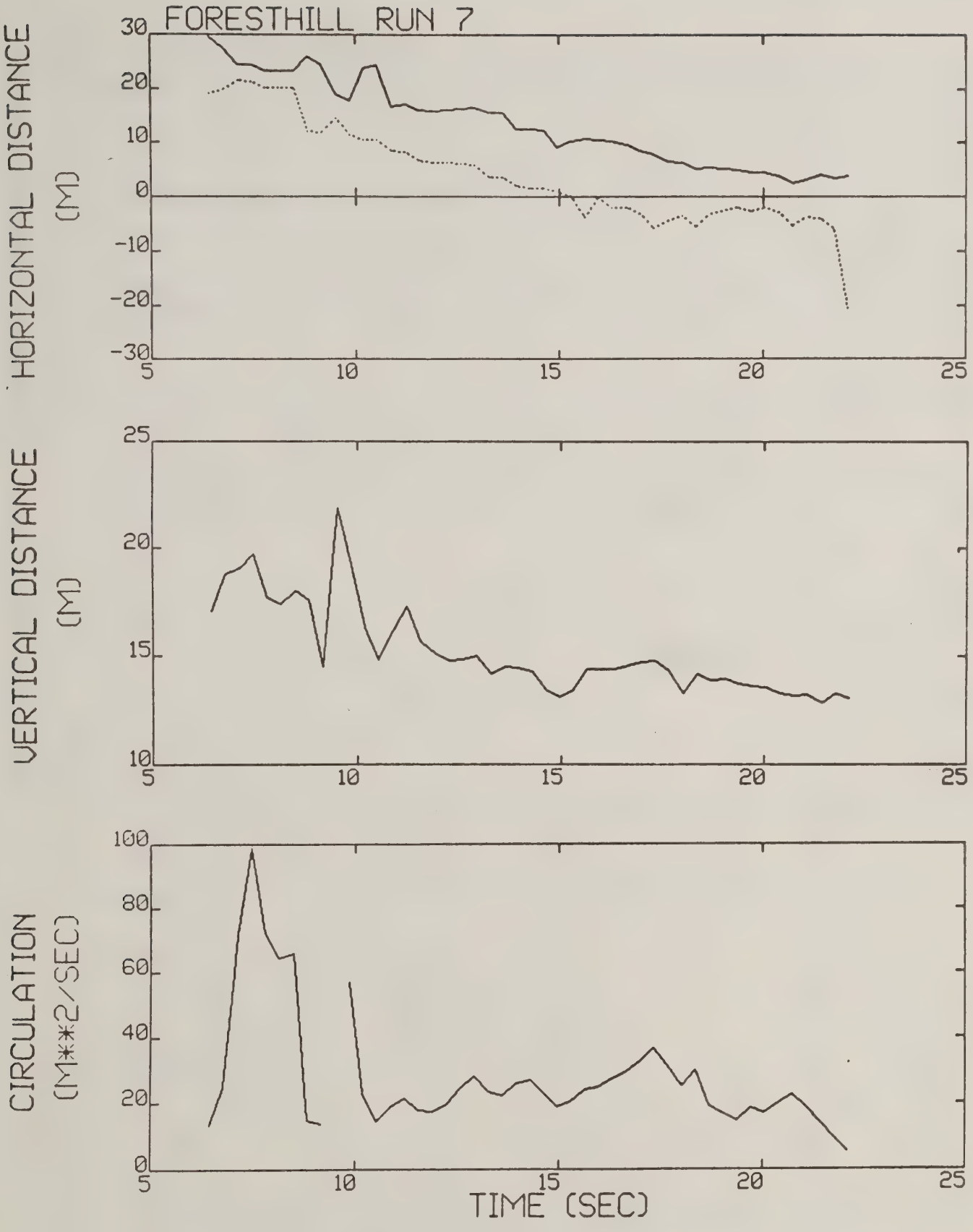

Figure A-2. Foresthill test run 7 generalized algorithm results (*).

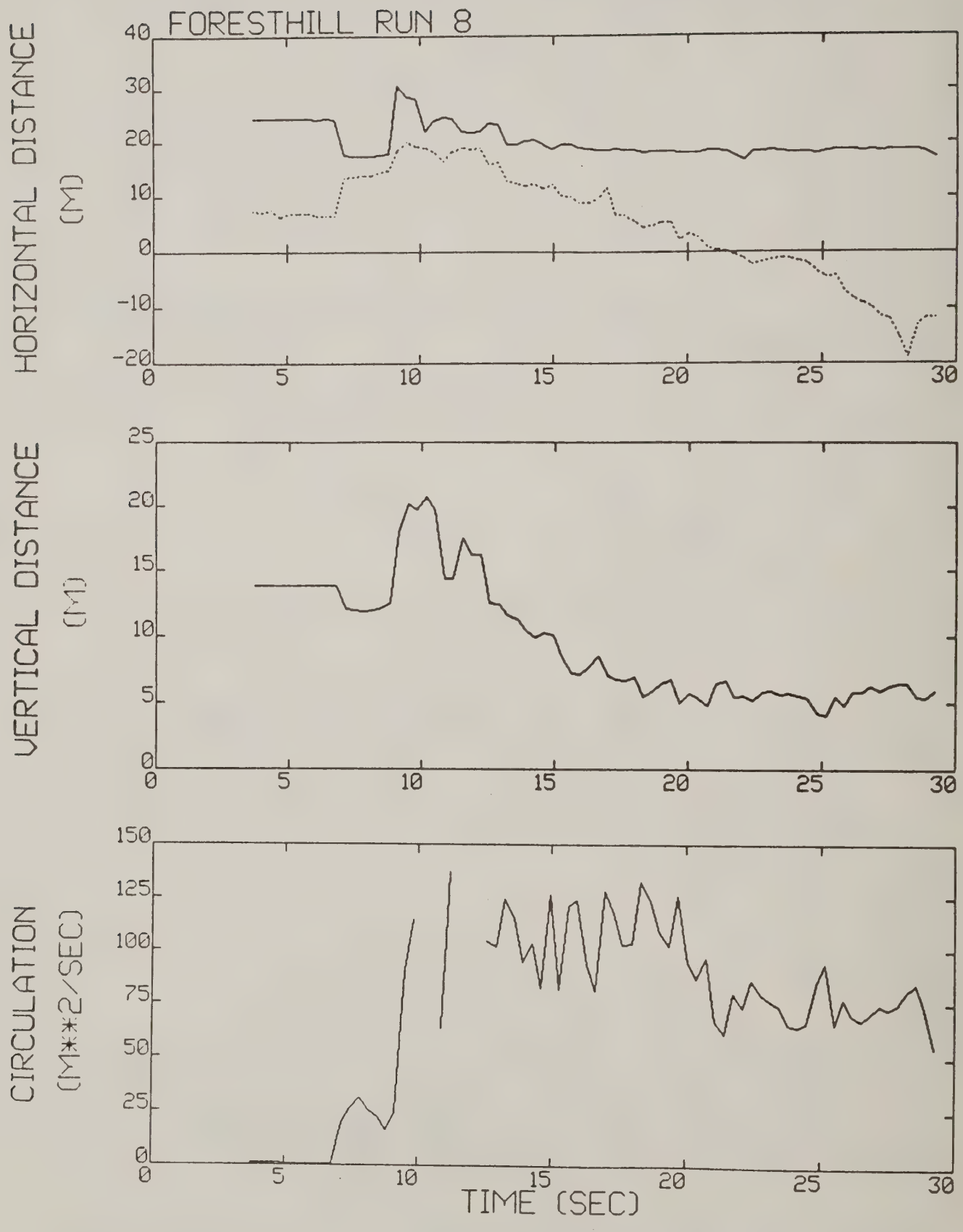

Figure A-3. Foresthill test run 8 generalized algorithm results (*).

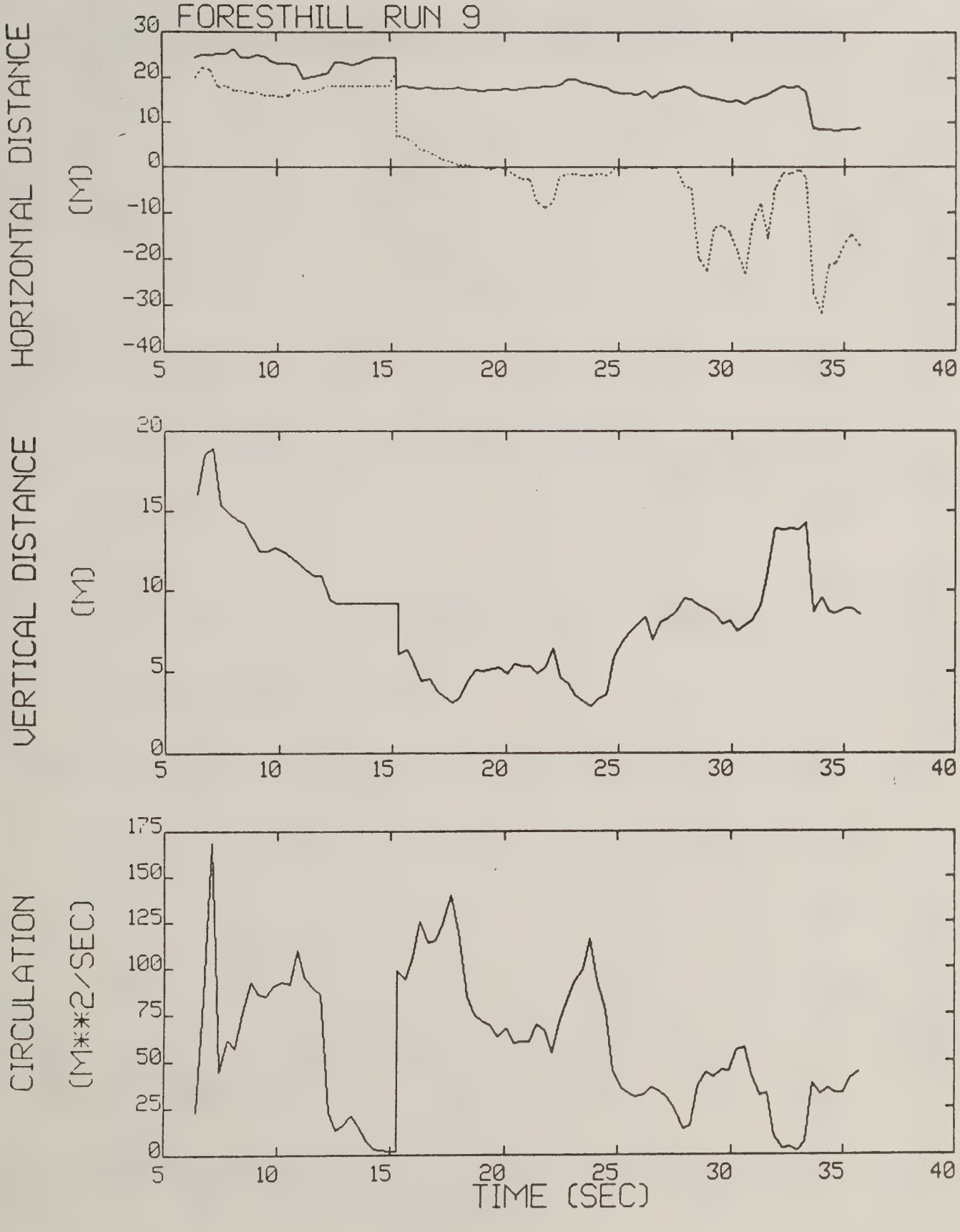

Figure A-4. Foresthill test run 9 generalized algorithm results (*).

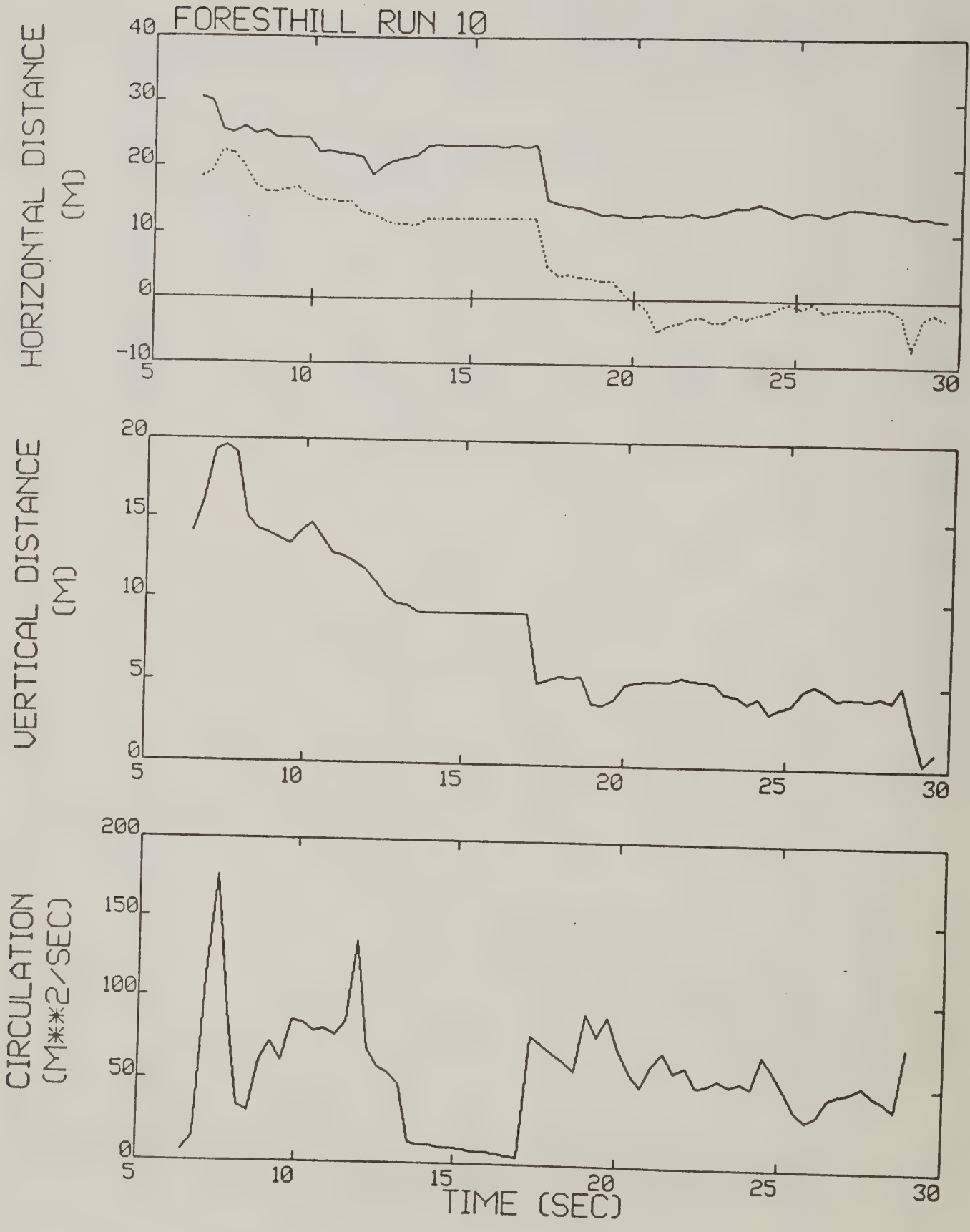

Figure A-5. Foresthill test run 10 generalized algorithm results.

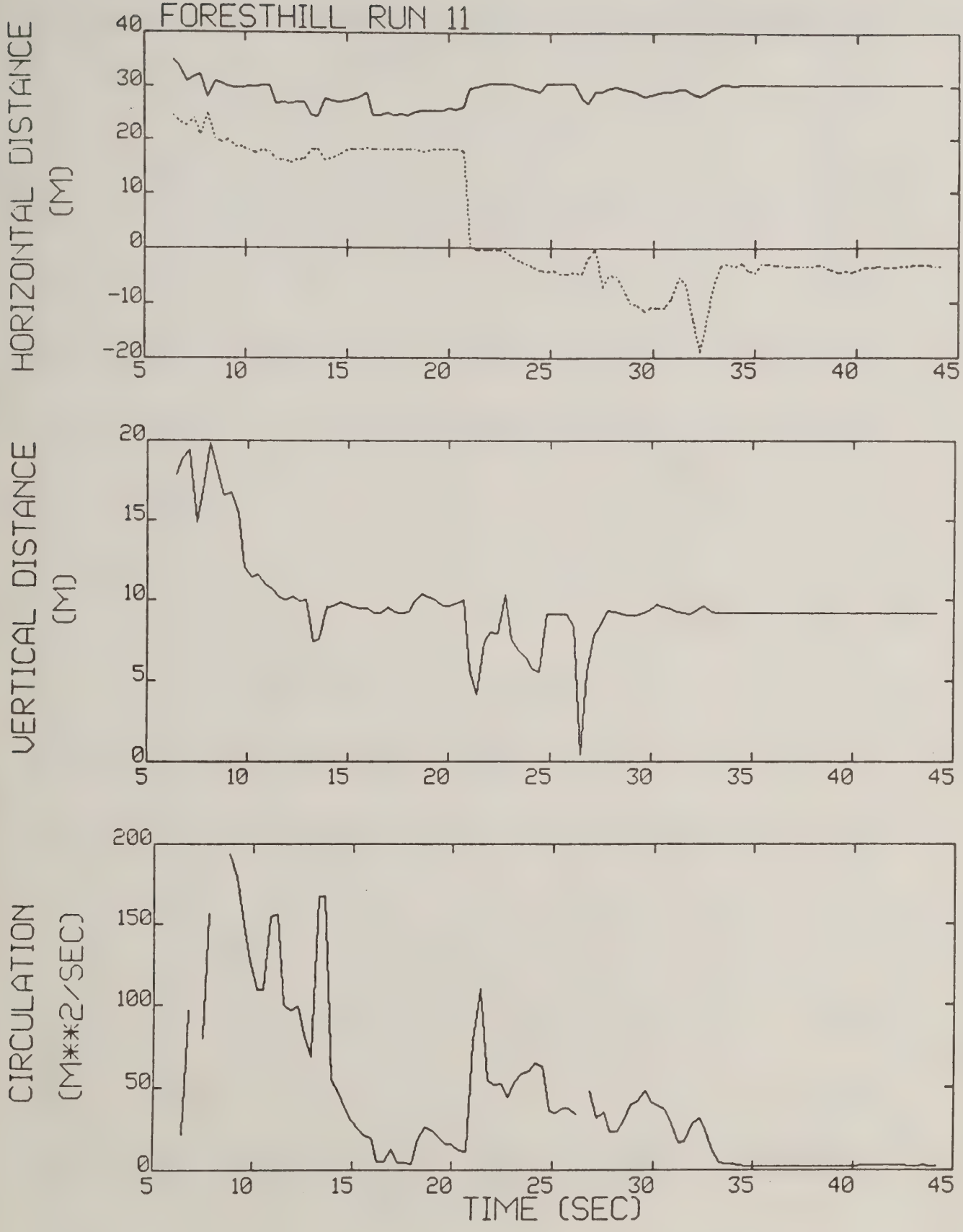

Figure A-6. Foresthill test run 11 generalized algorithm results (*).

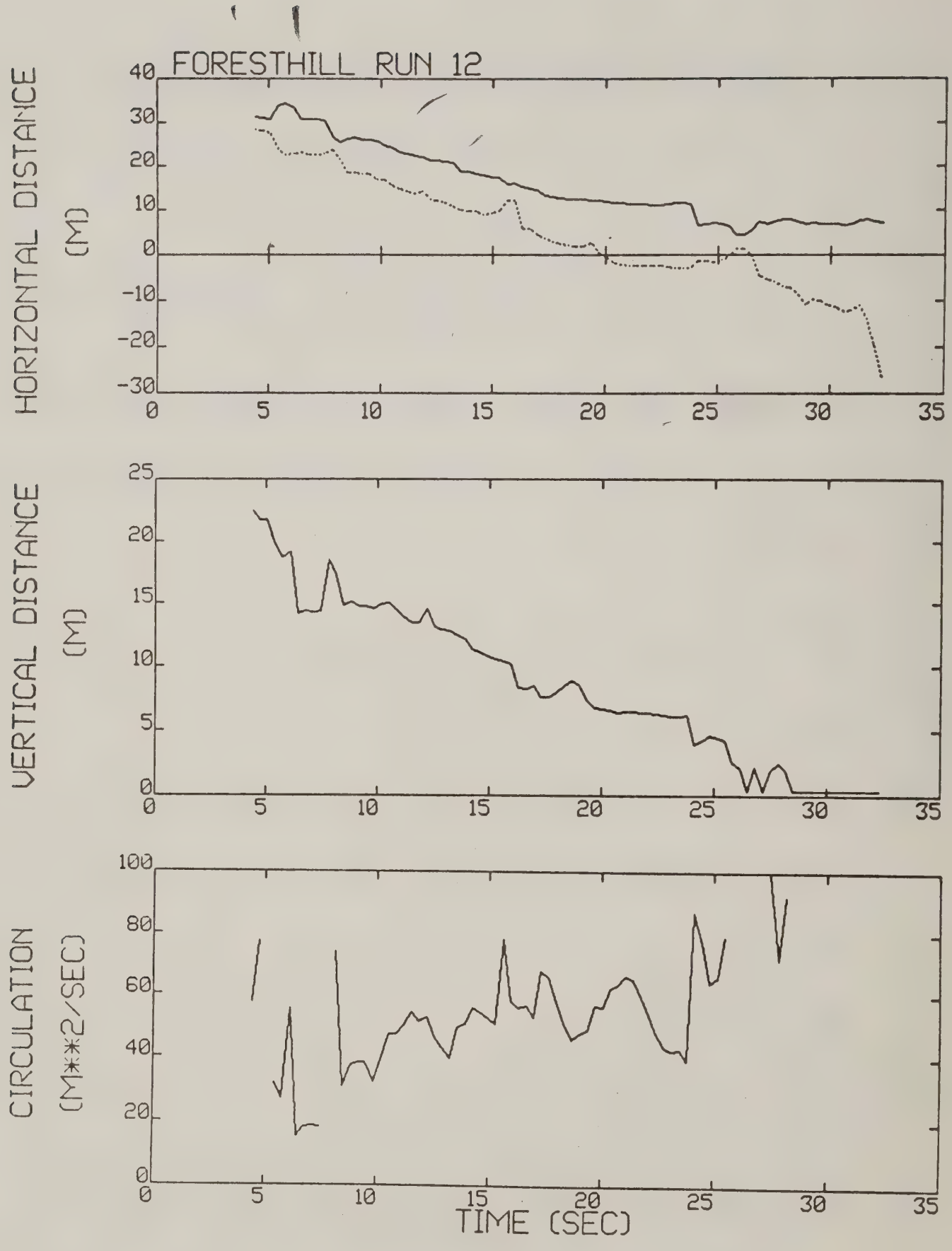

Figure A-7. Foresthill test run 12 generalized algorithm results.

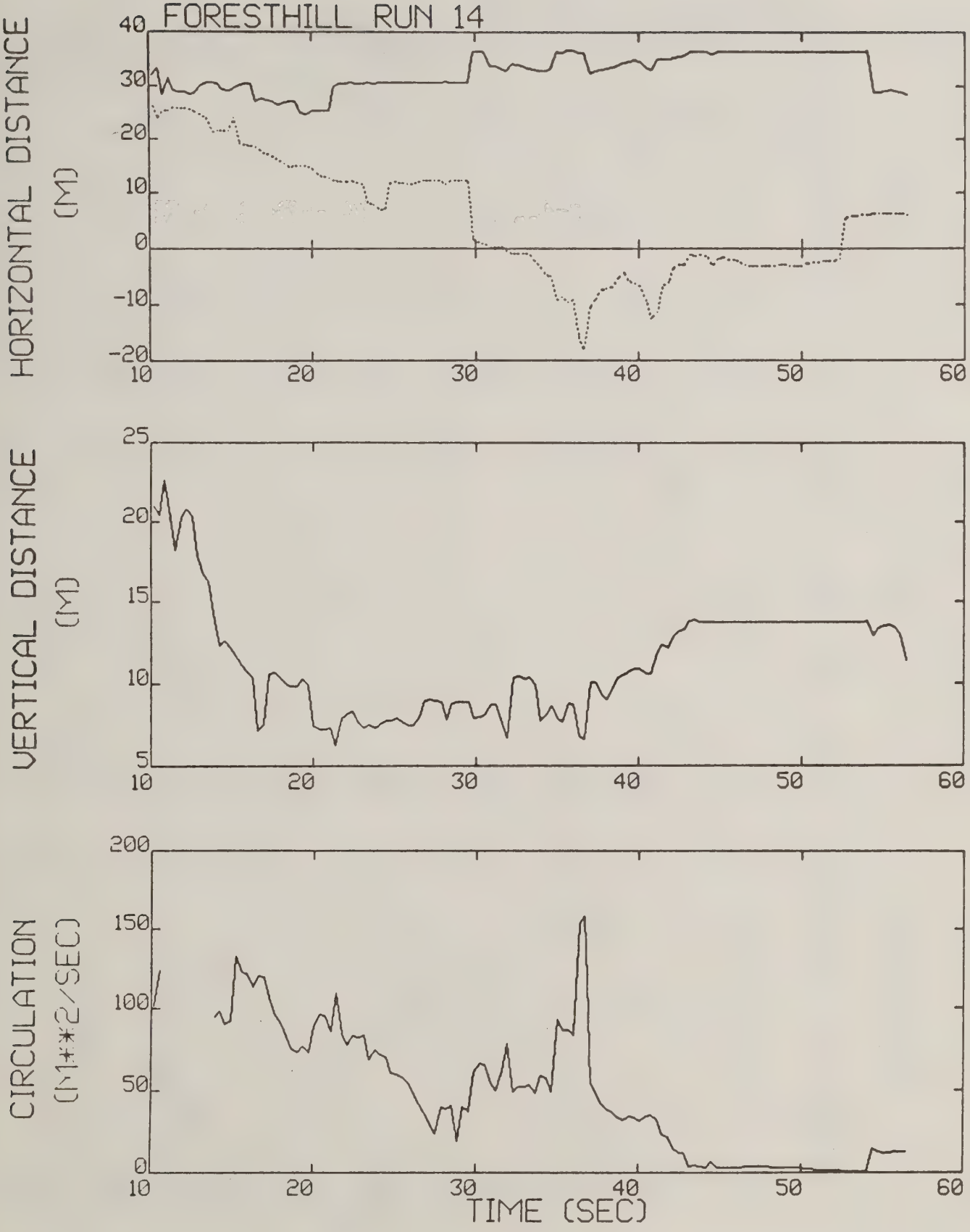

Figure A-8. Foresthill test run 14 generalized algorithm results (*).

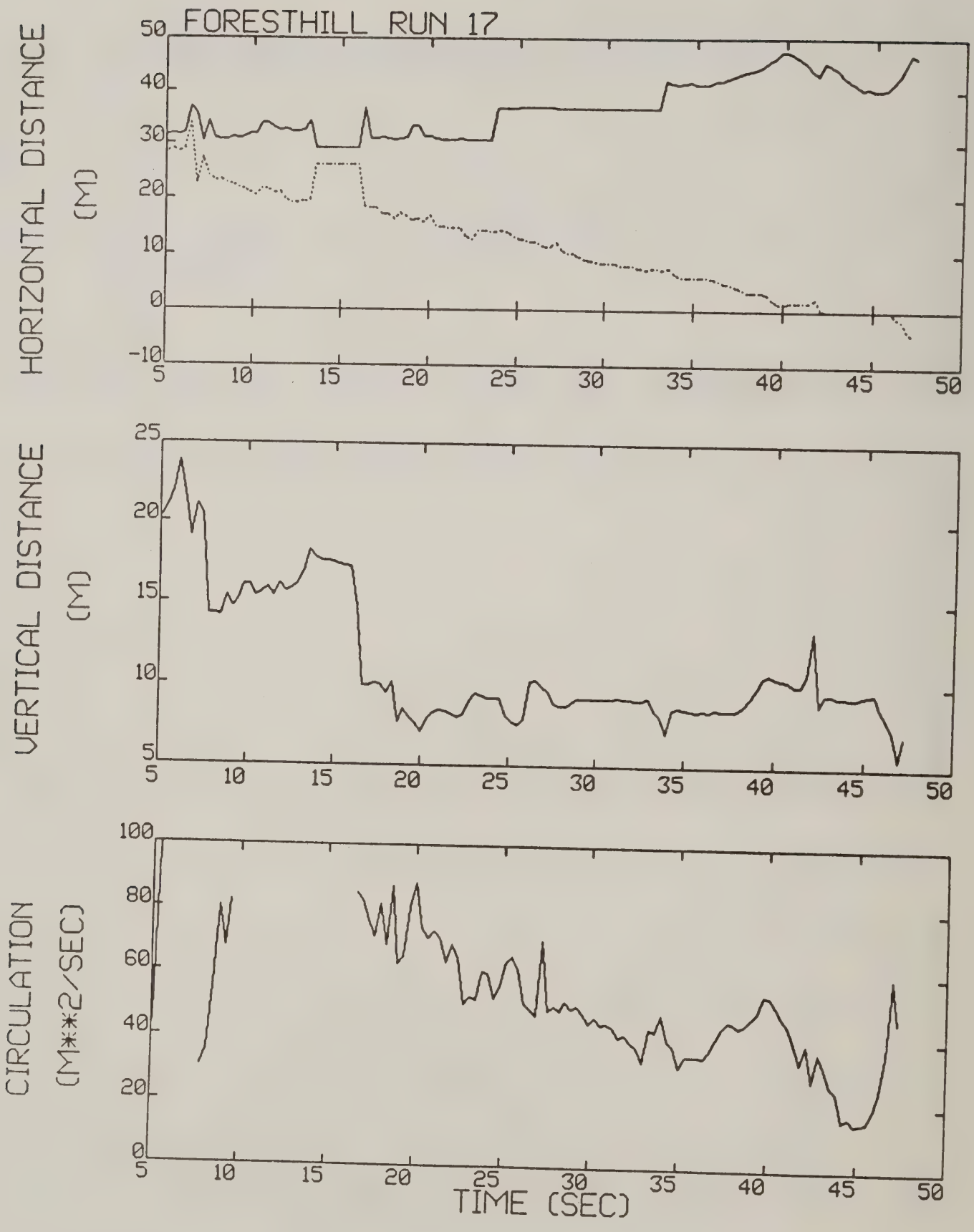

Figure A-9. Foresthill test run 17 generalized algorithm results (*).

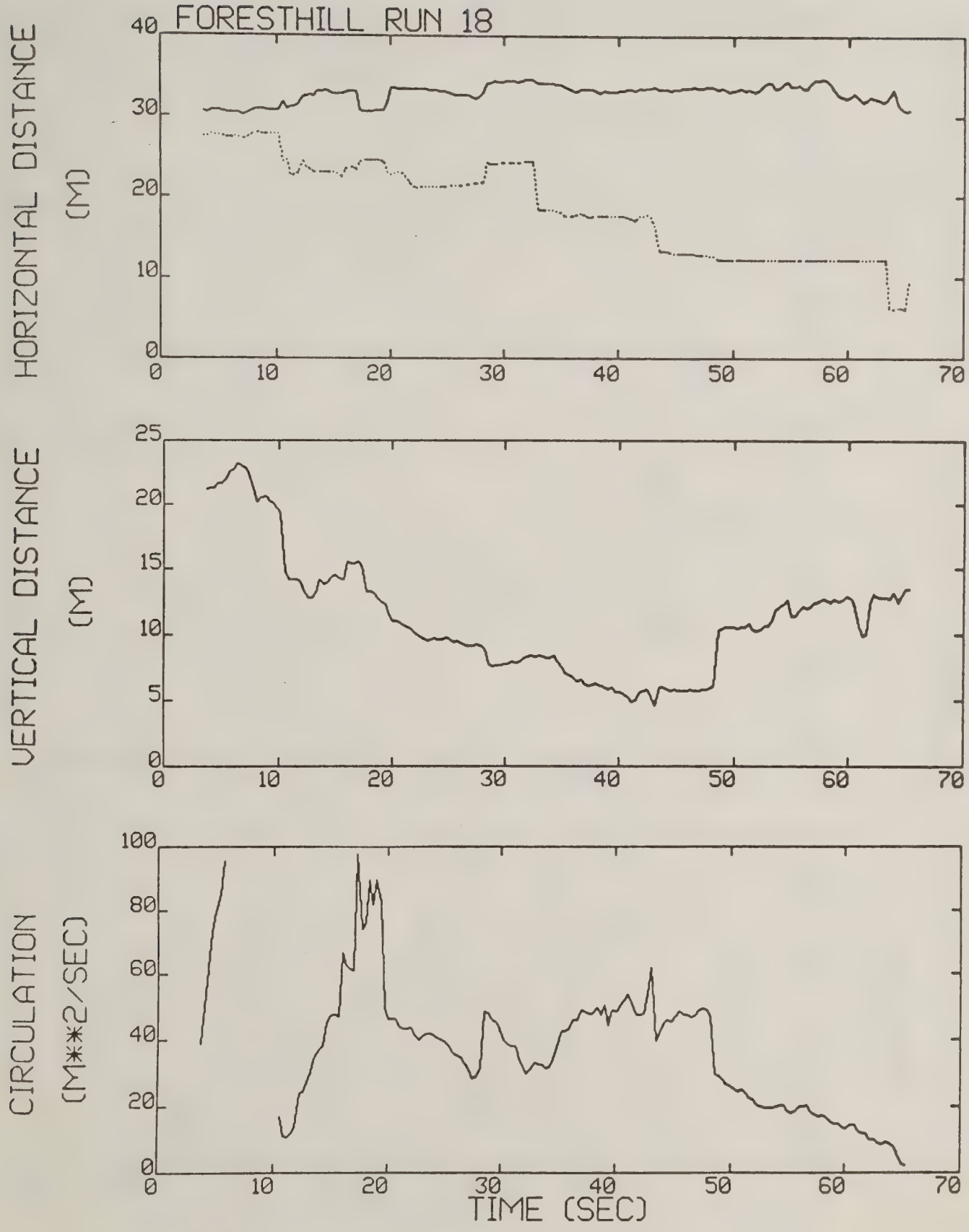

Figure A-10. Foresthill test run 18 generalized algorithm results (*).

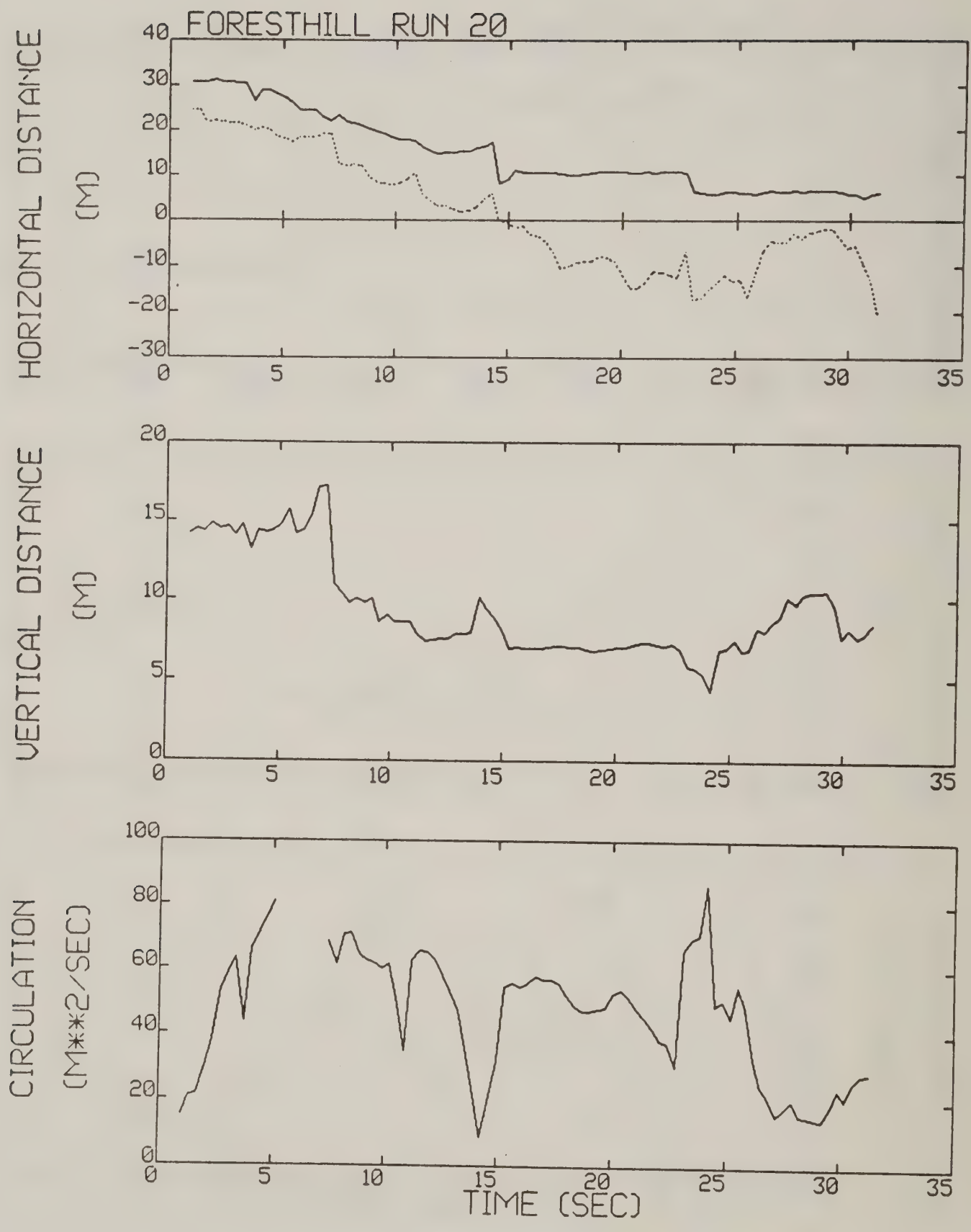

Figure A-11. Foresthill test run 20 generalized algorithm results (*).

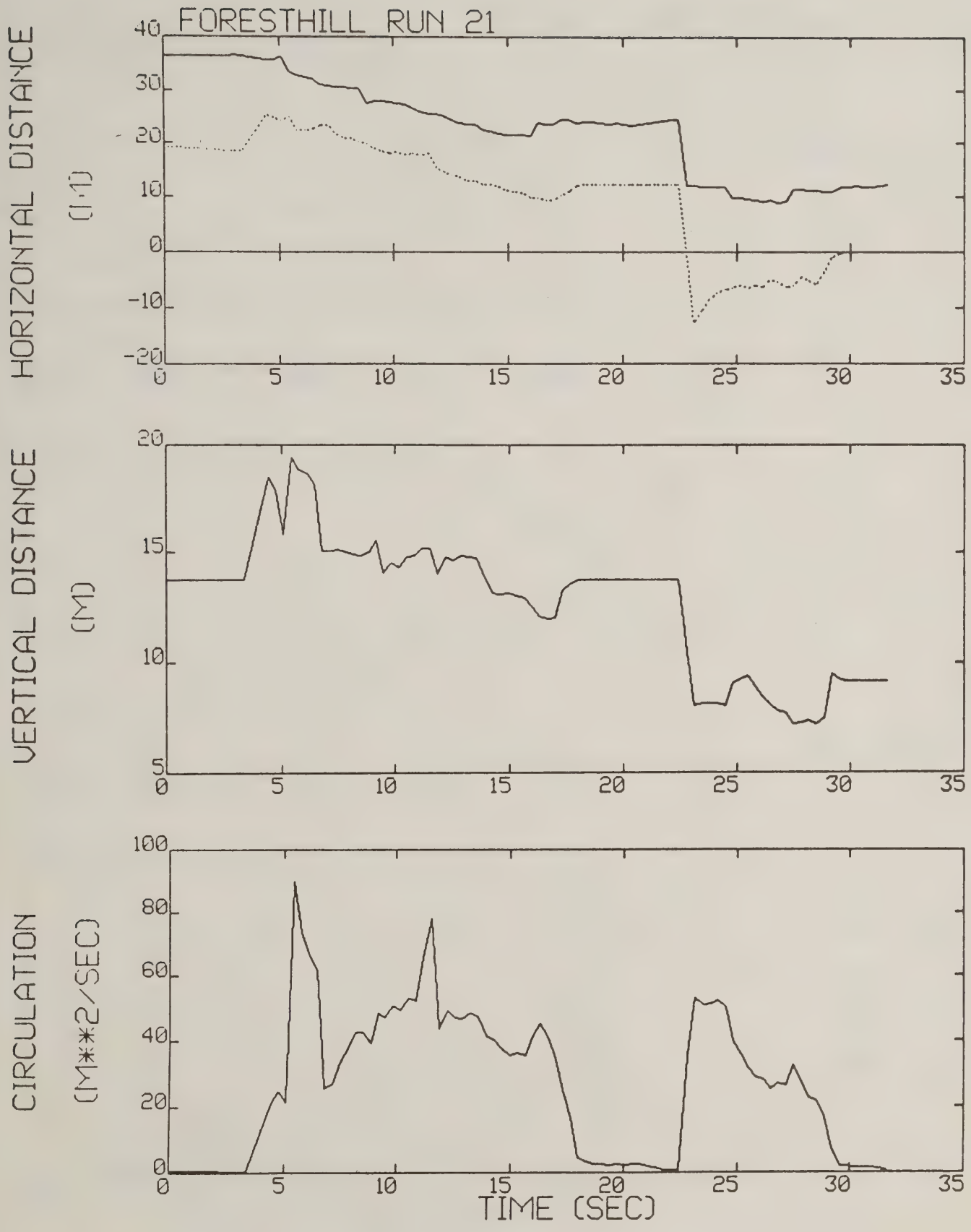

Figure A-12. Foresthill test run 21 generalized algorithm results.

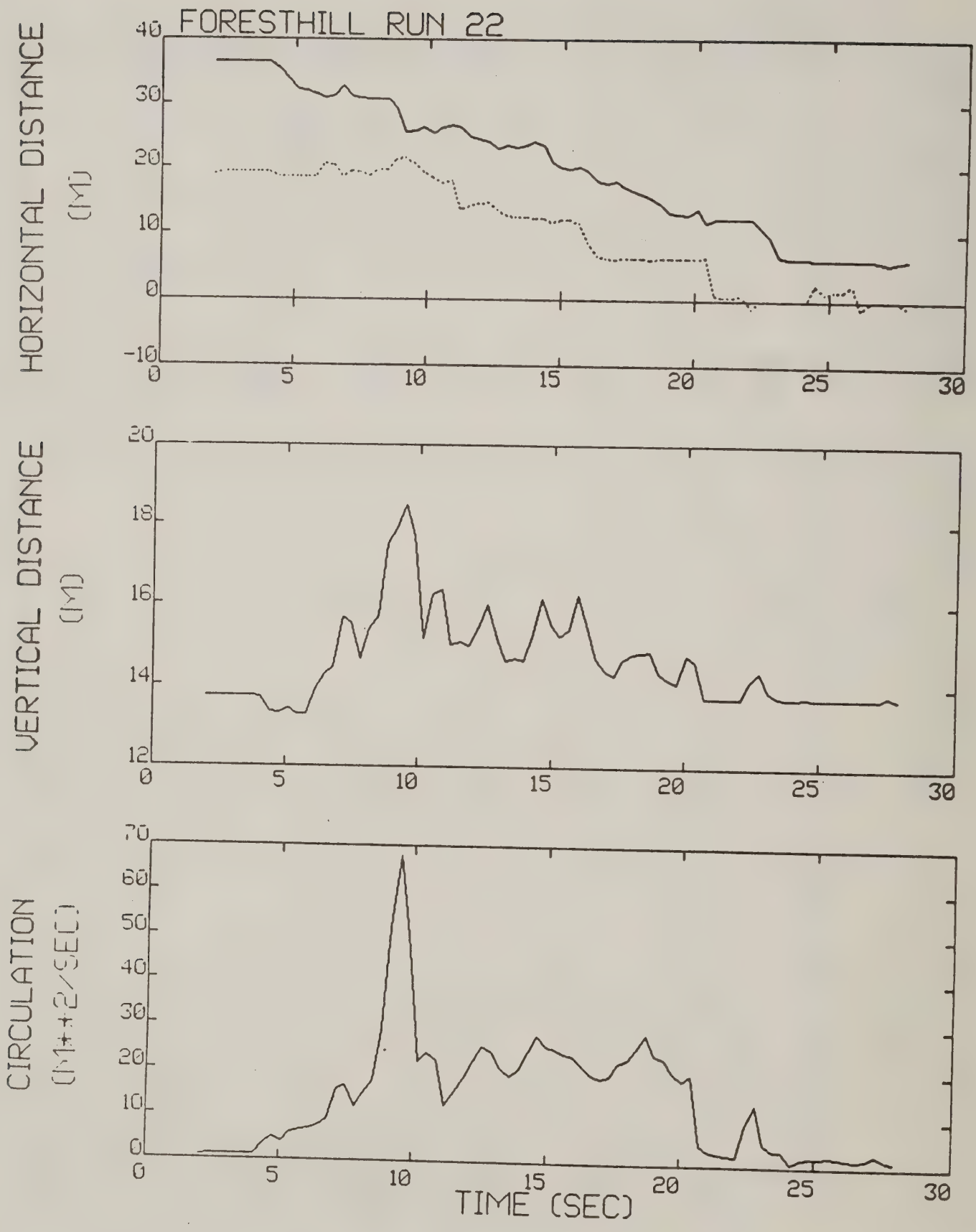

Figure A-13. Foresthill test run 22 generalized algorithm results.

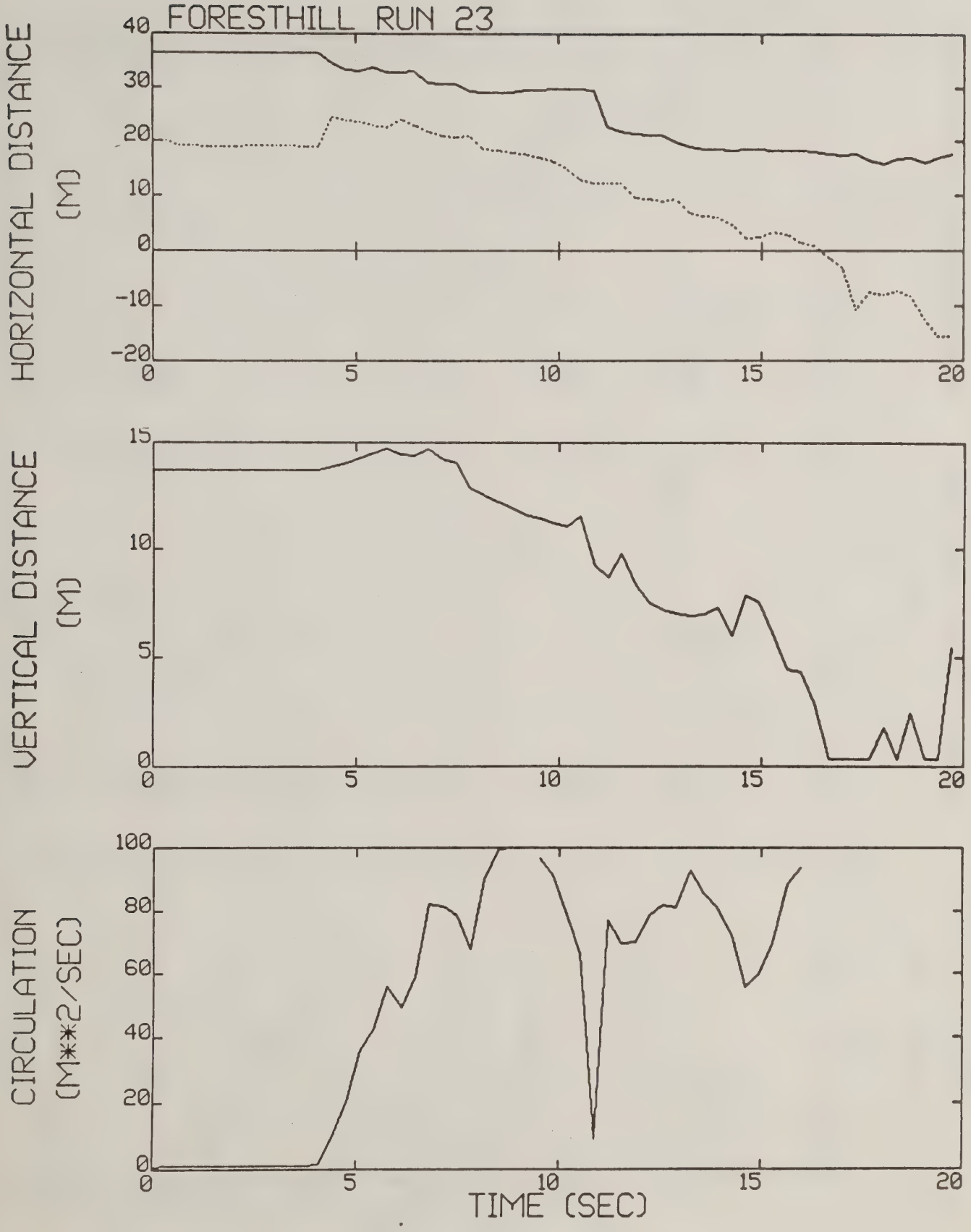

Figure A-14. Foresthill test run 23 generalized algorithm results.

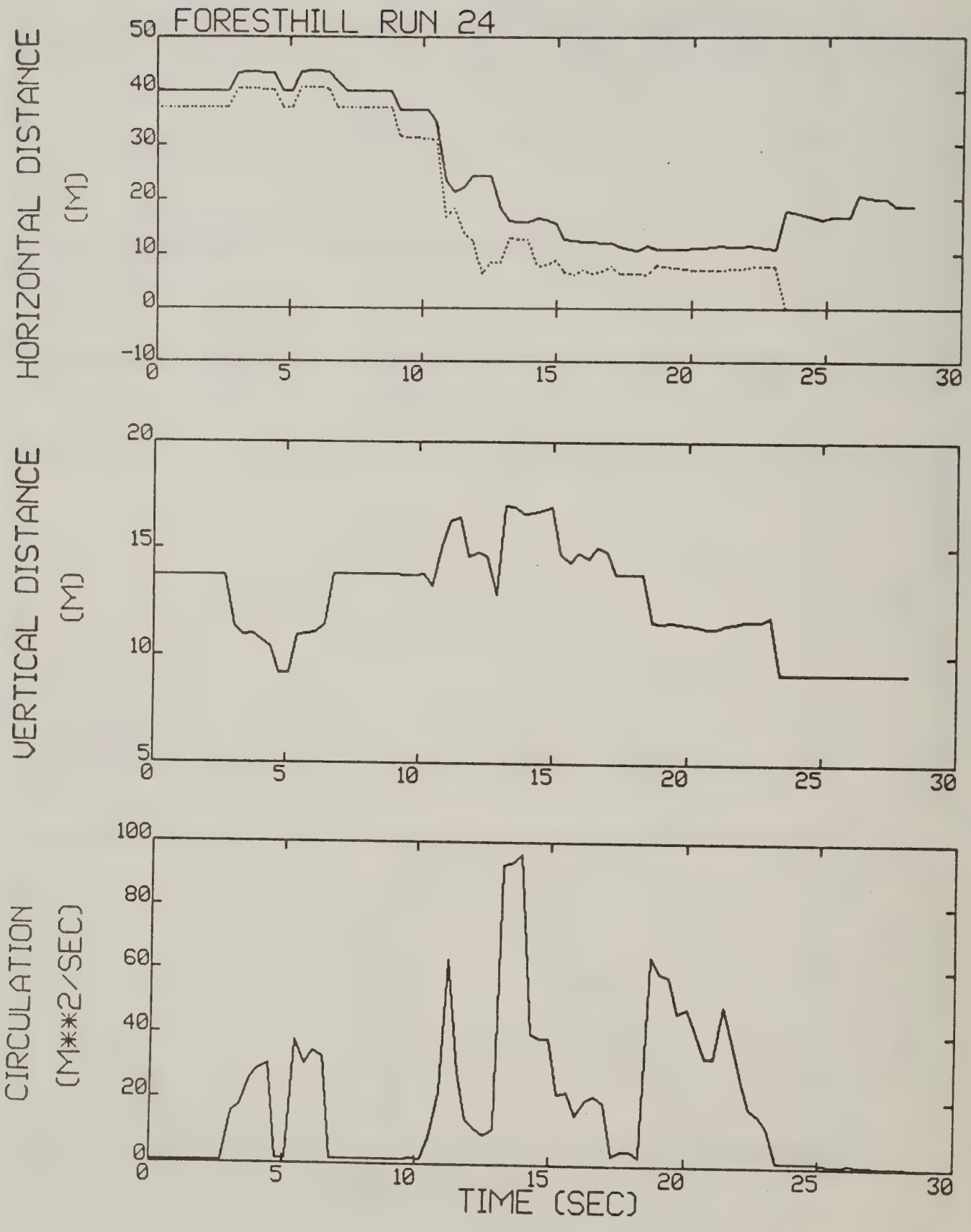

Figure A-15. Foresthill test run 24 generalized algorithm results.

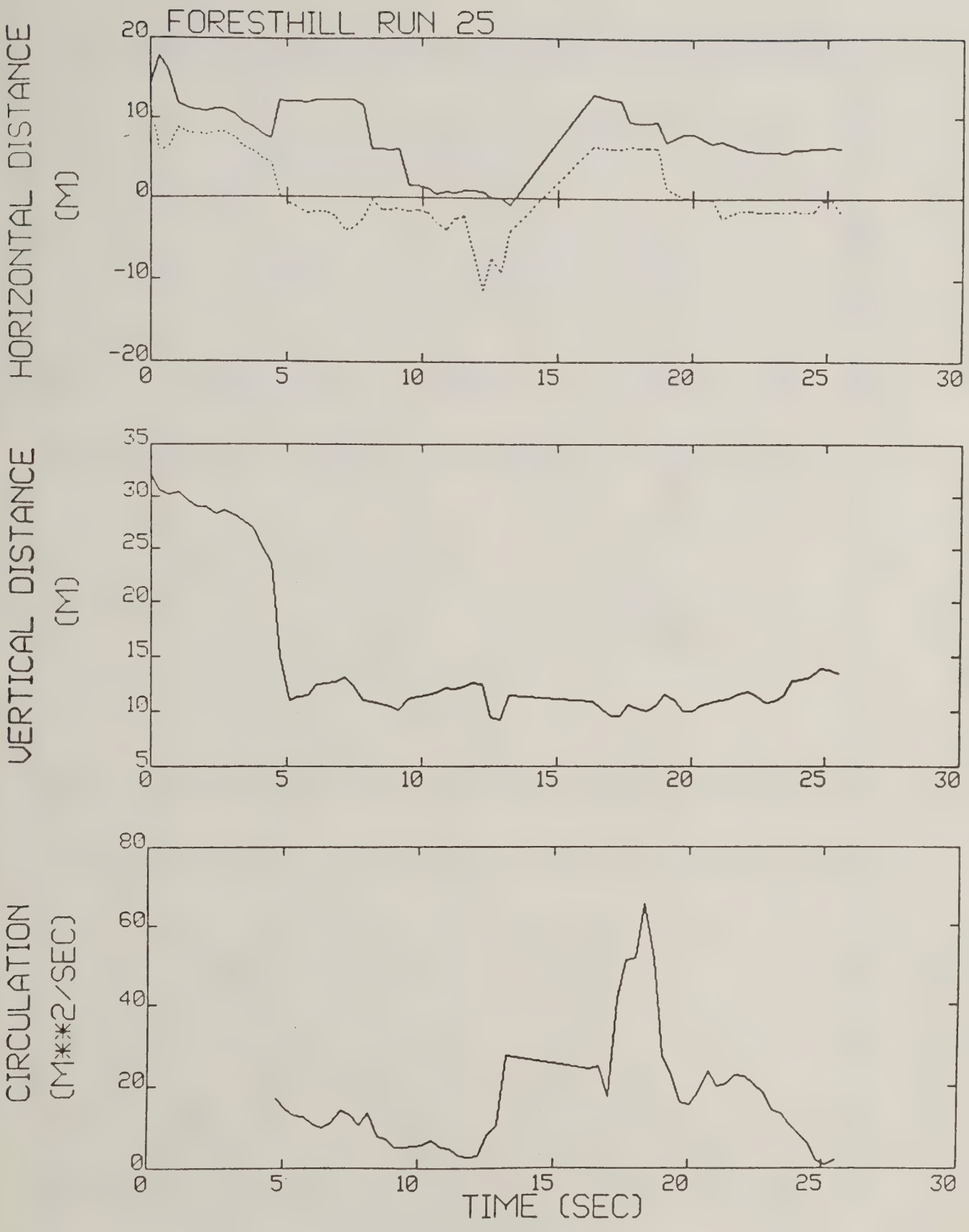

Figure A-16. Foresthill test run 25 generalized algorithm results.

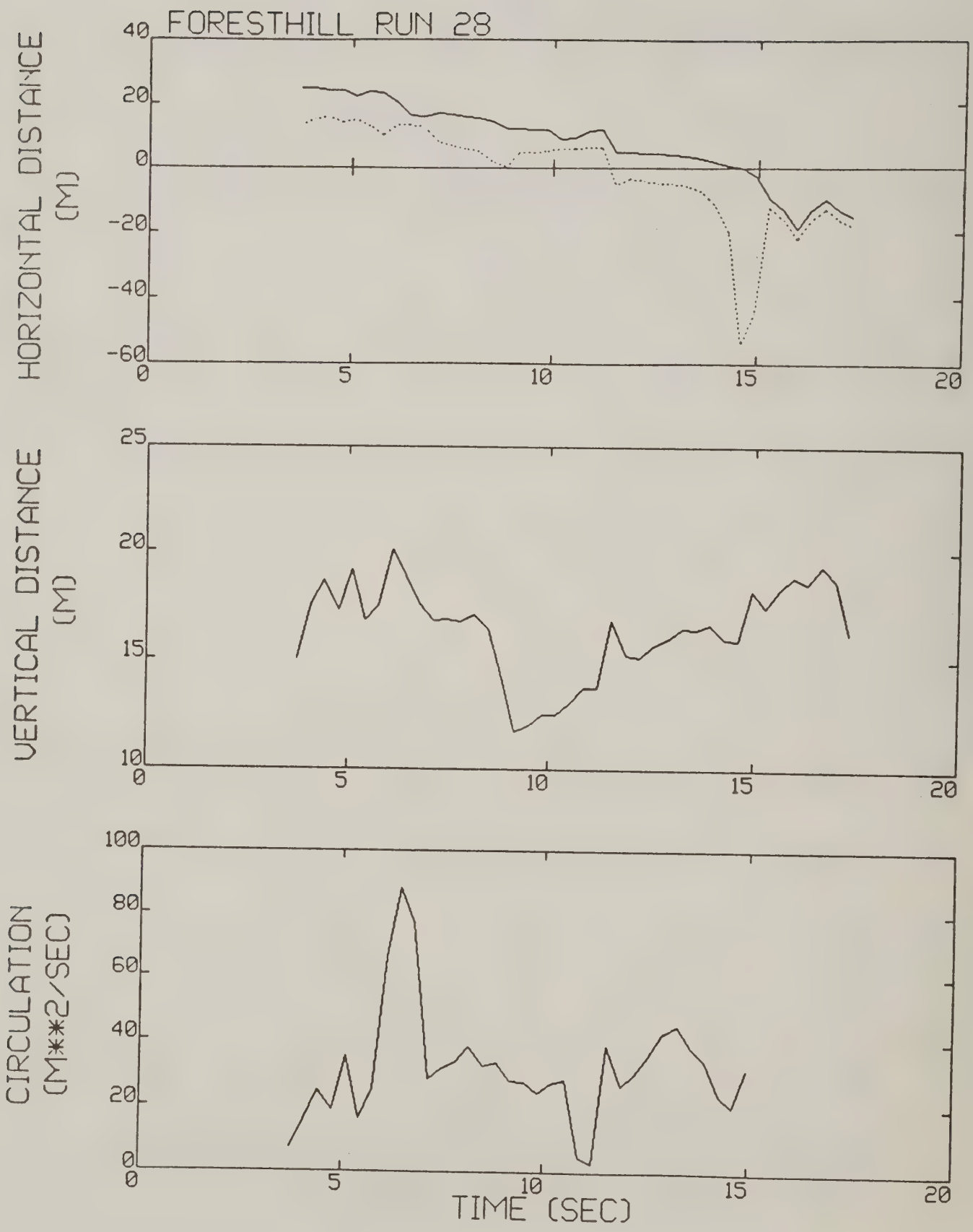

Figure A-17. Foresthill test run 28 generalized algorithm results.

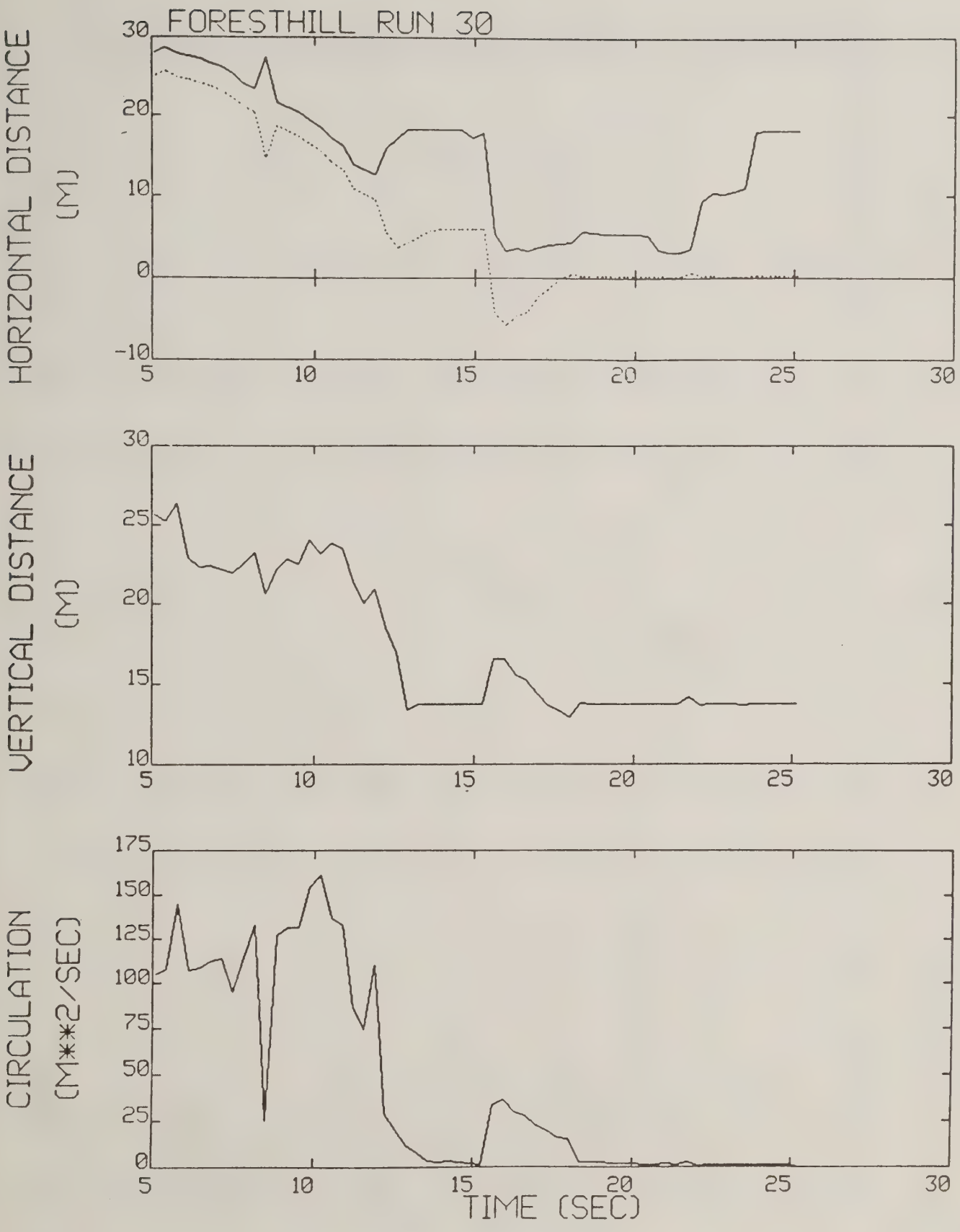

Figure A-18. Foresthill test run 30 generalized algorithm results.

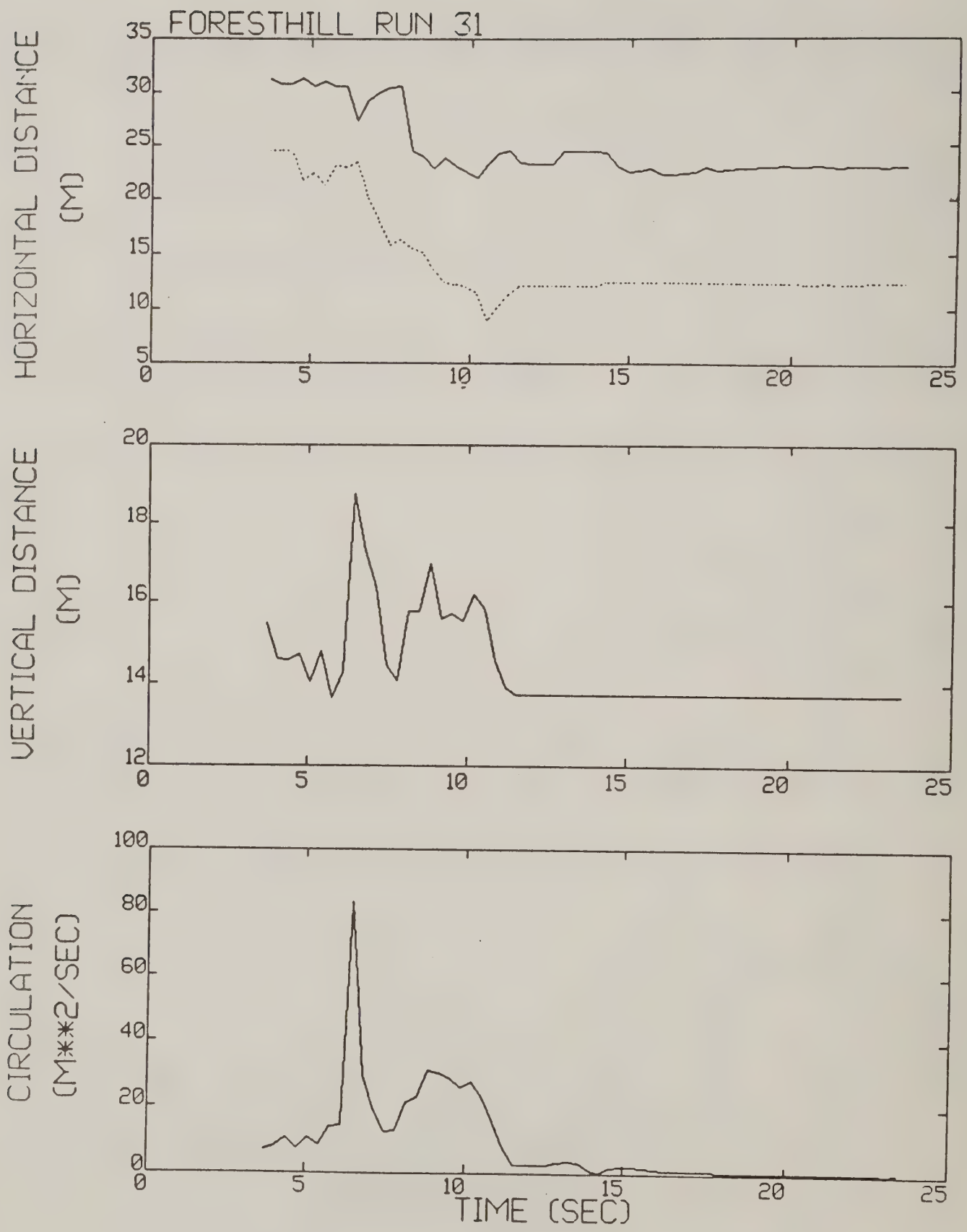

Figure A-19. Foresthill test run 31 generalized algorithm results.

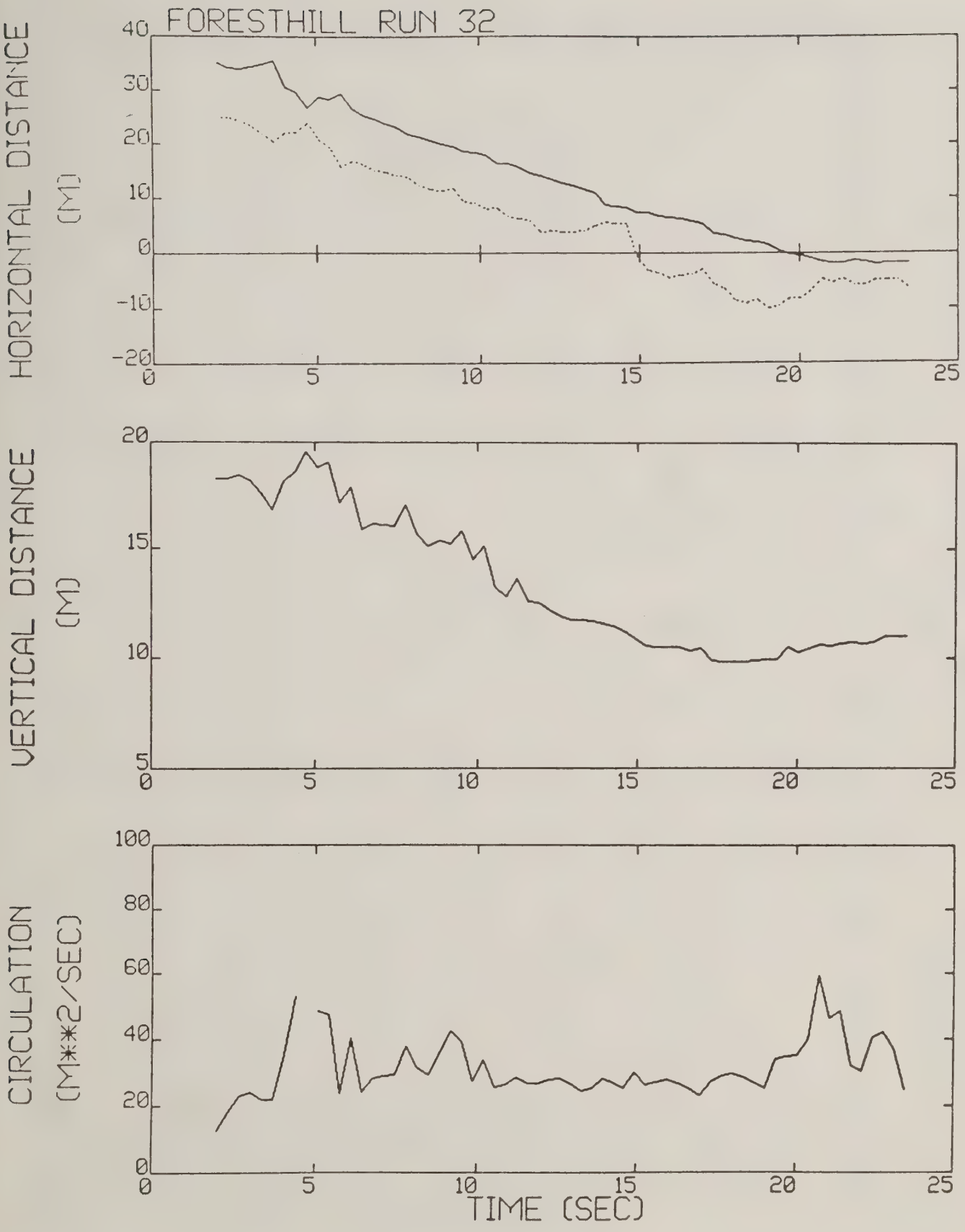

Figure A-20. Foresthill test run 32 generalized algorithm results.

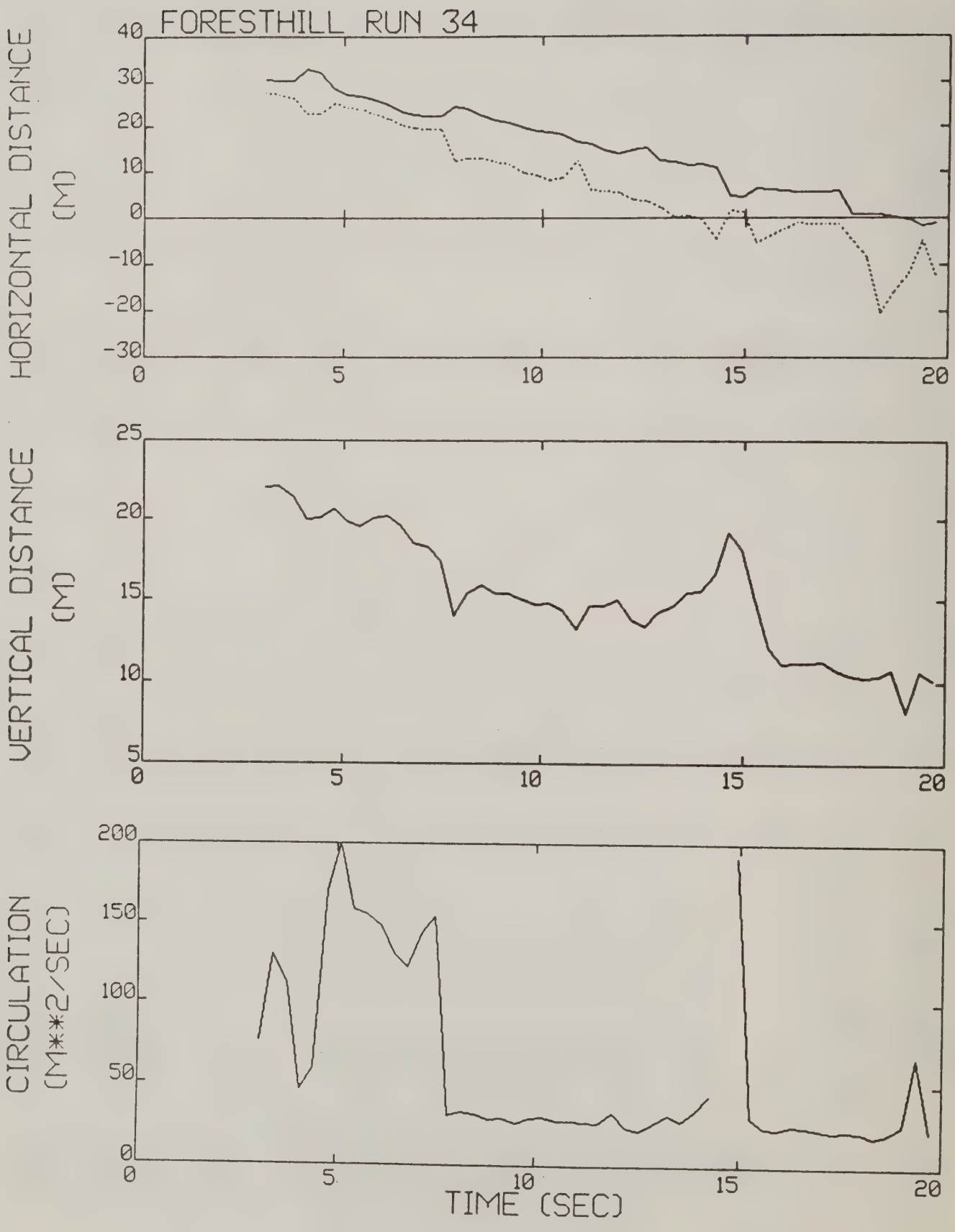

Figure A-21. Foresthill test run 34 generalized algorithm results.

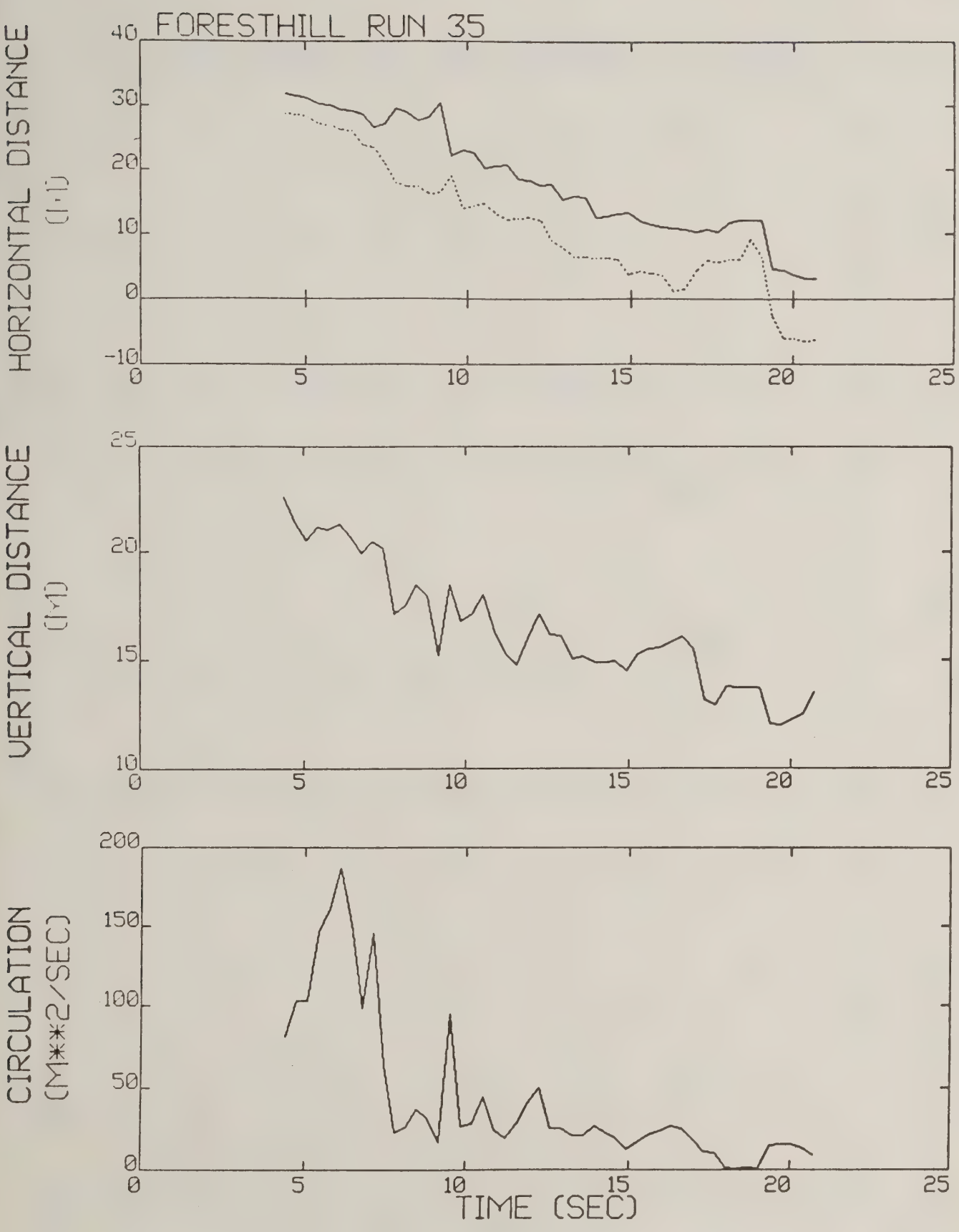

Figure A-22. Foresthill test run 35 generalized algorithm results (*).

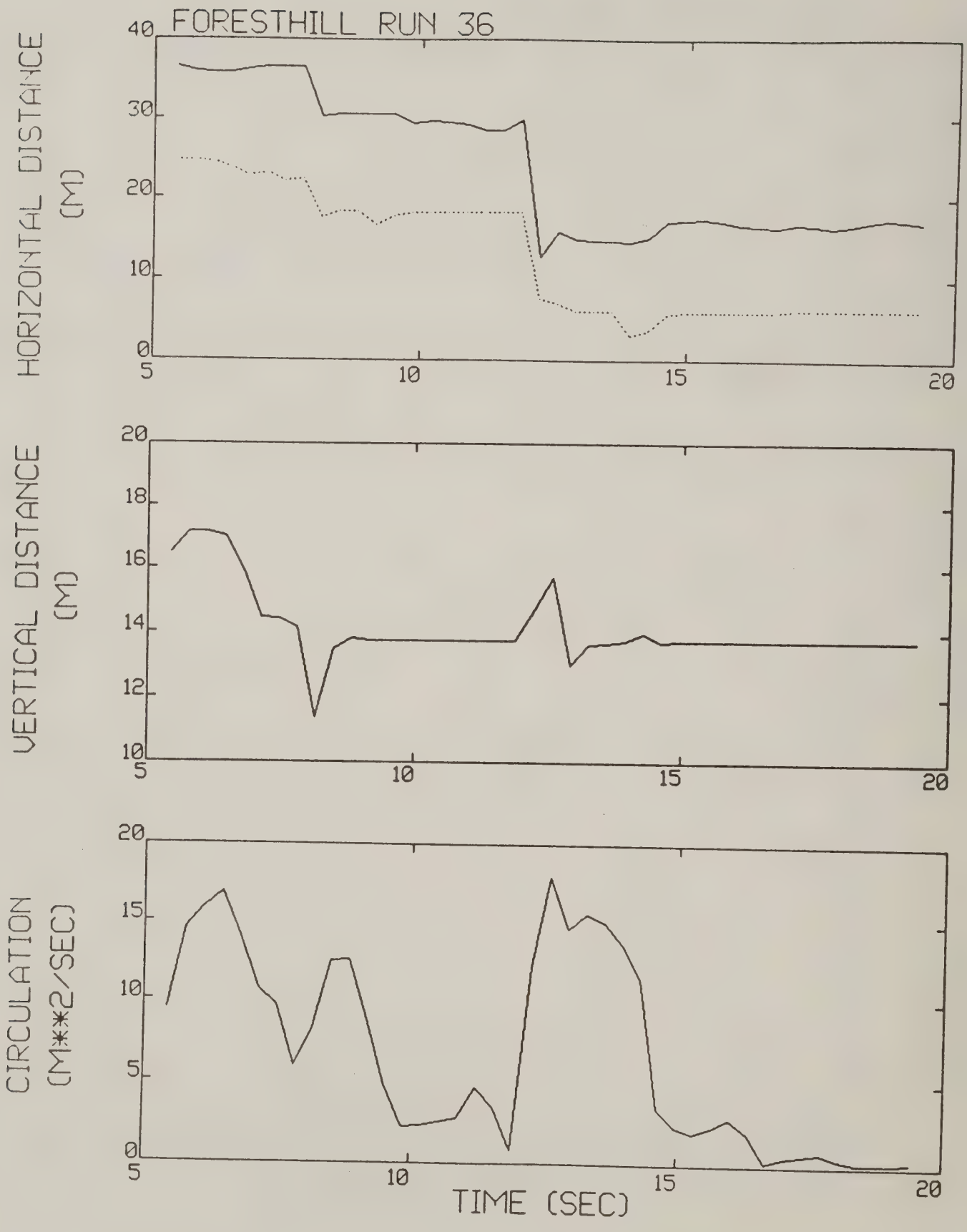

Figure A-23. Foresthill test run 36 generalized algorithm results.

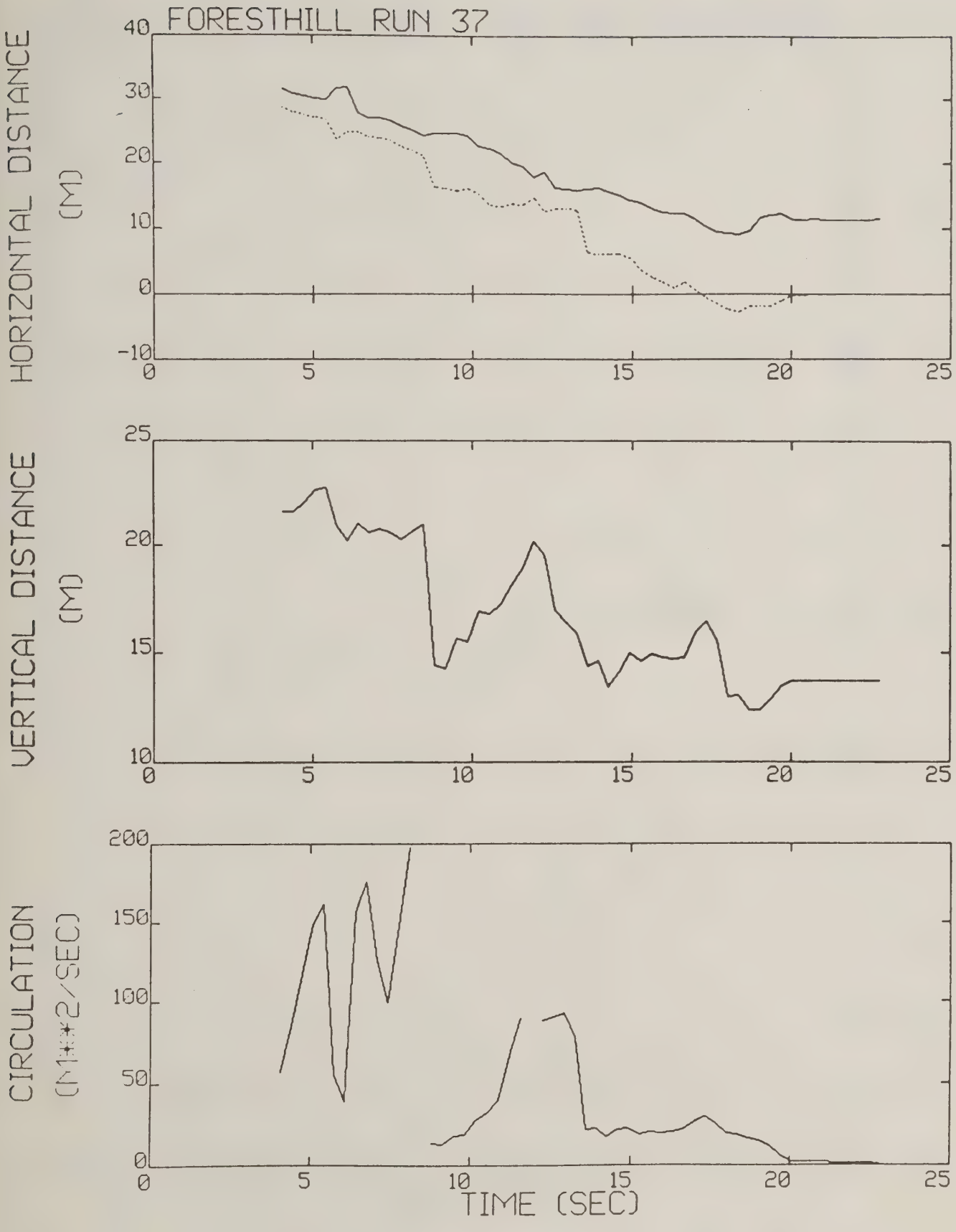

Figure A-24. Foresthill test run 37 generalized algorithm results.

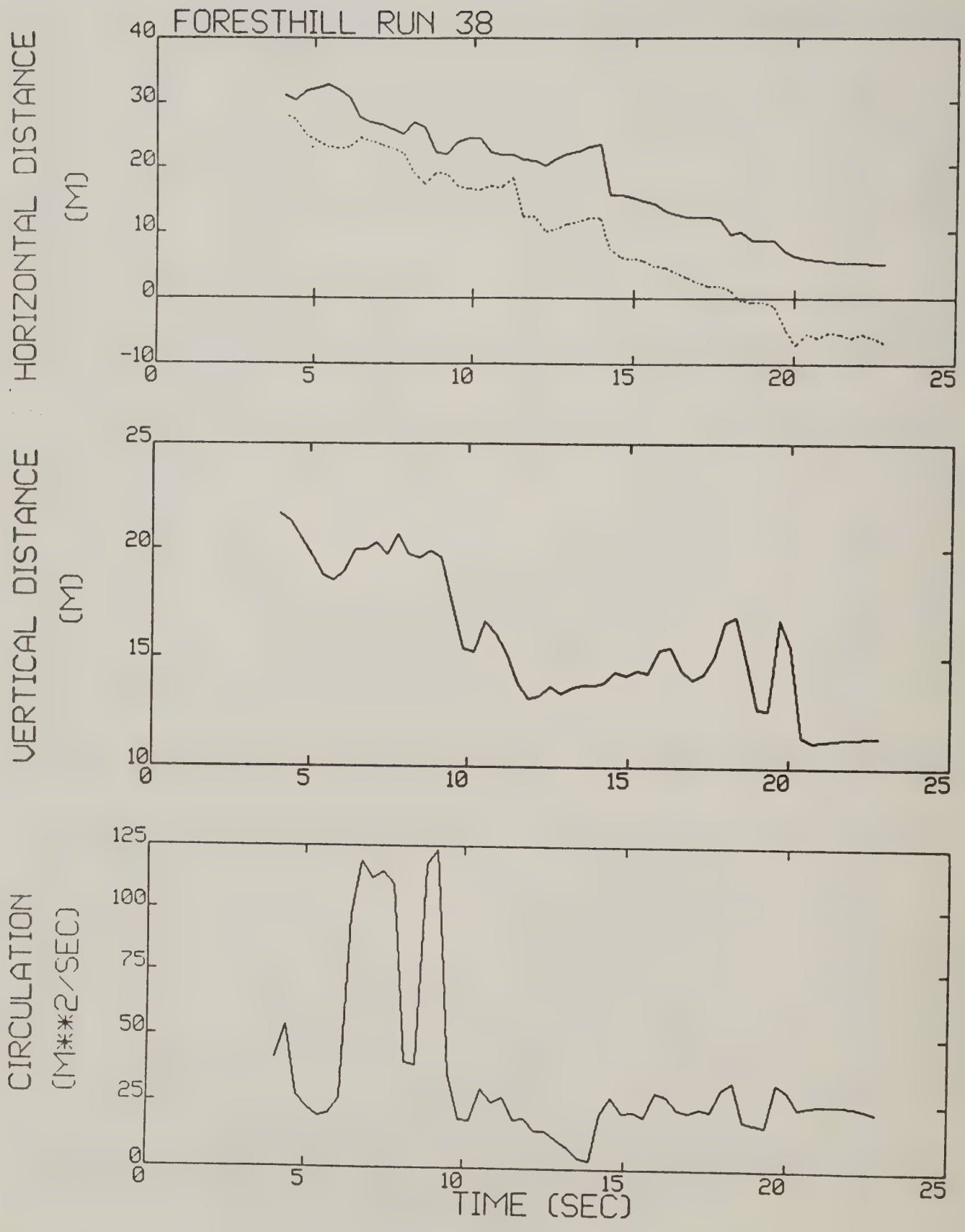

Figure A-25. Foresthill test run 38 generalized algorithm results.

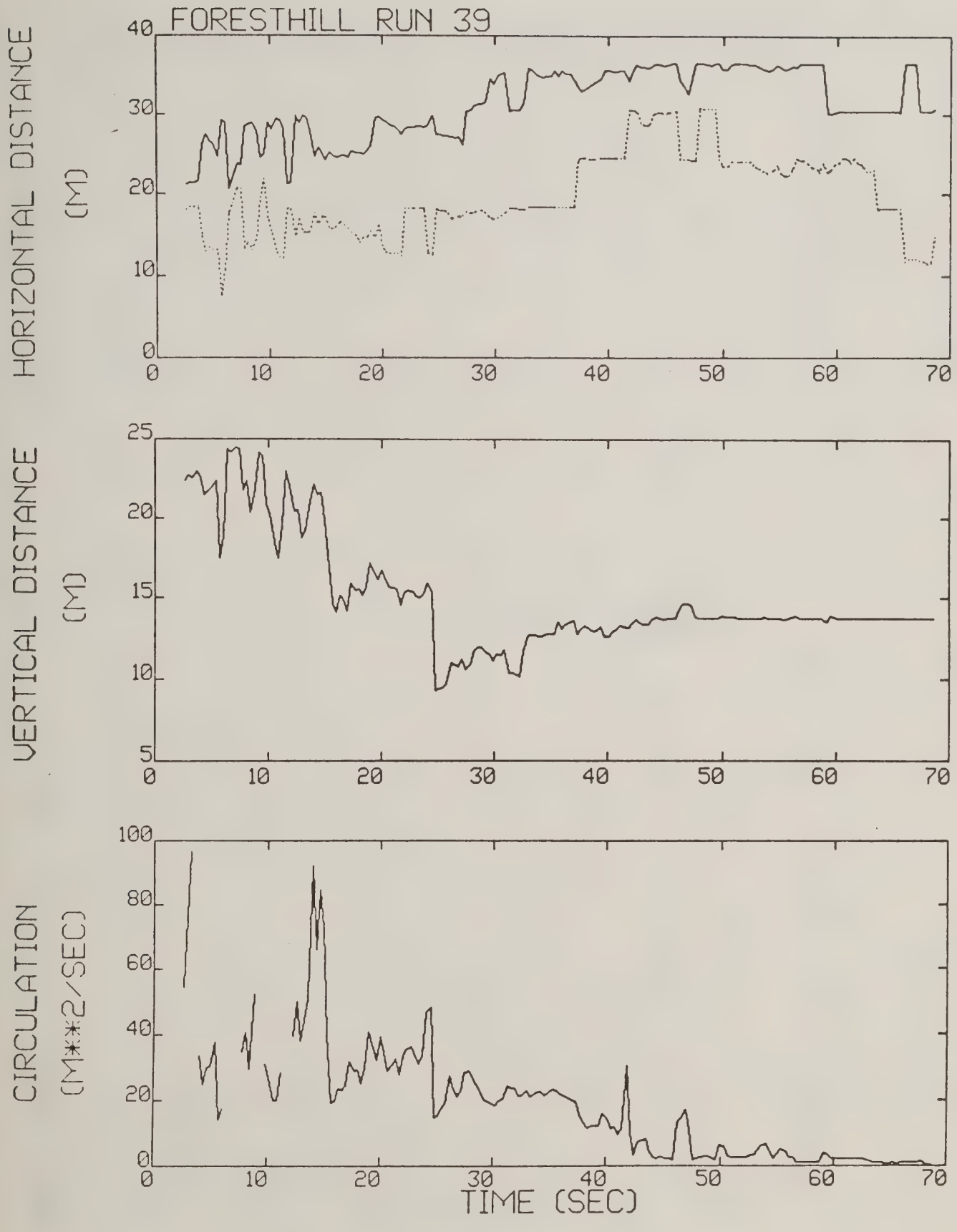

Figure A-26. Foresthill test run 39 generalized algorithm results (*).

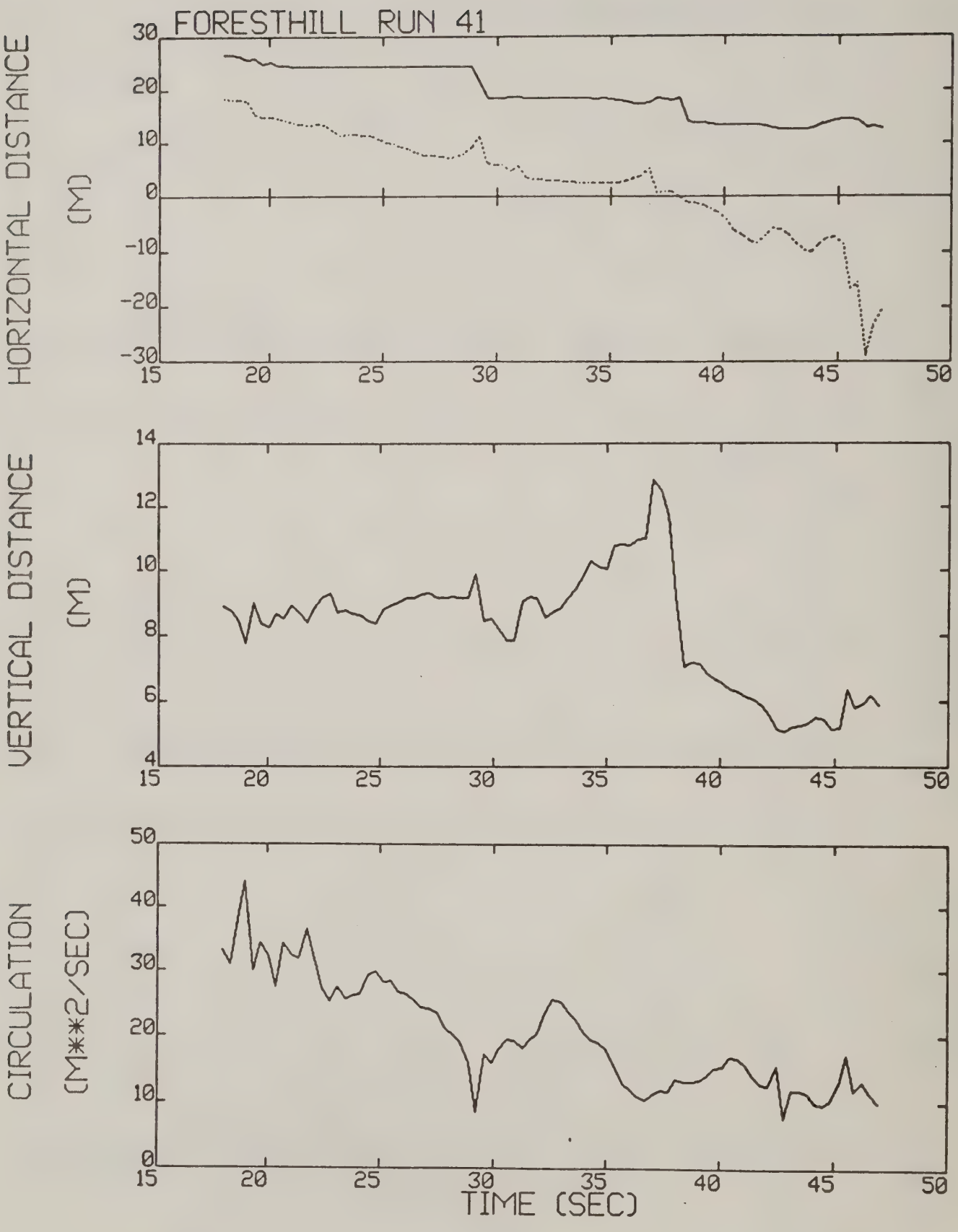

Figure A-27. Foresthill test run 41 generalized algorithm results (*).

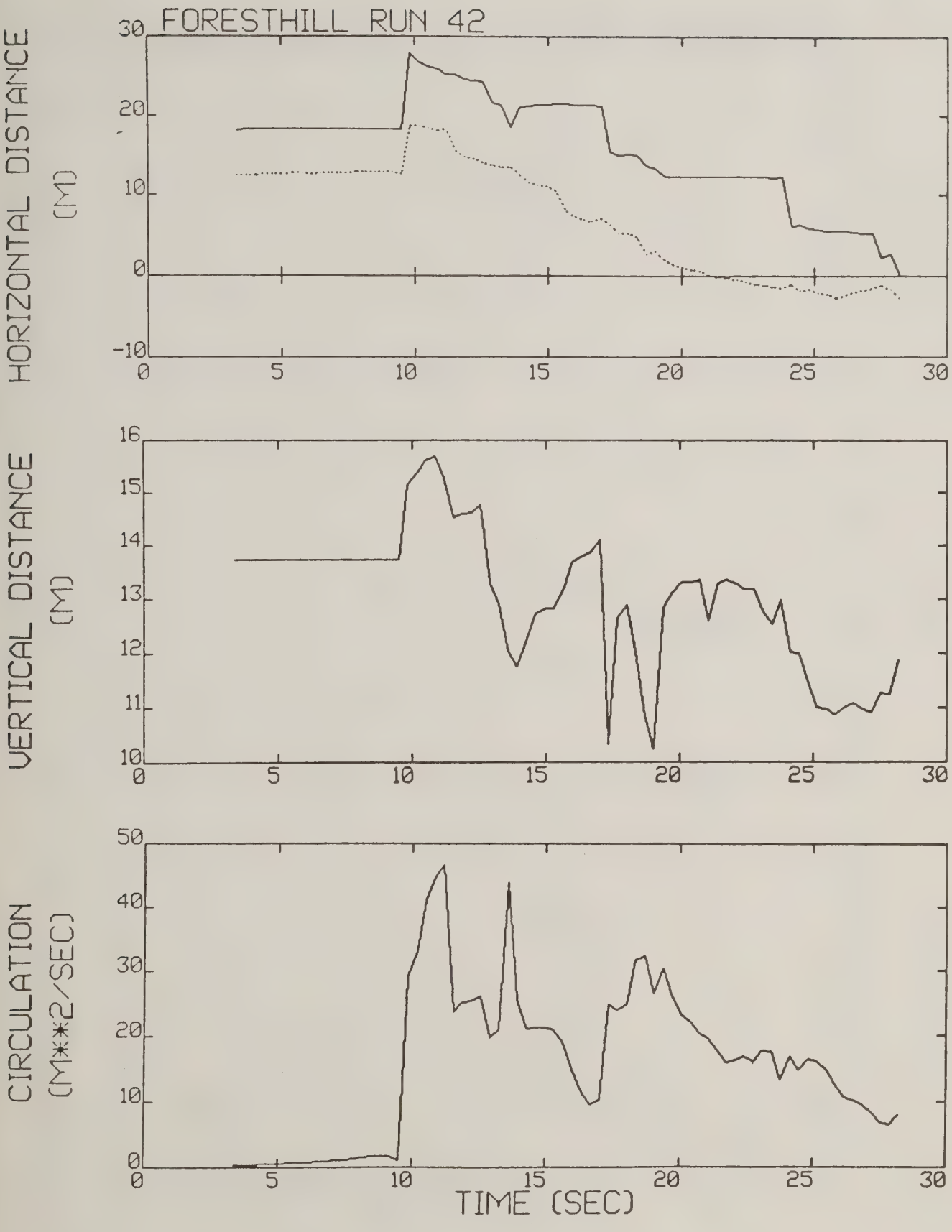

Figure A-28. Foresthill test run 42 generalized algorithm results (*).

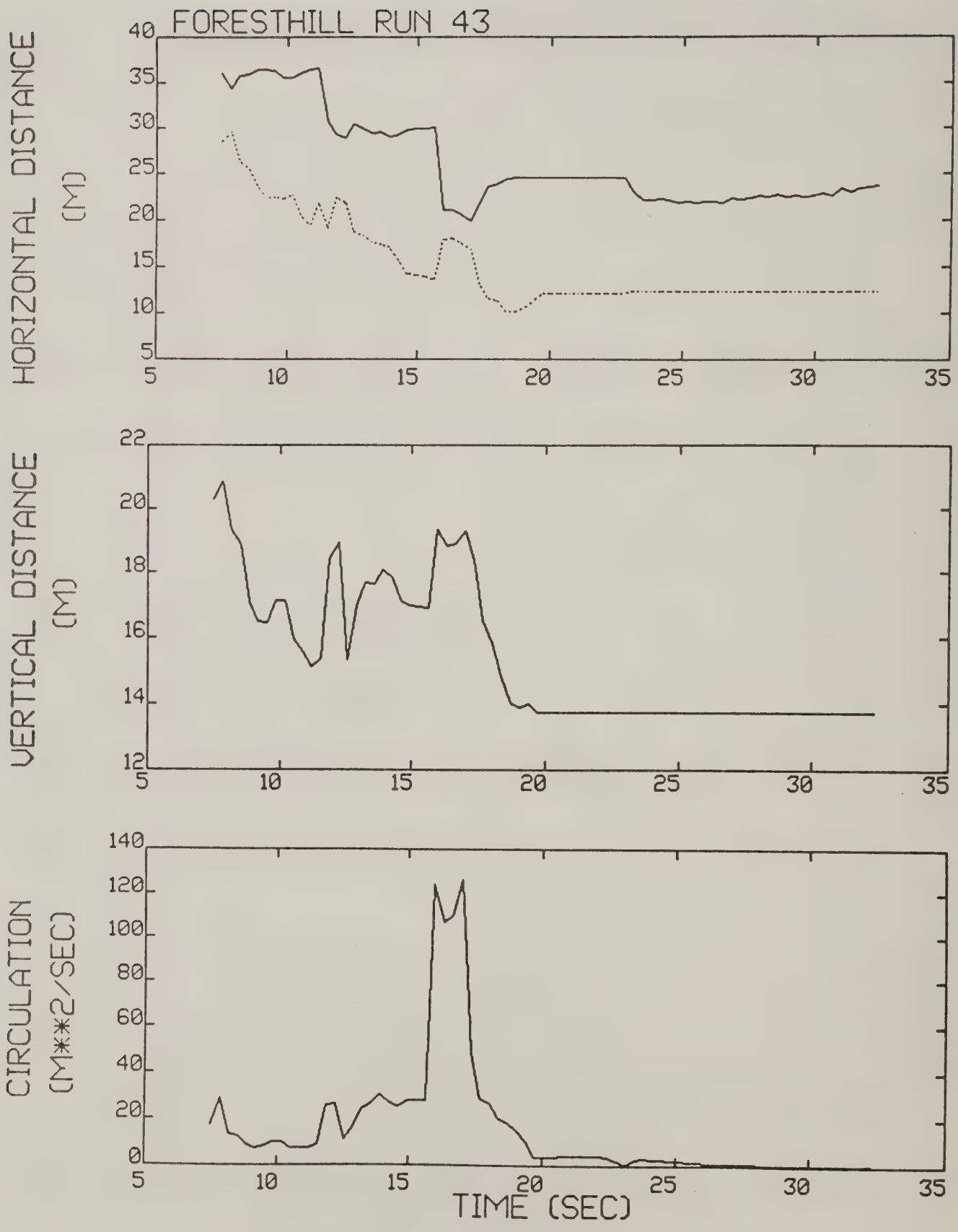

Figure A-29. Foresthill test run 43 generalized algorithm results.

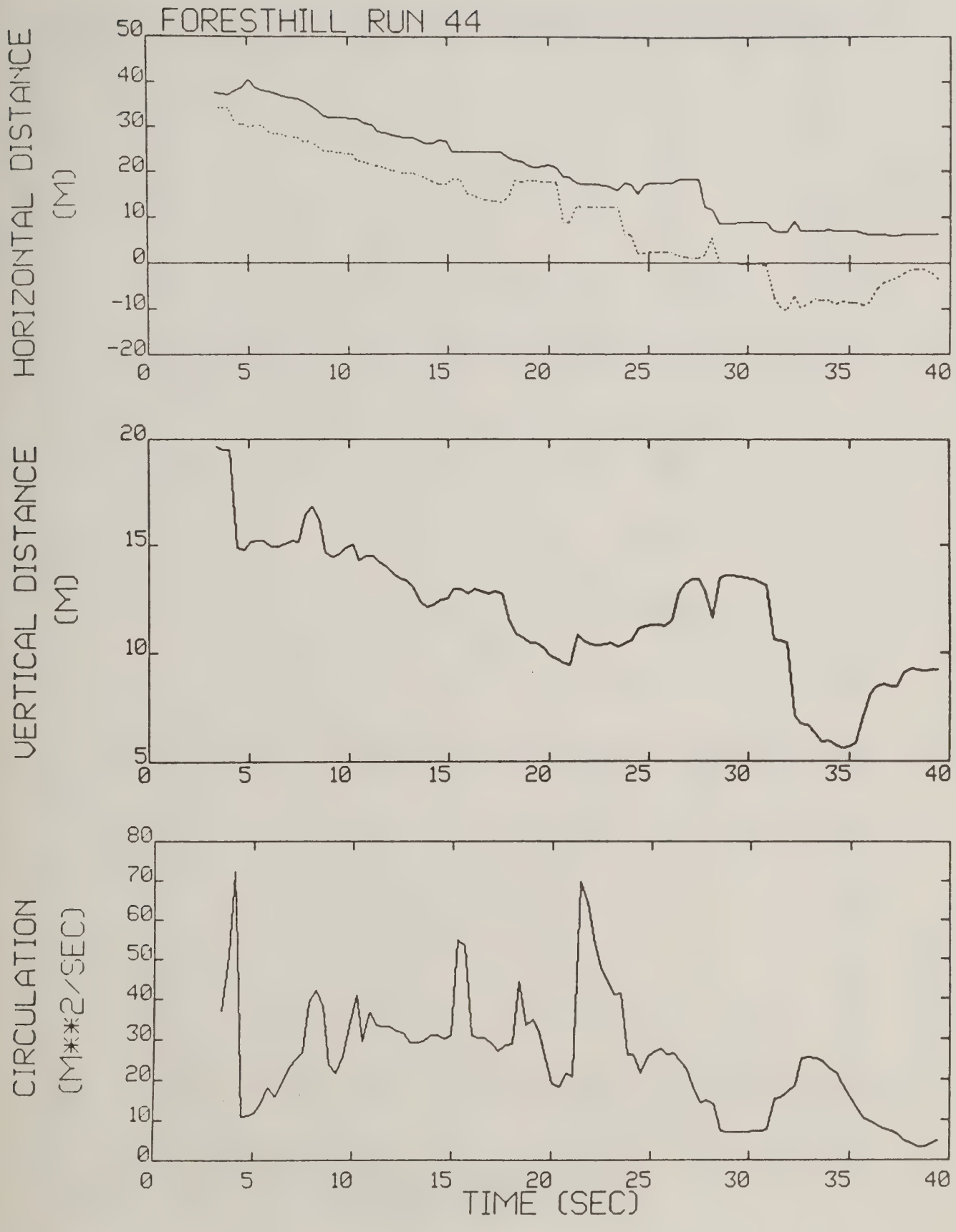

Figure A-30. Foresthill test run 44 generalized algorithm results (*).

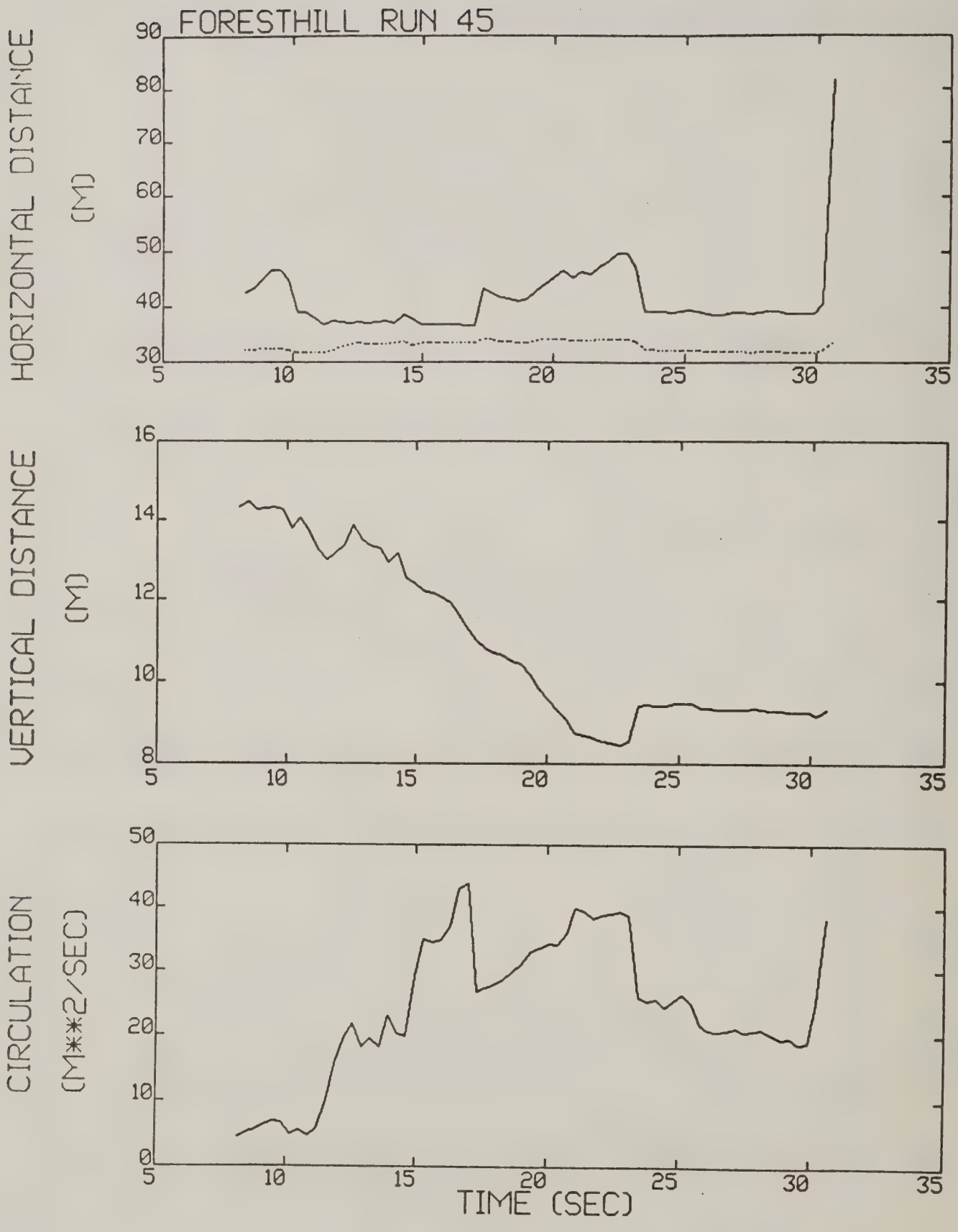

Figure A-31. Foresthill test run 45 generalized algorithm results.

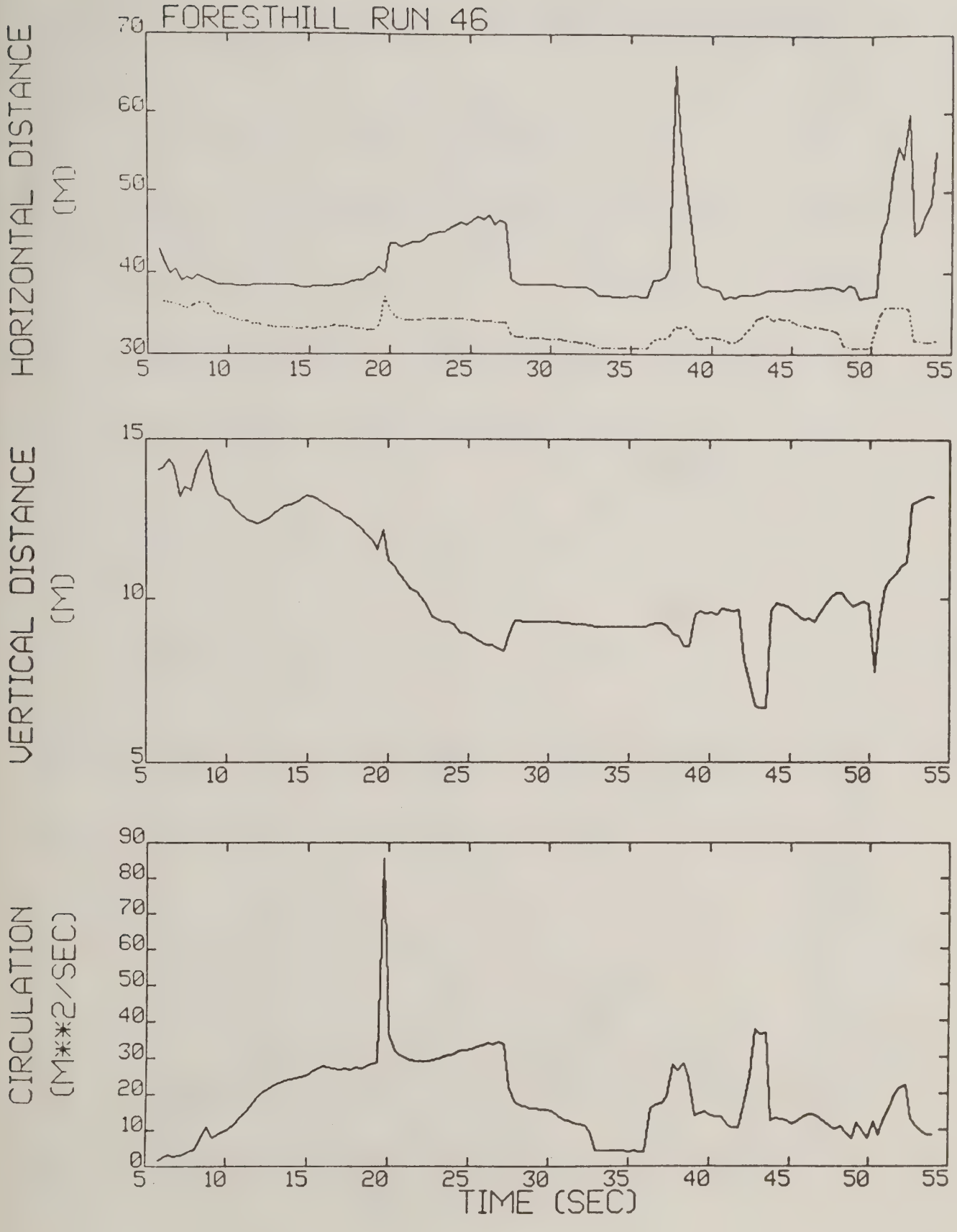

Figure A-32. Foresthill test run 46 generalized algorithm results.

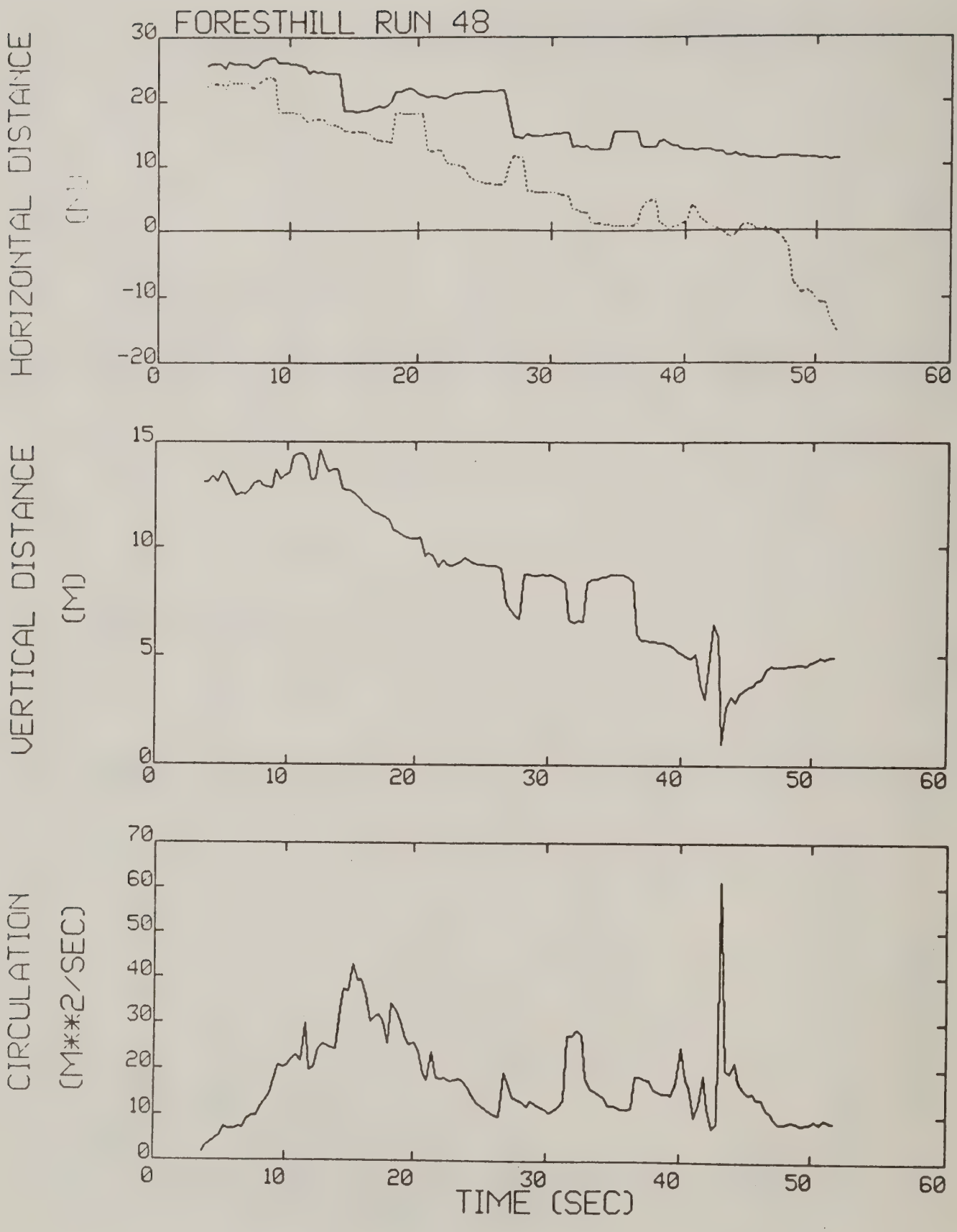

Figure A-33. Foresthill test run 48 generalized algorithm results (*).

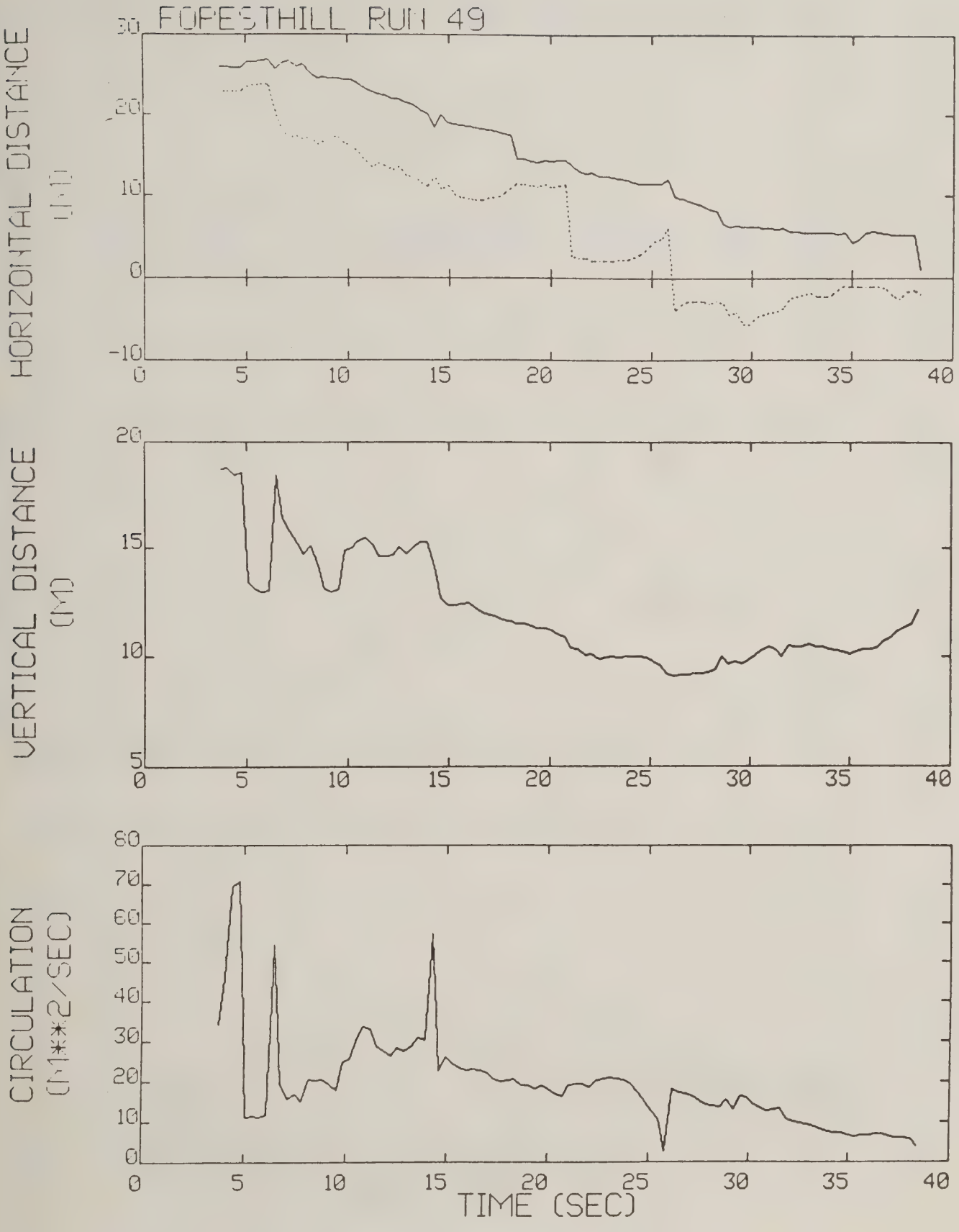

Figure A-34. Foresthill test run 49 generalized algorithm results (*).

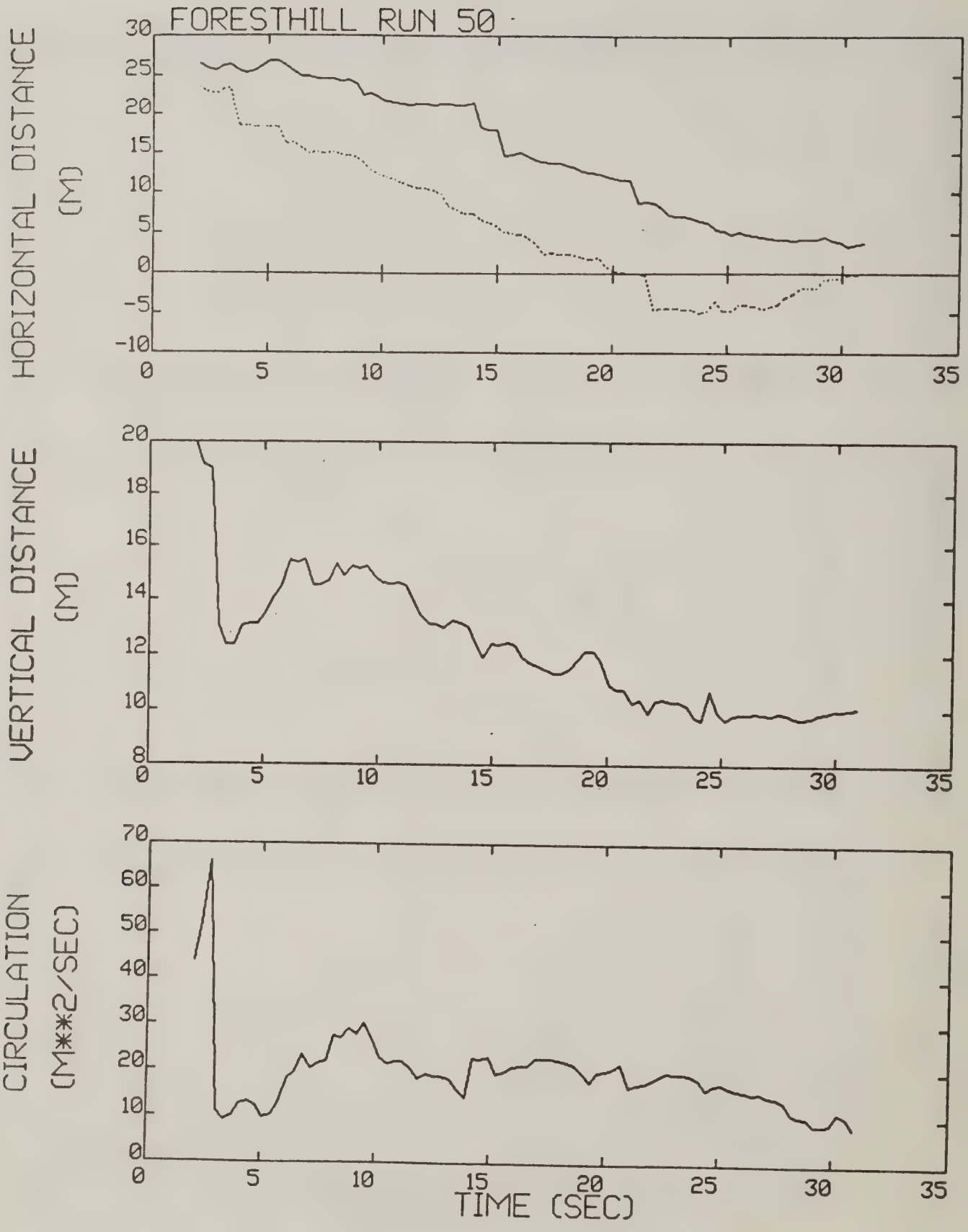

Figure A-35. Foresthill test run 50 generalized algorithm results (*).

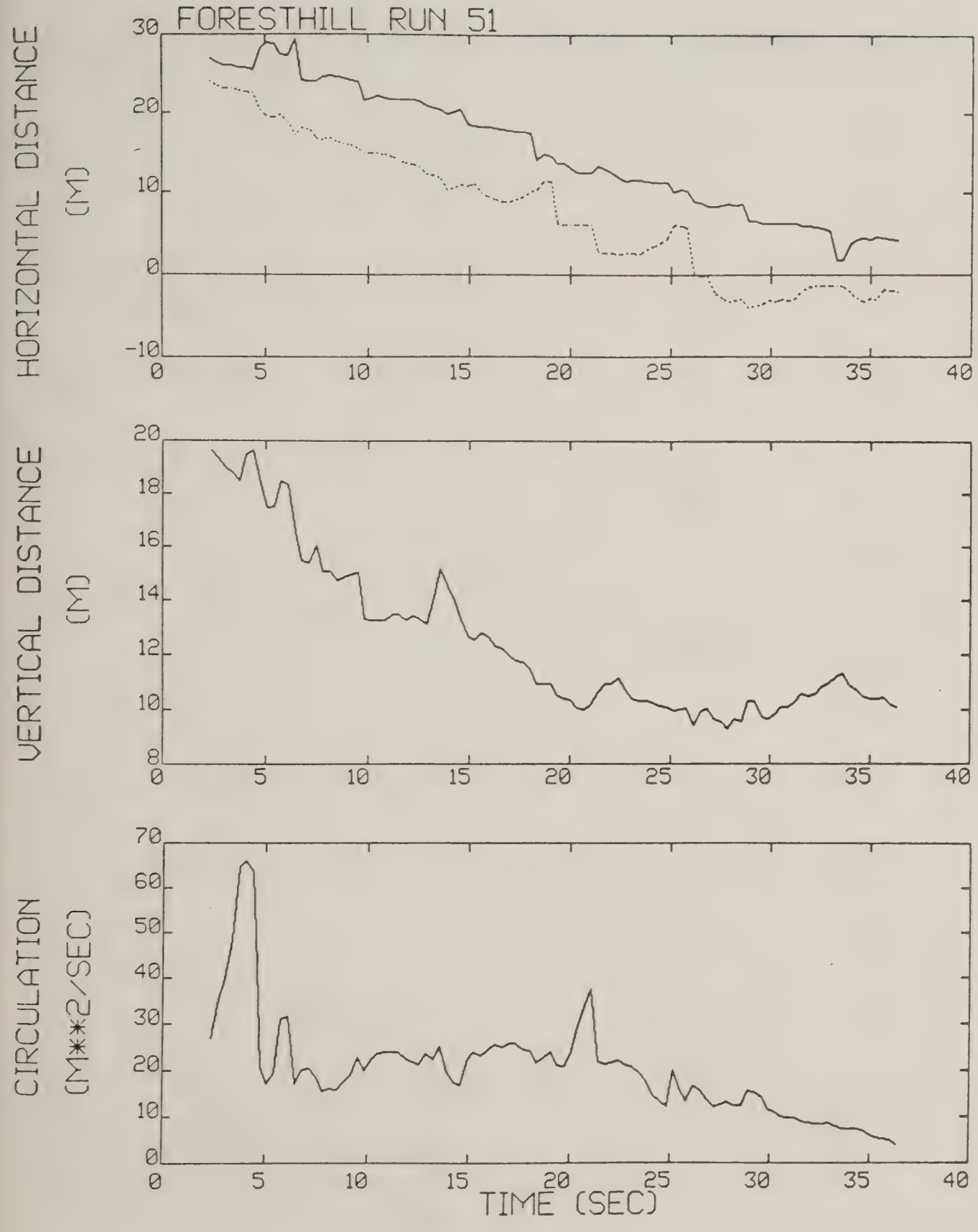

Figure A-36. Foresthill test run 51 generalized algorithm results (*).

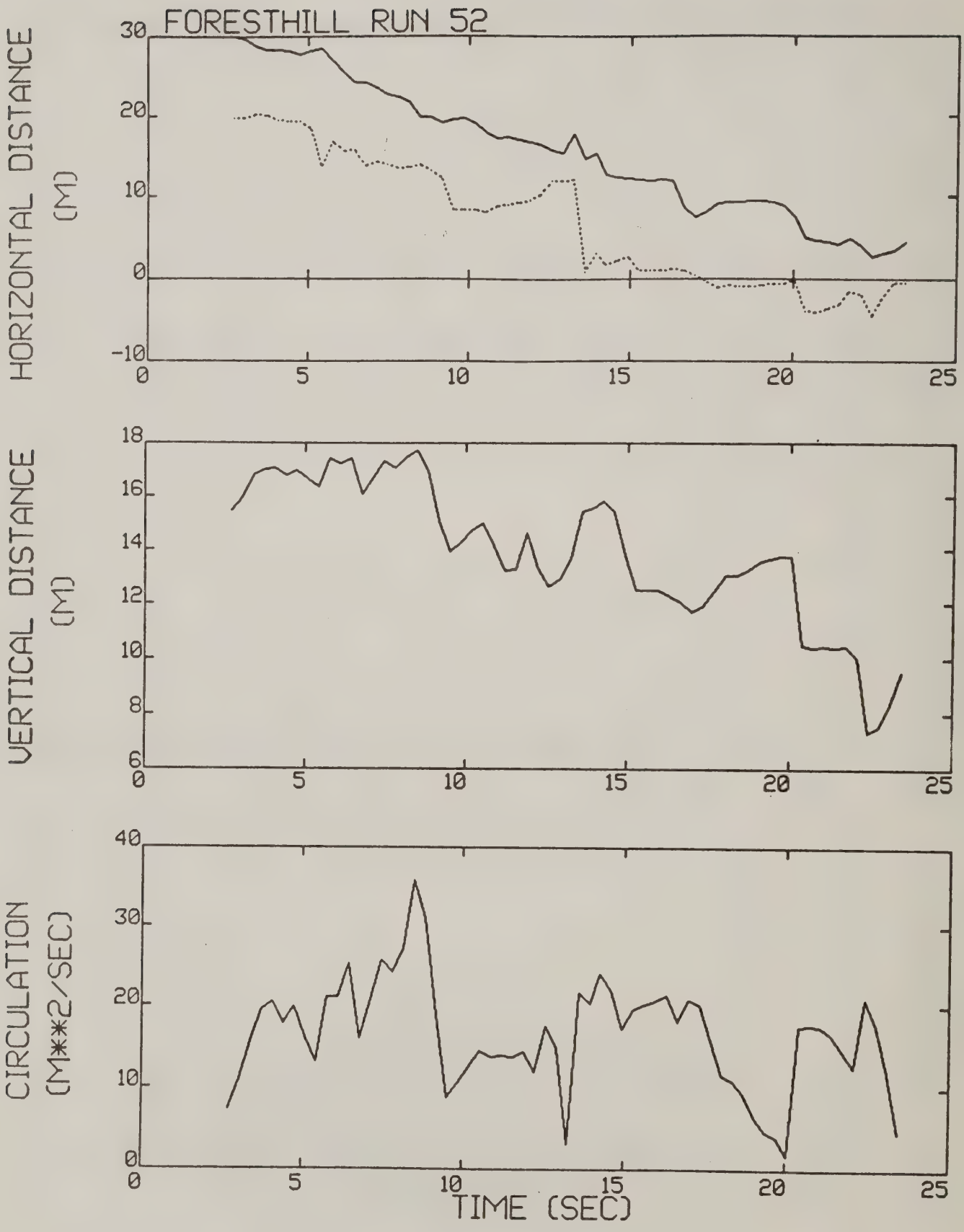

Figure A-37. Foresthill test run 52 generalized algorithm results.

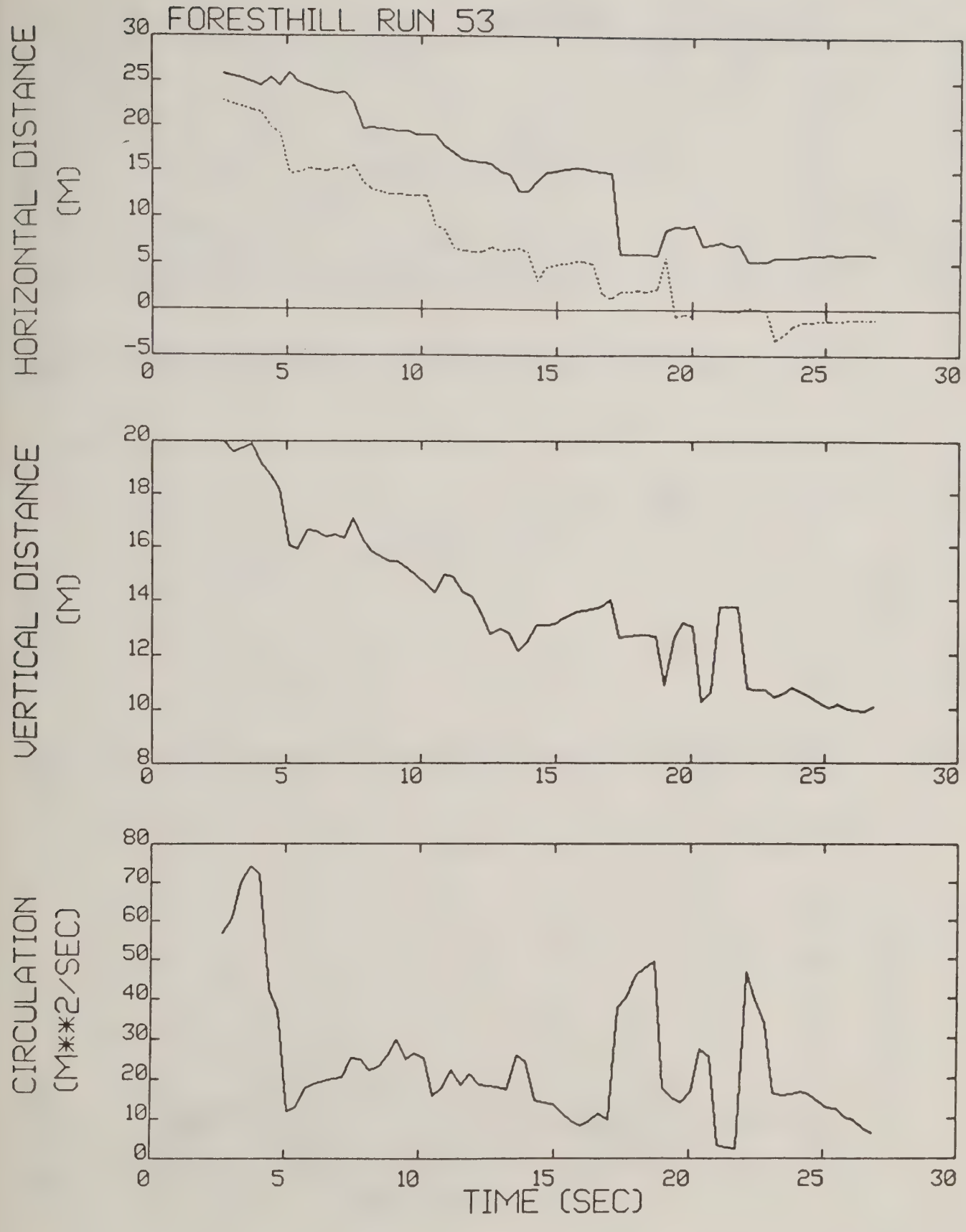

Figure A-38. Foresthill test run 53 generalized algorithm results (*).

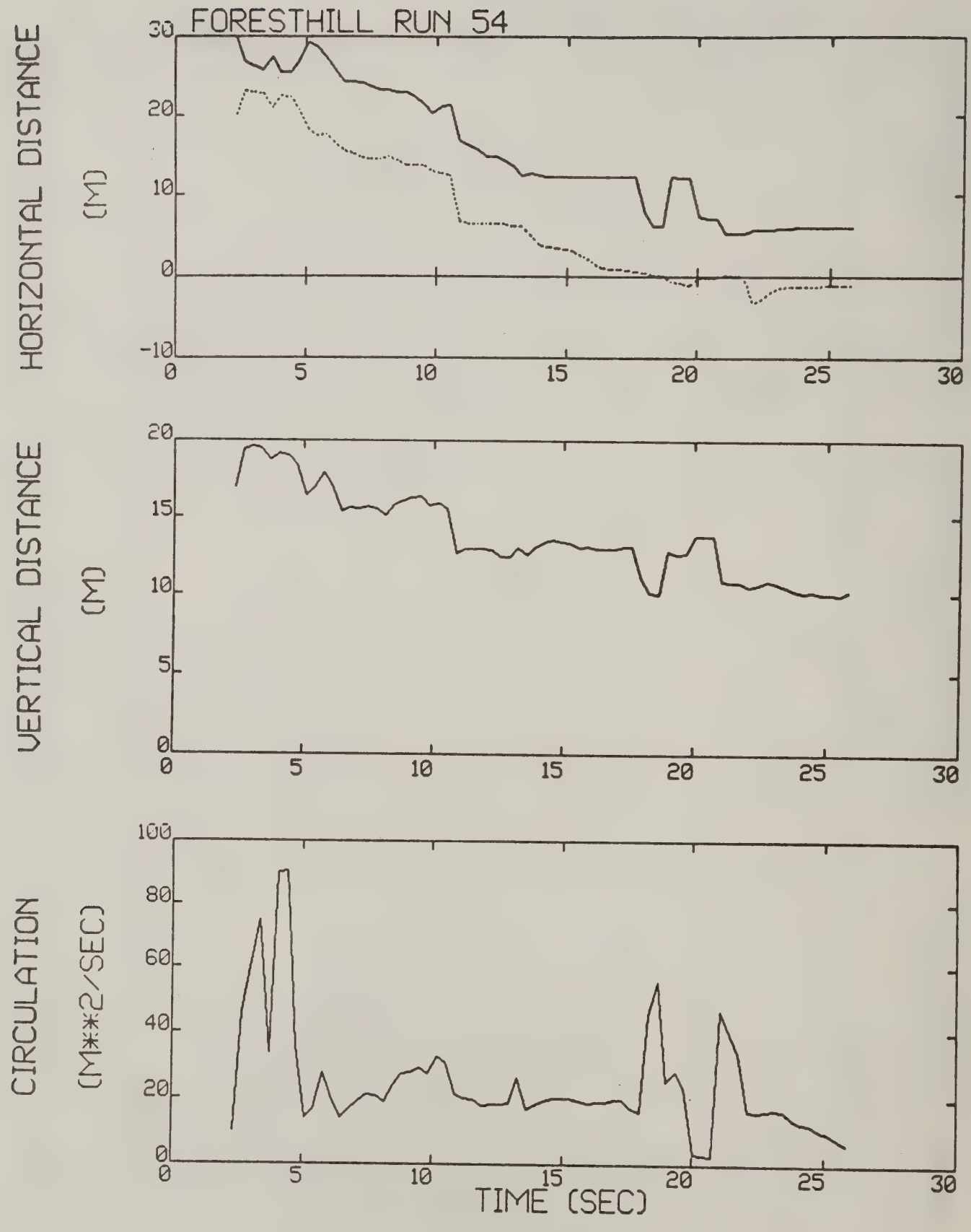

Figure A-39. Foresthill test run 54 generalized algorithm results (*).

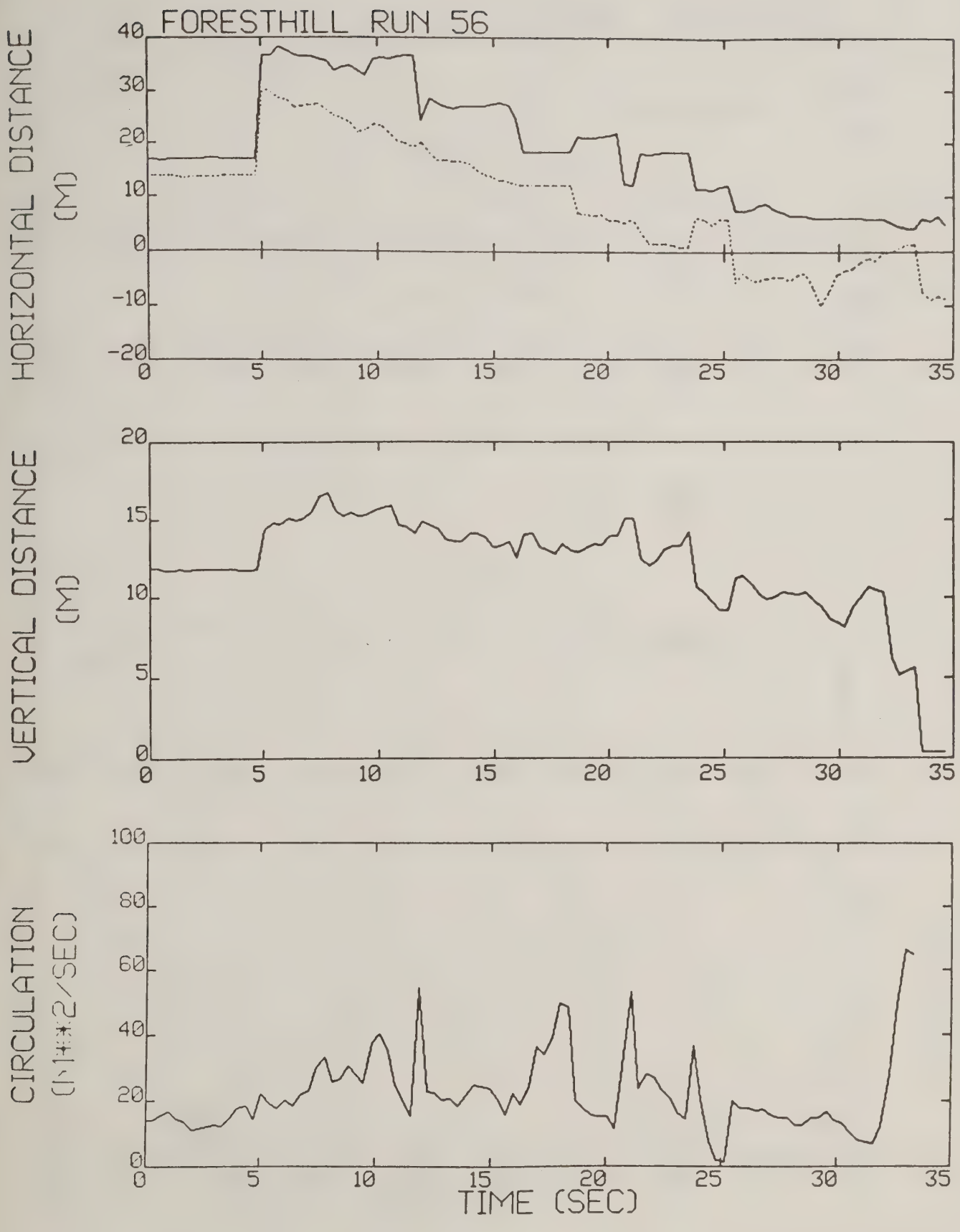

Figure A-40. Foresthill test run 56 generalized algorithm results.

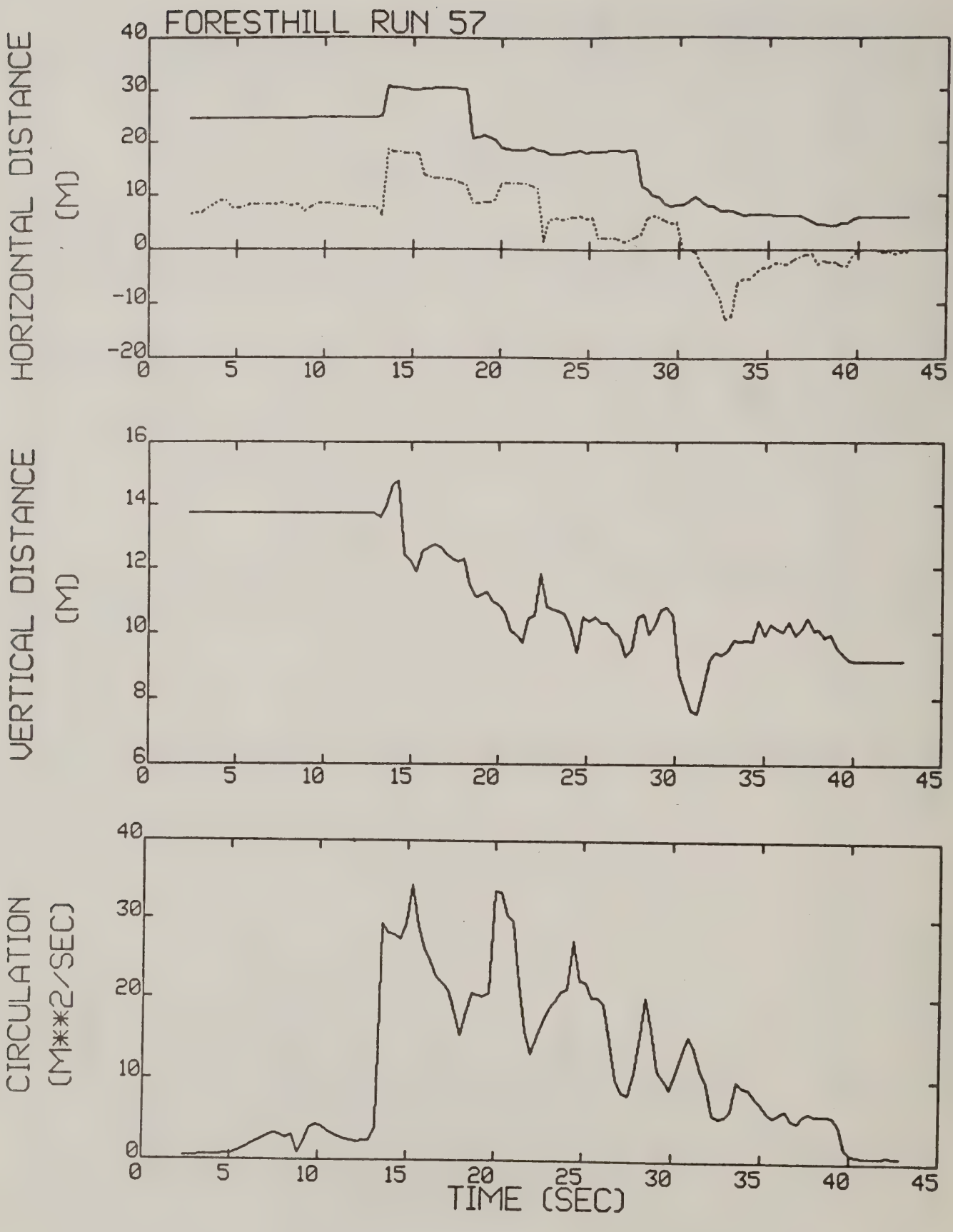

Figure A-41. Foresthill test run 57 generalized algorithm results (*).

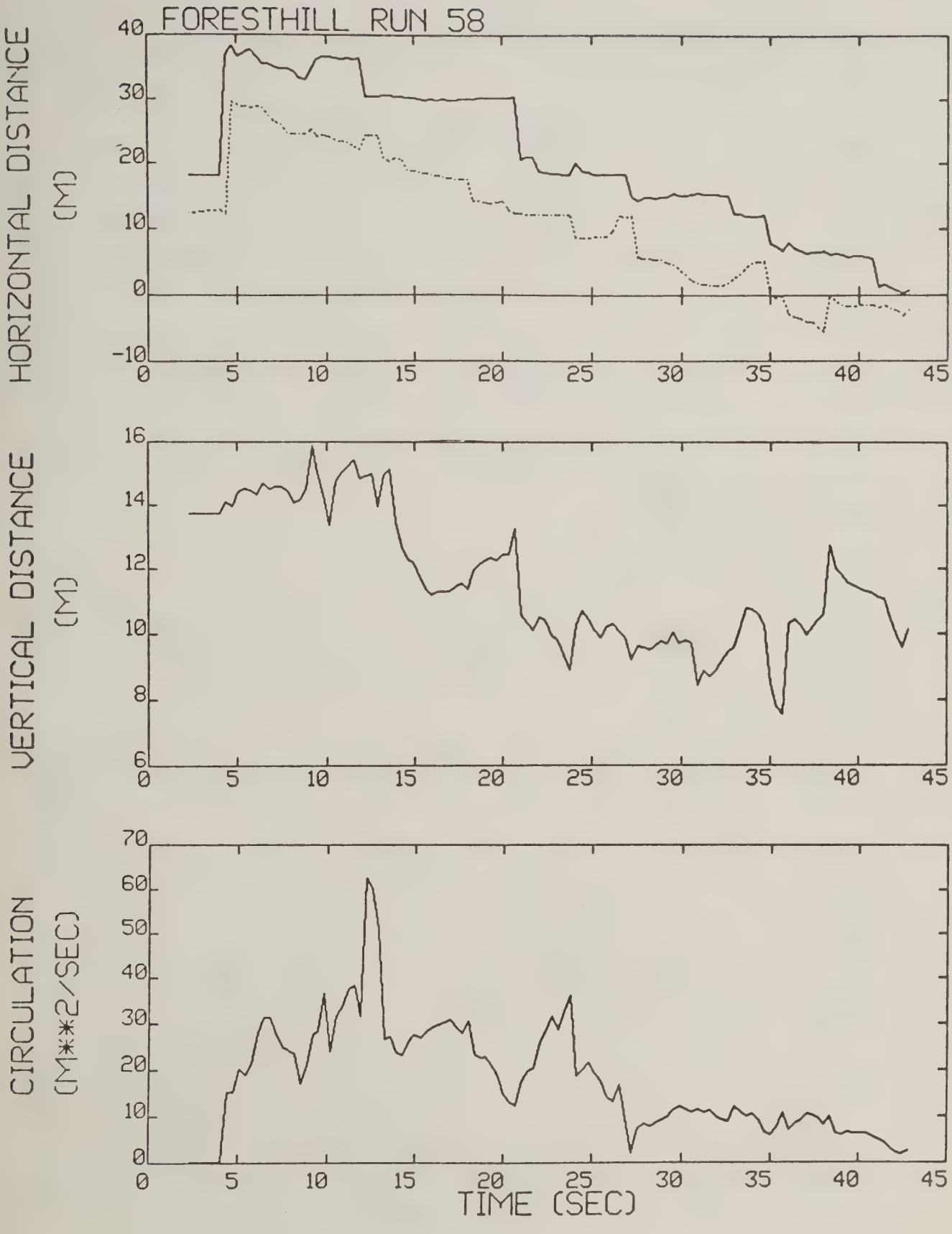

Figure A-42. Foresthill test run 58 generalized algorithm results (*).

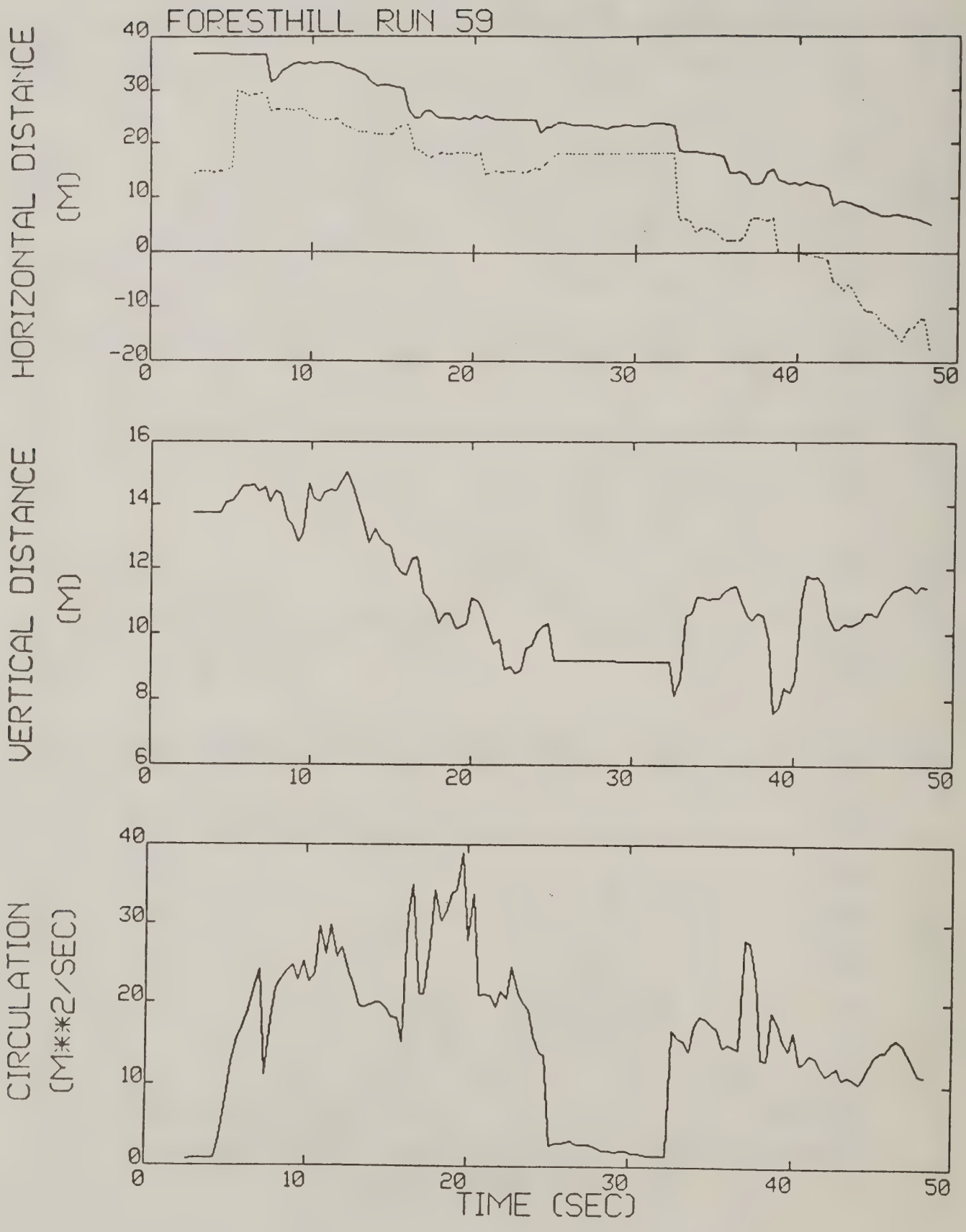

Figure A-43. Foresthill test run 59 generalized algorithm results.

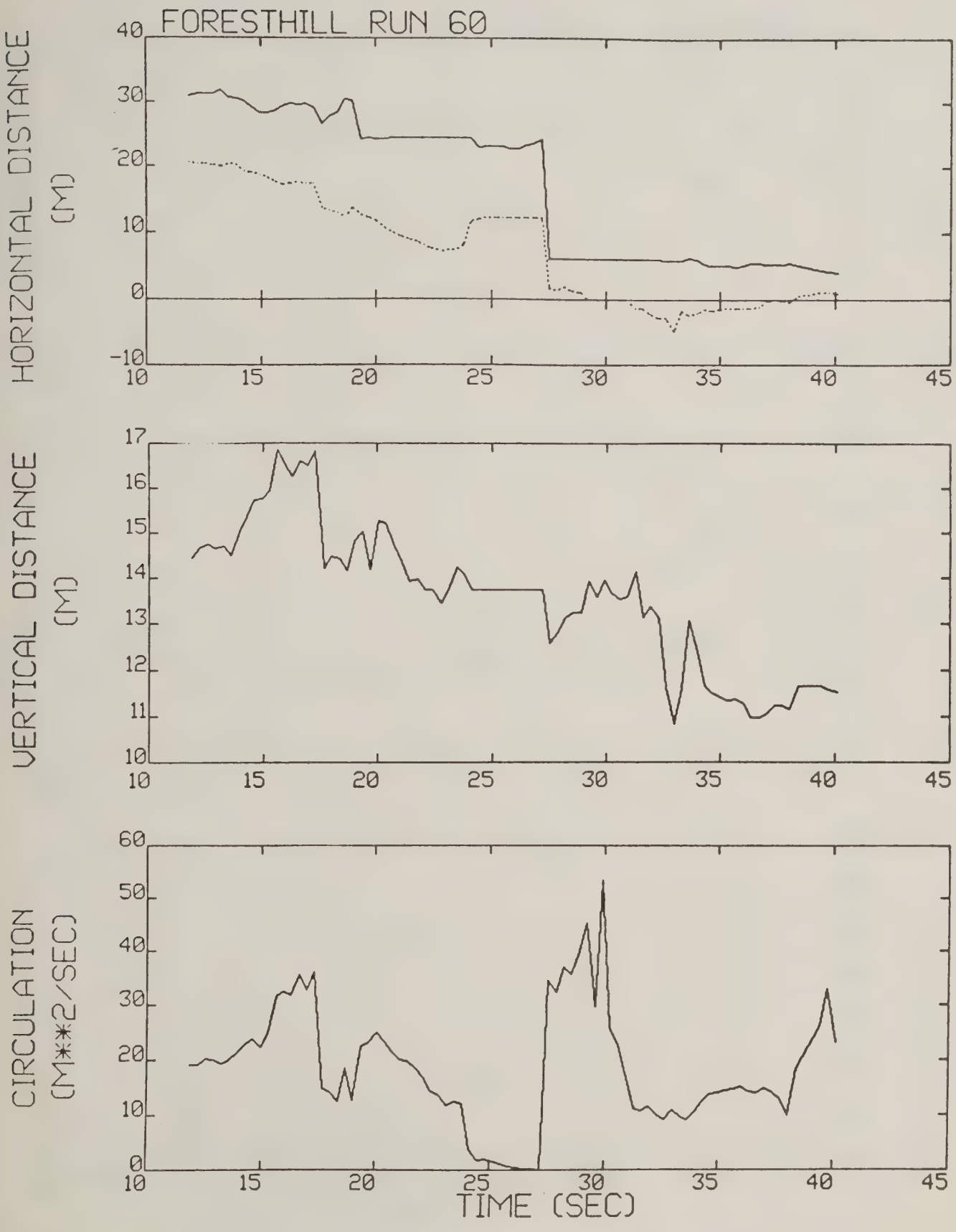

Figure A-44. Foresthill test run 60 generalized algorithm results.

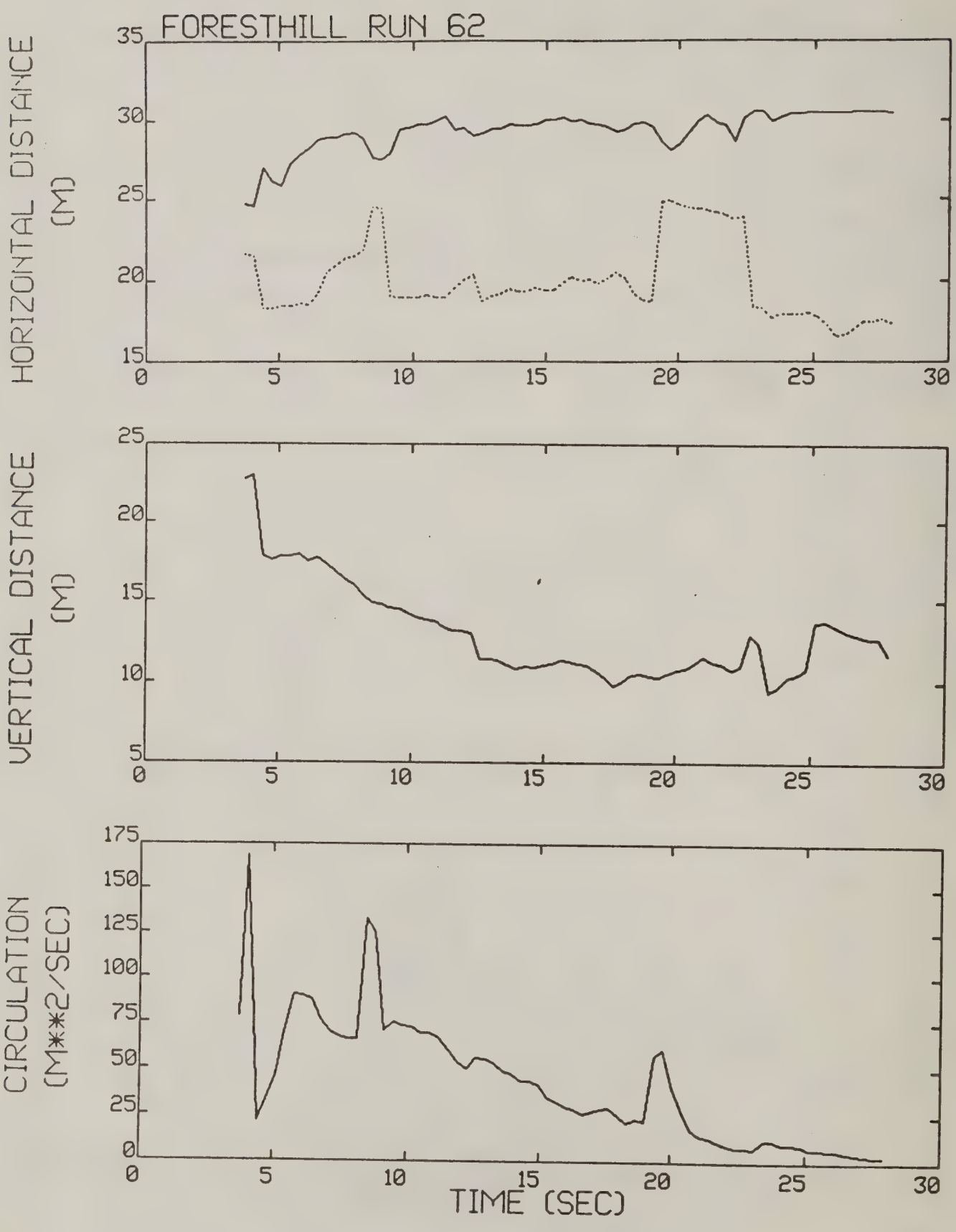

Figure A-45. Foresthill test run 62 generalized algorithm results (*).

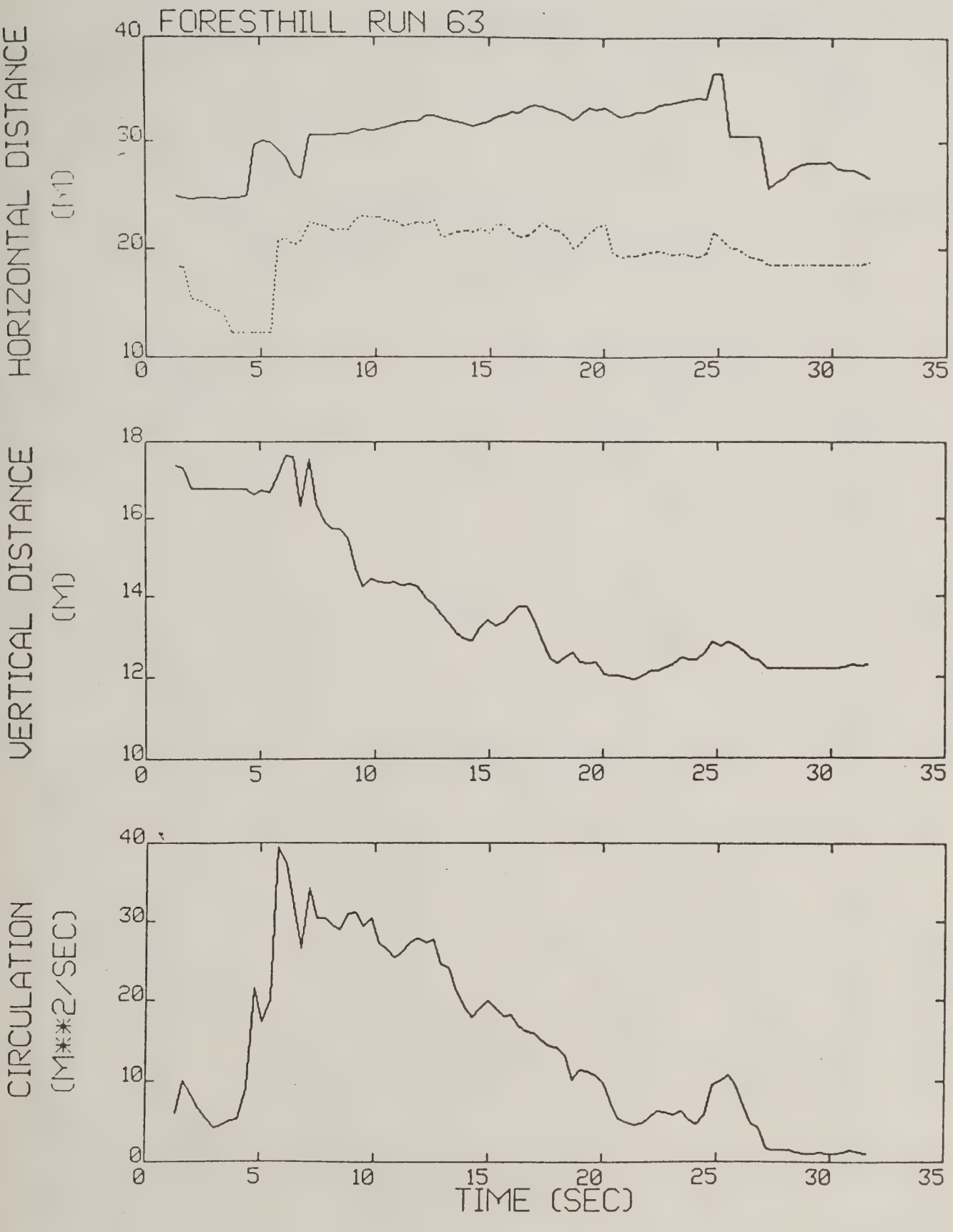

Figure A-46. Foresthill test run 63 generalized algorithm results (*).

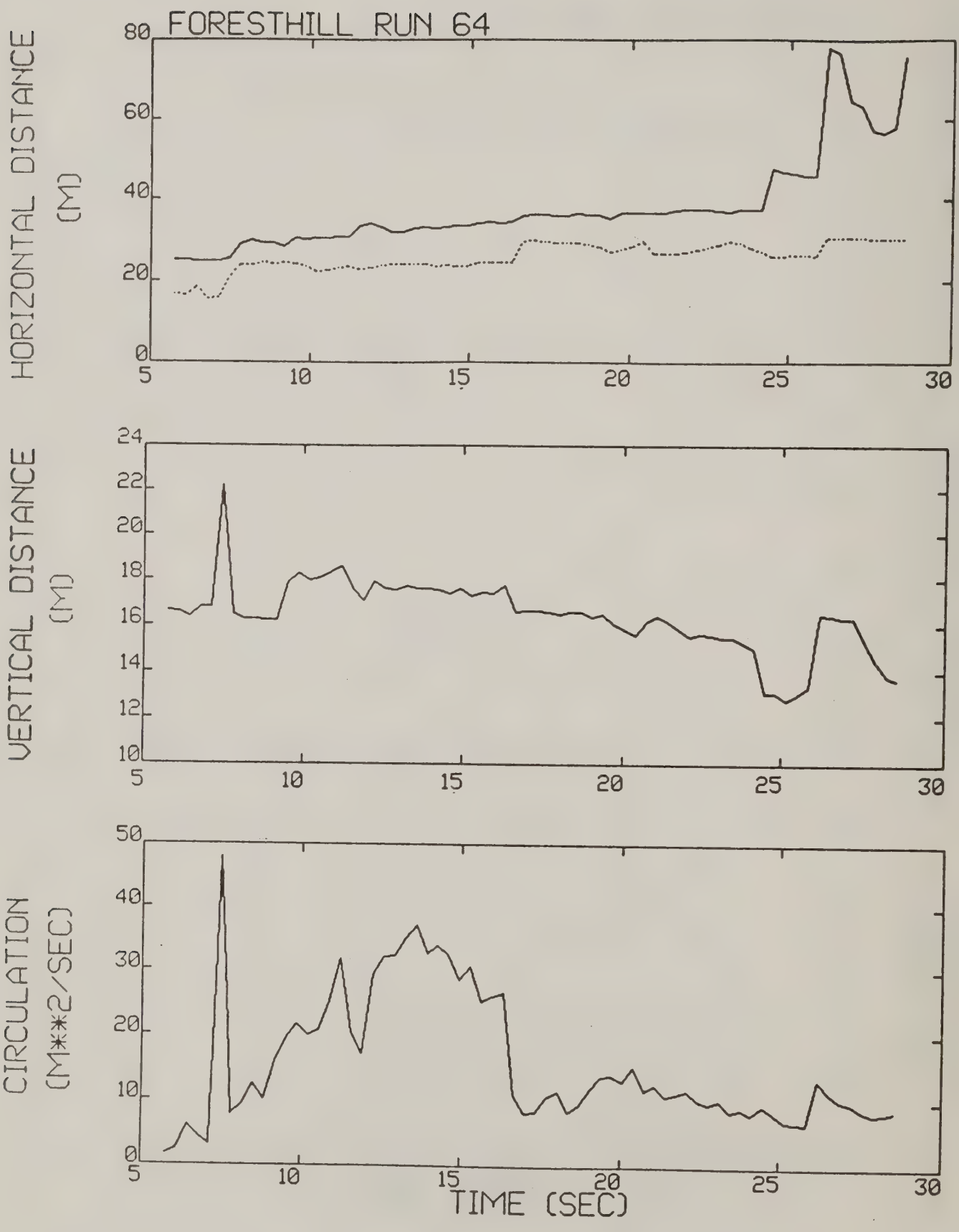

Figure A-47. Foresthill test run 64 generalized algorithm results.

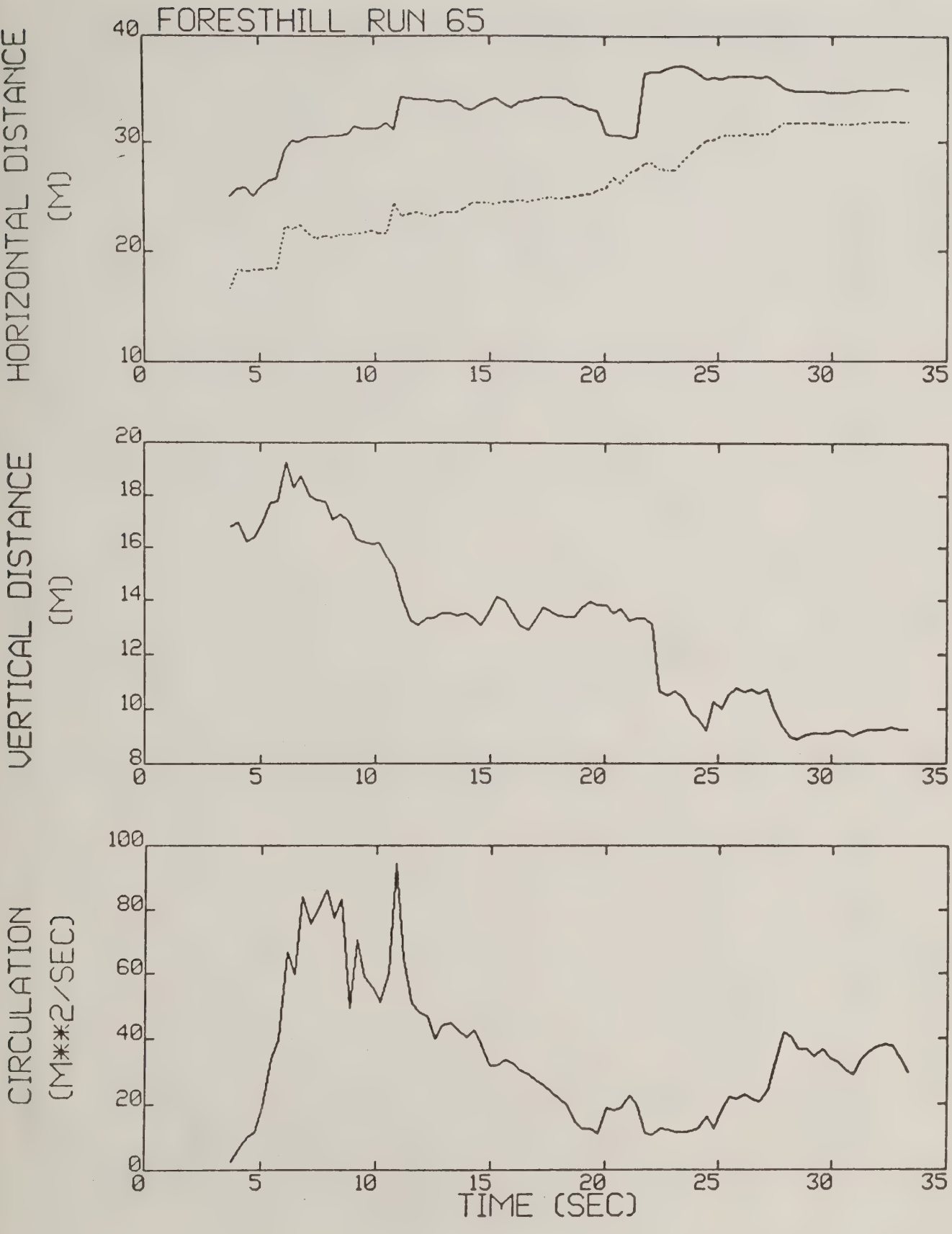

Figure A-48. Foresthill test run 65 generalized algorithm results (*).

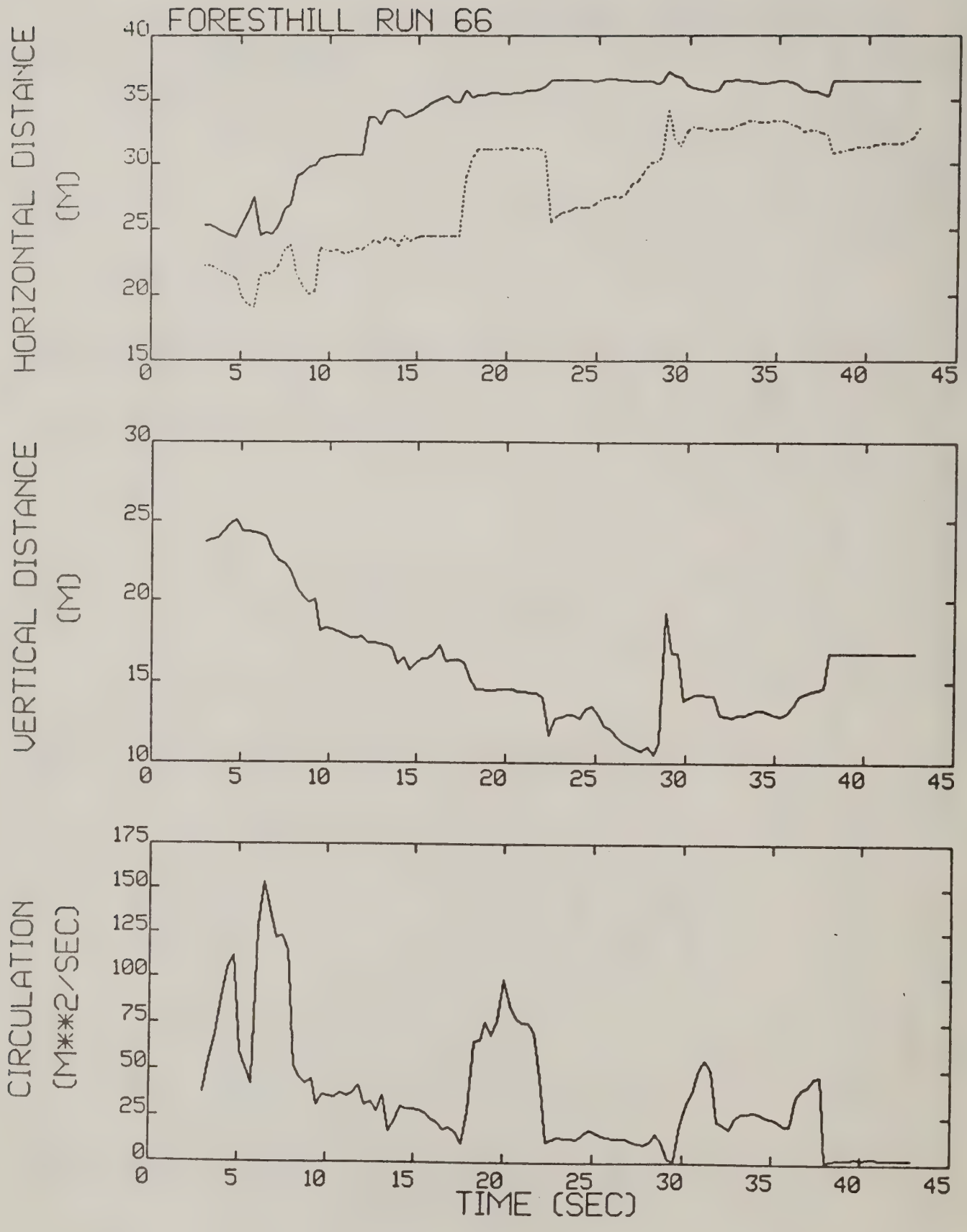

Figure A-49. Foresthill test run 66 generalized algorithm results (*).

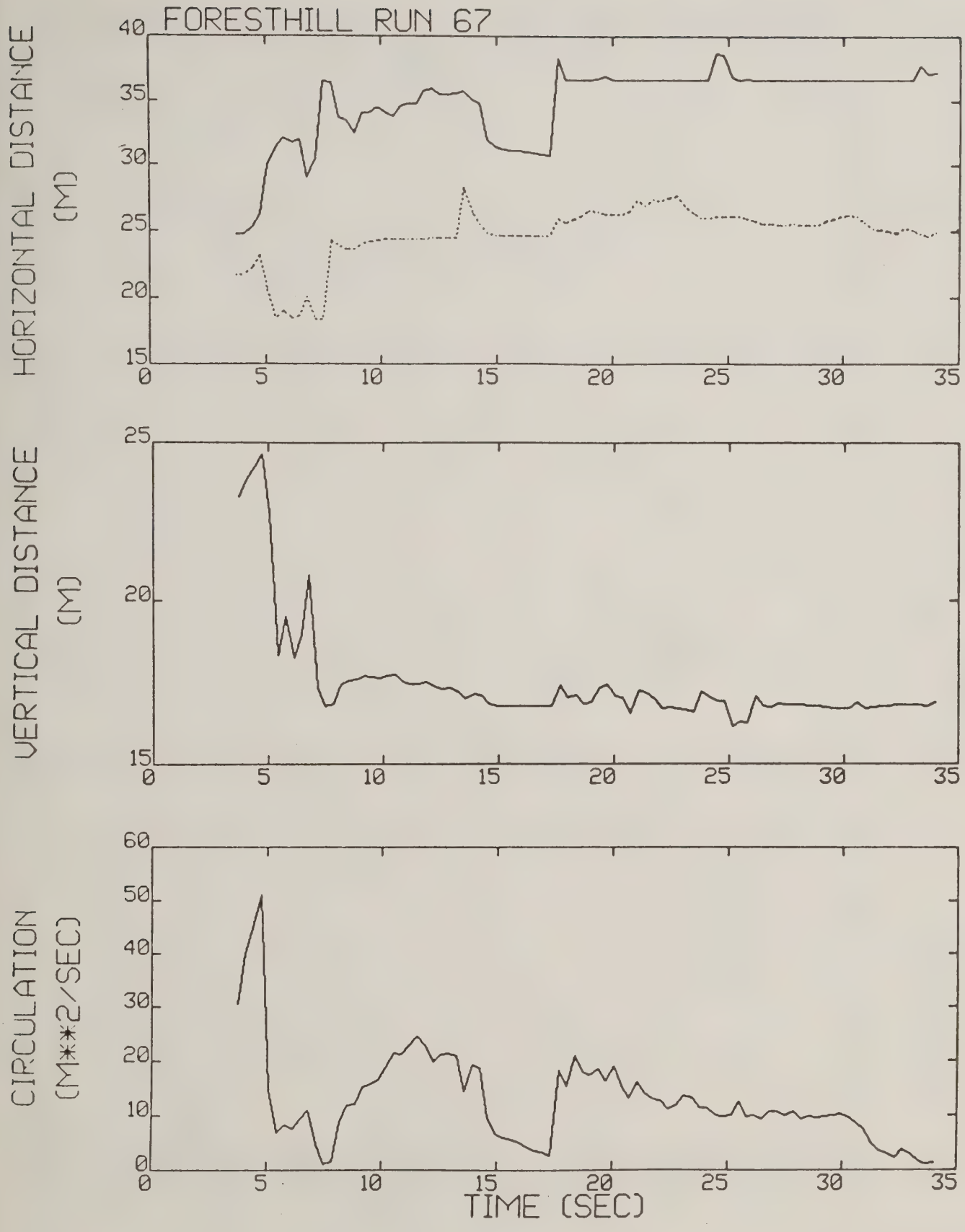

Figure A-50. Foresthill test run 67 generalized algorithm results (*).

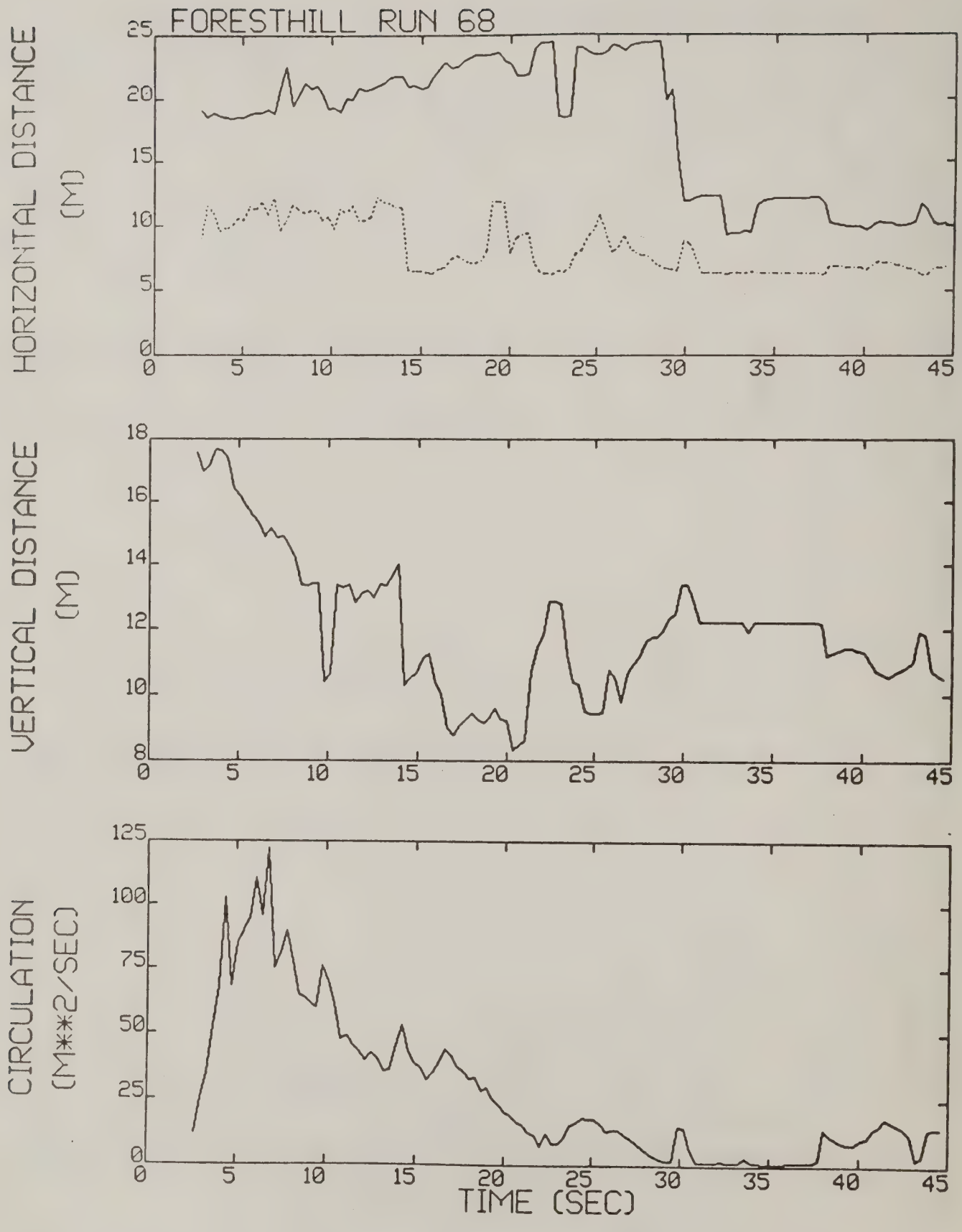

Figure A-51. Foresthill test run 68 generalized algorithm results (*).

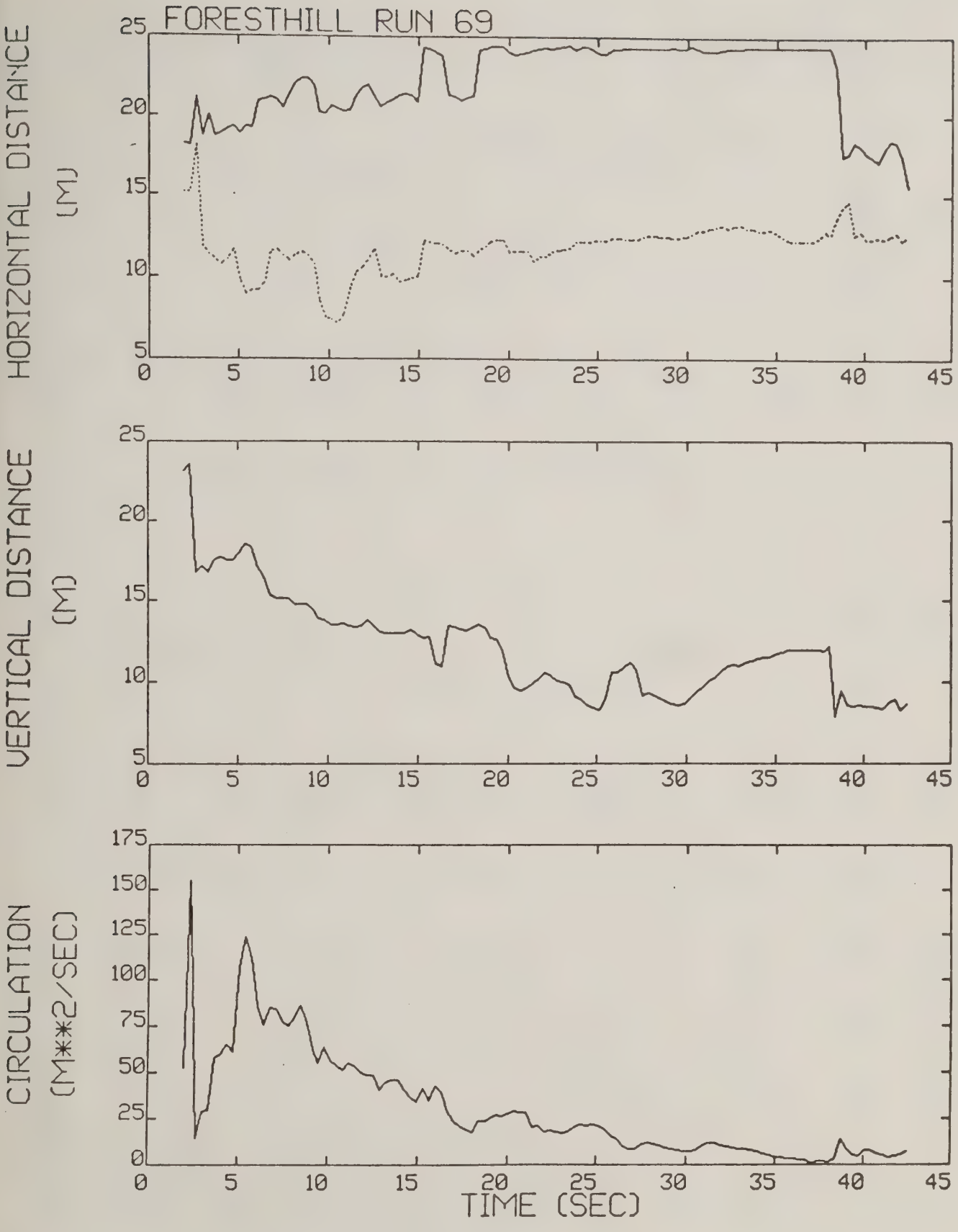

Figure A-52. Foresthill test run 69 generalized algorithm results (*).

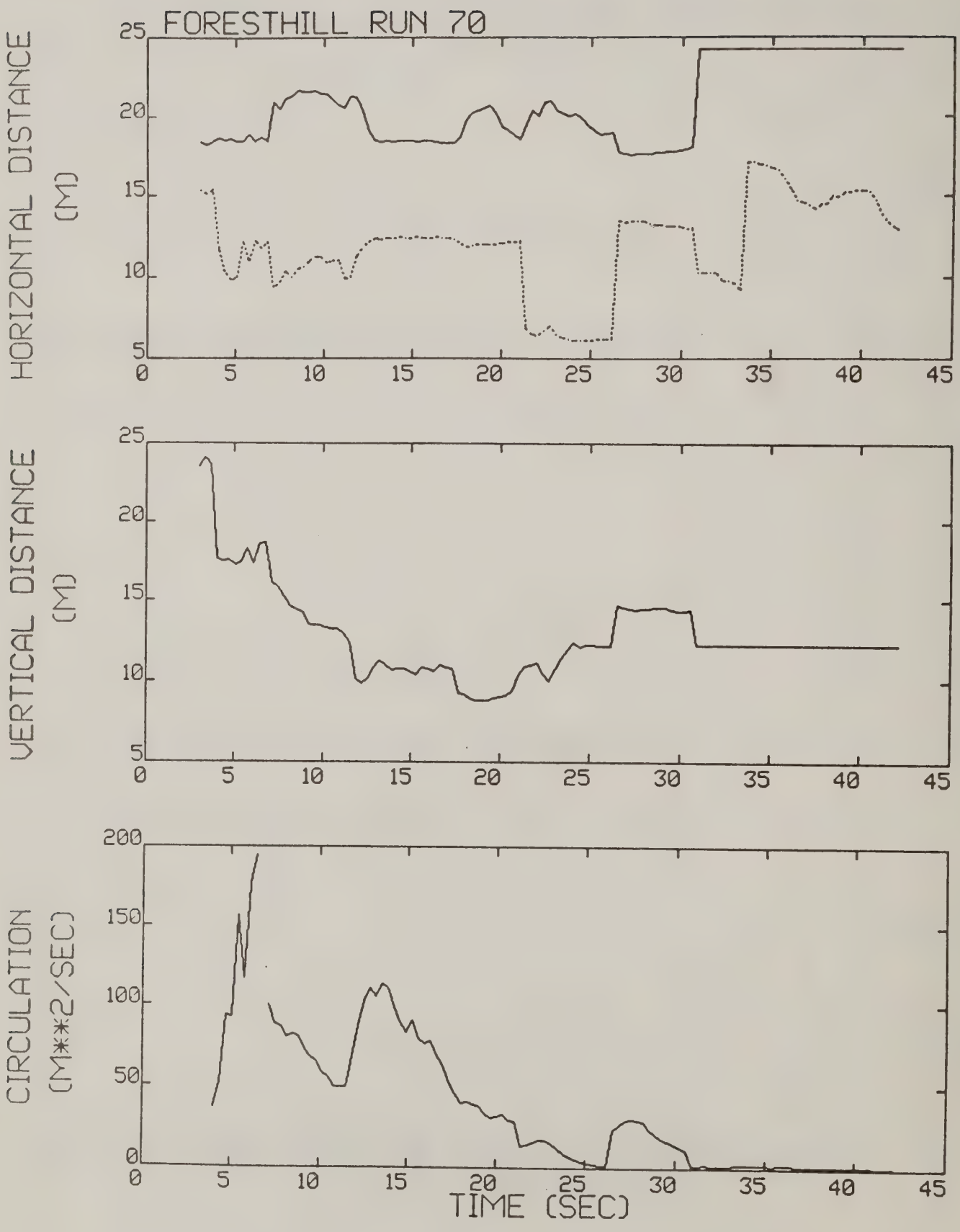

Figure A-53. Foresthill test run 70 generalized algorithm results (*).

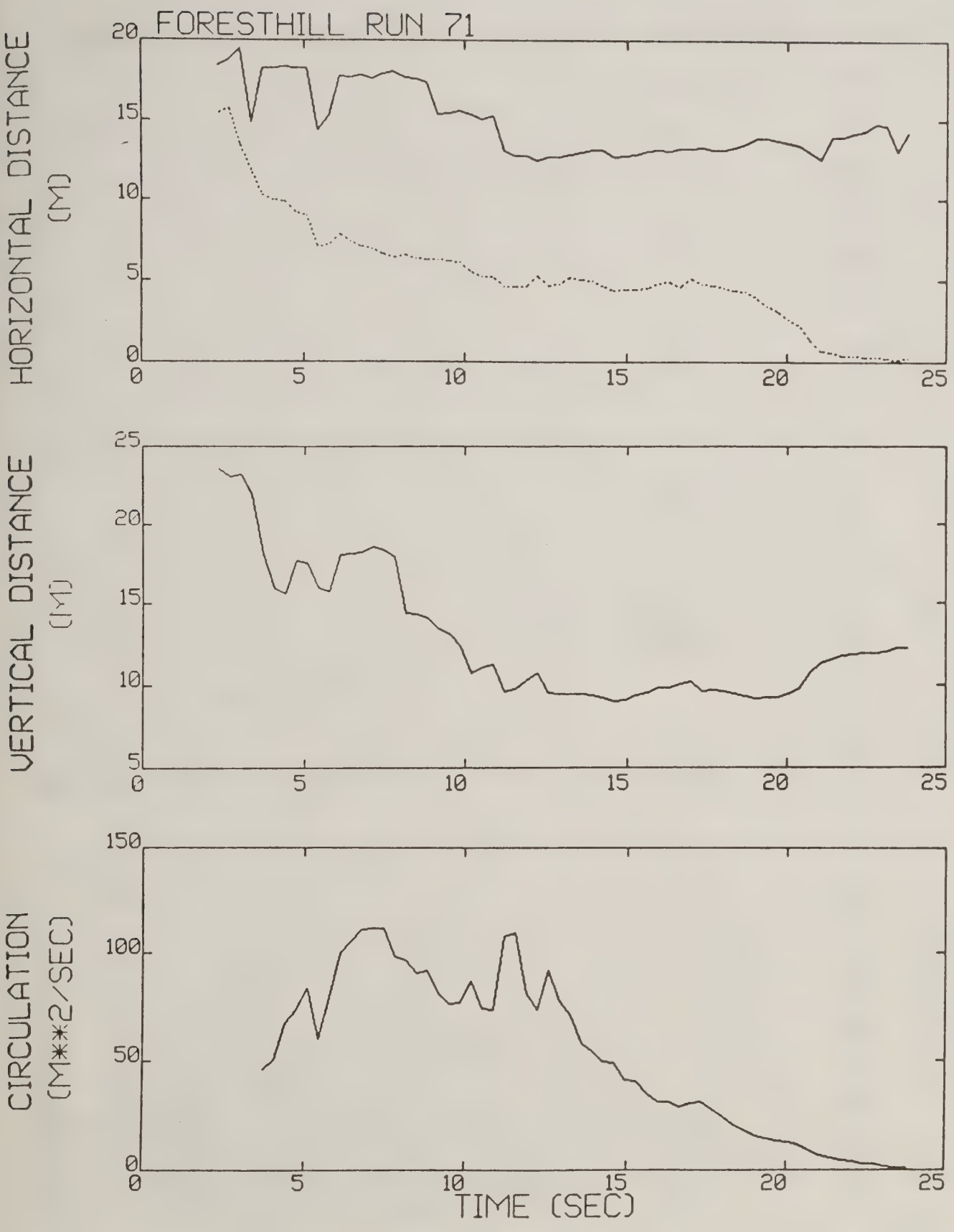

Figure A-54. Foresthill test run 71 generalized algorithm results (*).

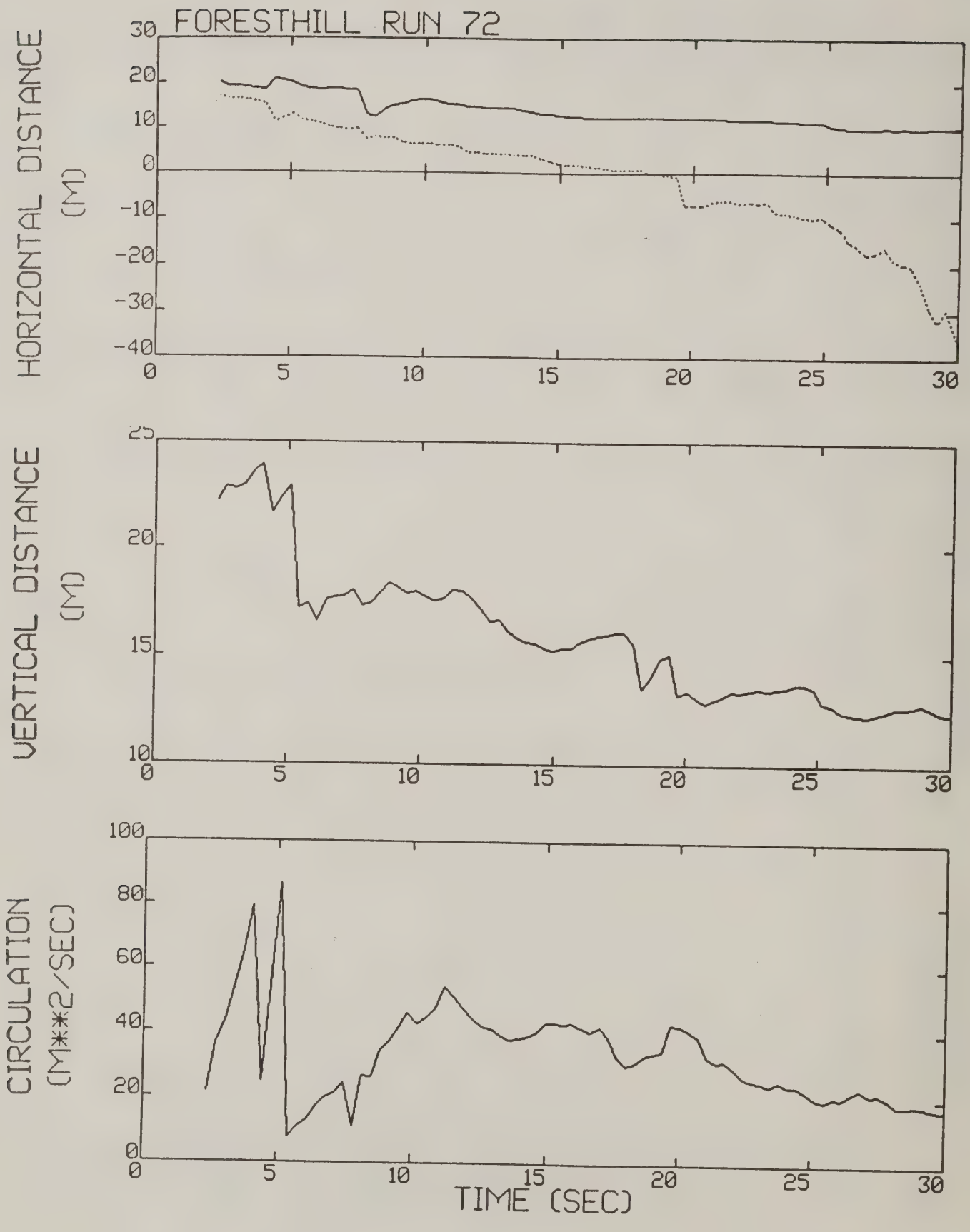

Figure A-55. Foresthill test run 72 generalized algorithm results.

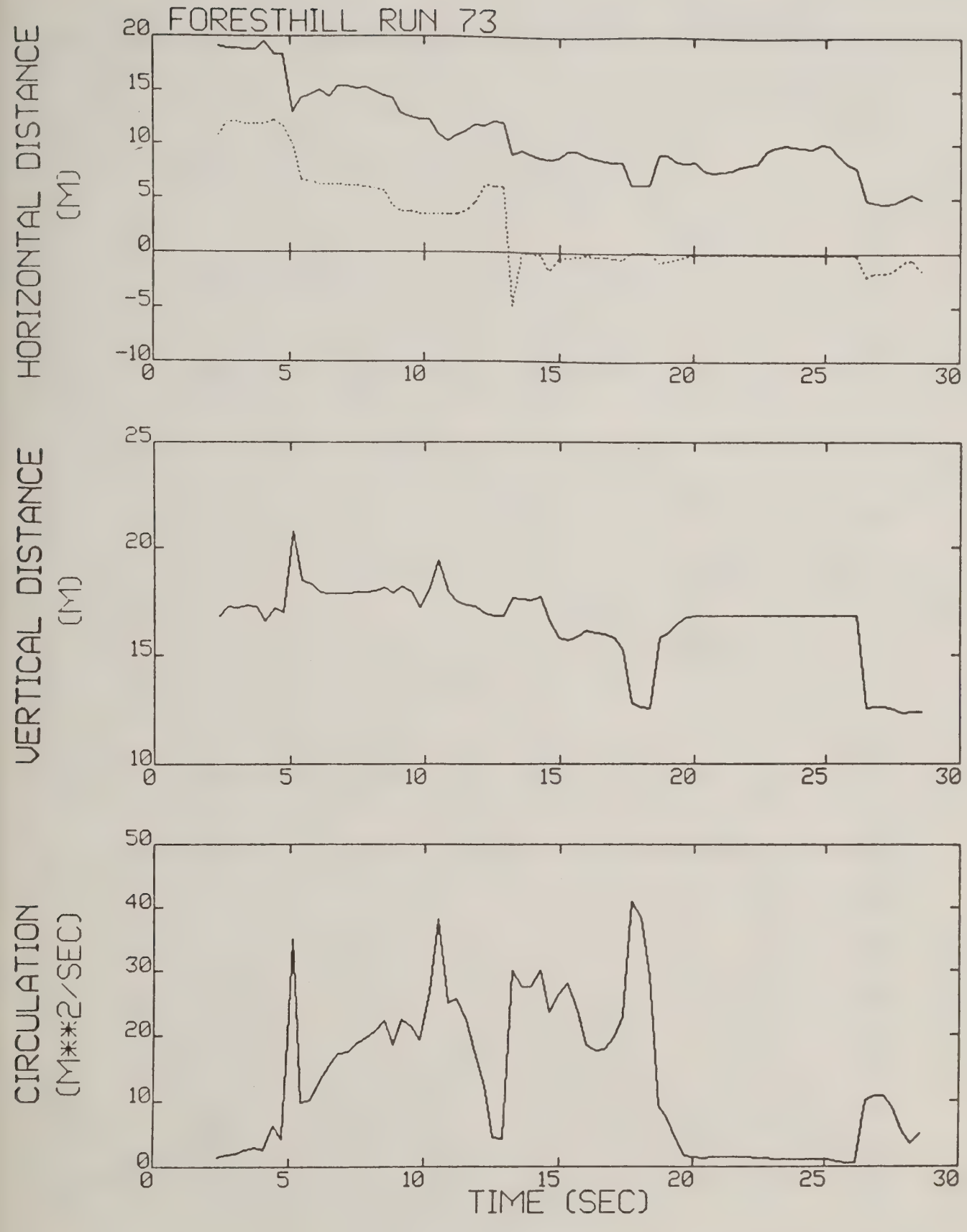

Figure A-56. Foresthill test run 73 generalized algorithm results.

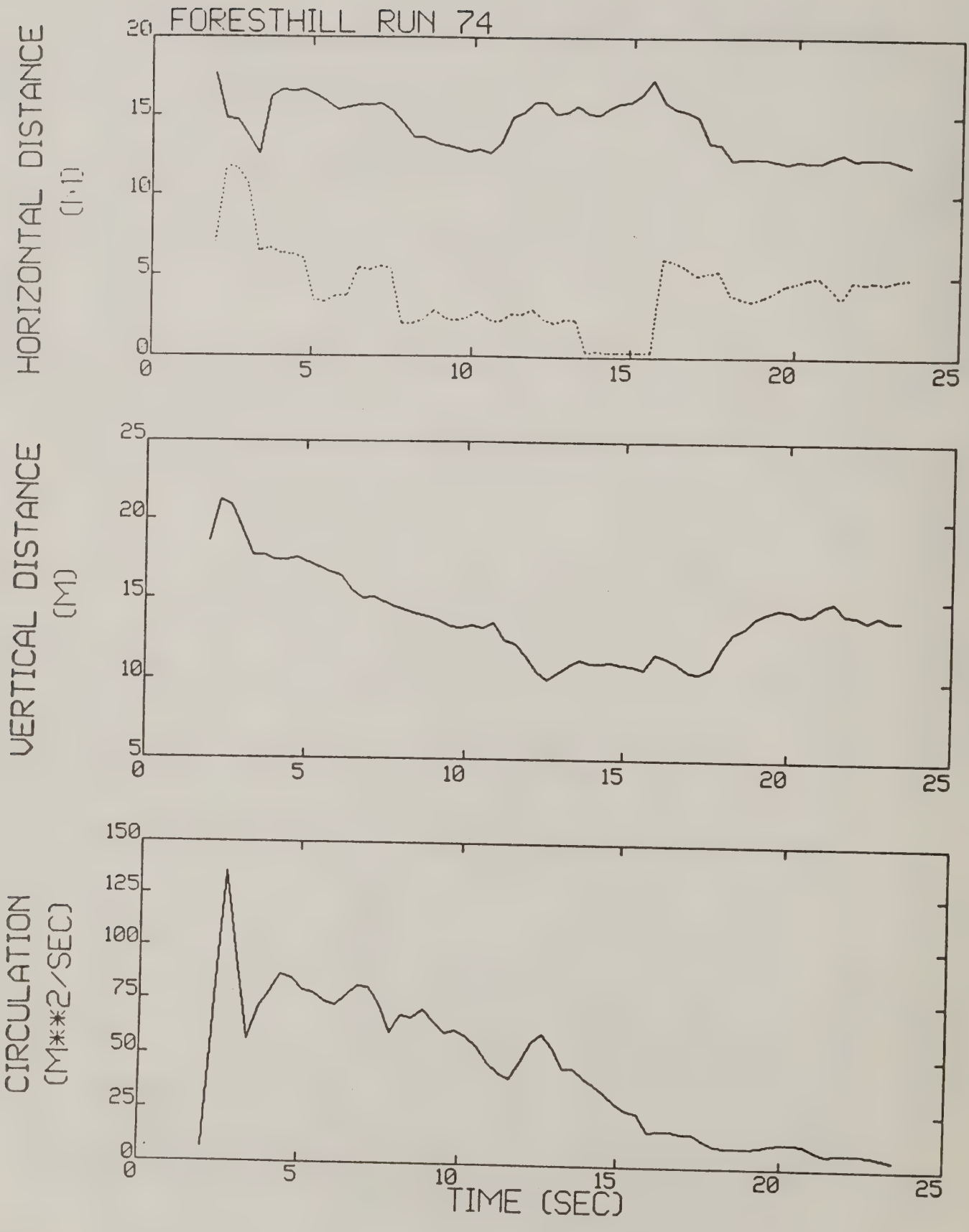

Figure A-57. Foresthill test run 74 generalized algorithm results (*).

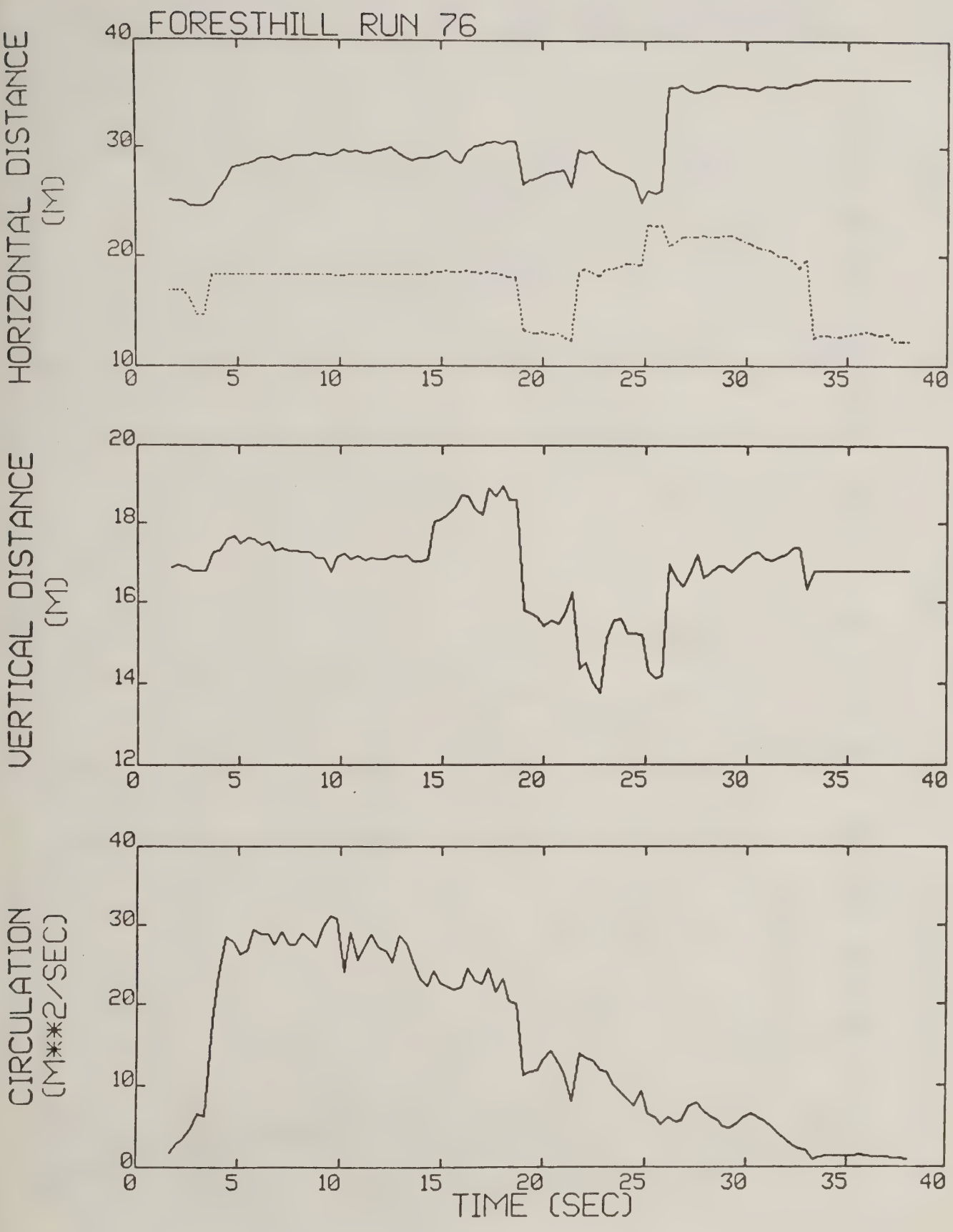

Figure A-58. Foresthill test run 76 generalized algorithm results (*).

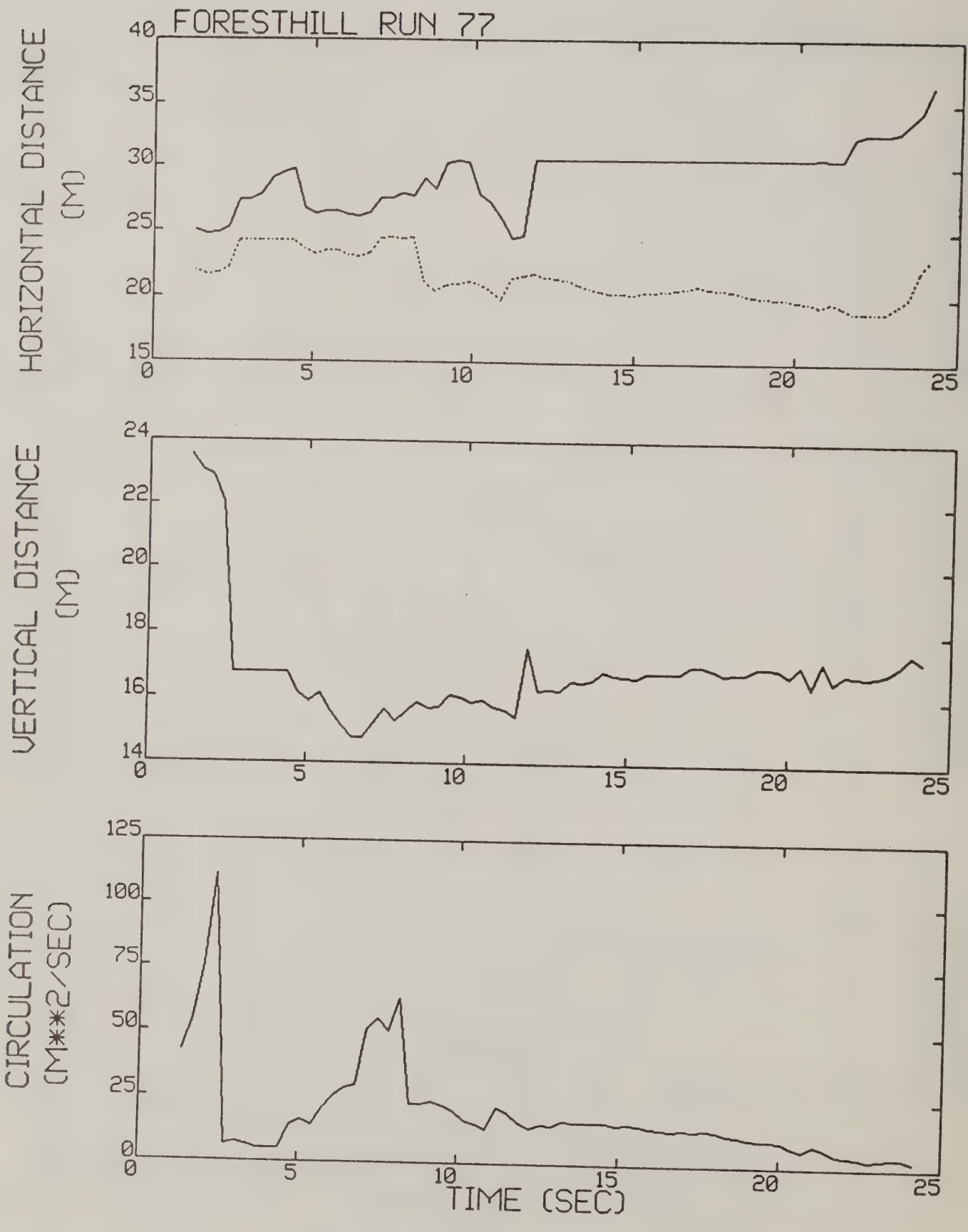

Figure A-59. Foresthill test run 77 generalized algorithm results.

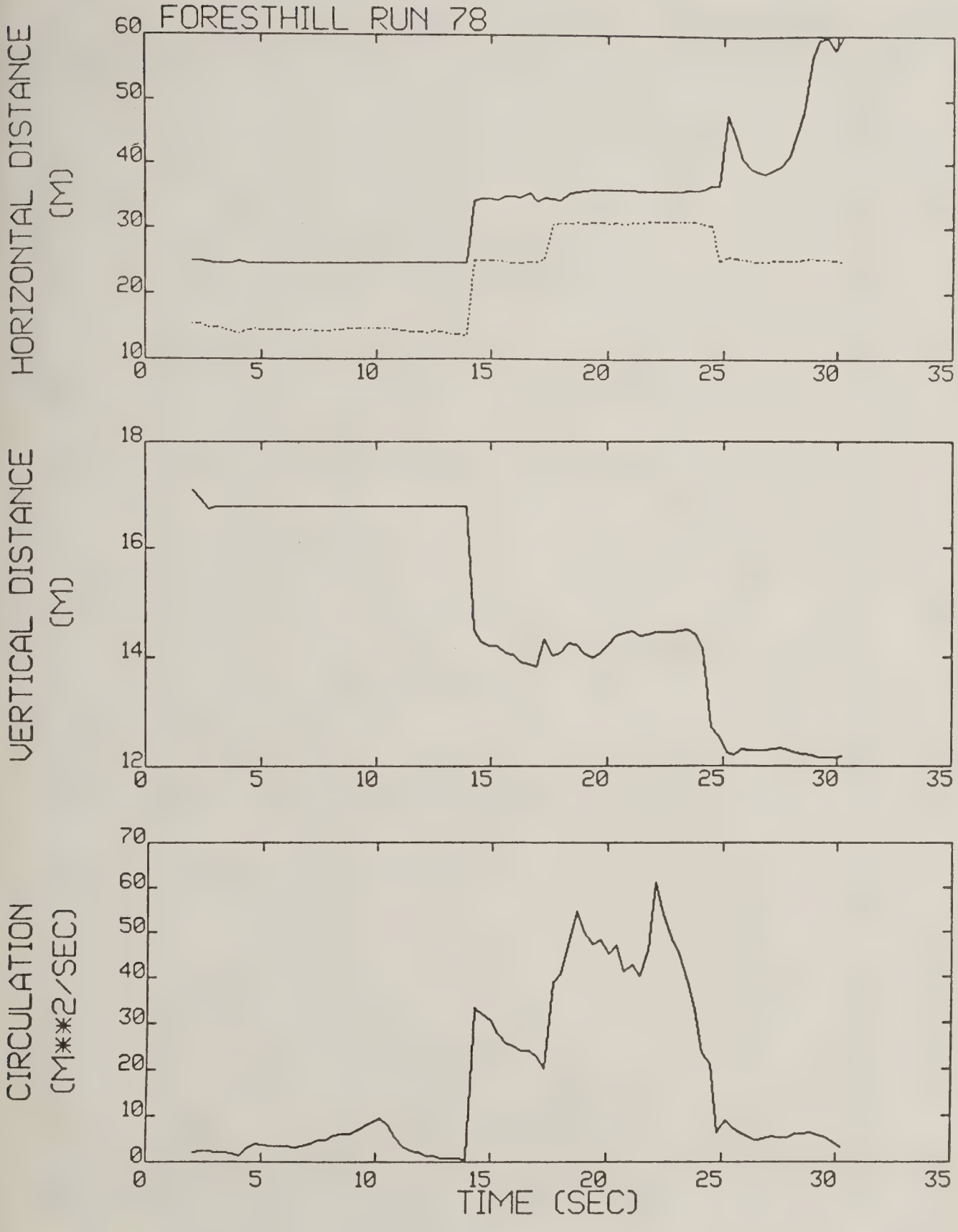

Figure A-60. Foresthill test run 78 generalized algorithm results.

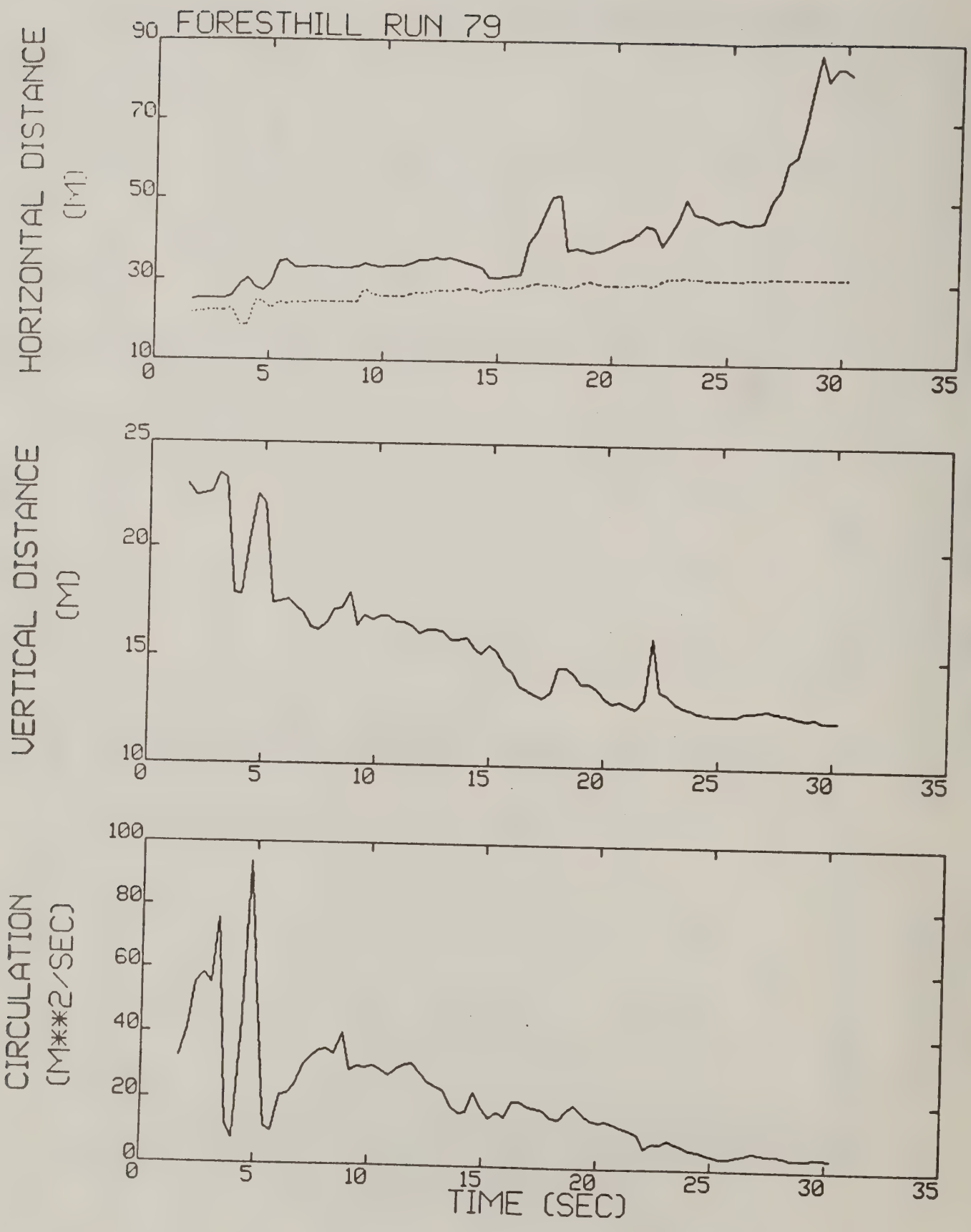

Figure A-61. Foresthill test run 79 generalized algorithm results (*).

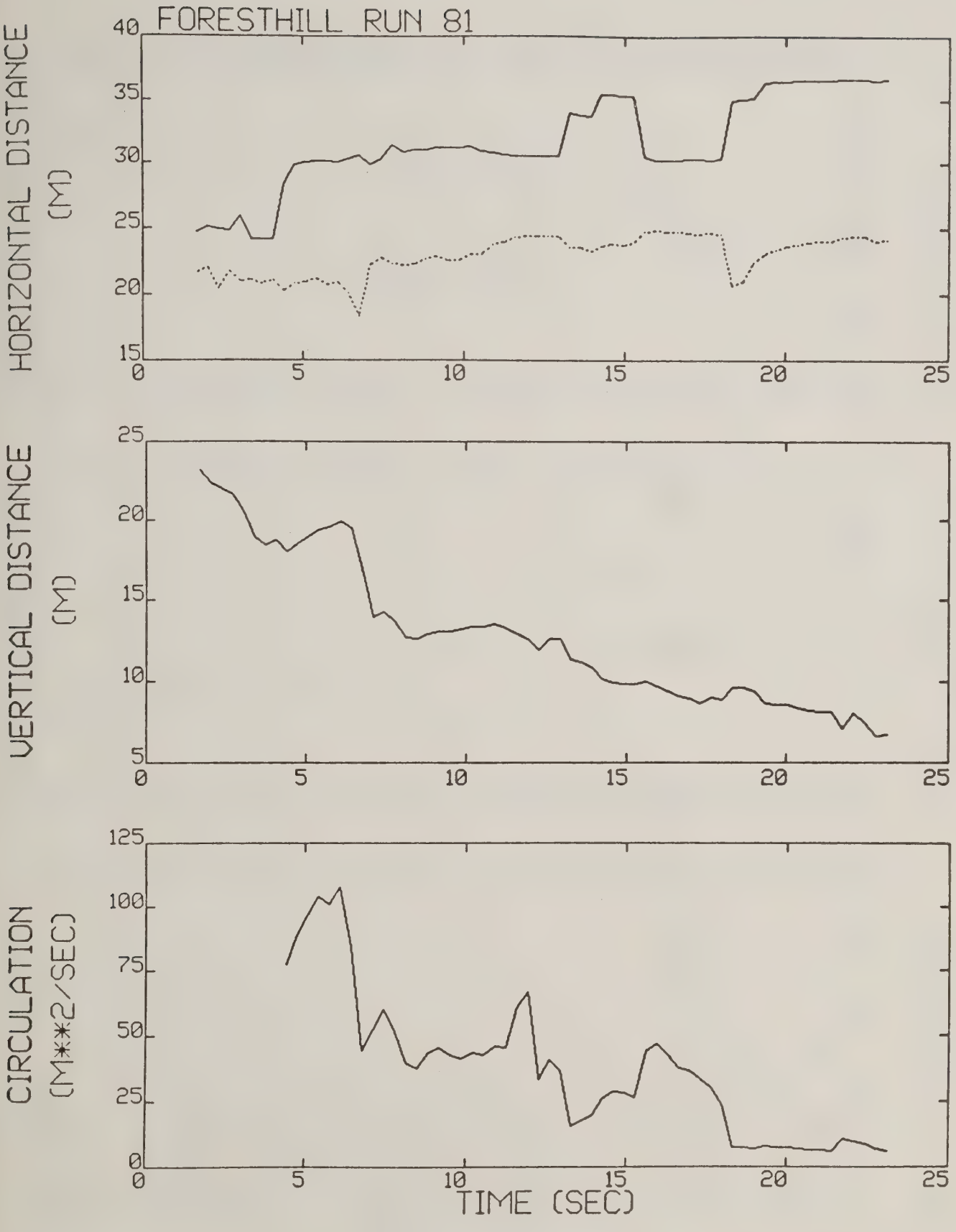

Figure A-62. Foresthill test run 81 generalized algorithm results (*).

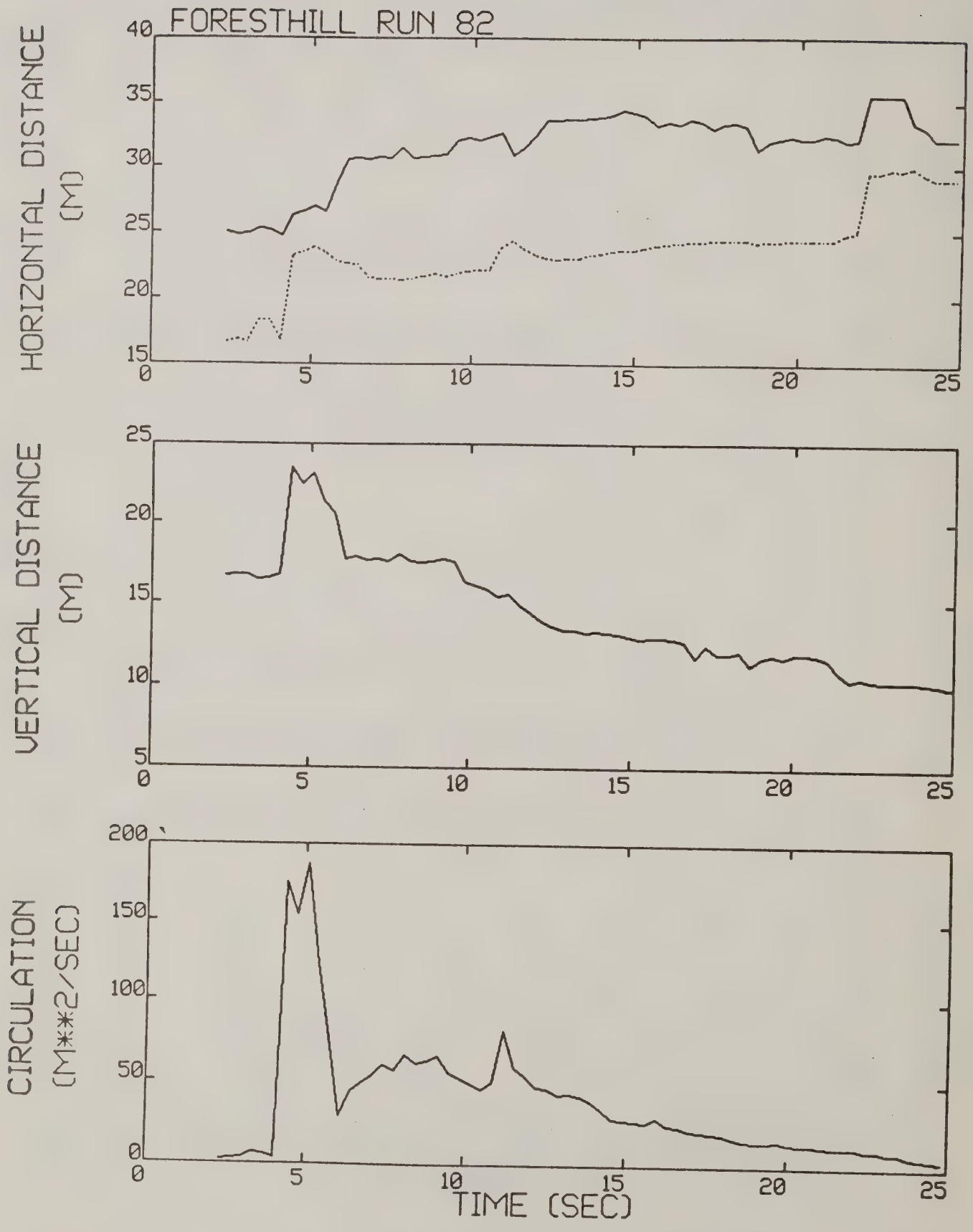

Figure A-63. Foresthill test run 82 generalized algorithm results (*).

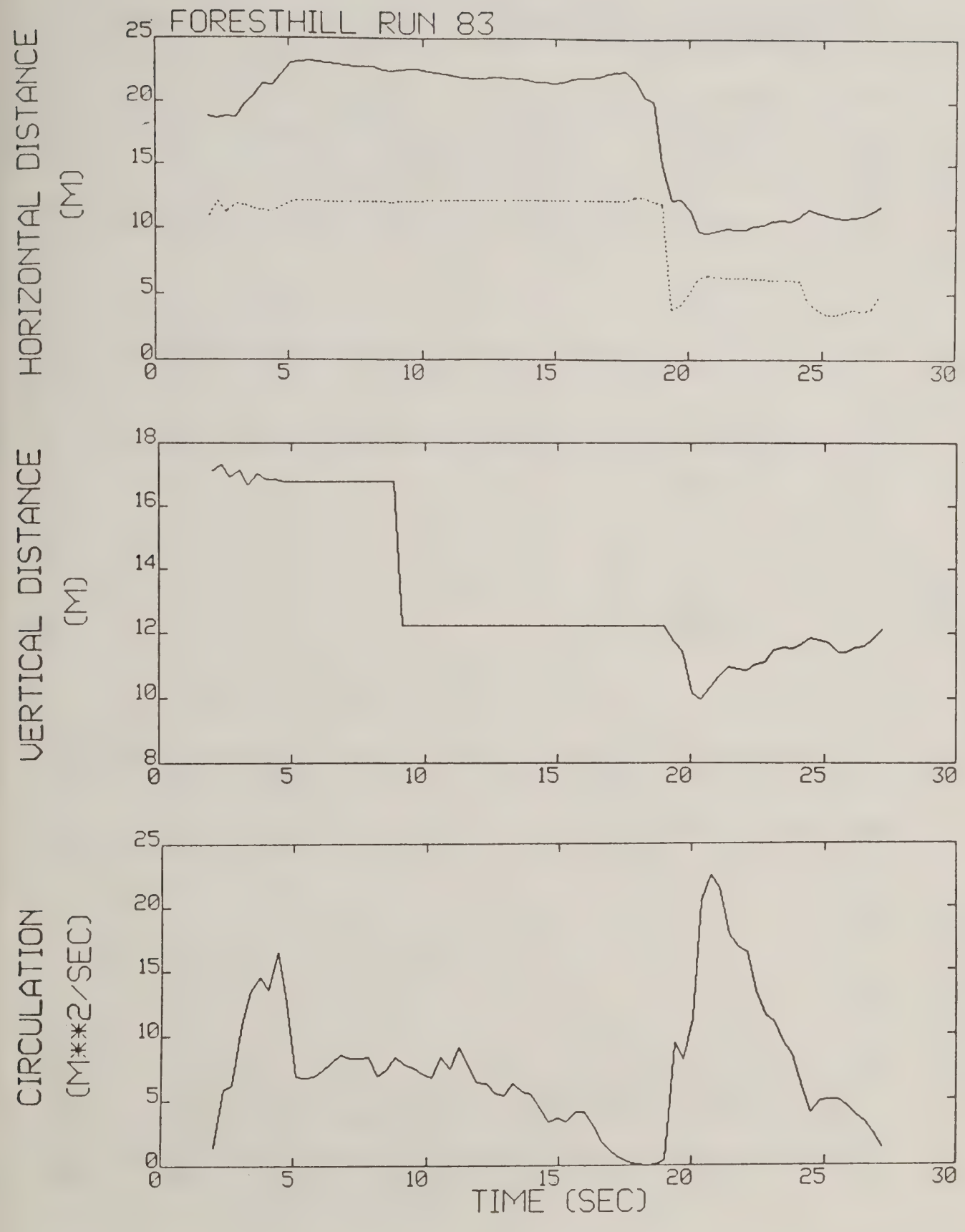

Figure A-64. Foresthill test run 83 generalized algorithm results.

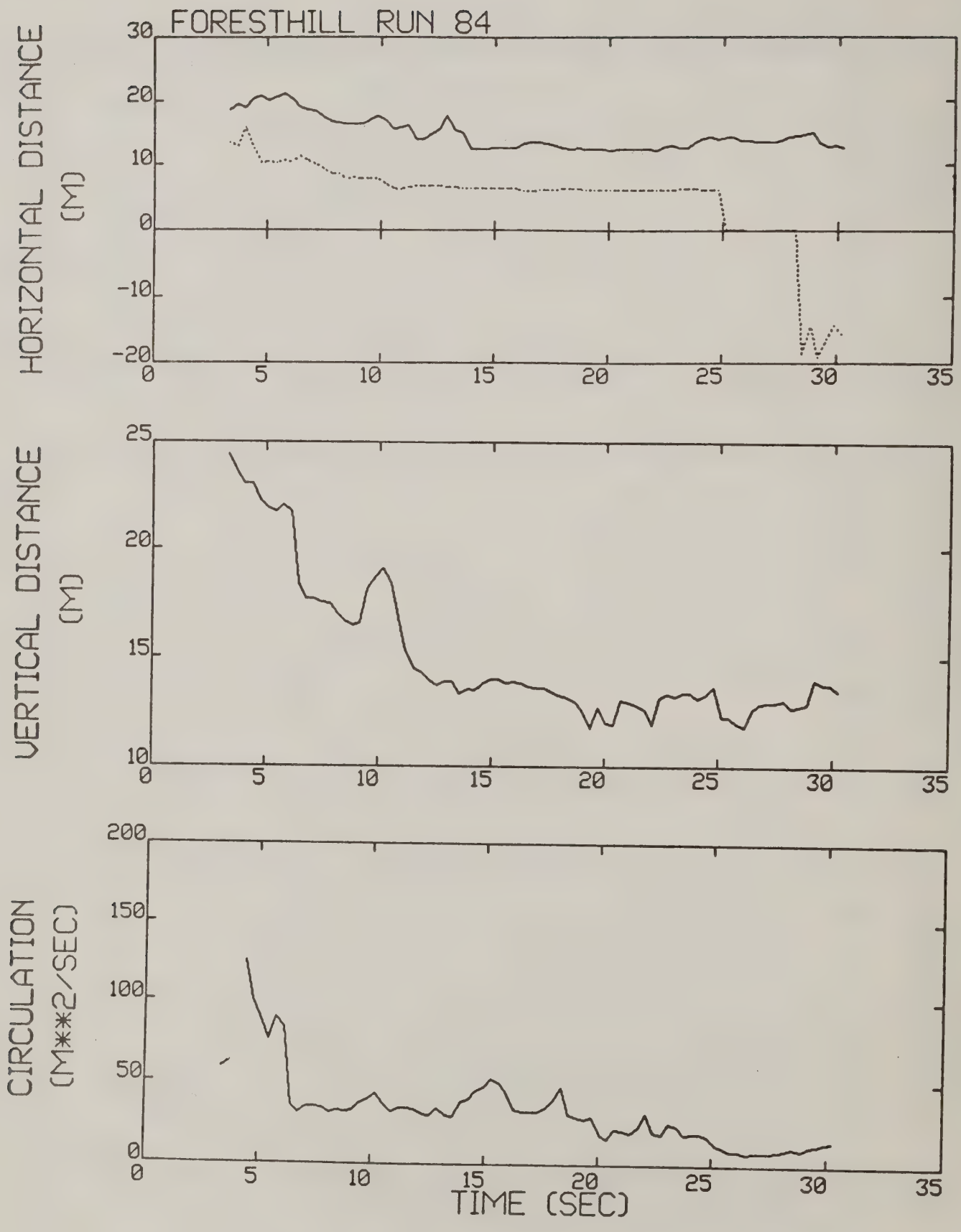

Figure A-65. Foresthill test run 84 generalized algorithm results (*).

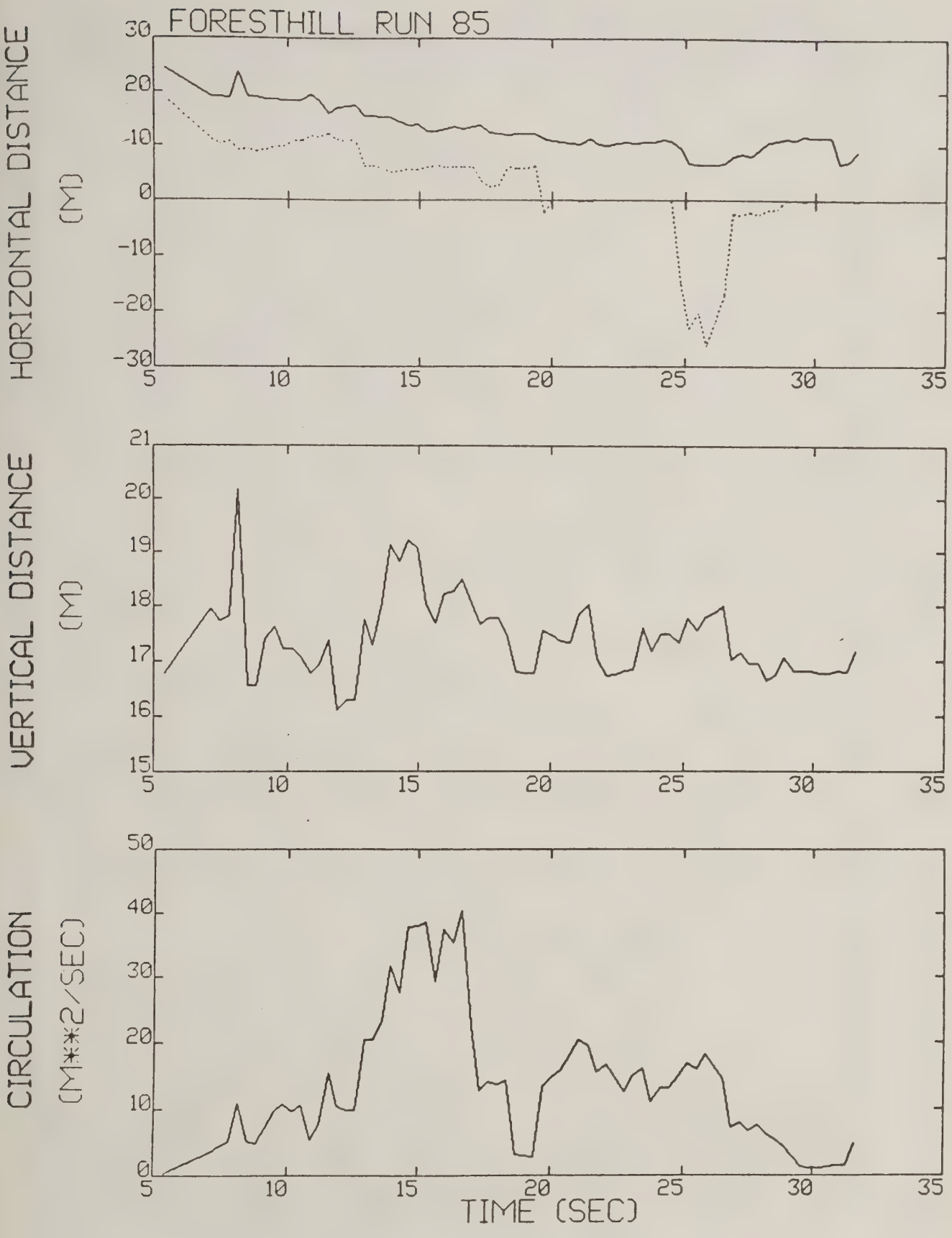

Figure A-66. Foresthill test run 85 generalized algorithm results.

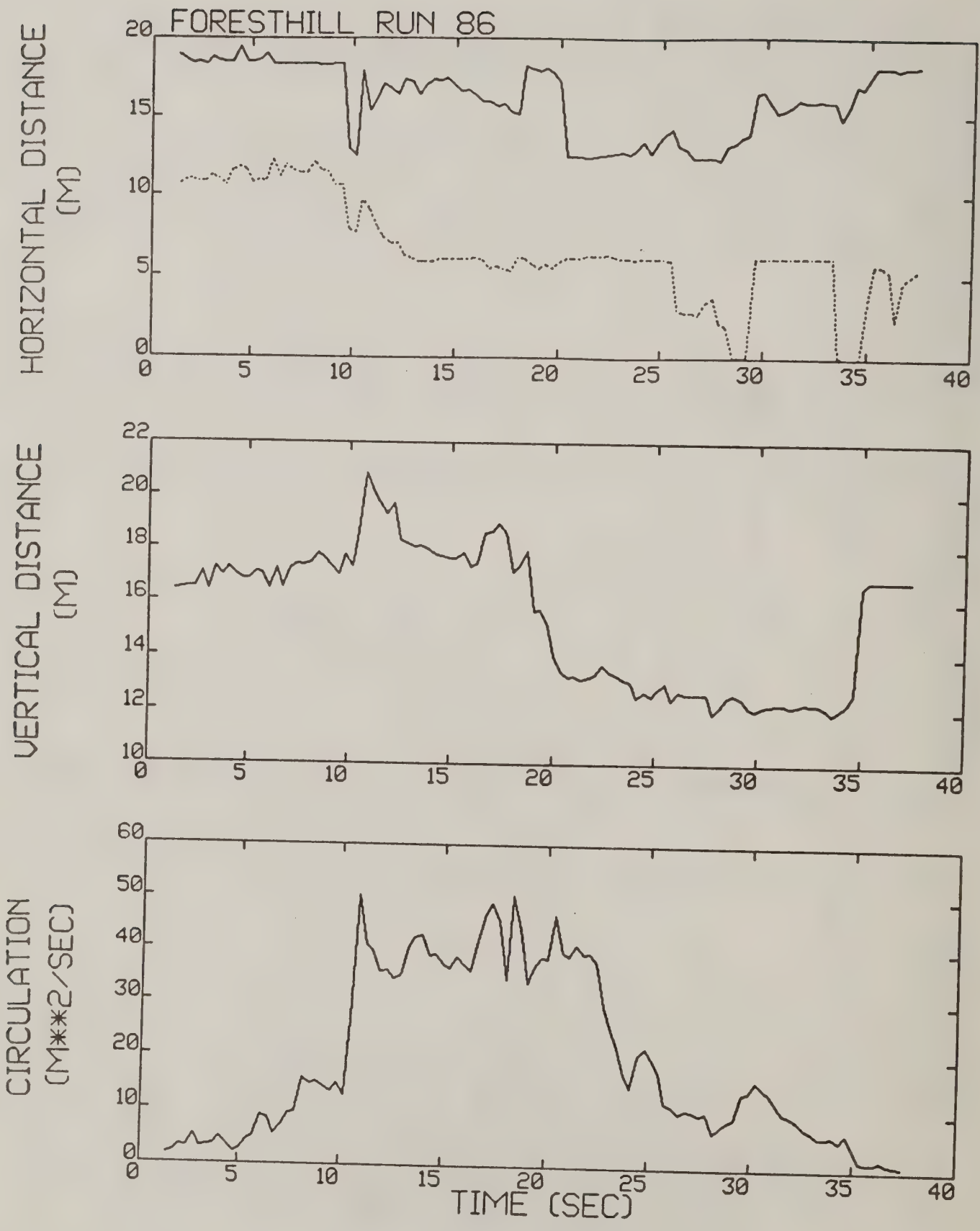

Figure A-67. Foresthill test run 86 generalized algorithm results (*).

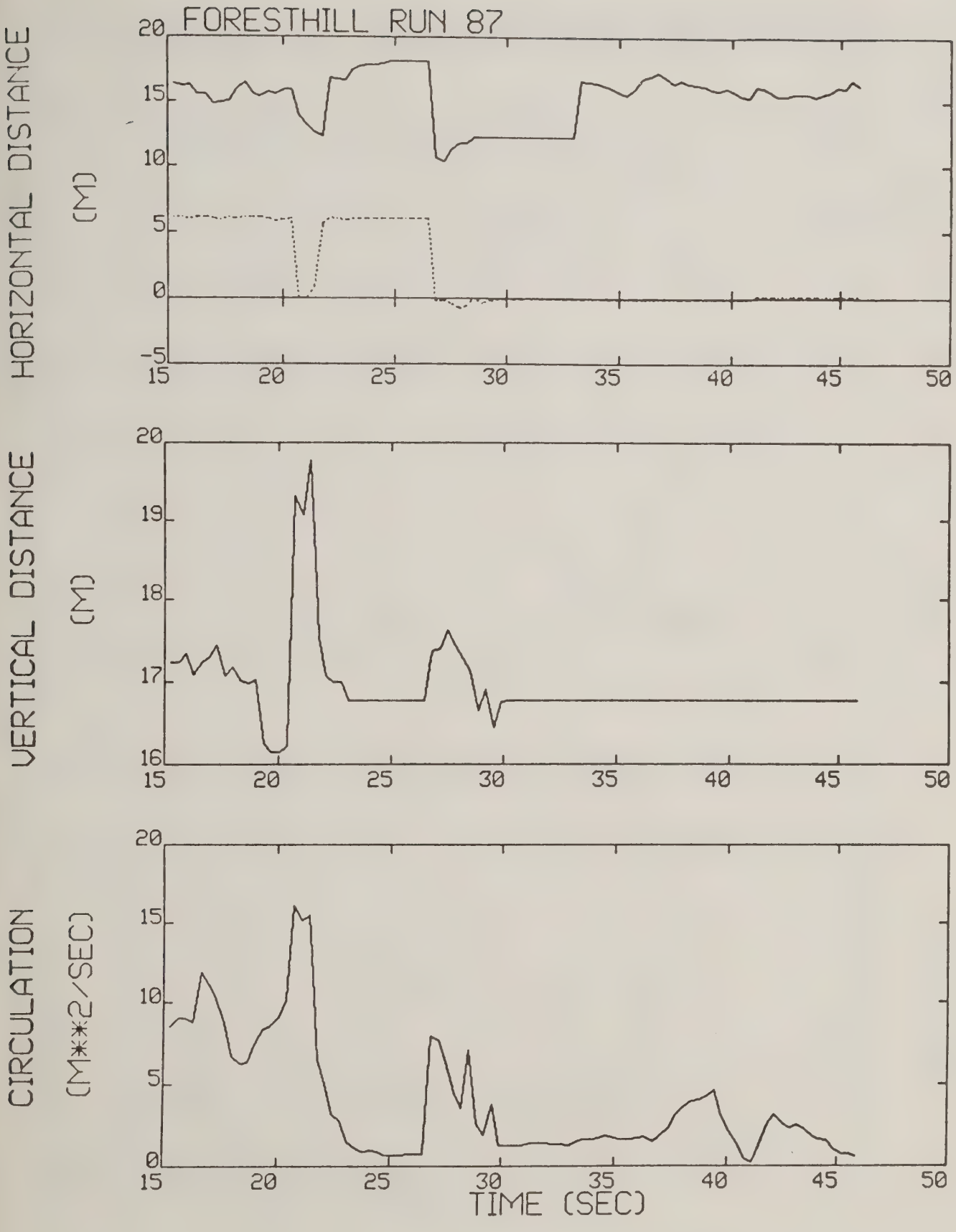

Figure A-68. Foresthill test run 87 generalized algorithm results.

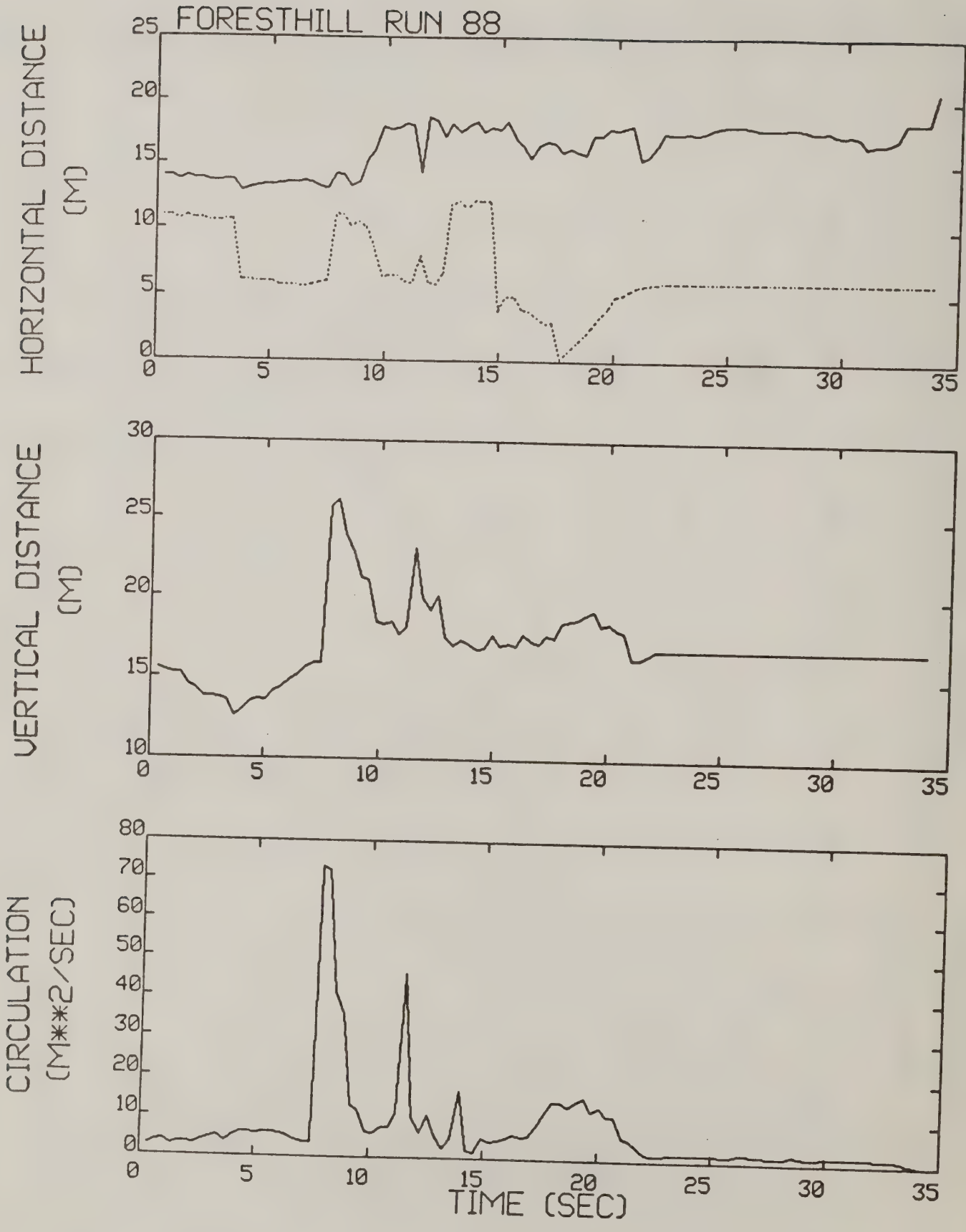

Figure A-69. Foresthill test run 88 generalized algorithm results.

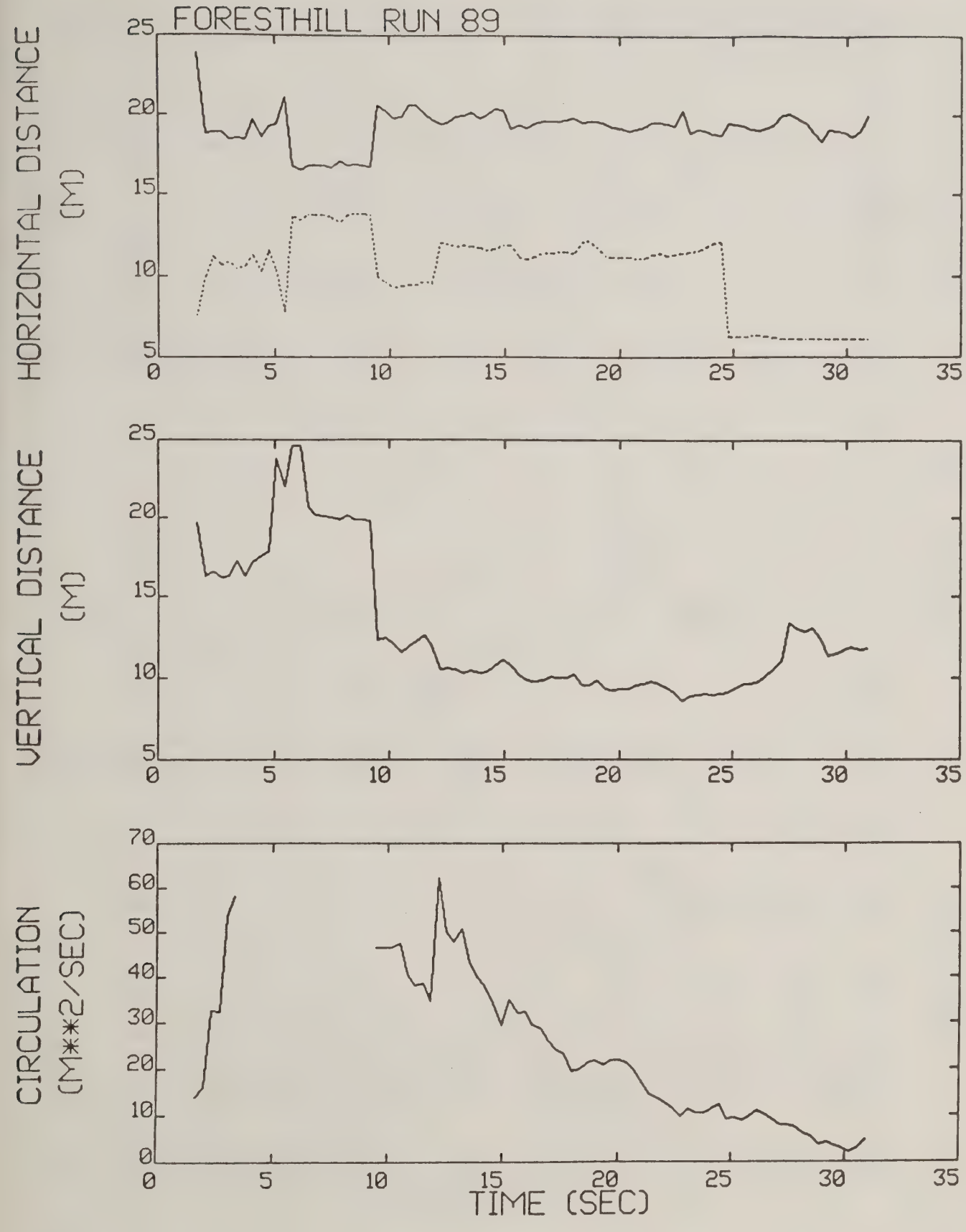

Figure A-70. Foresthill test run 89 generalized algorithm results (*).

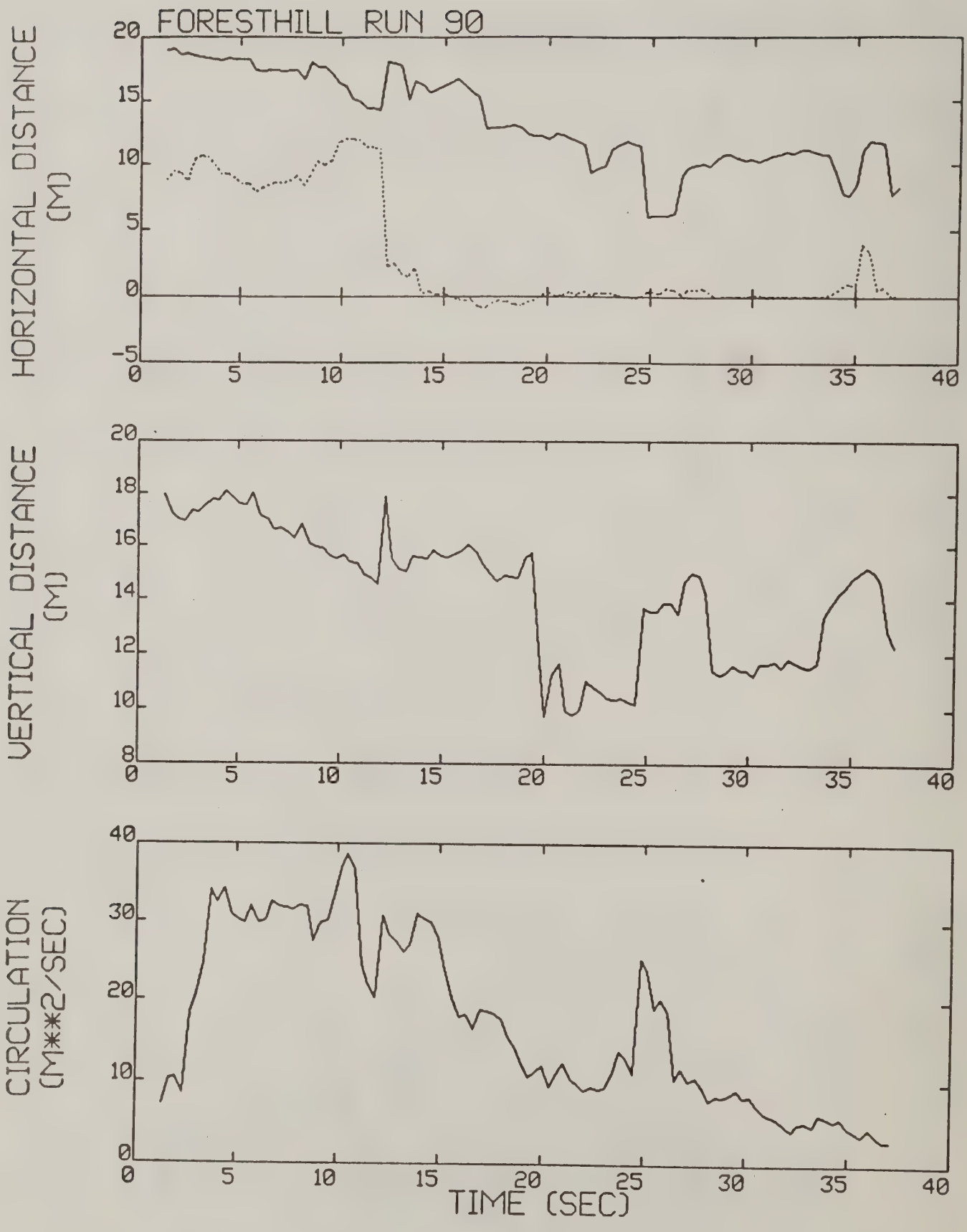

Figure A-71. Foresthill test run 90 generalized algorithm results (*).

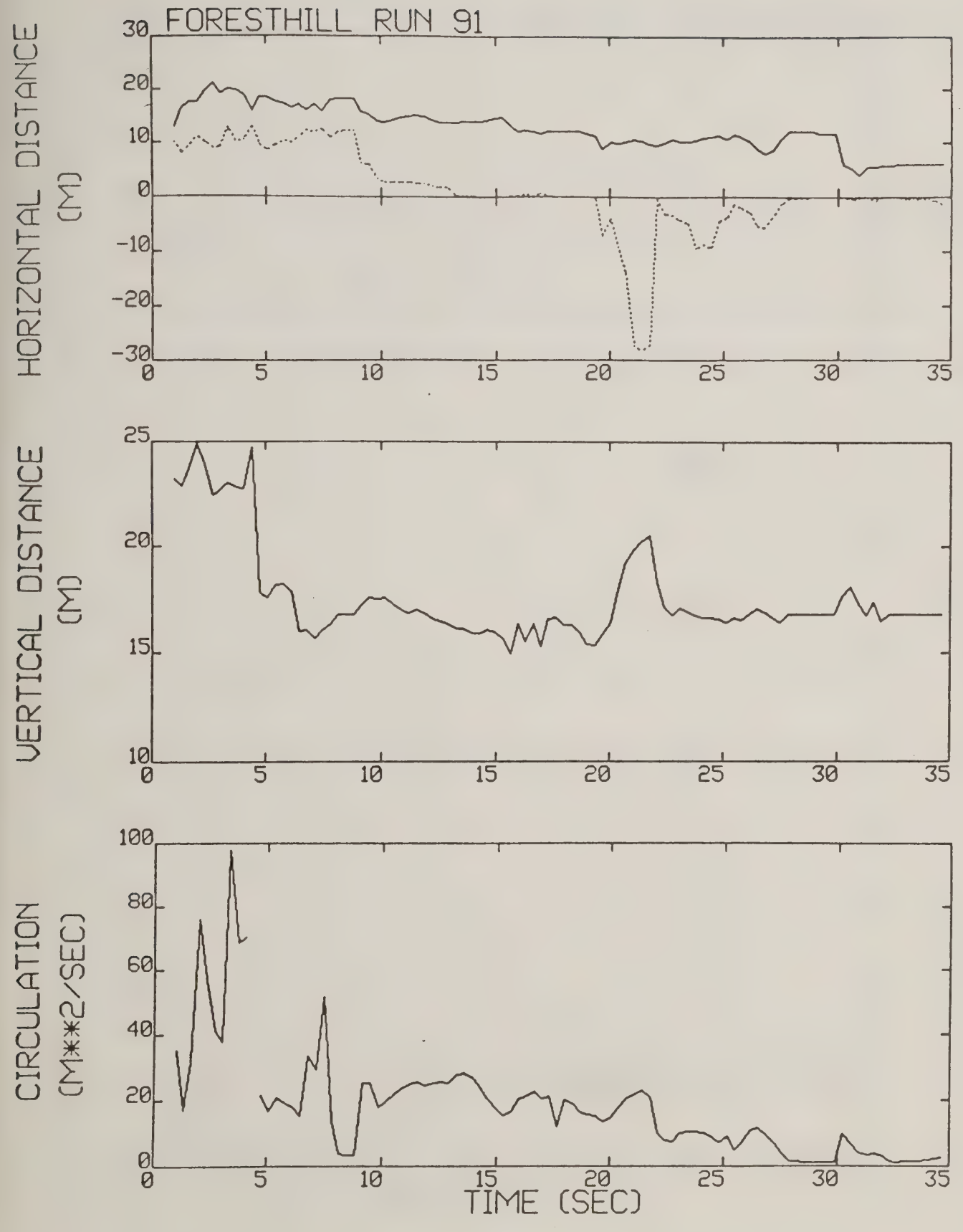

Figure A-72. Foresthill test run 91 generalized algorithm results (*).

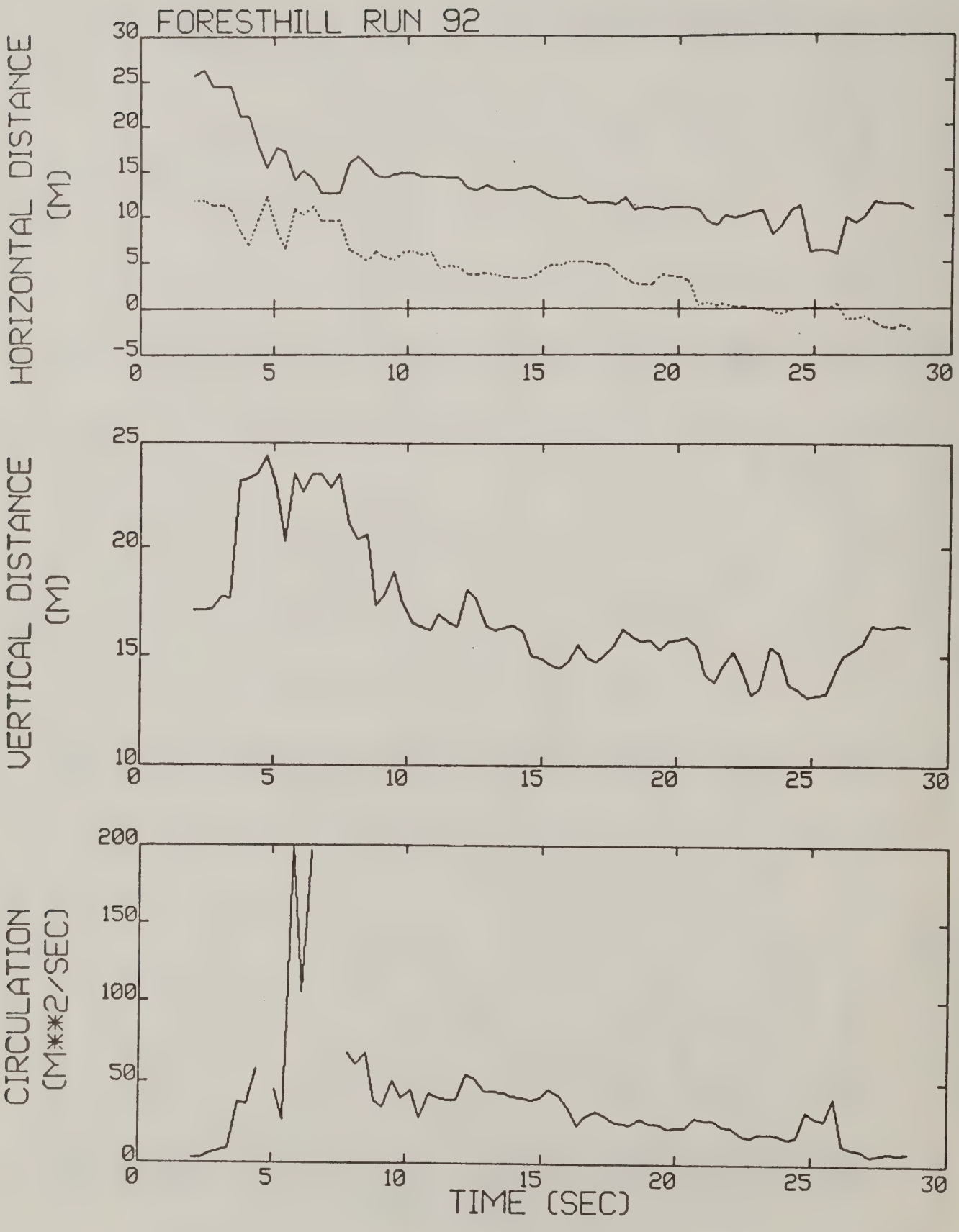

Figure A-73. Foresthill test run 92 generalized algorithm results (*).

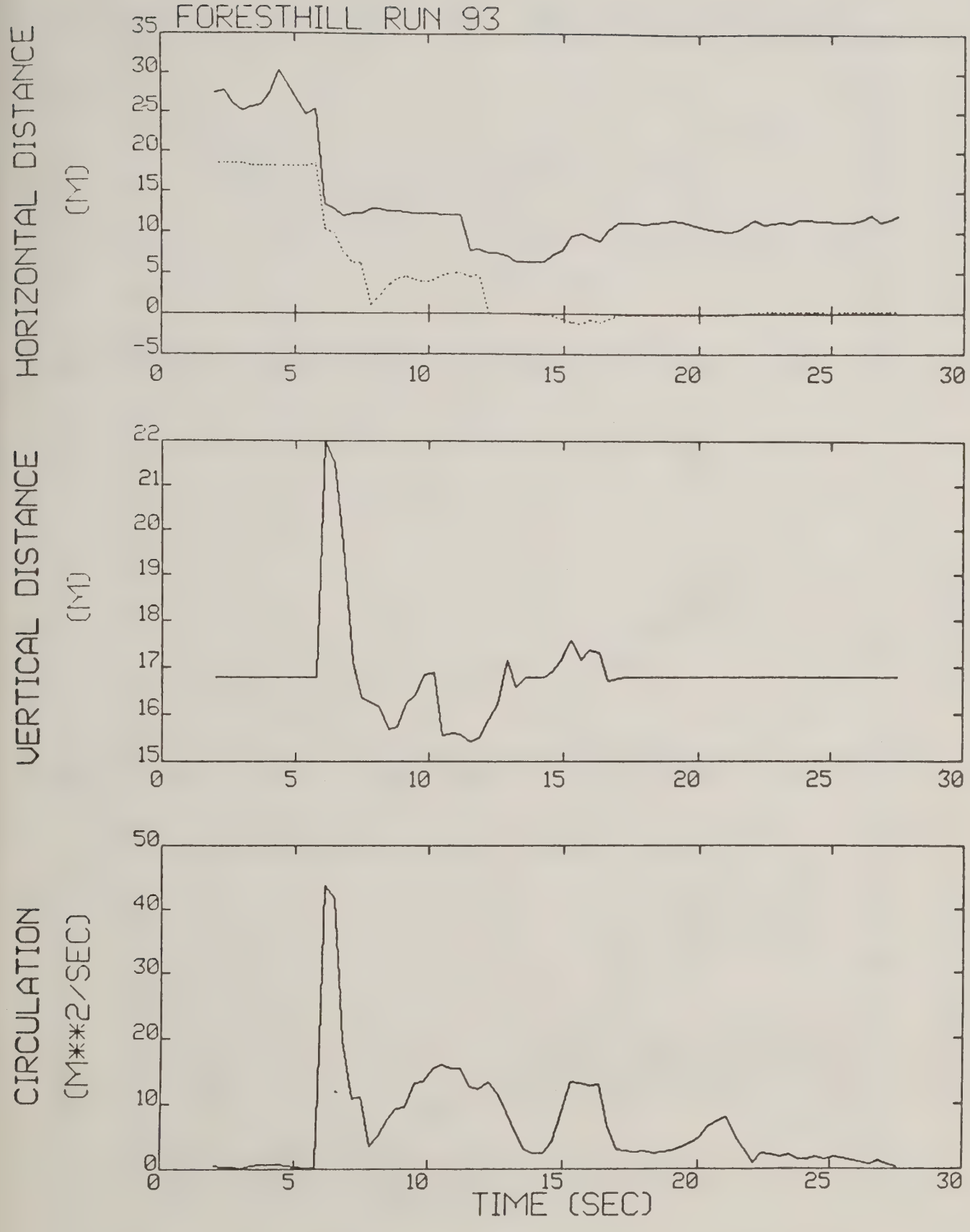

Figure A-74. Foresthill test run 93 generalized algorithm results (*).

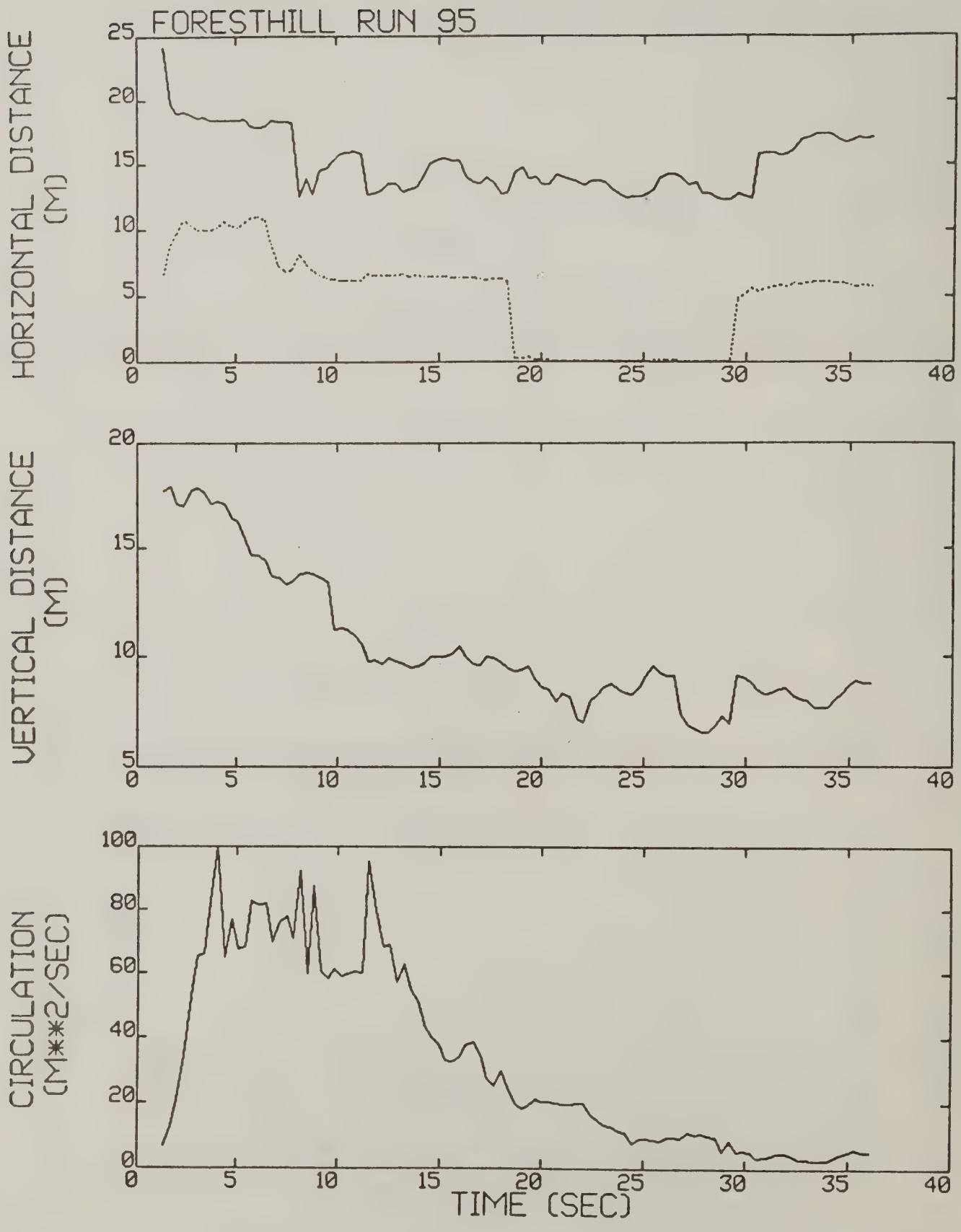

Figure A-75. Foresthill test run 95 generalized algorithm results (*).

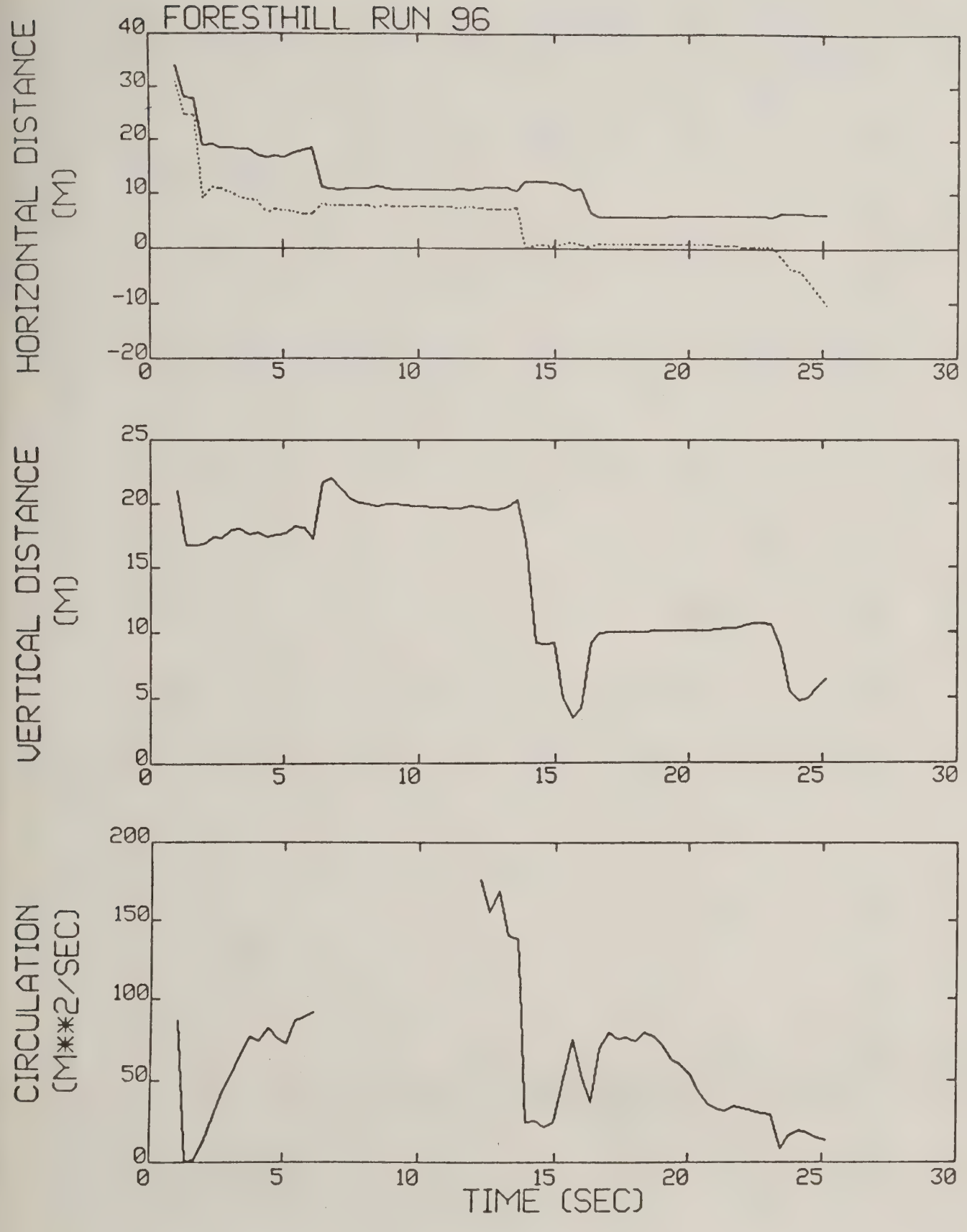

Figure A-76. Foresthill test run 96 generalized algorithm results.

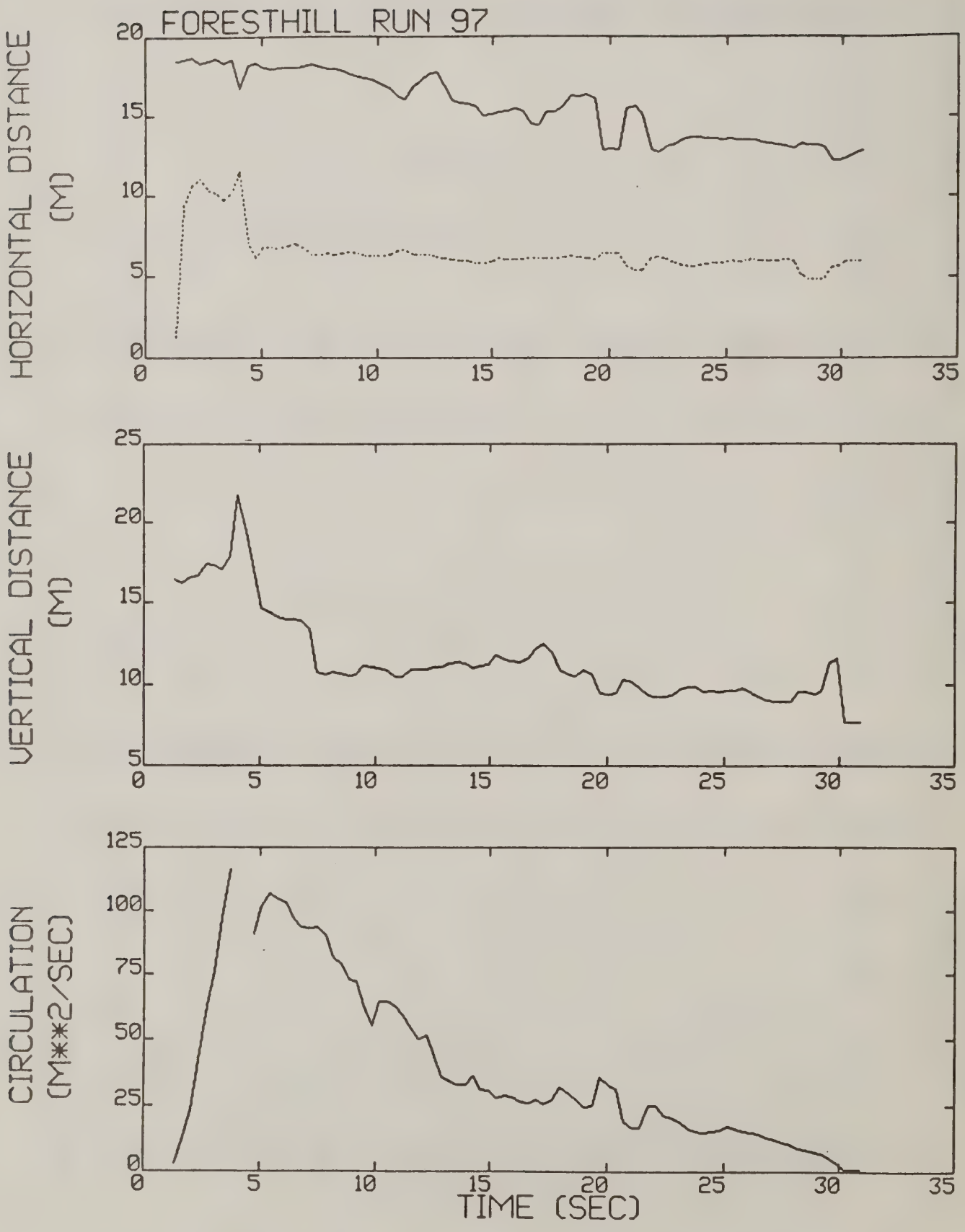

Figure A-77. Foresthill test run 97 generalized algorithm results (*).

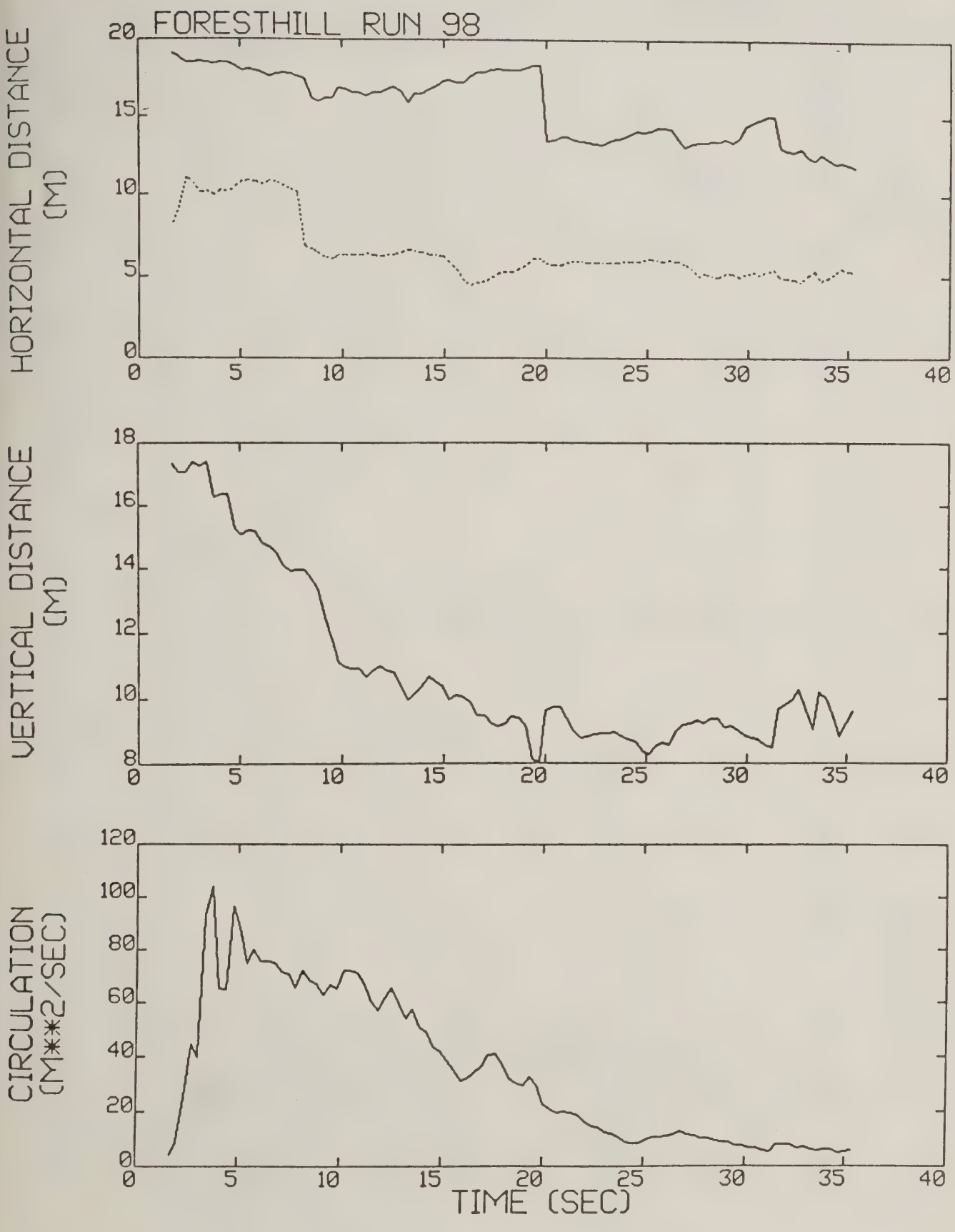

Figure A-78. Foresthill test run 98 generalized algorithm results (*).

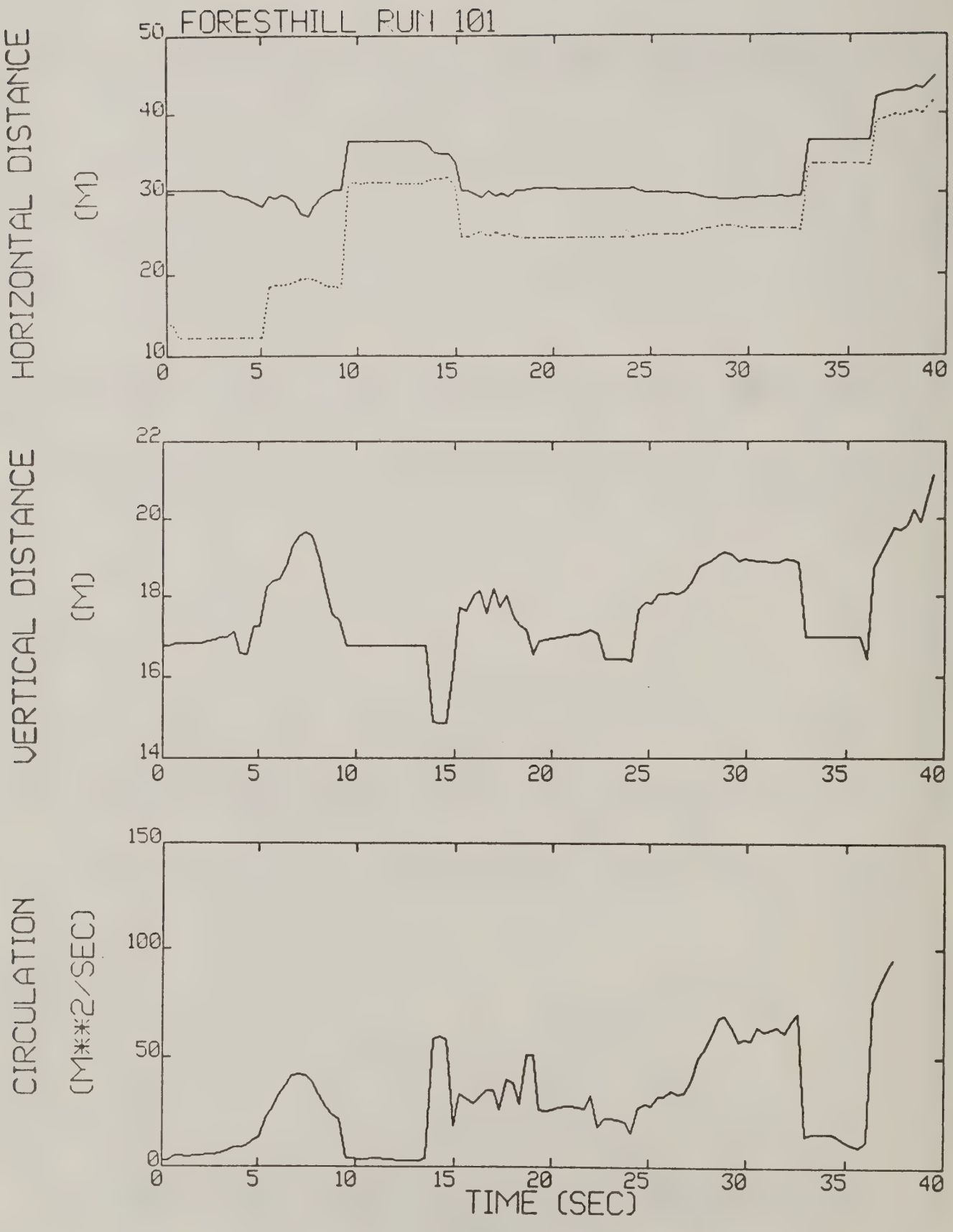

Figure A-79. Foresthill test run 101 generalized algorithm results.

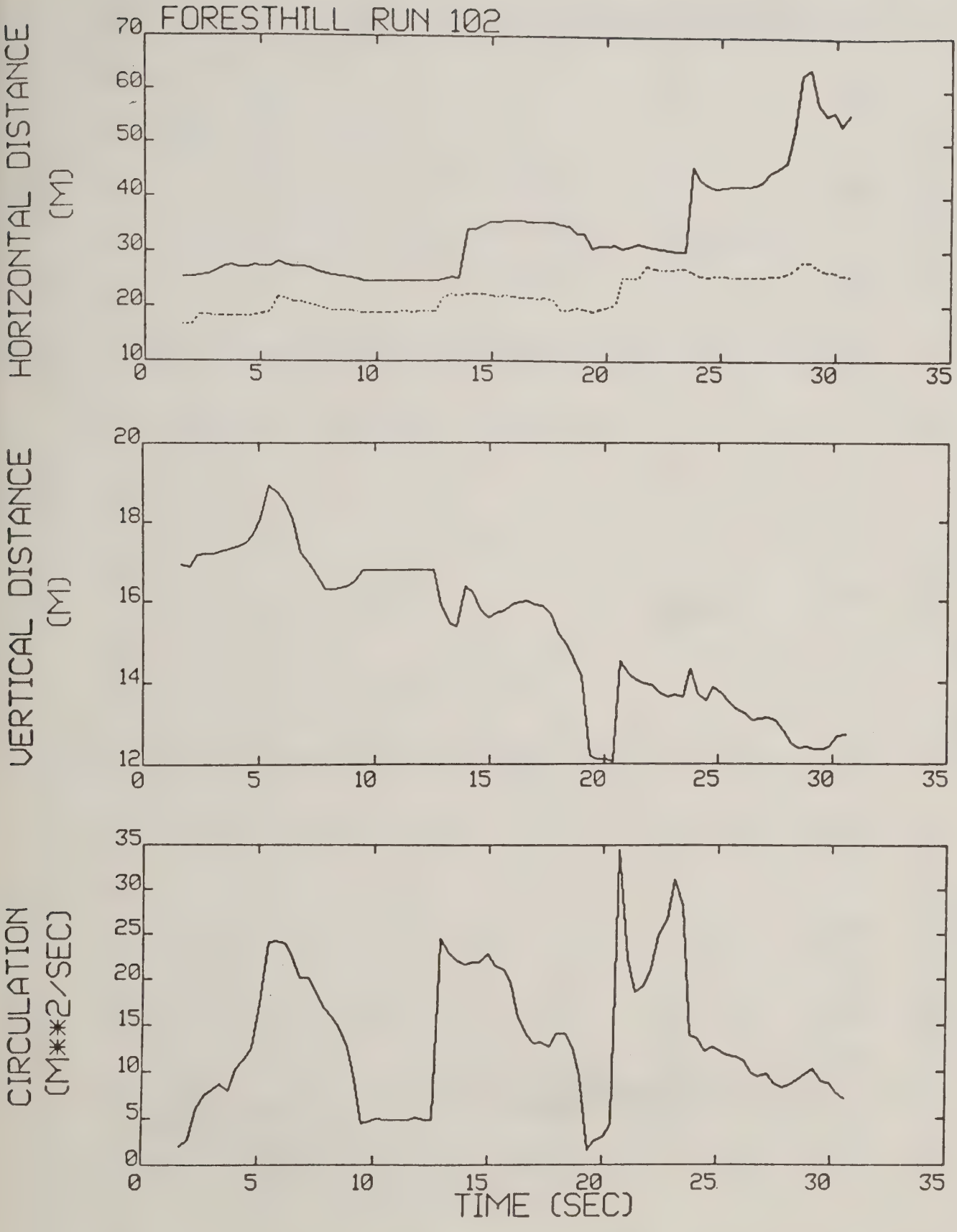

Figure A-80. Foresthill test run 102 generalized algorithm results.

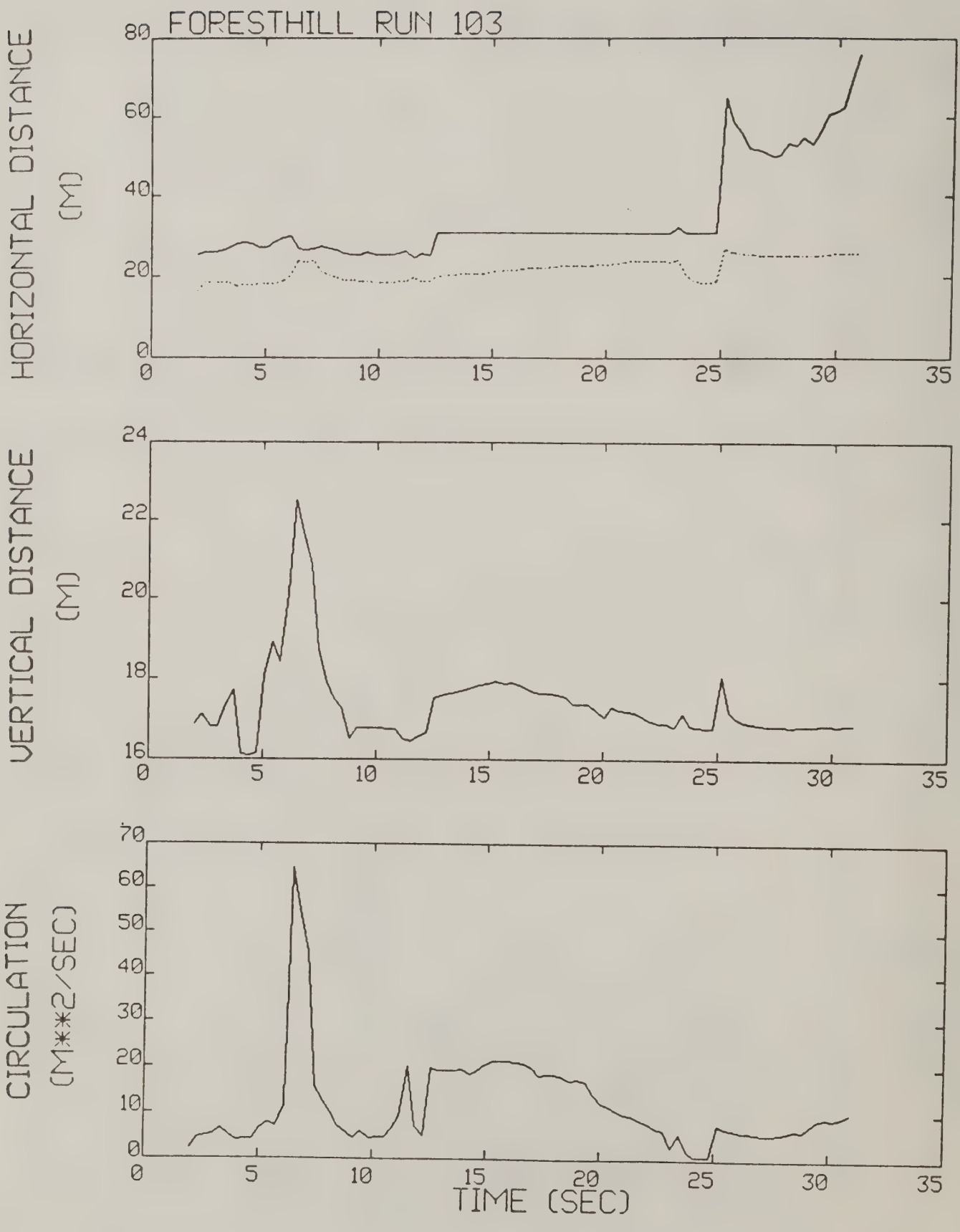

Figure A-81. Foresthill test run 103 generalized algorithm results.

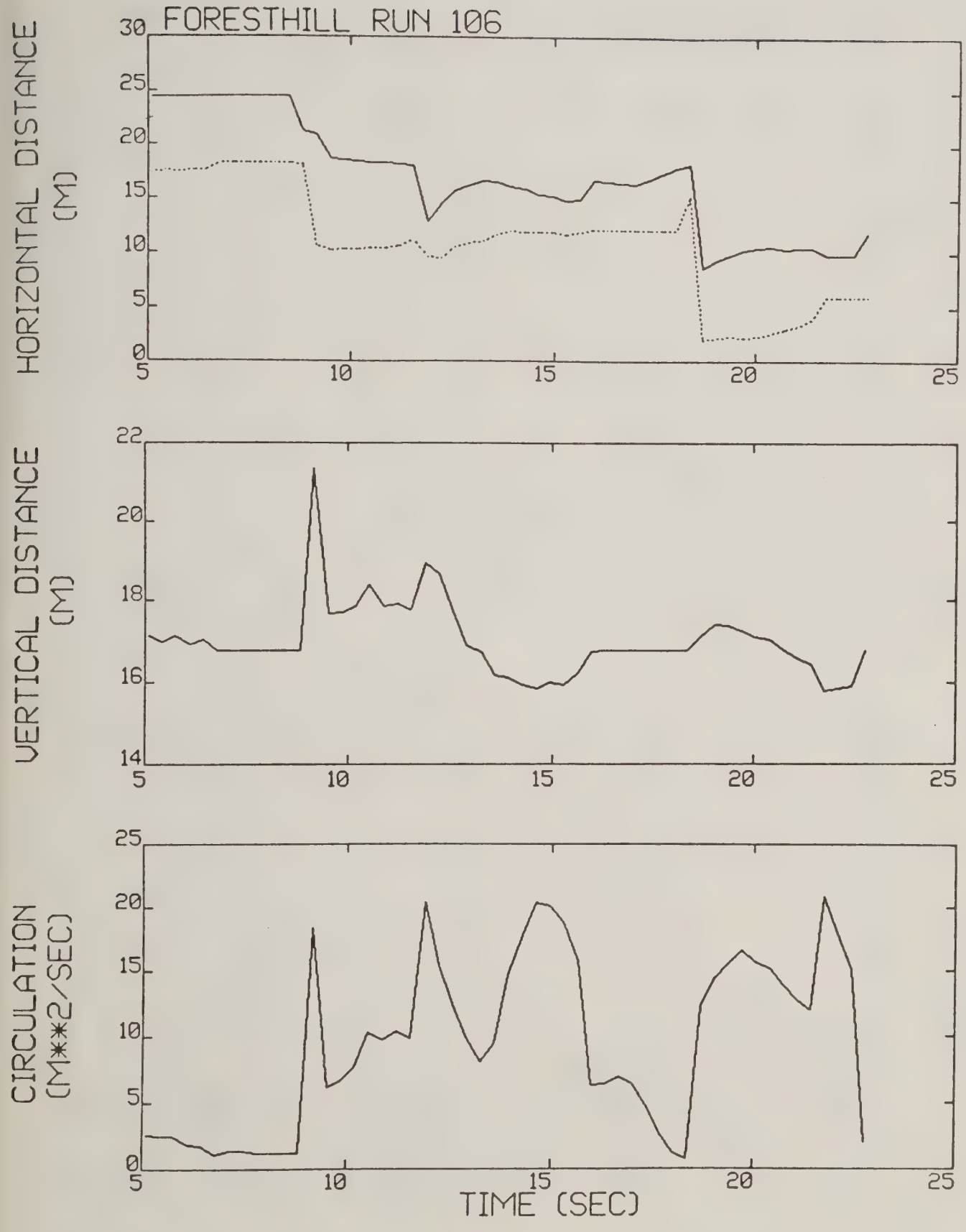

Figure A-82. Foresthill test run 106 generalized algorithm results.

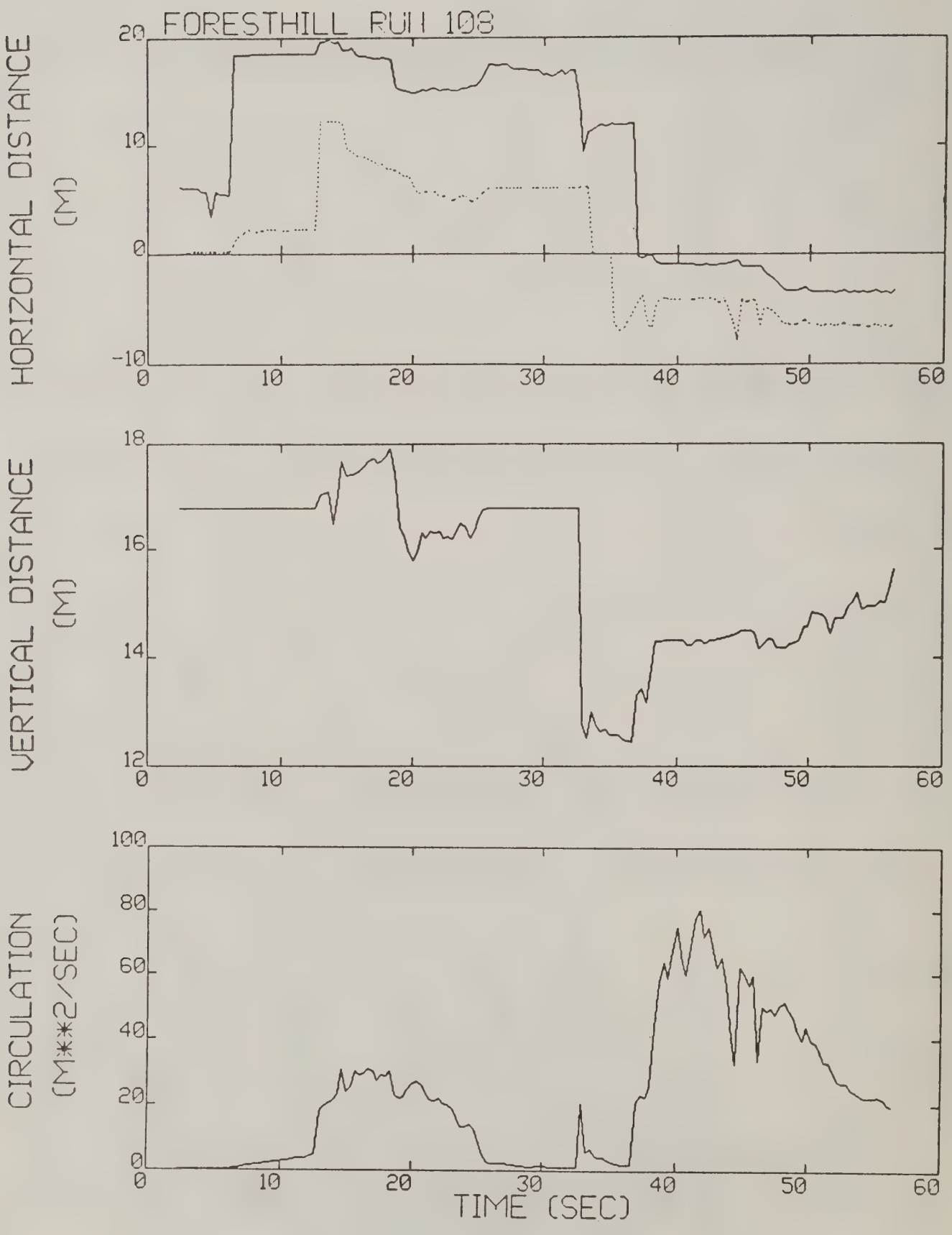

Figure A-83. Foresthill test run 108 generalized algorithm results.

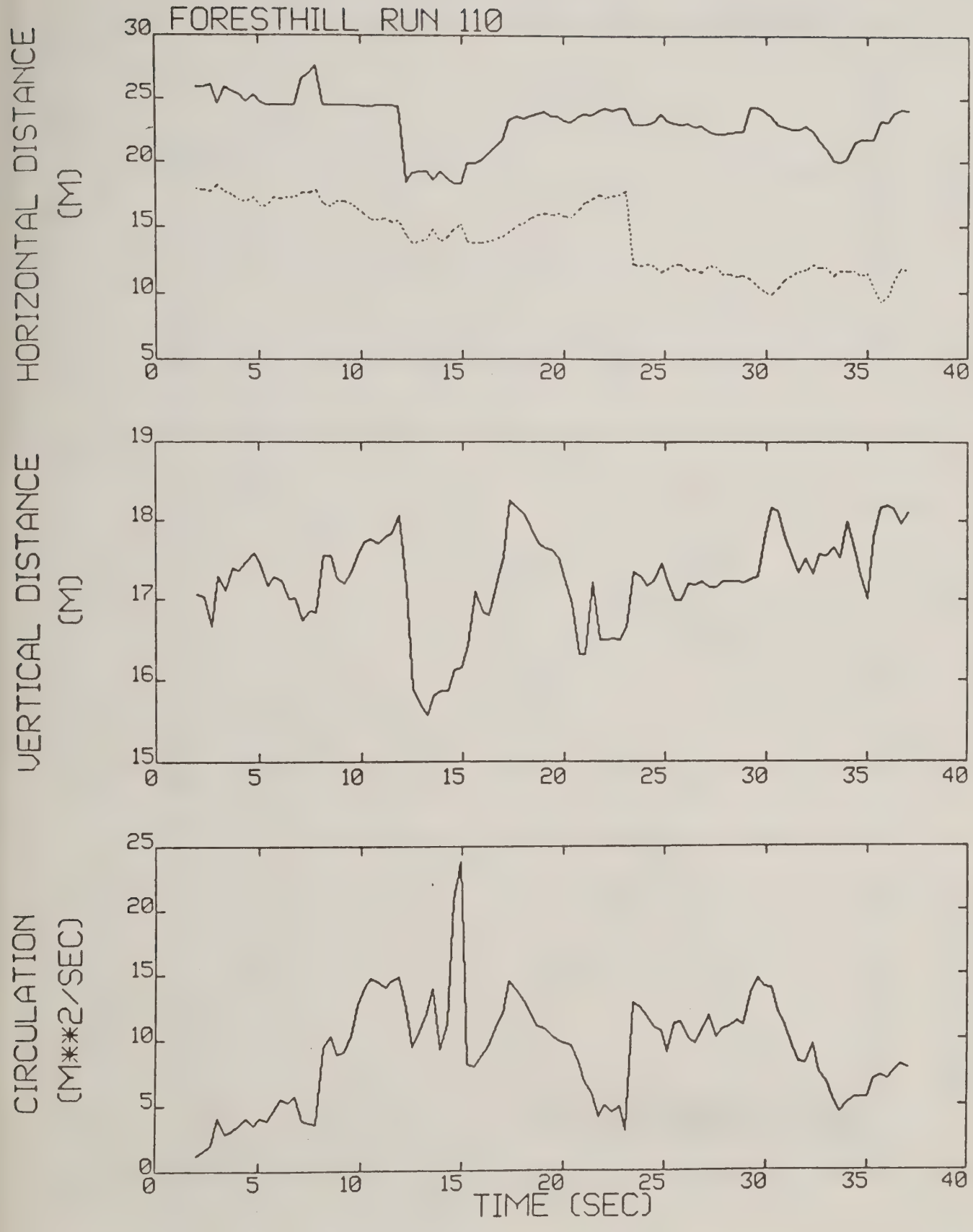

Figure A-84. Foresthill test run 110 generalized algorithm results.

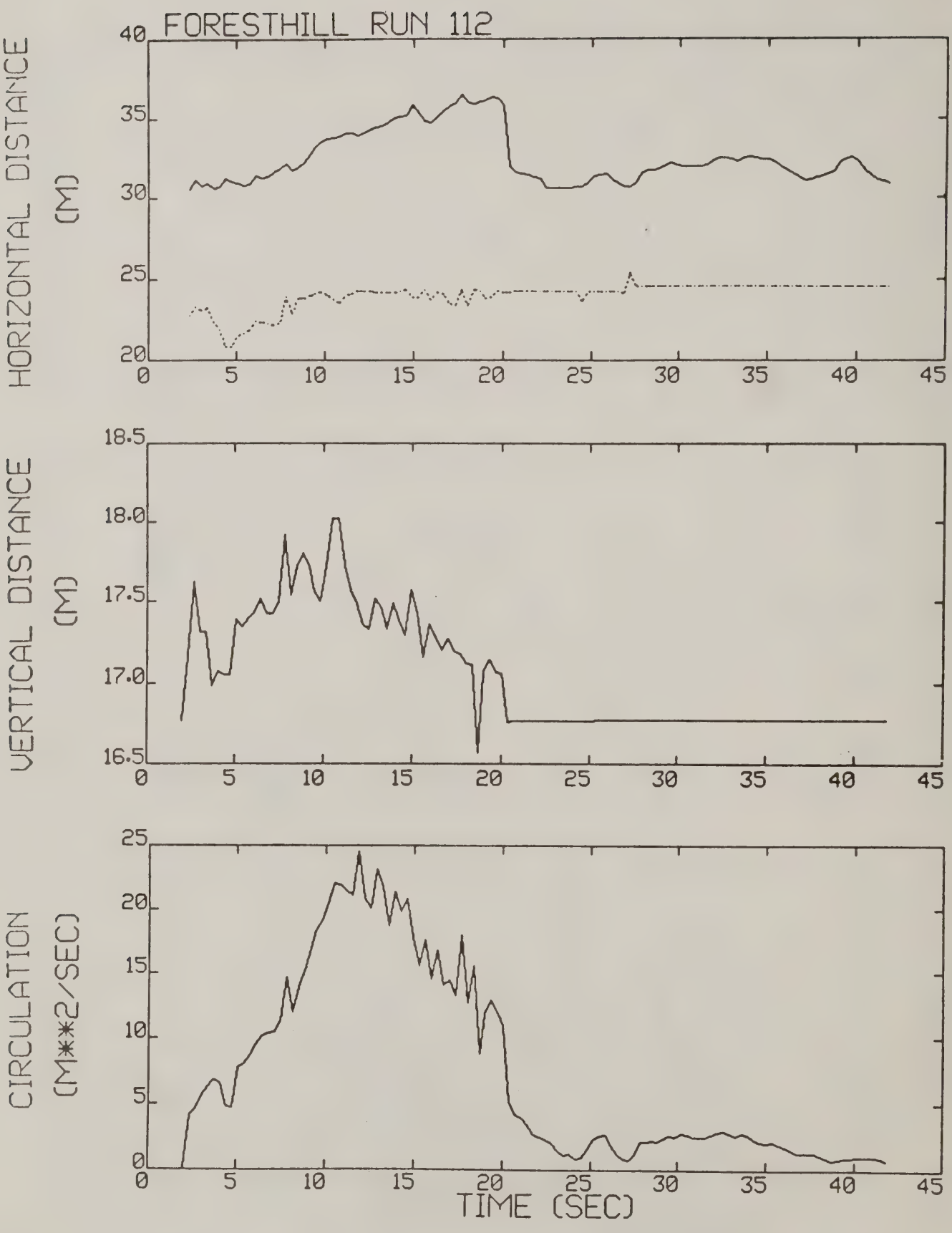

Figure A-85. Foresthill test run 112 generalized algorithm results (*).

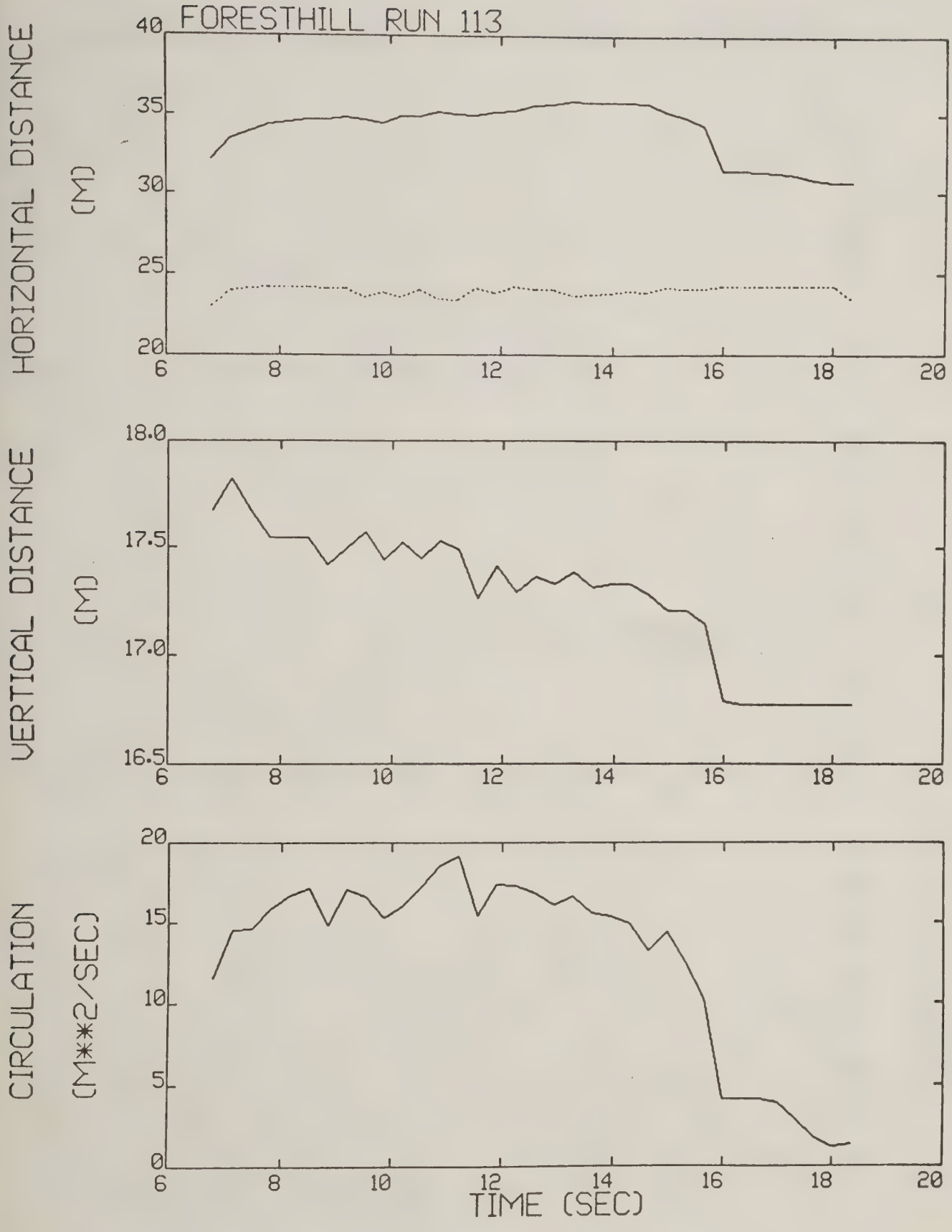

Figure A-86. Foresthill test run 113 generalized algorithm results.

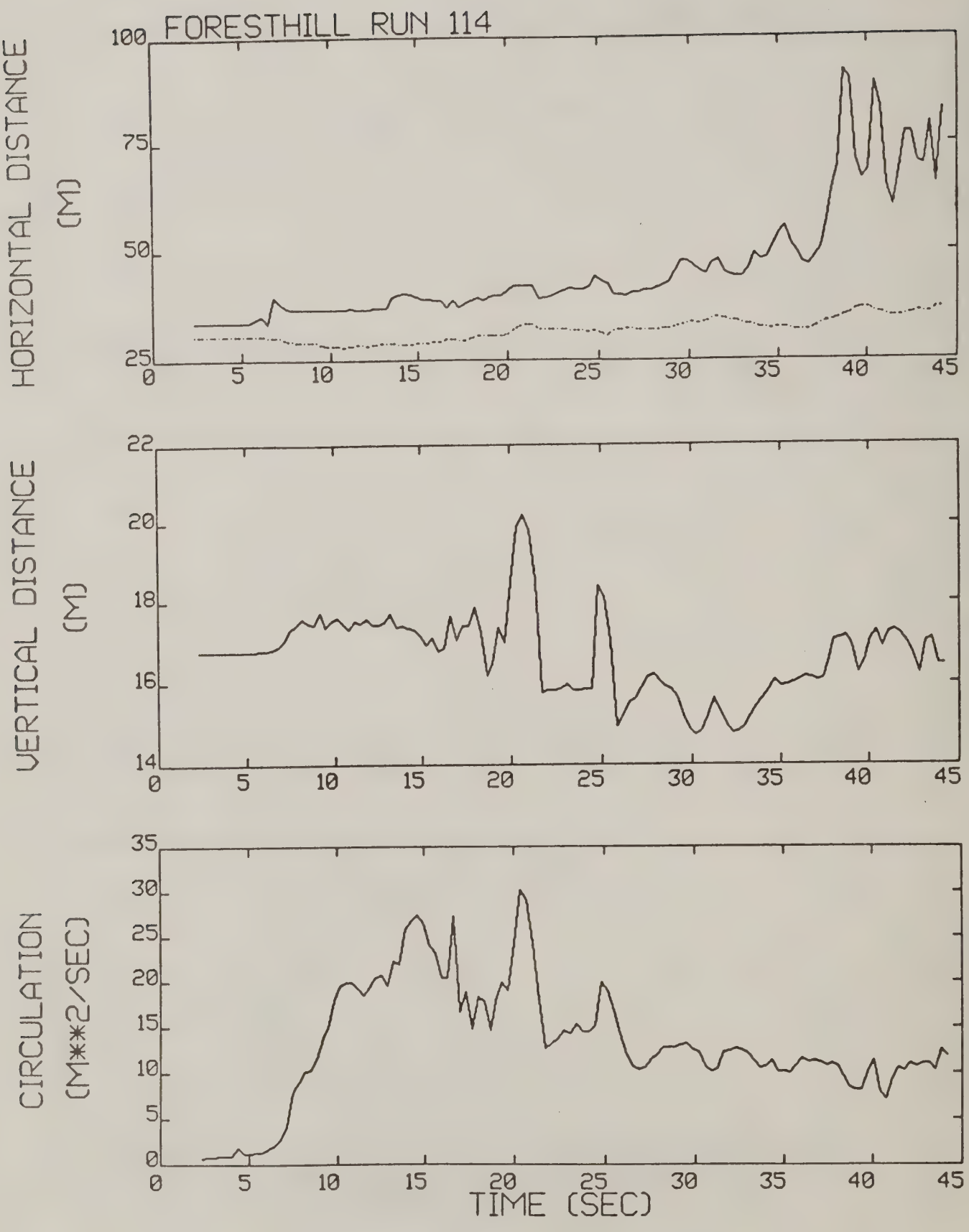

Figure A-87. Foresthill test run 114 generalized algorithm results (*).

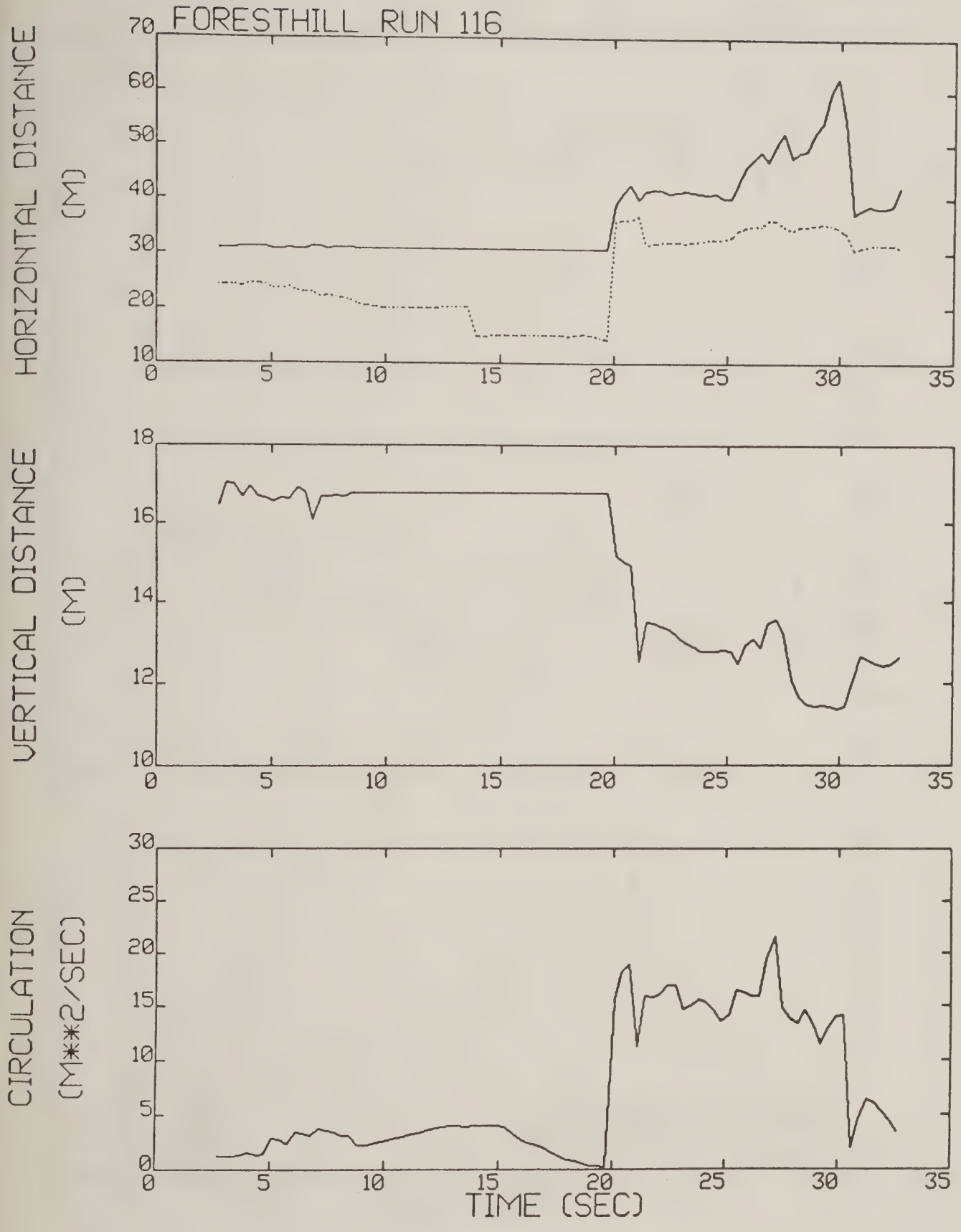

Figure A-88. Foresthill test run 116 generalized algorithm results.

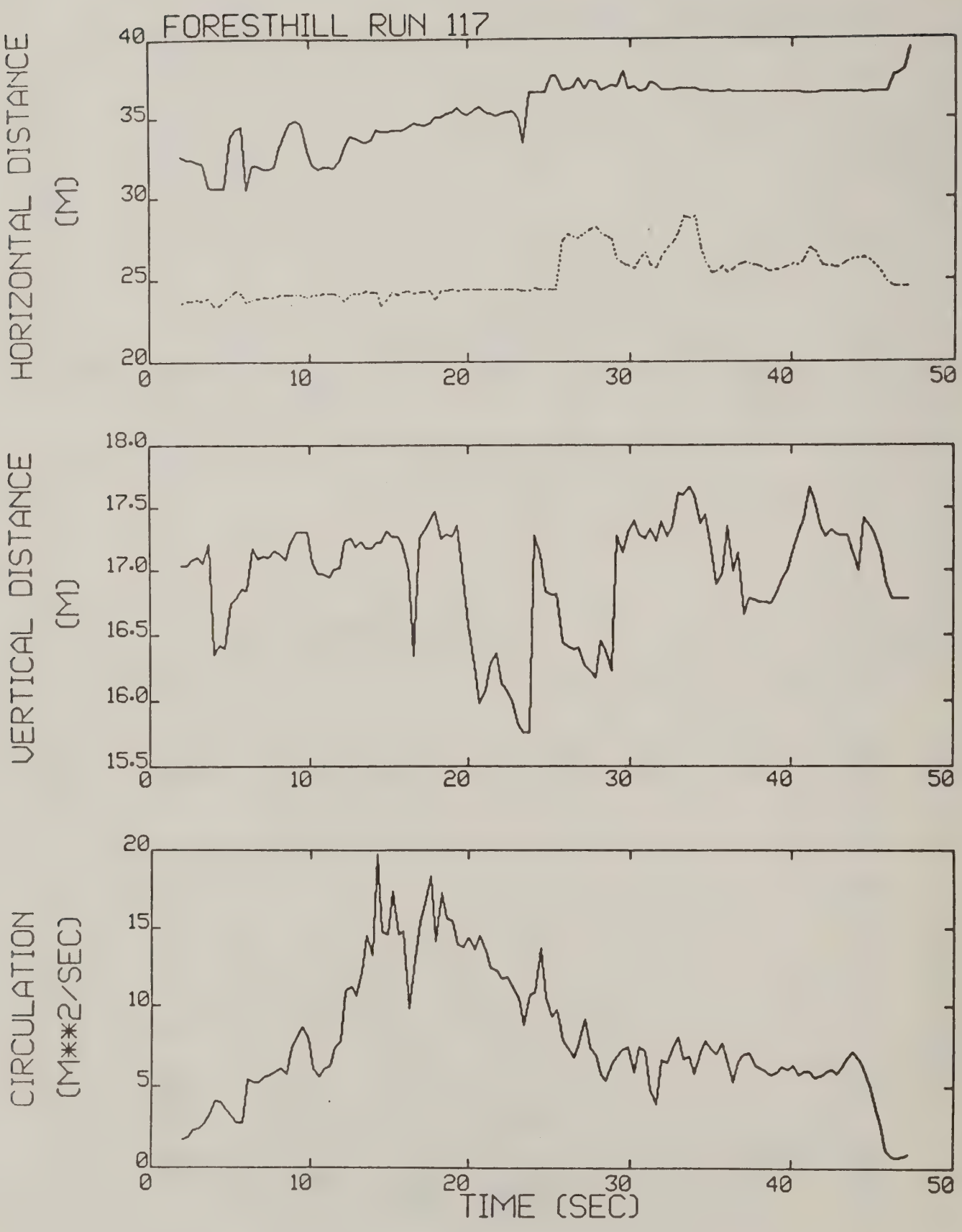

Figure A-89. Foresthill test run 117 generalized algorithm results (*).

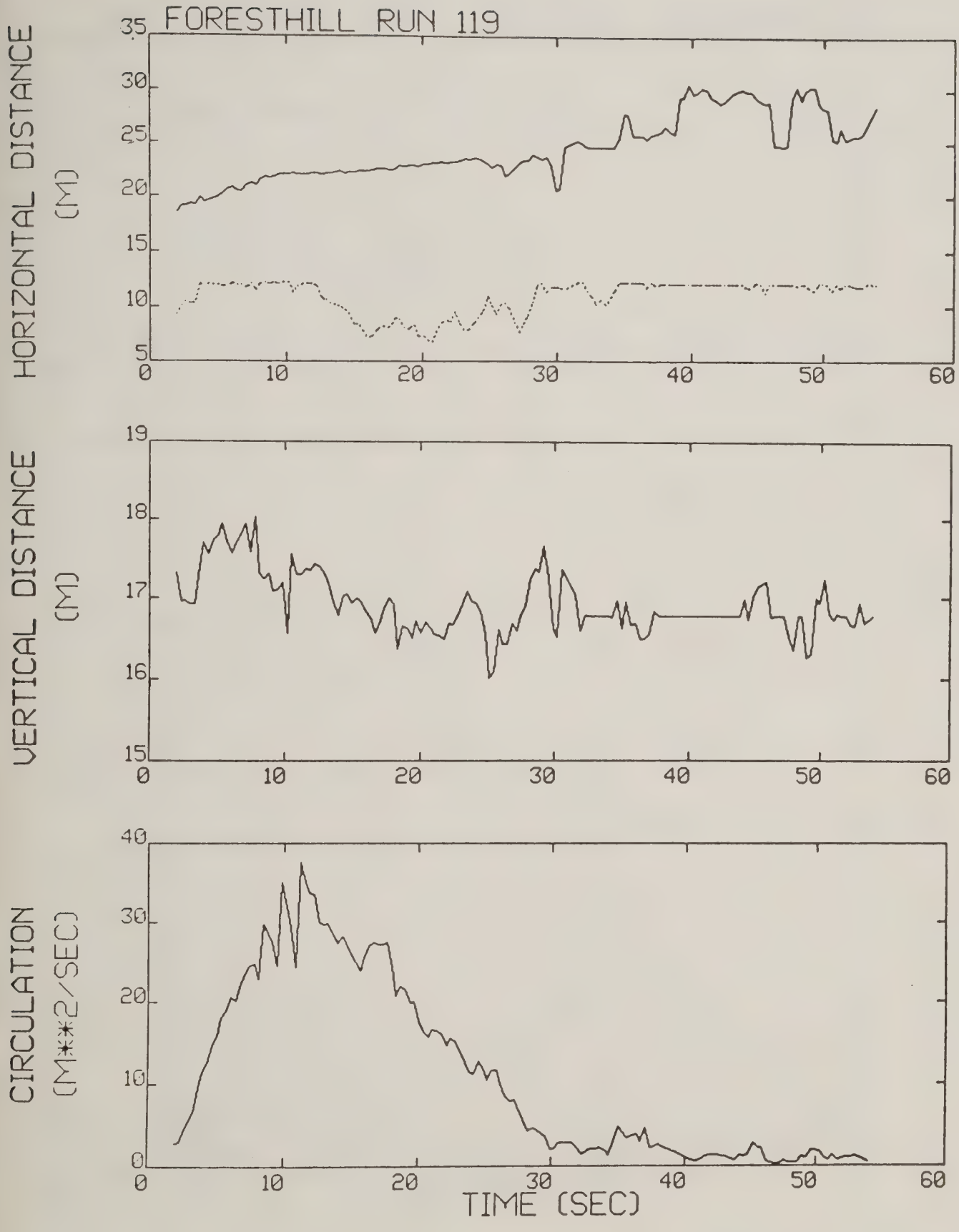

Figure A-90. Foresthill test run 119 generalized algorithm results (*).

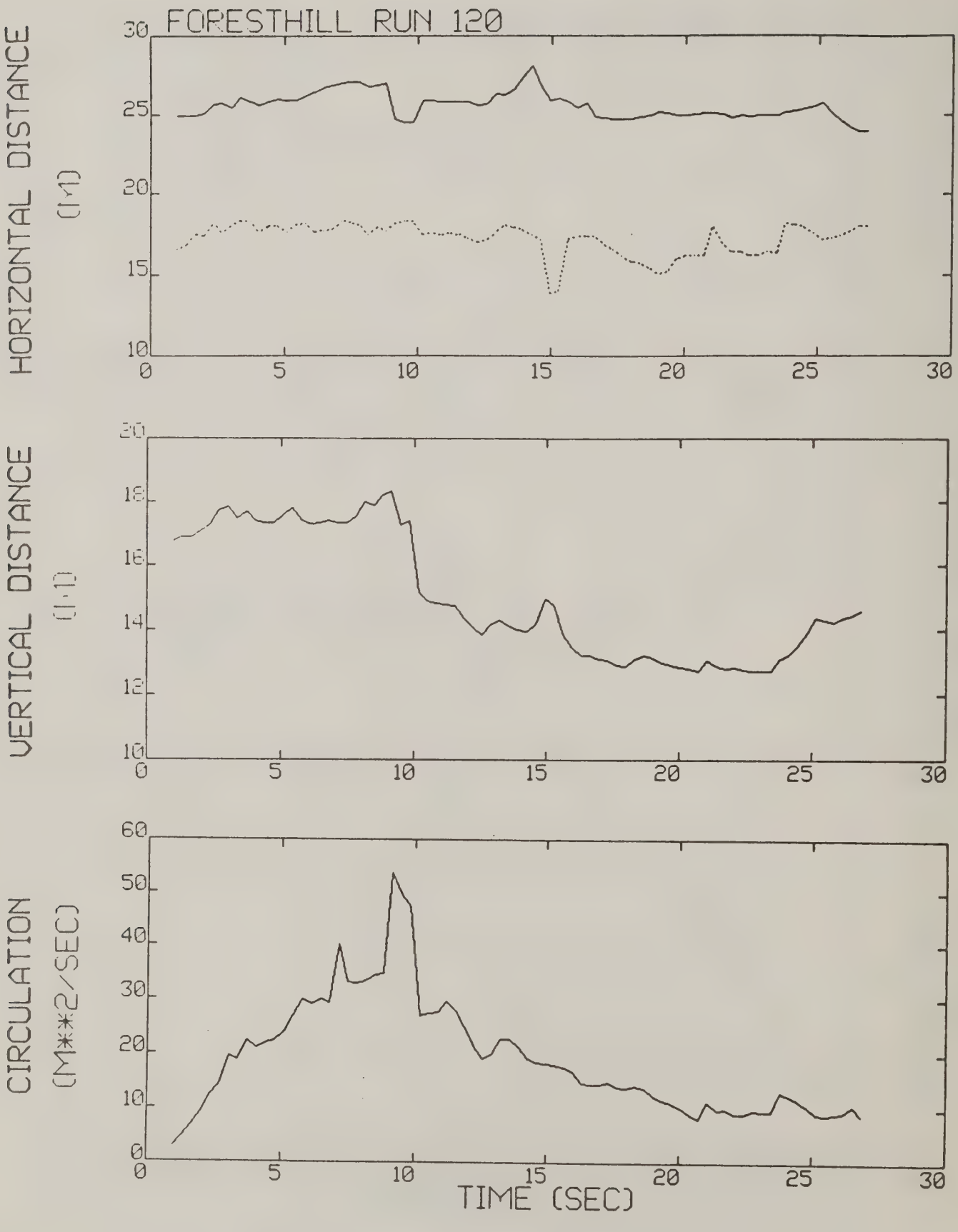

Figure A-91. Foresthill test run 120 generalized algorithm results (*).

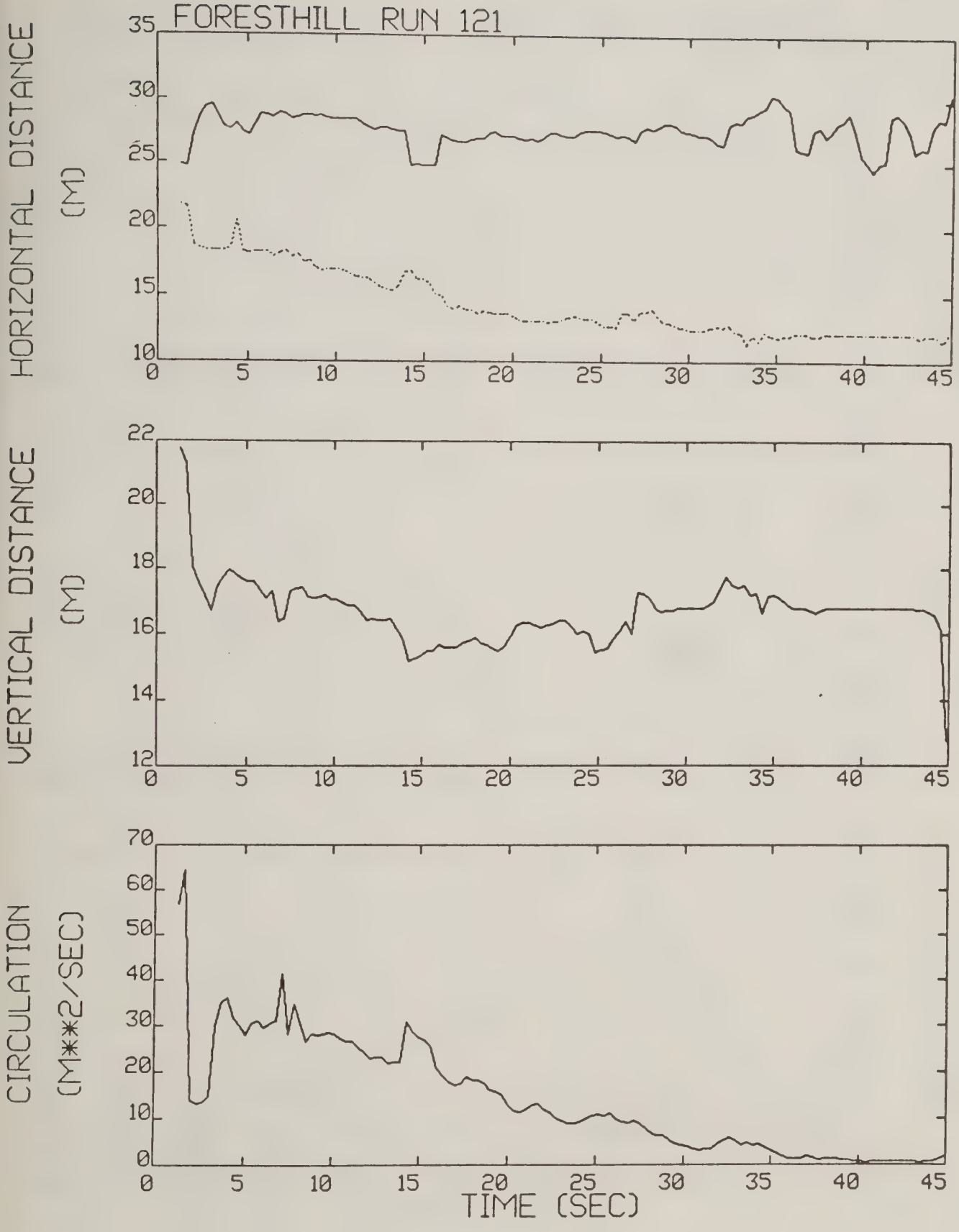

Figure A-92. Foresthill test run 121 generalized algorithm results (*).

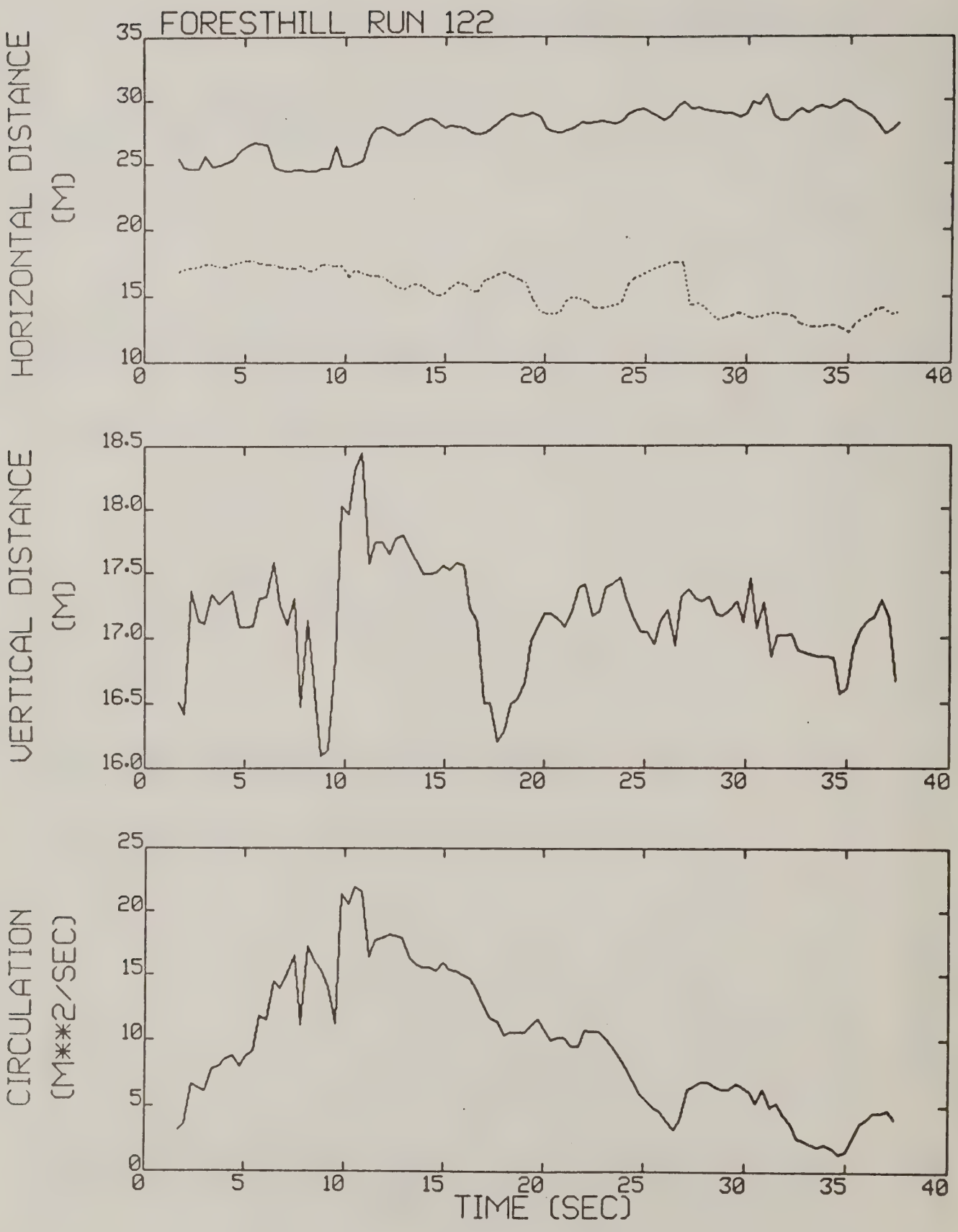

Figure A-93. Foresthill test run 122 generalized algorithm results (*).

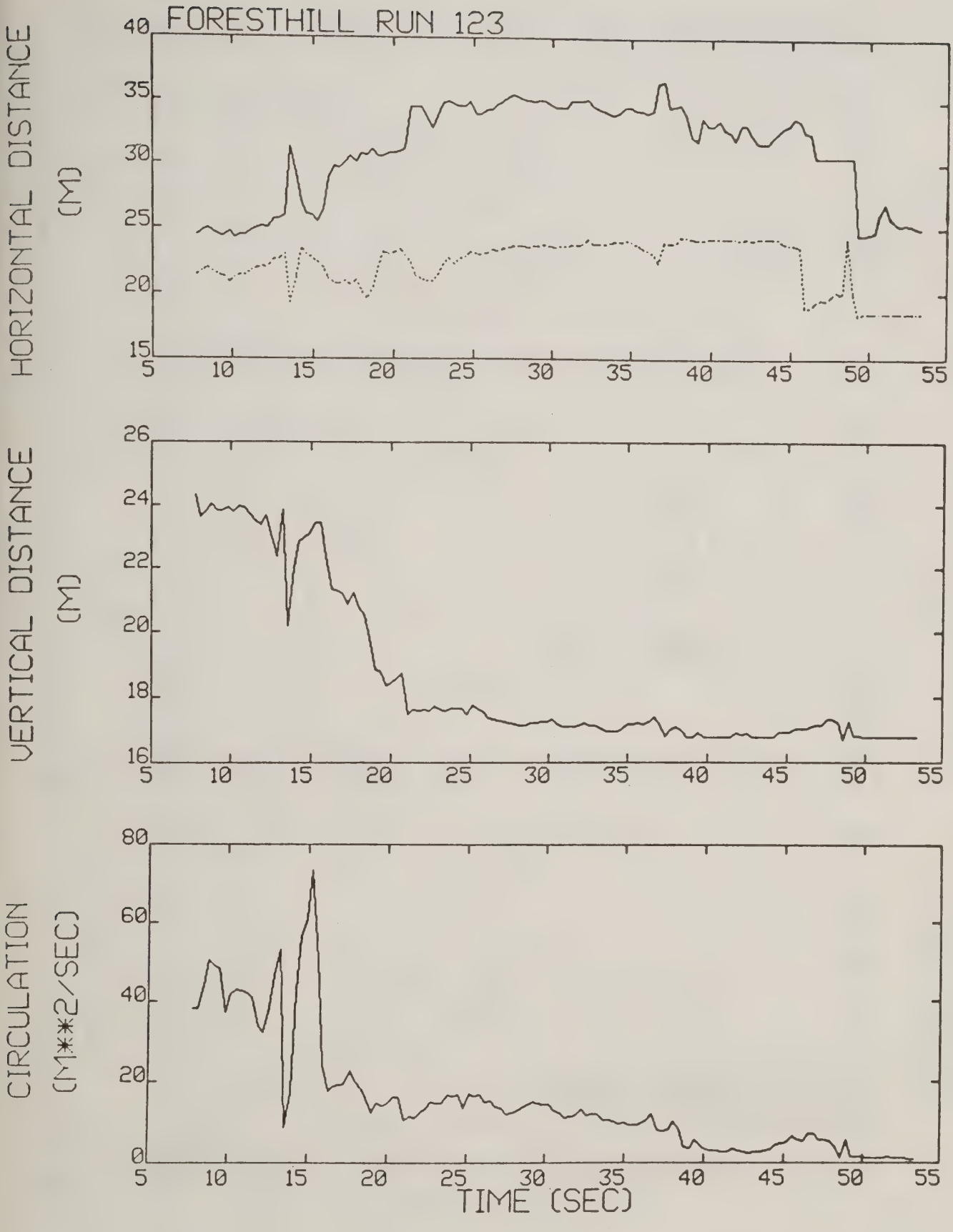

Figure A-94. Foresthill test run 123 generalized algorithm results (*).

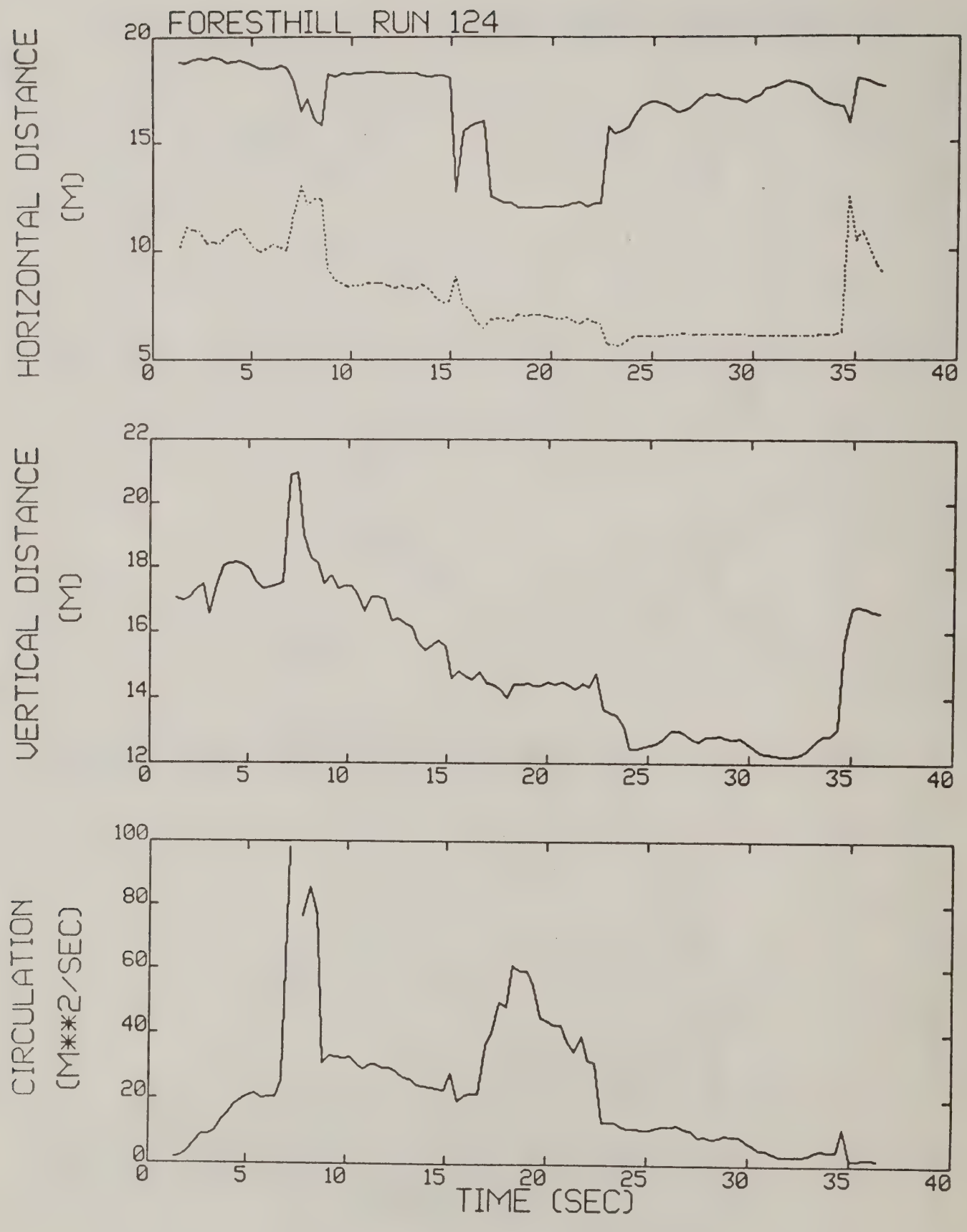

Figure A-95. Foresthill test run 124 generalized algorithm results.

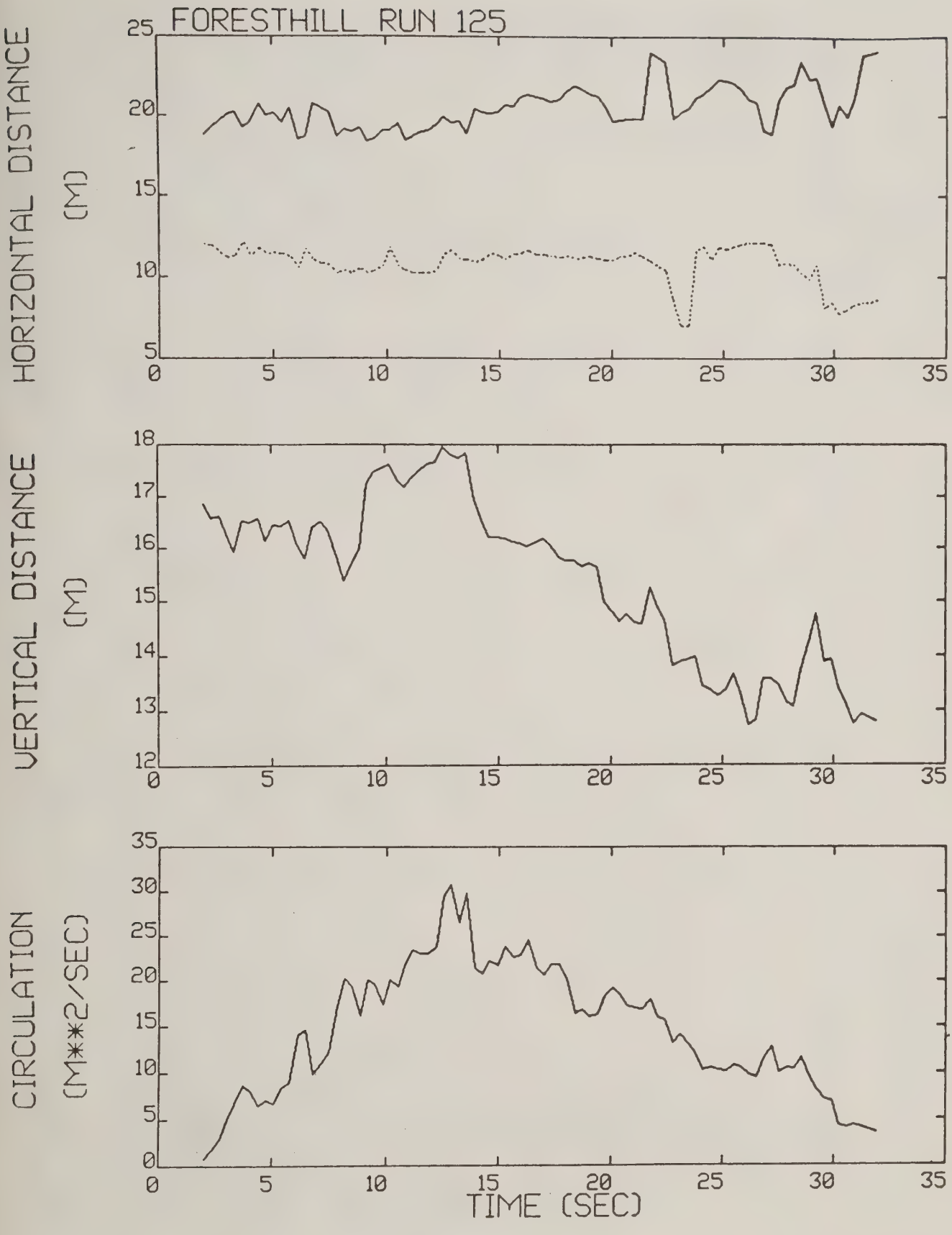

Figure A-96. Foresthill test run 125 generalized algorithm results (*).

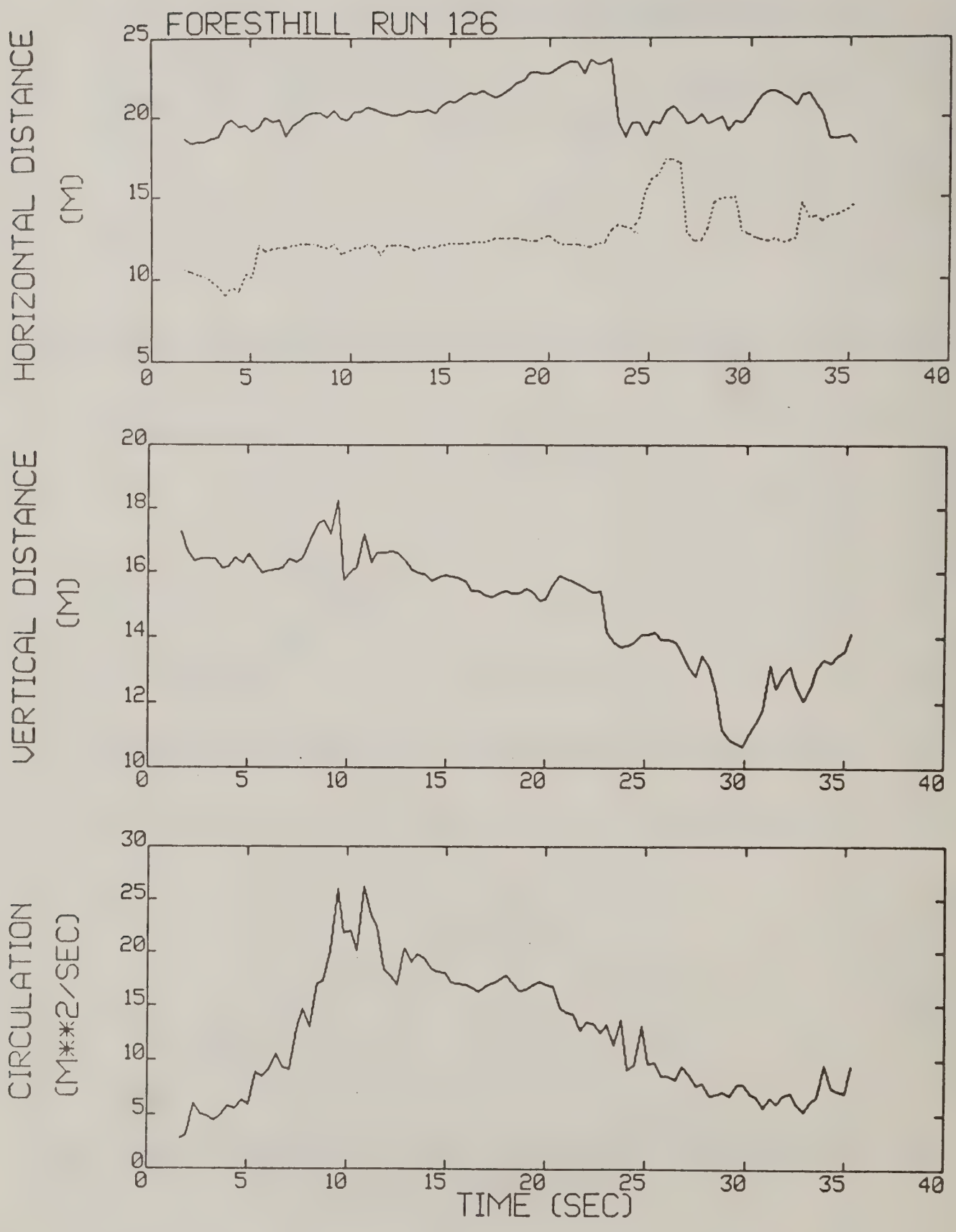

Figure A-97. Foresthill test run 126 generalized algorithm results (*).

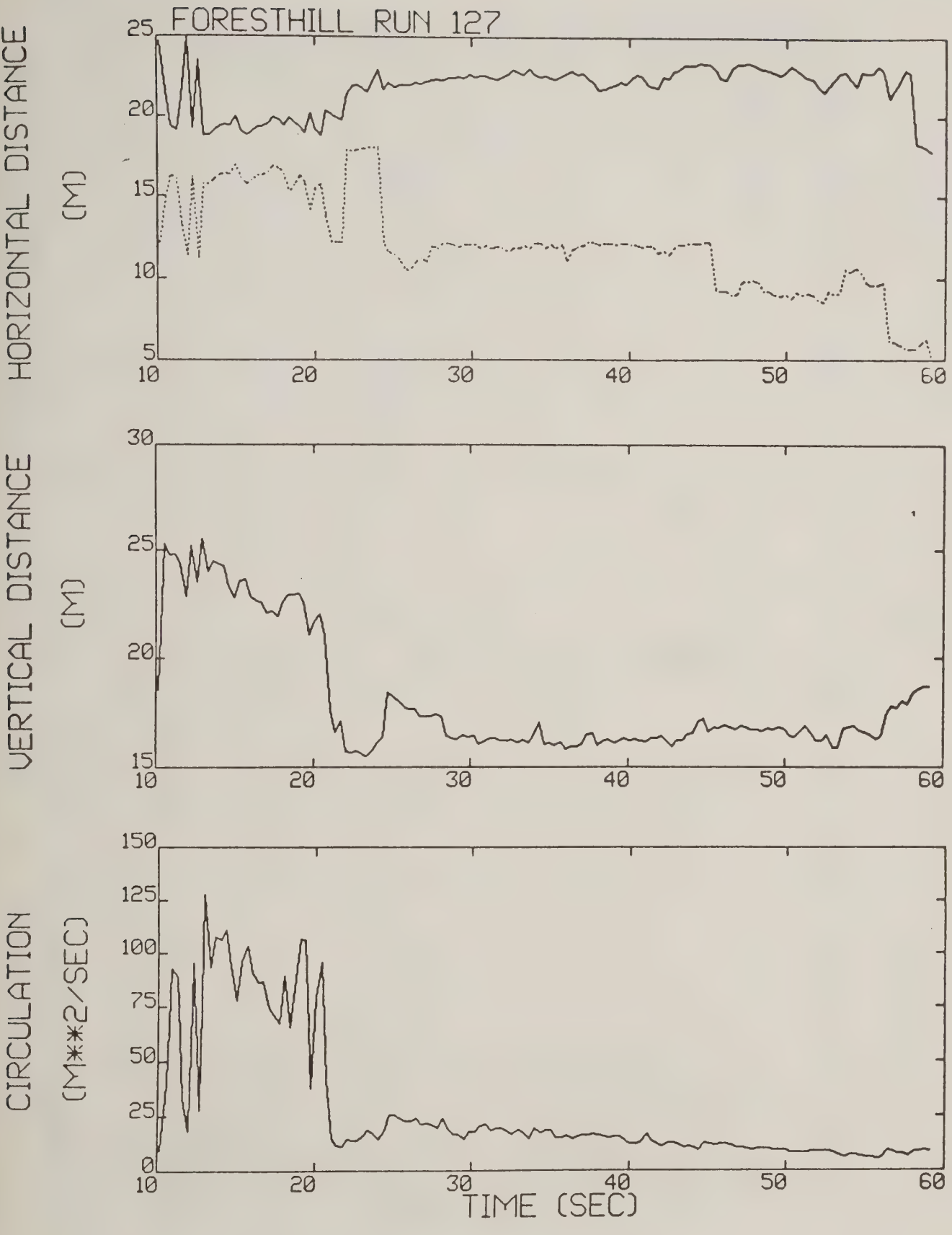

Figure A-98. Foresthill test run 127 generalized algorithm results (*).

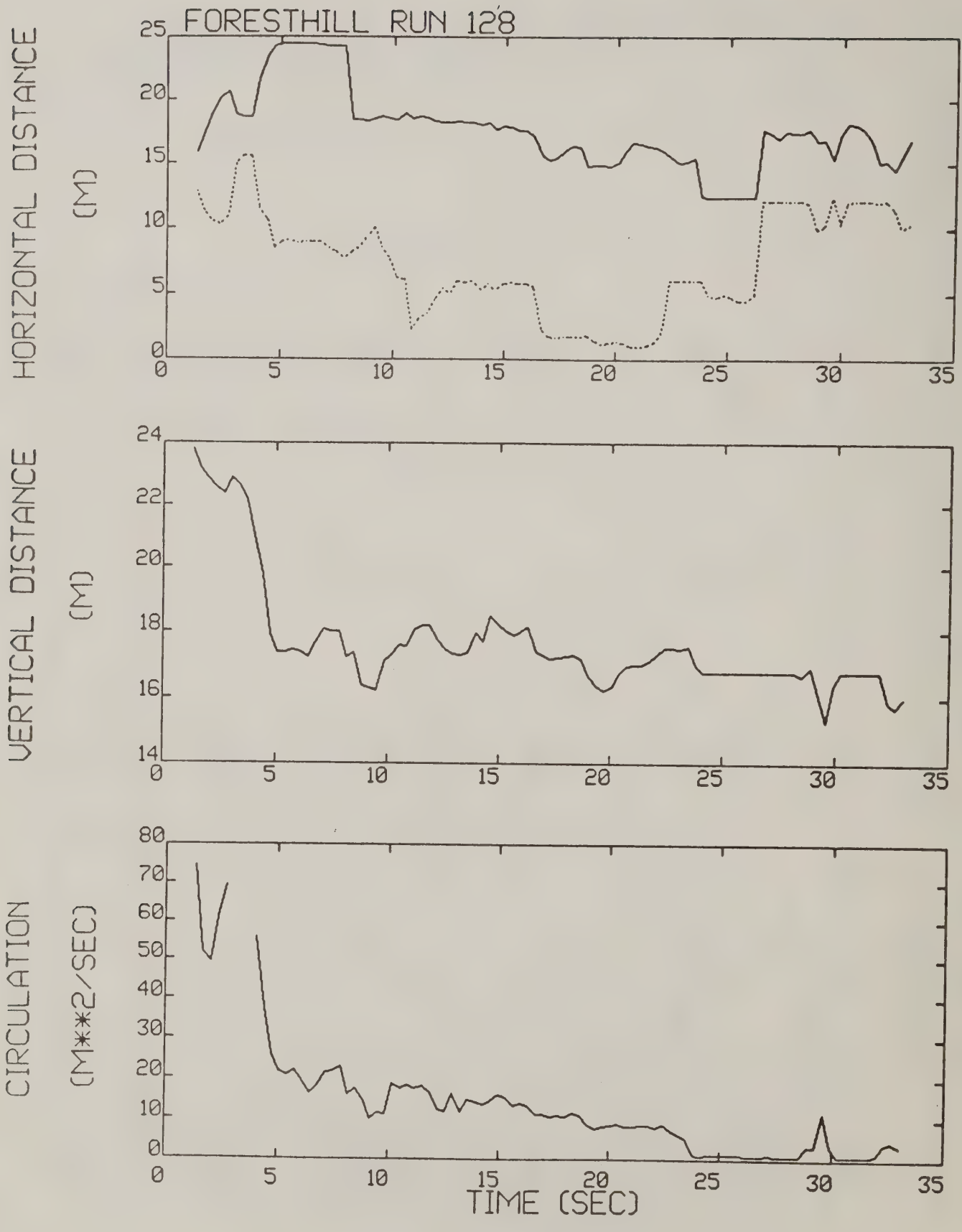

Figure A-99. Foresthill test run 128 generalized algorithm results (*).

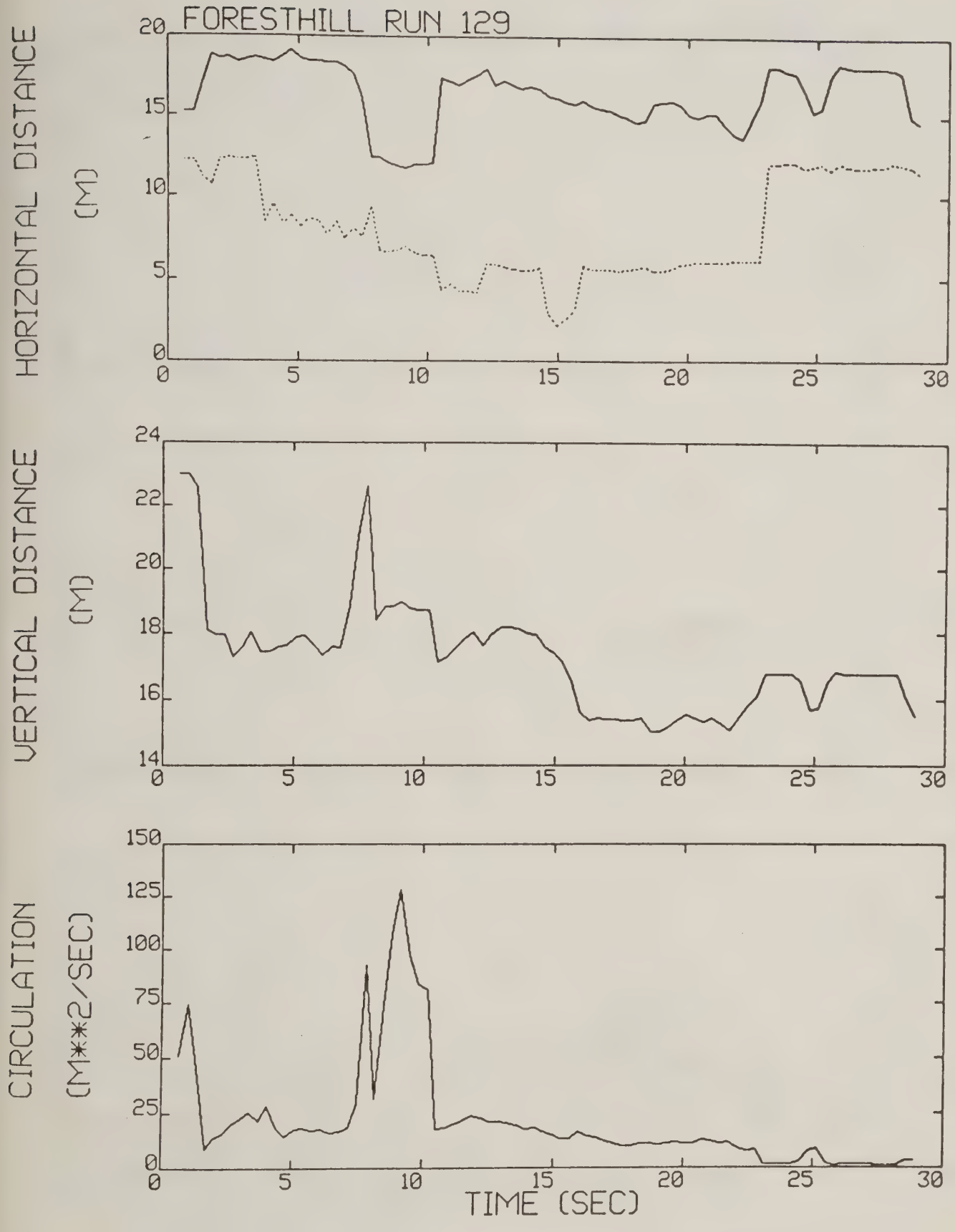

Figure A-100. Foresthill test run 129 generalized algorithm results.

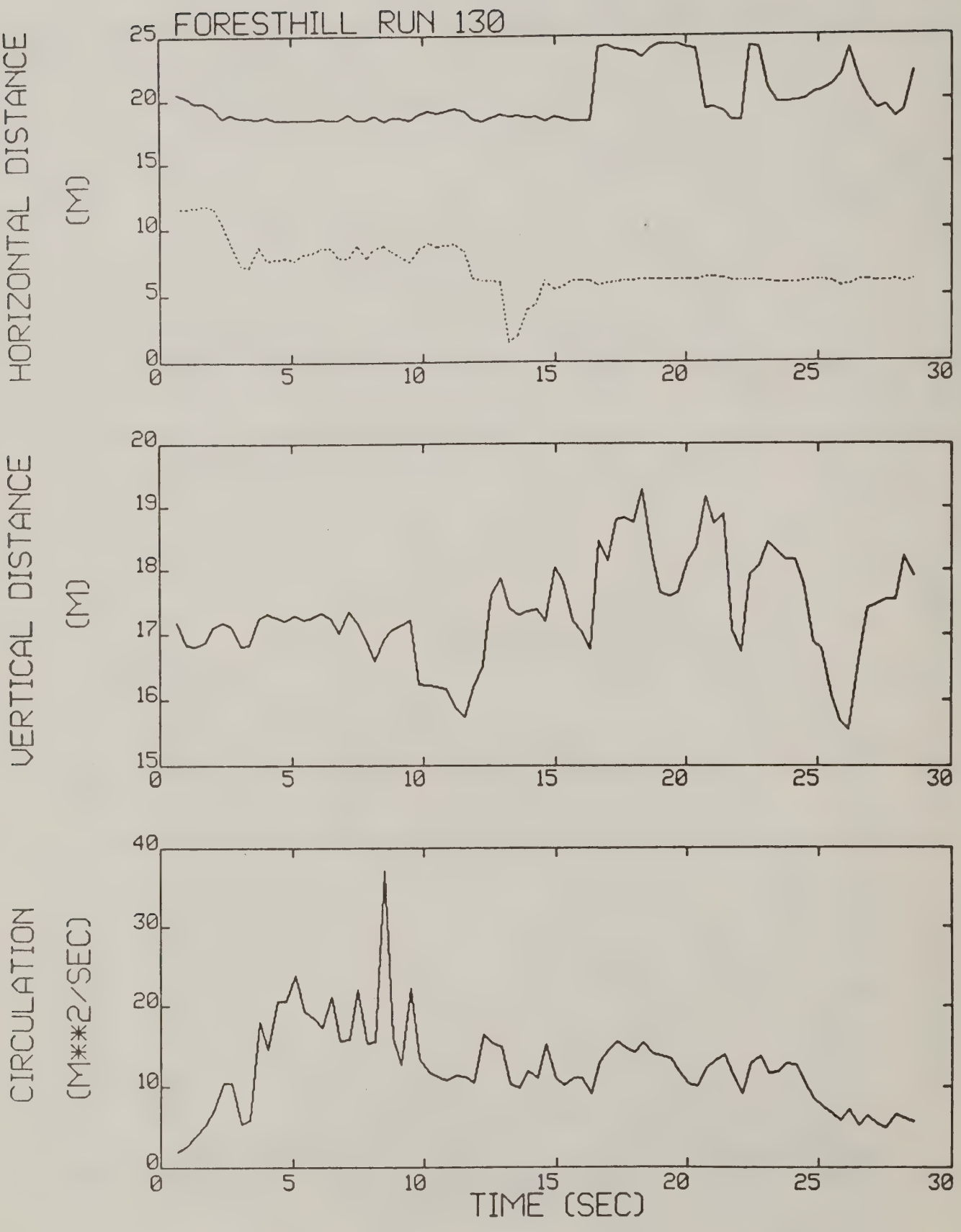

Figure A-101. Foresthill test run 130 generalized algorithm results.

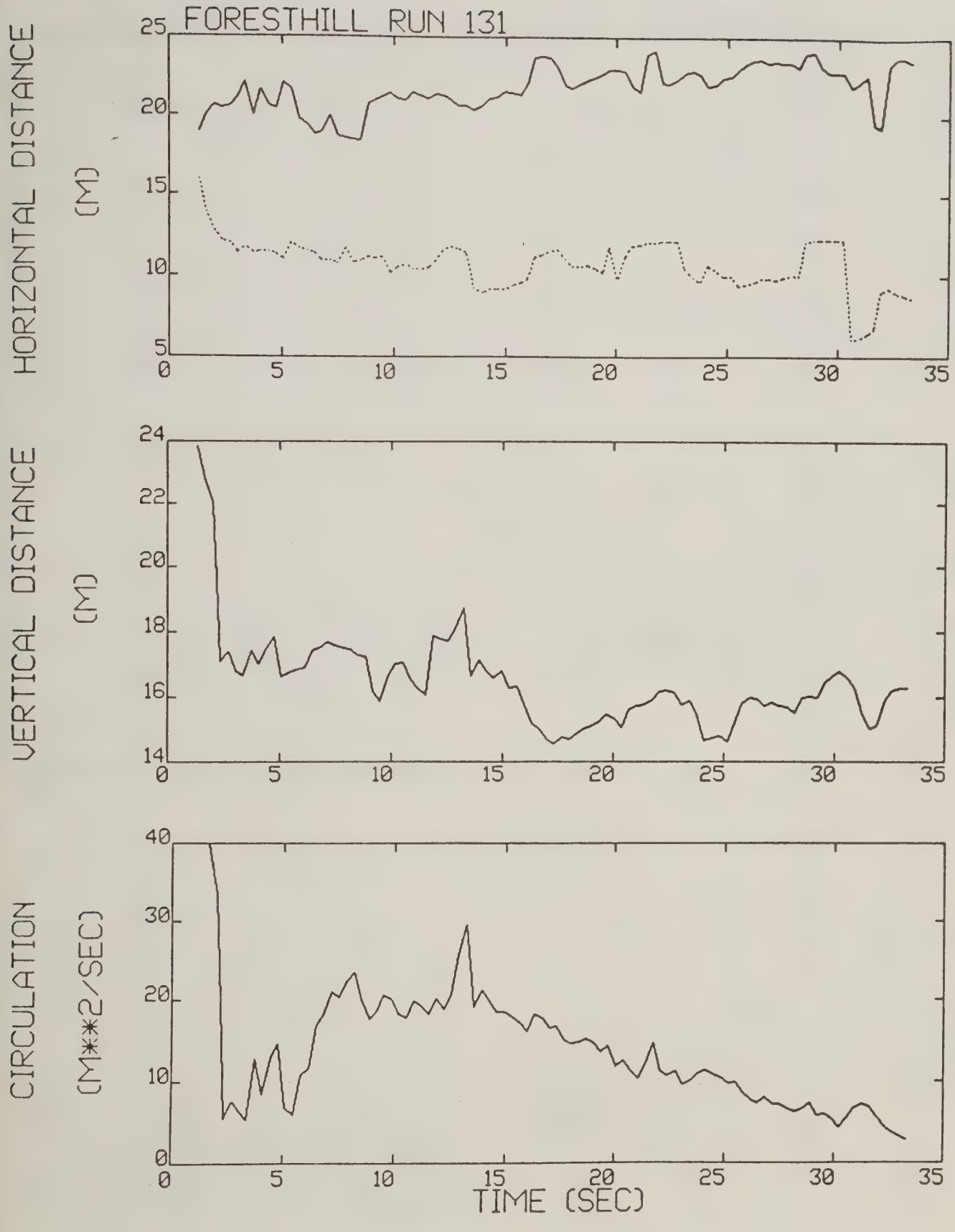

Figure A-102. Foresthill test run 131 generalized algorithm results (*).

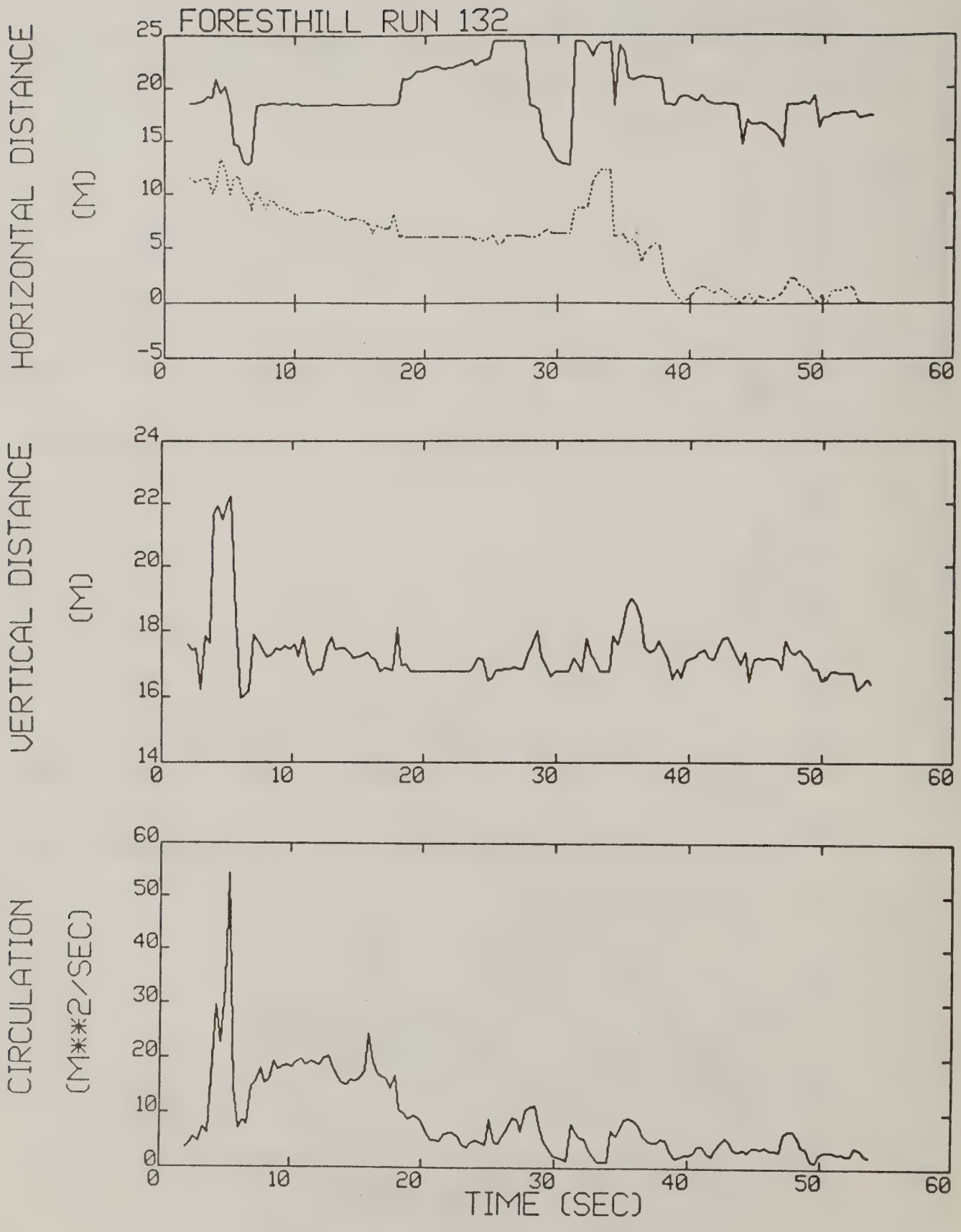

Figure A-103. Foresthill test run 132 generalized algorithm results.

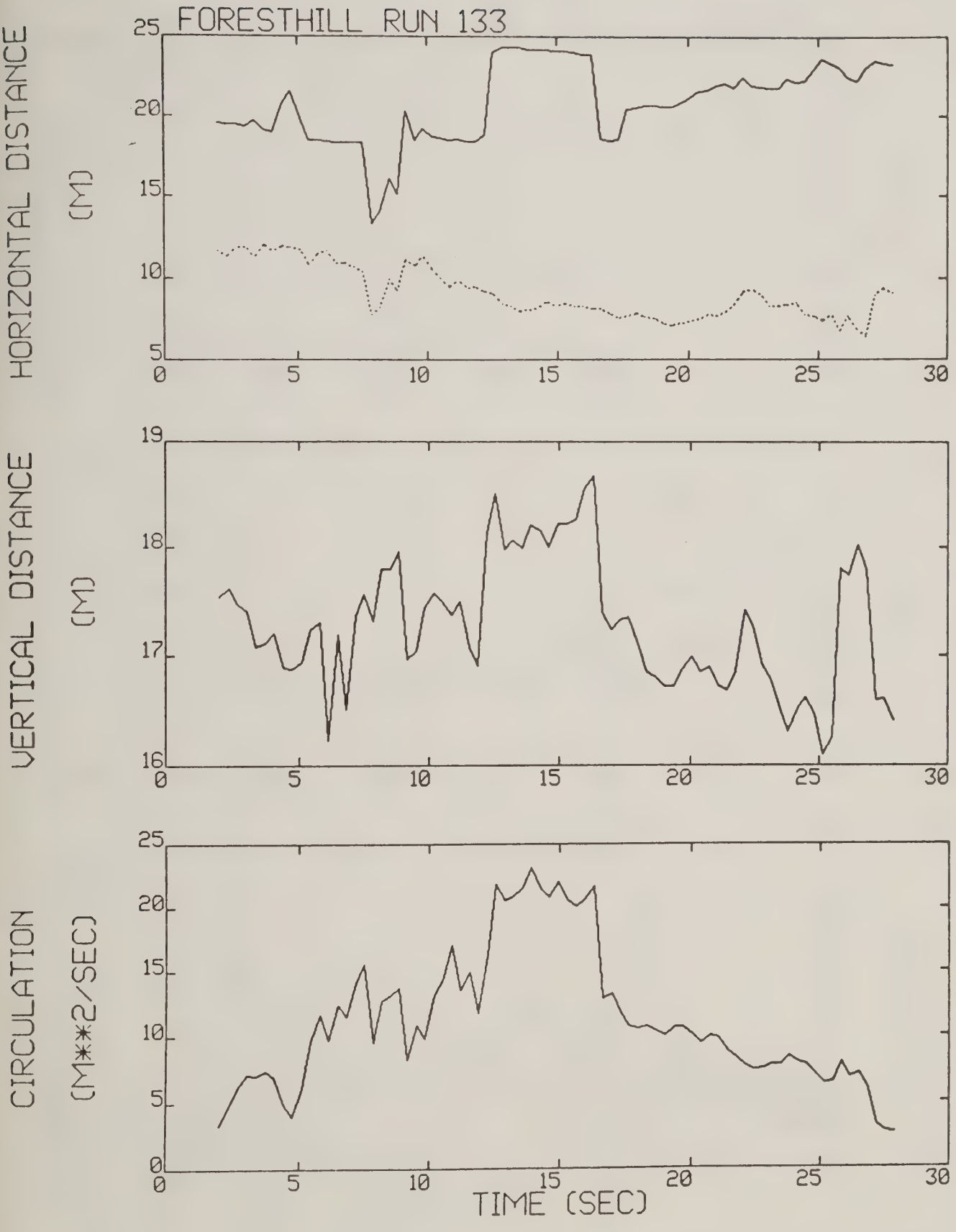

Figure A-104. Foresthill test run 133 generalized algorithm results.

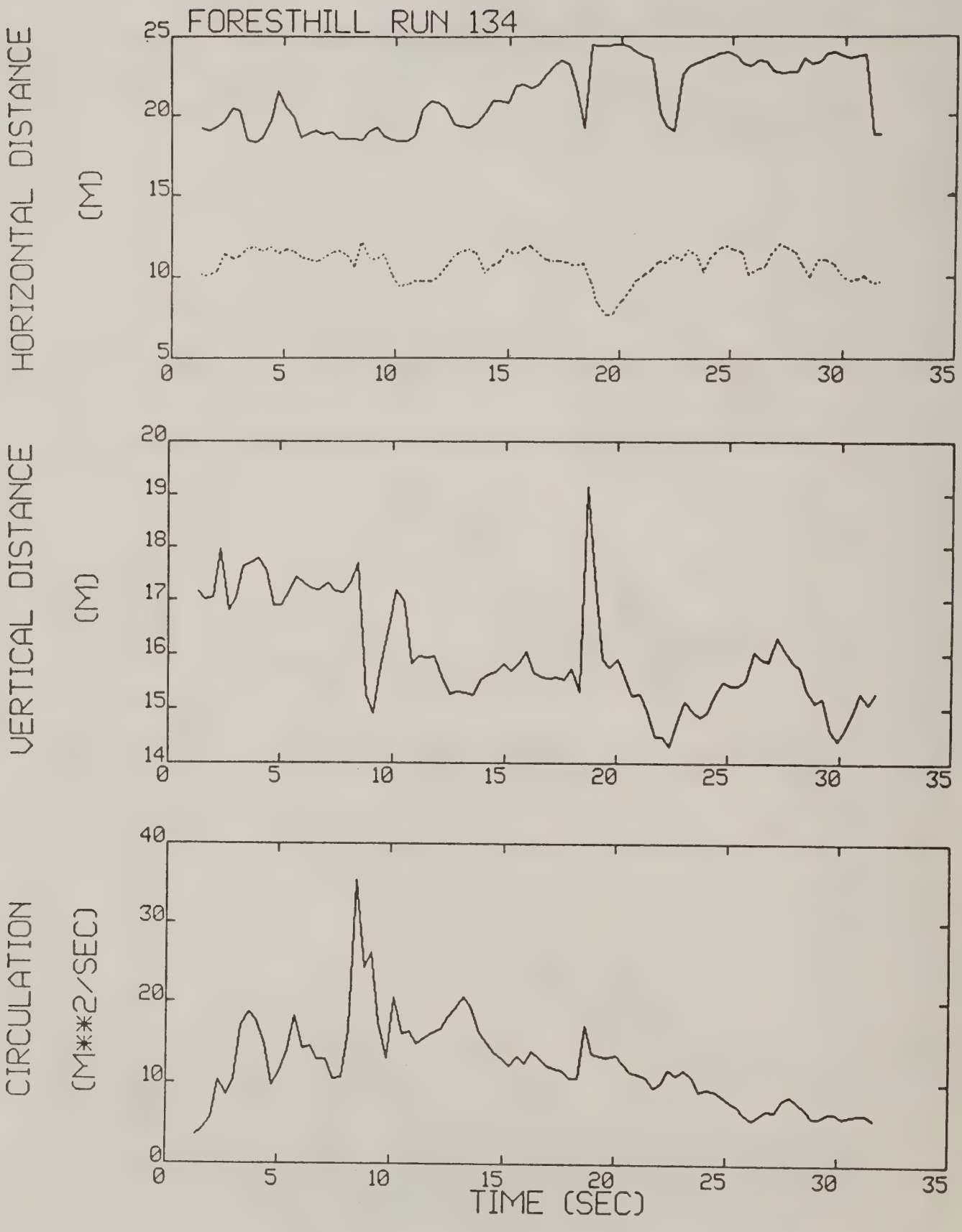

Figure A-105. Foresthill test run 134 generalized algorithm results (*).

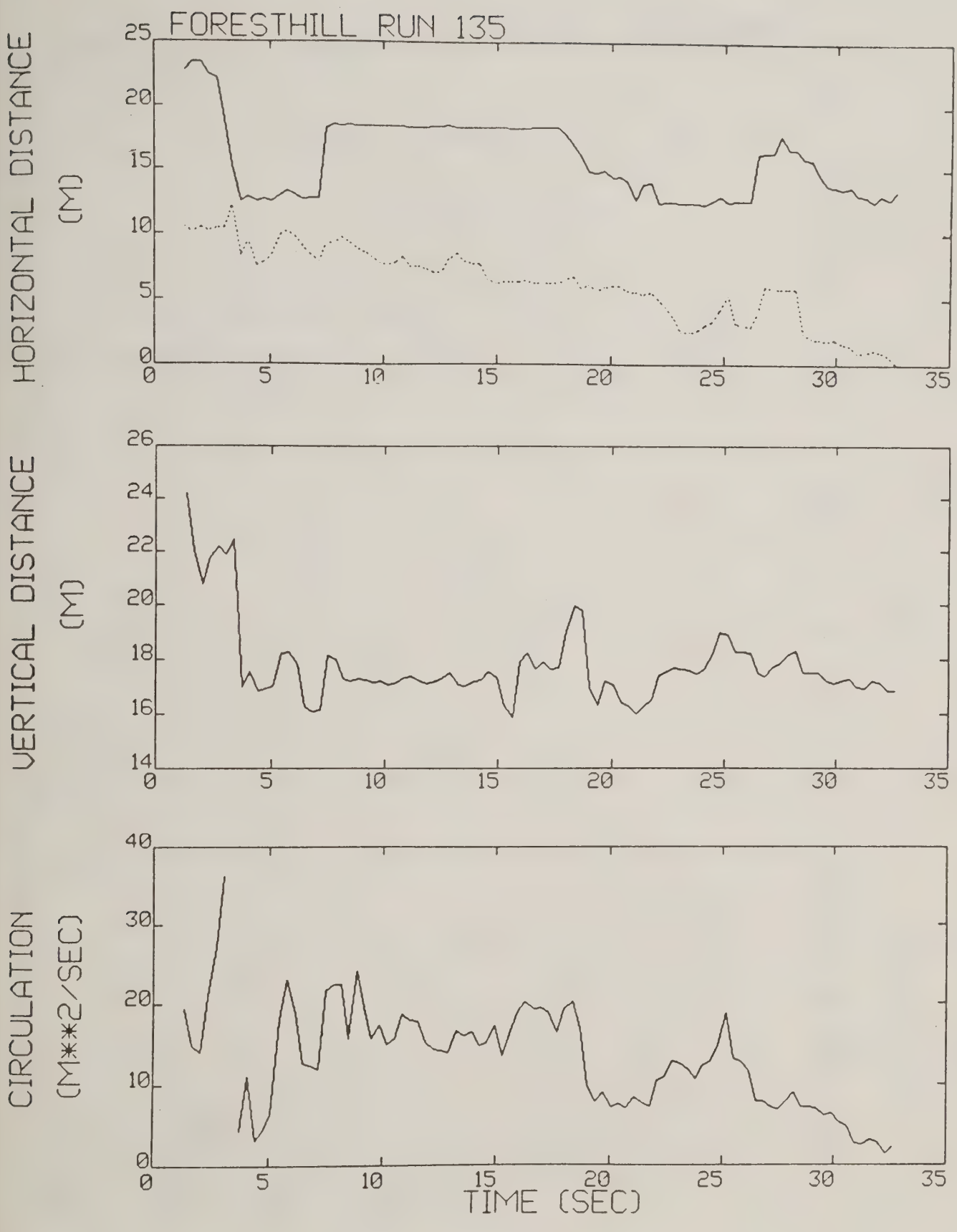

Figure A-106. Foresthill test run 135 generalized algorithm results (*).

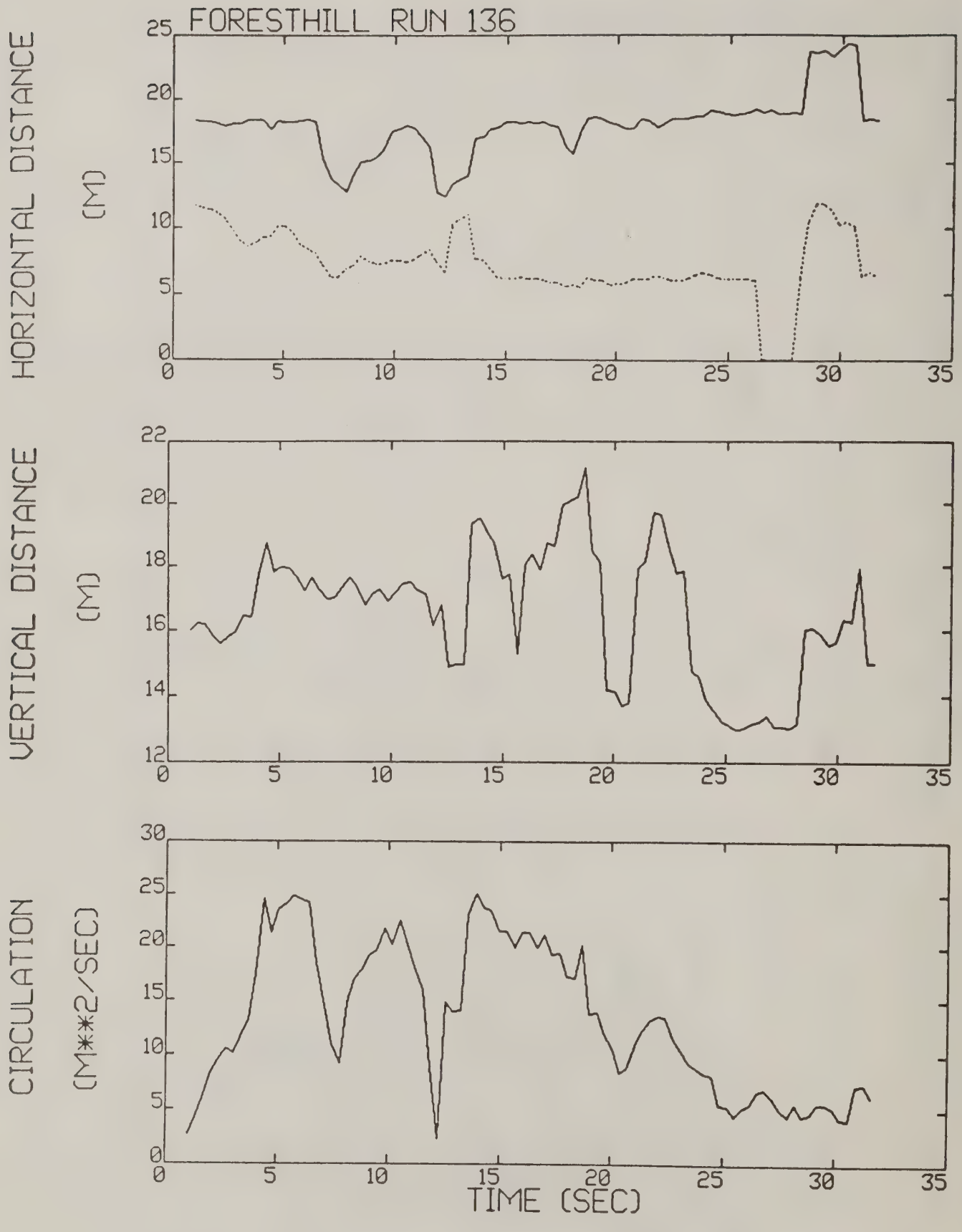

Figure A-107. Foresthill test run 136 generalized algorithm results (*).

APPENDIX B

Chico Reduced Plots

Generalized algorithm results for Program WIND Phase I at Chico are plotted on the following pages in the same format as discussed in Appendix A.

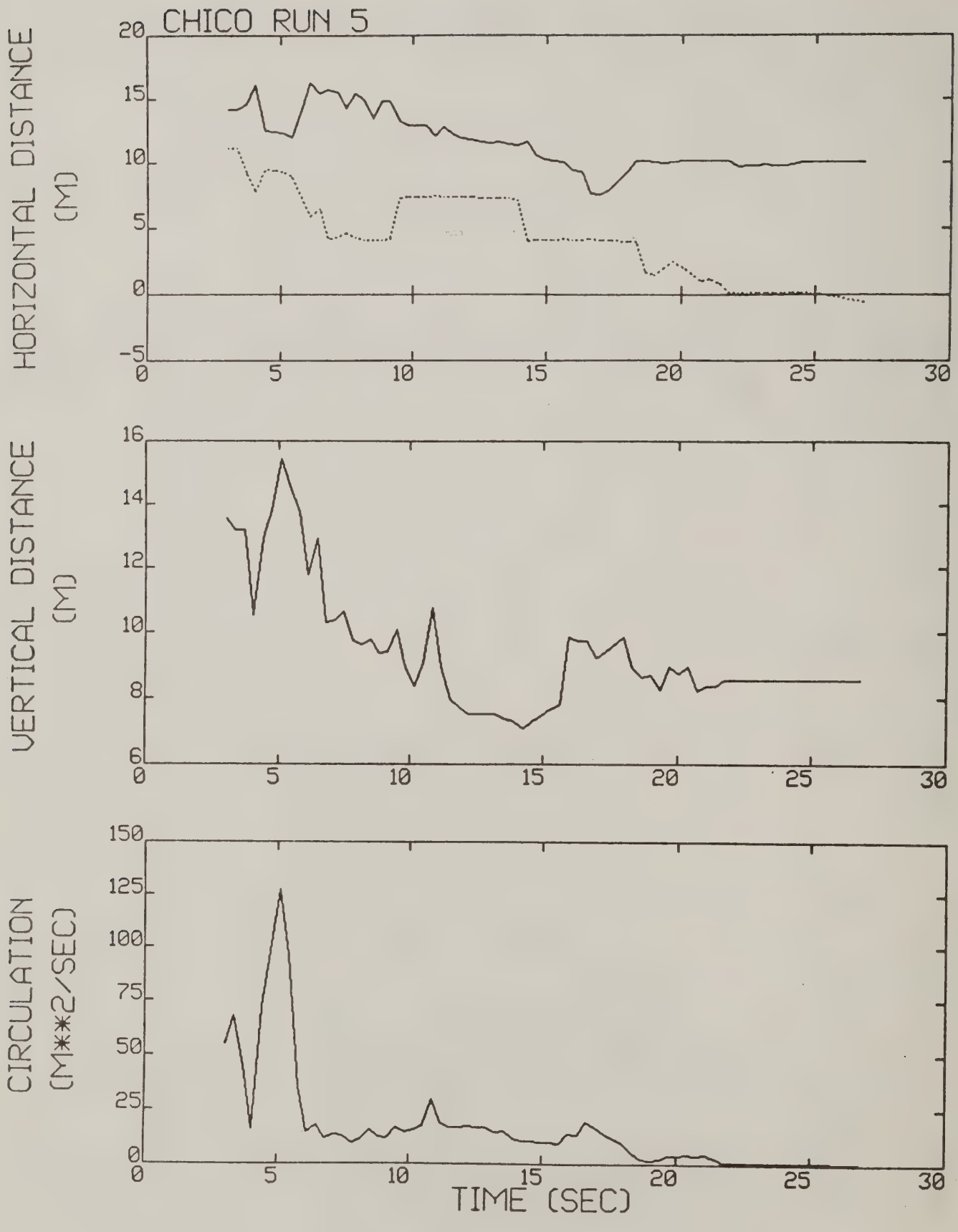

Figure B-1. Chico test run 5 generalized algorithm results.

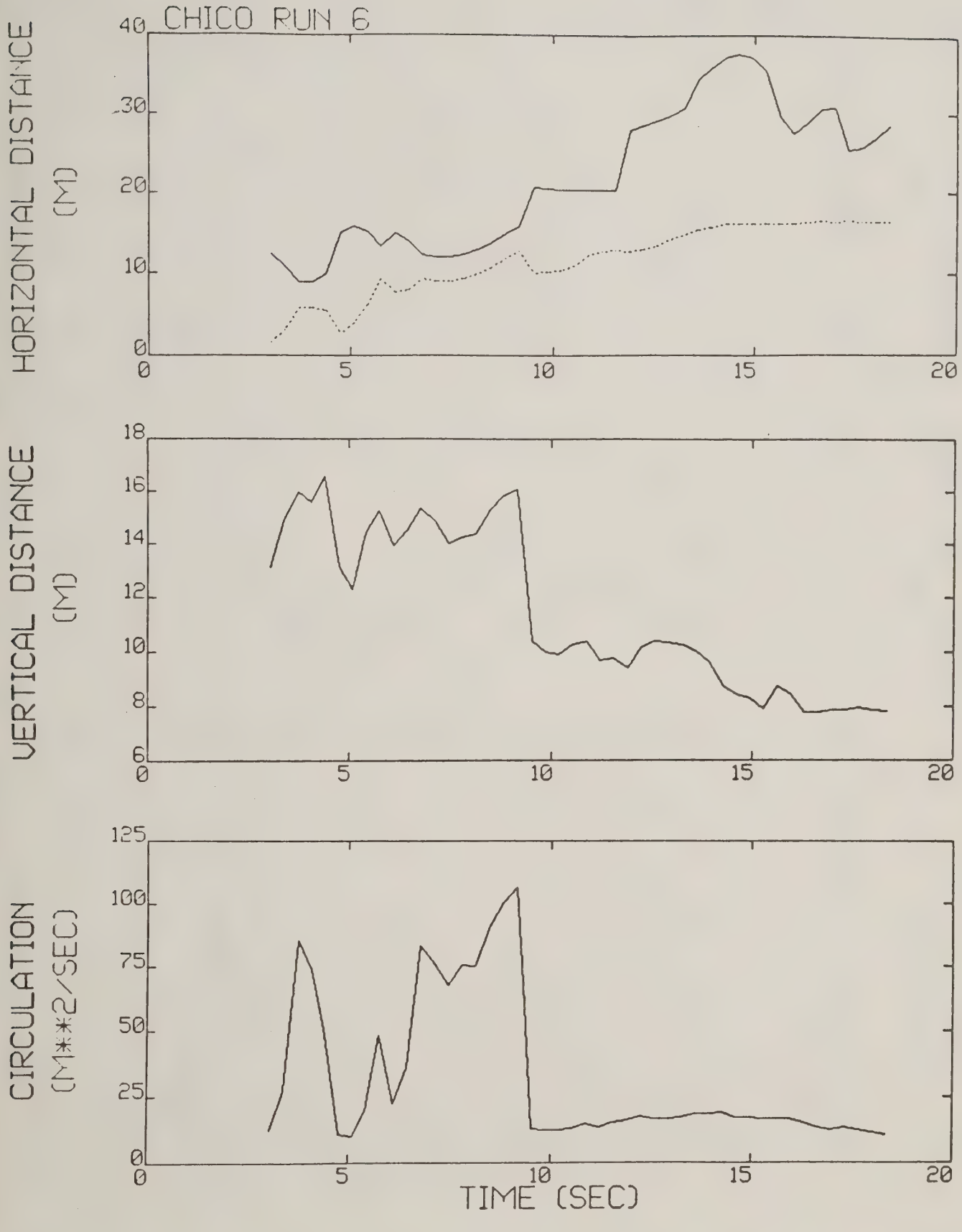

Figure B-2. Chico test run 6 generalized algorithm results.

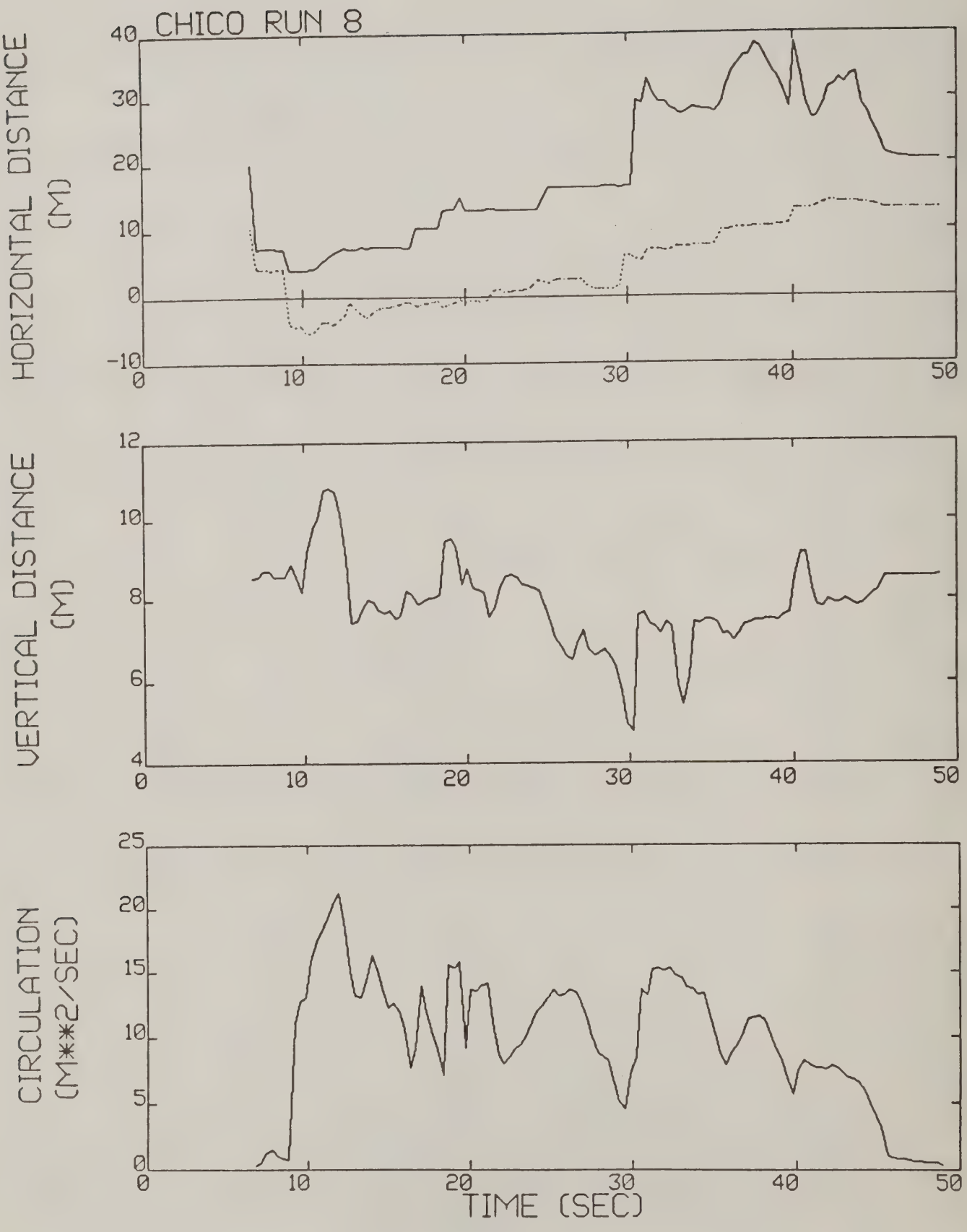

Figure B-3. Chico test run 8 generalized algorithm results (*).

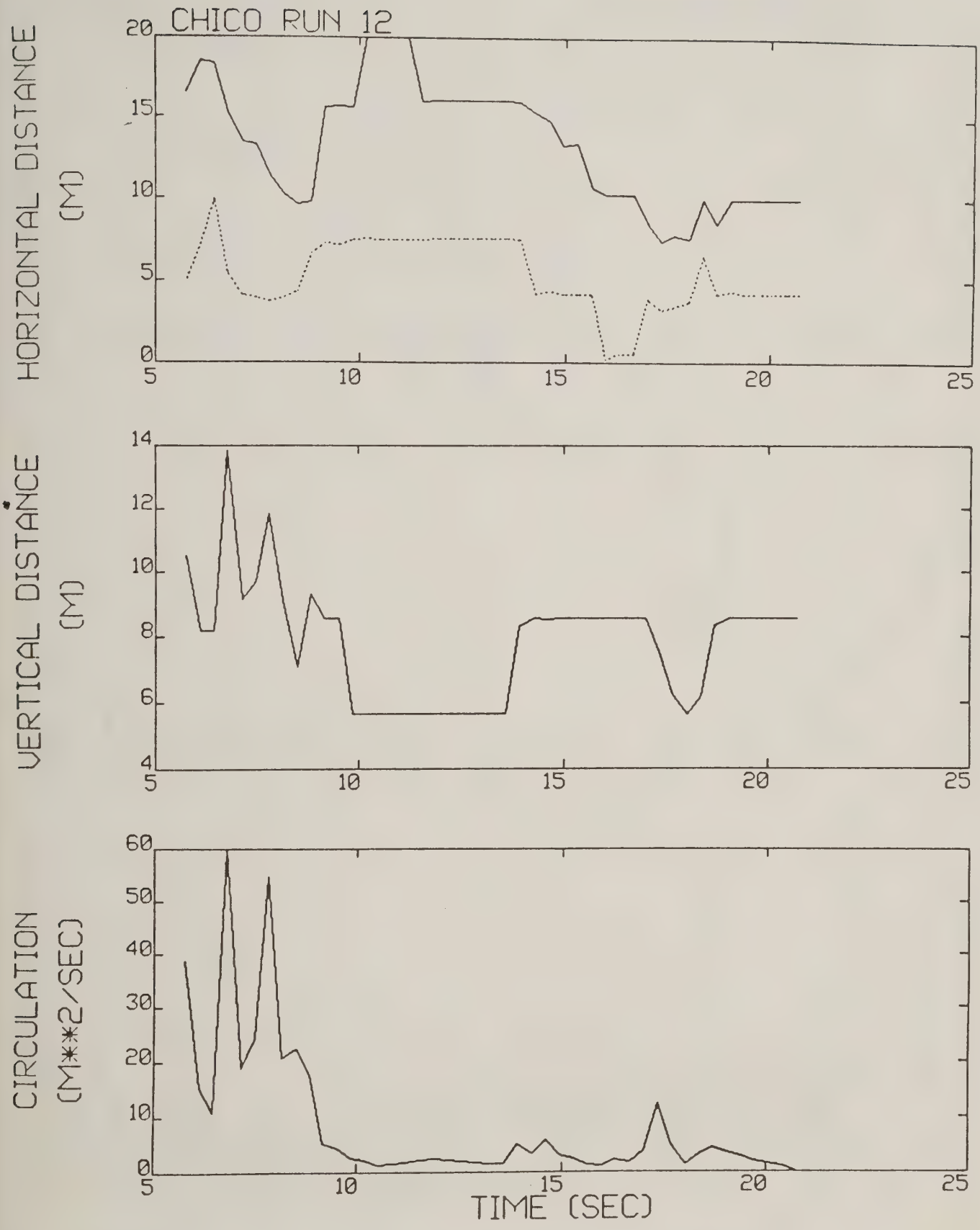

Figure B-4. Chico test run 12 generalized algorithm results.

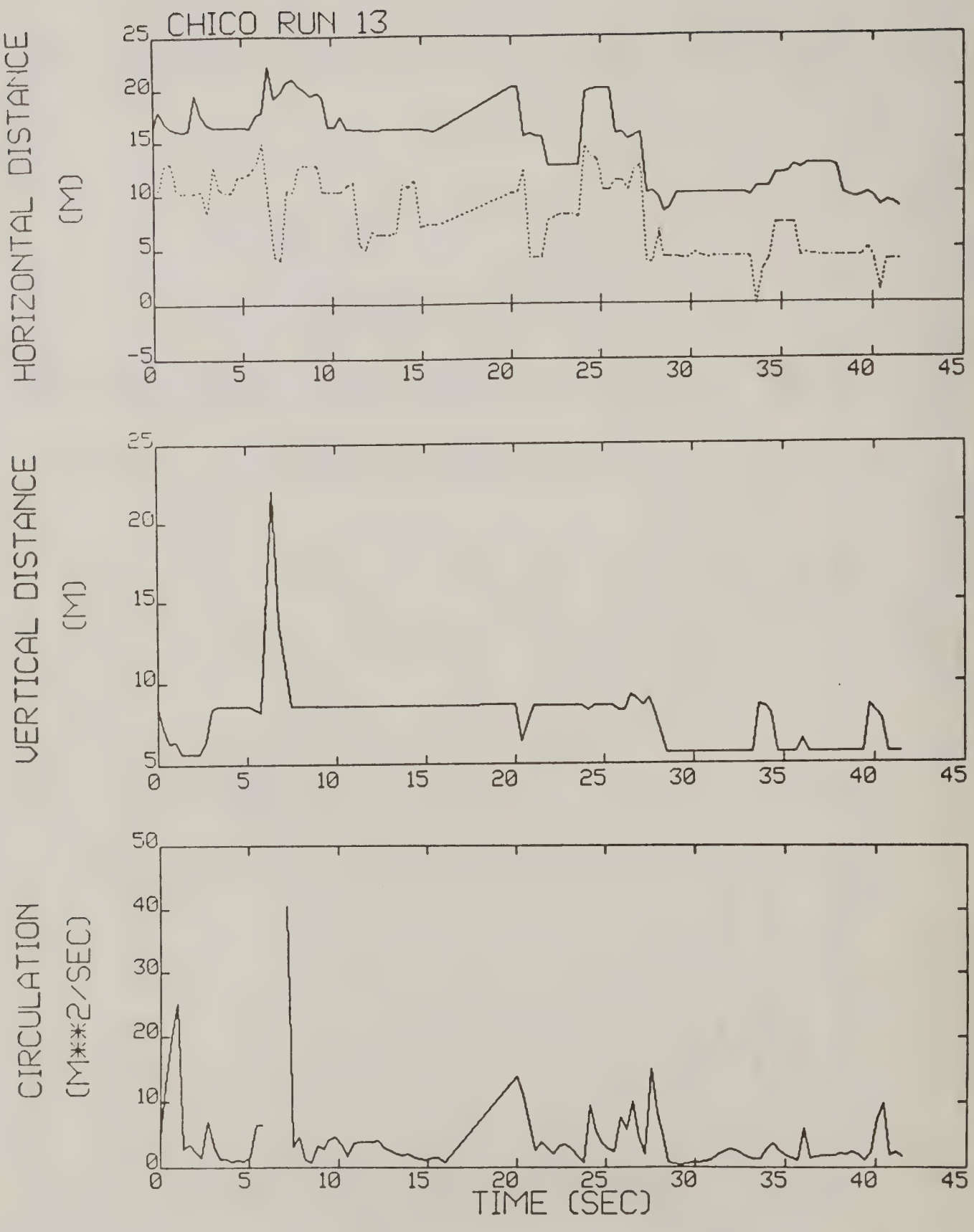

Figure B-5. Chico test run 13 generalized algorithm results.

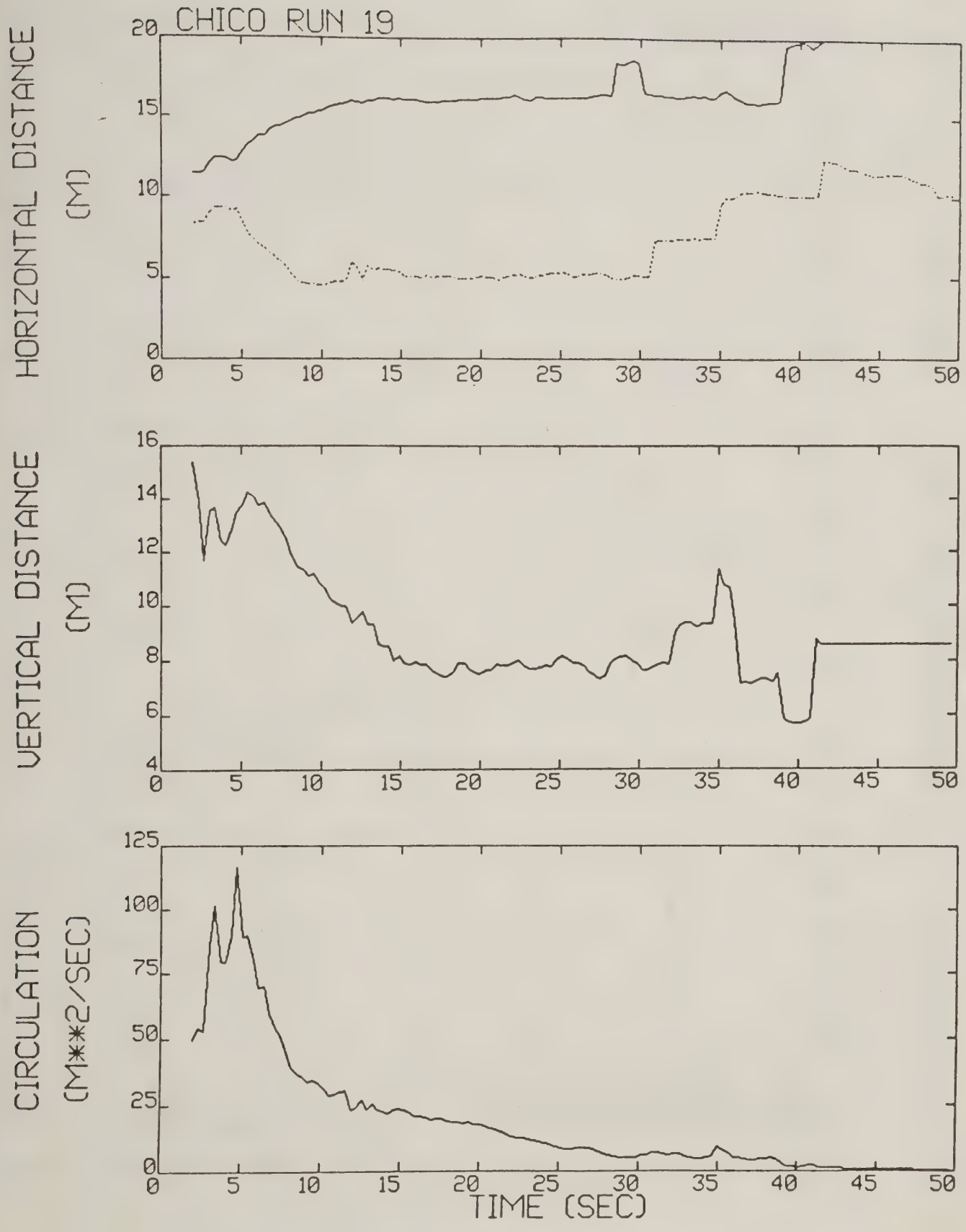

Figure B-6. Chico test run 19 generalized algorithm results (*).

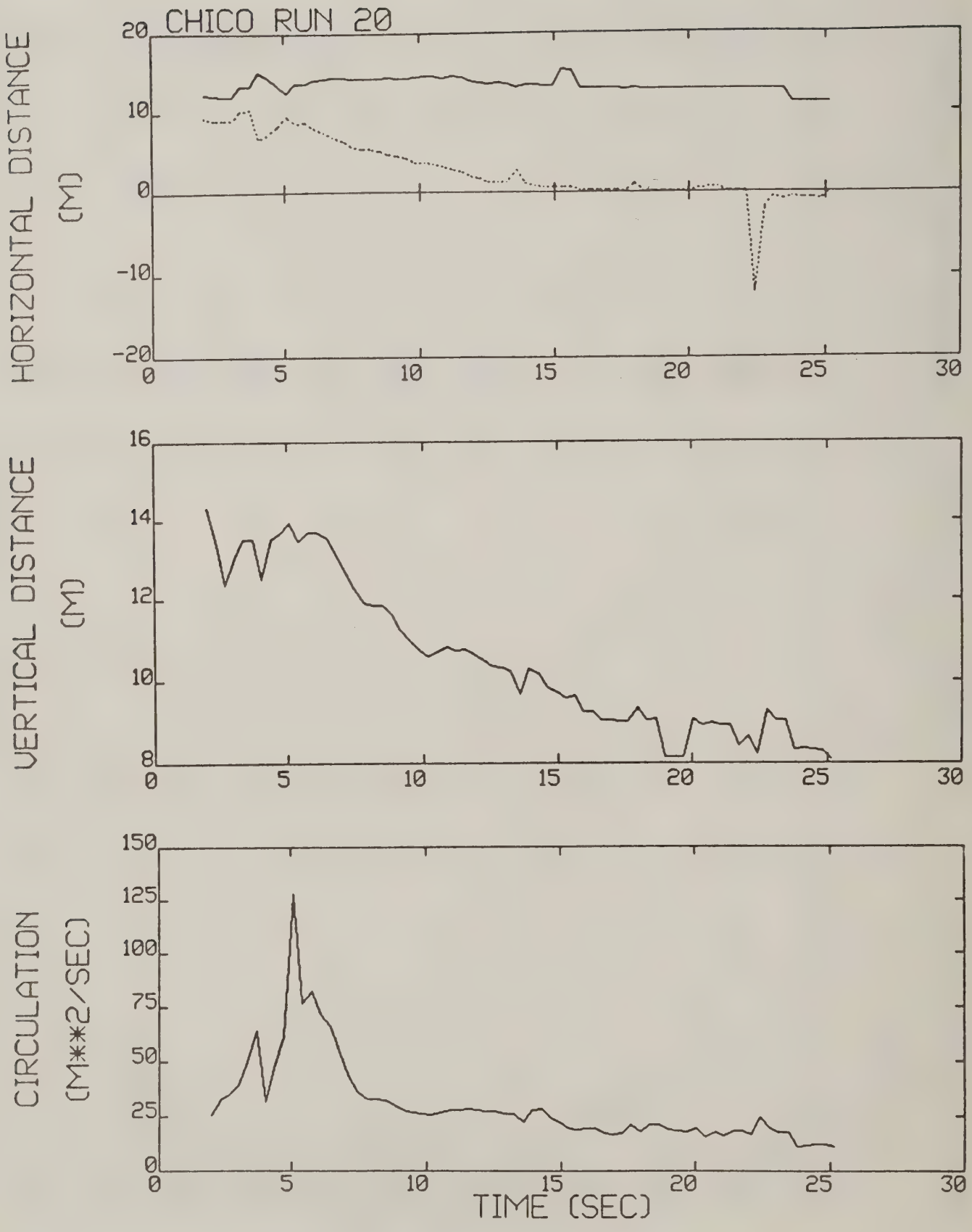

Figure B-7. Chico test run 20 generalized algorithm results (*).

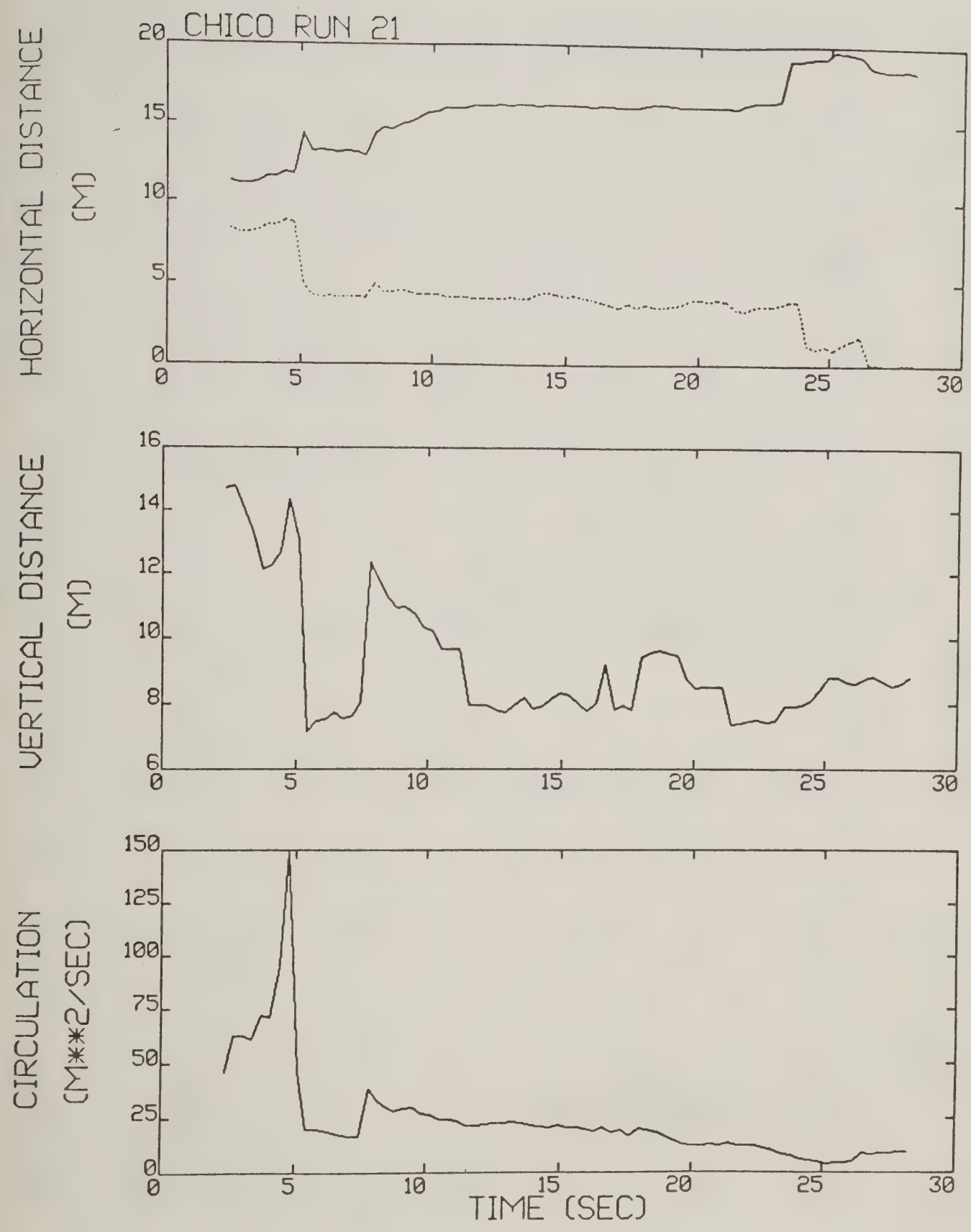

Figure B-8. Chico test run 21 generalized algorithm results.

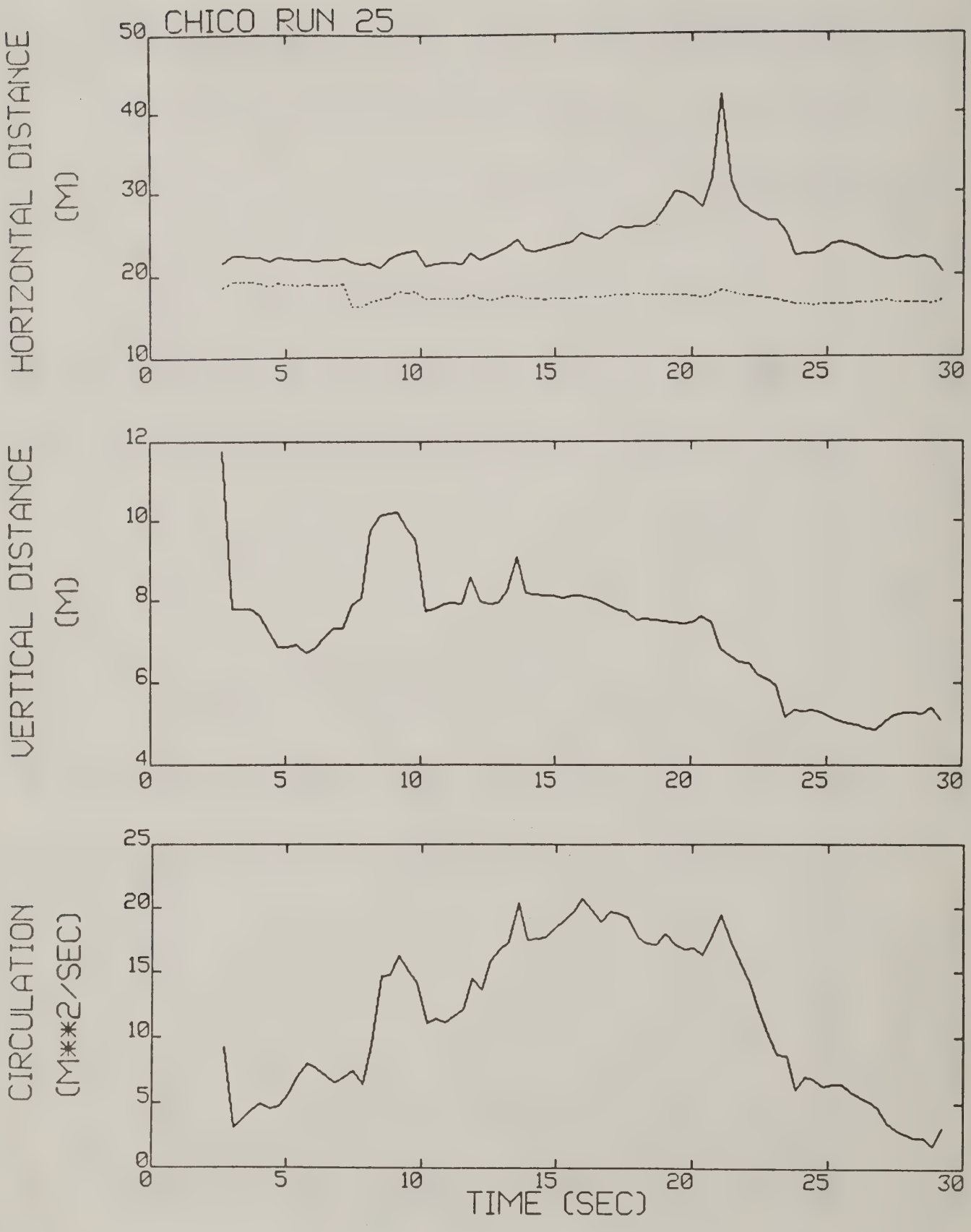

Figure B-9. Chico test run 25 generalized algorithm results.

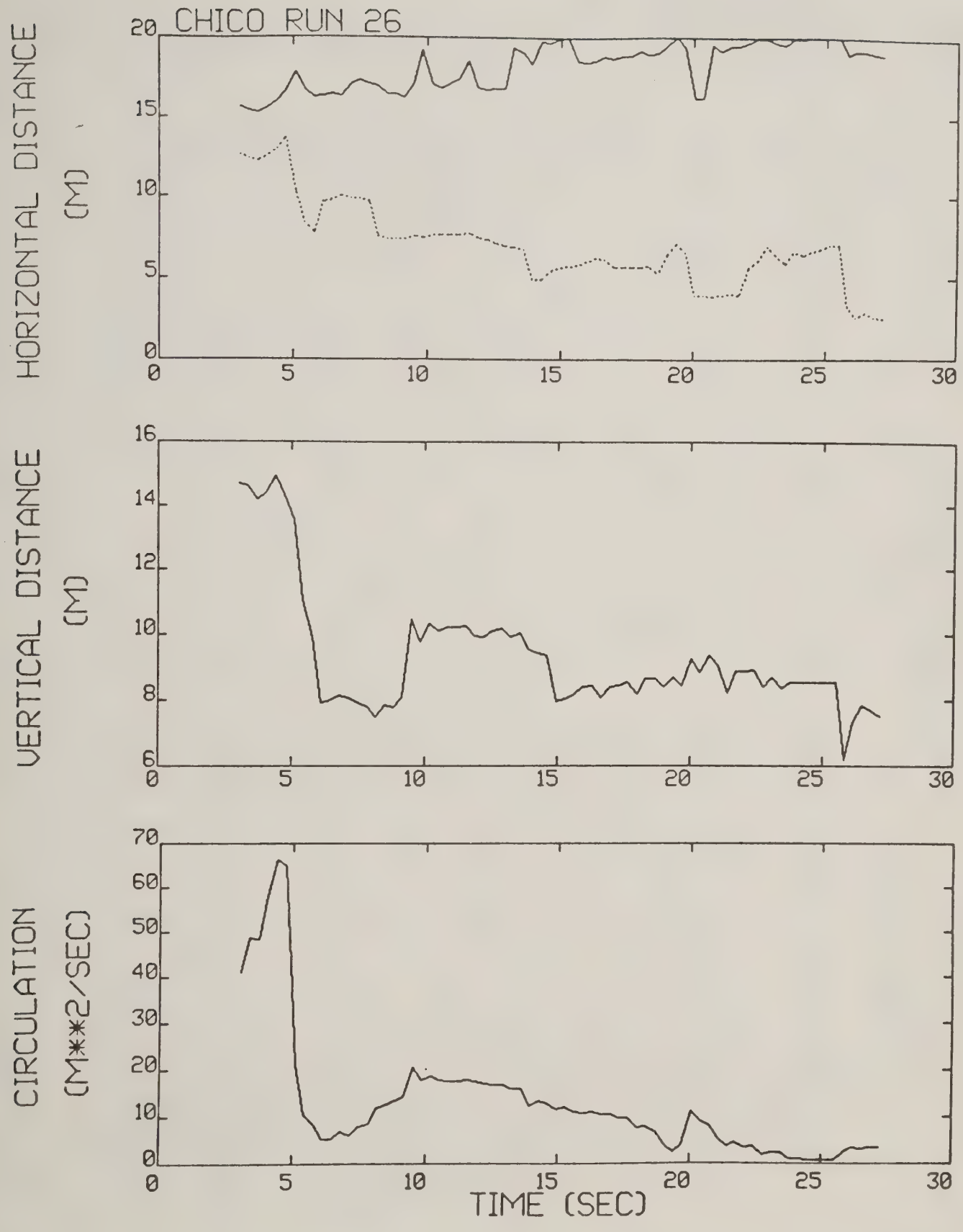

Figure B-10. Chico test run 26 generalized algorithm results (*).

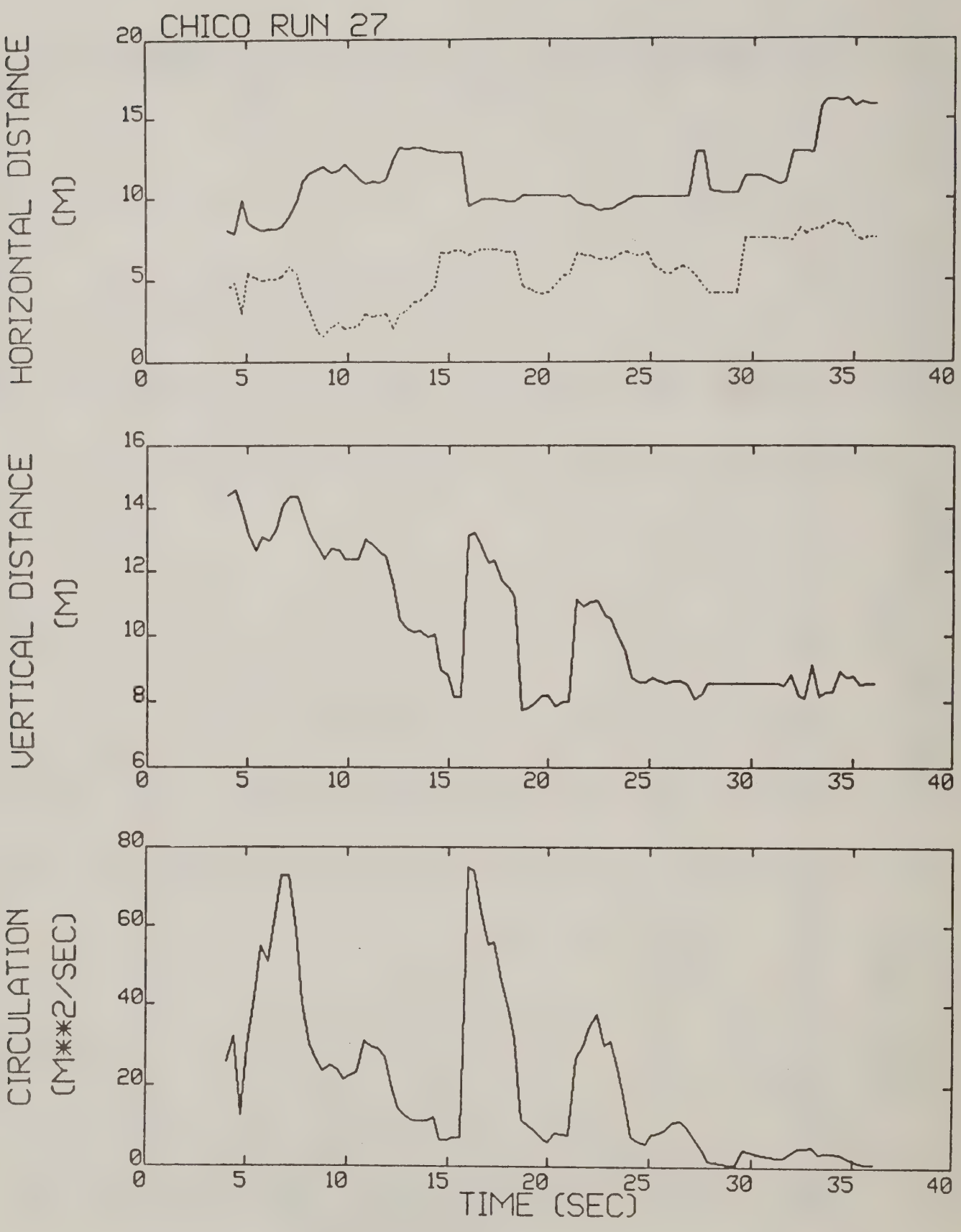

Figure B-11. Chico test run 27 generalized algorithm results (*).

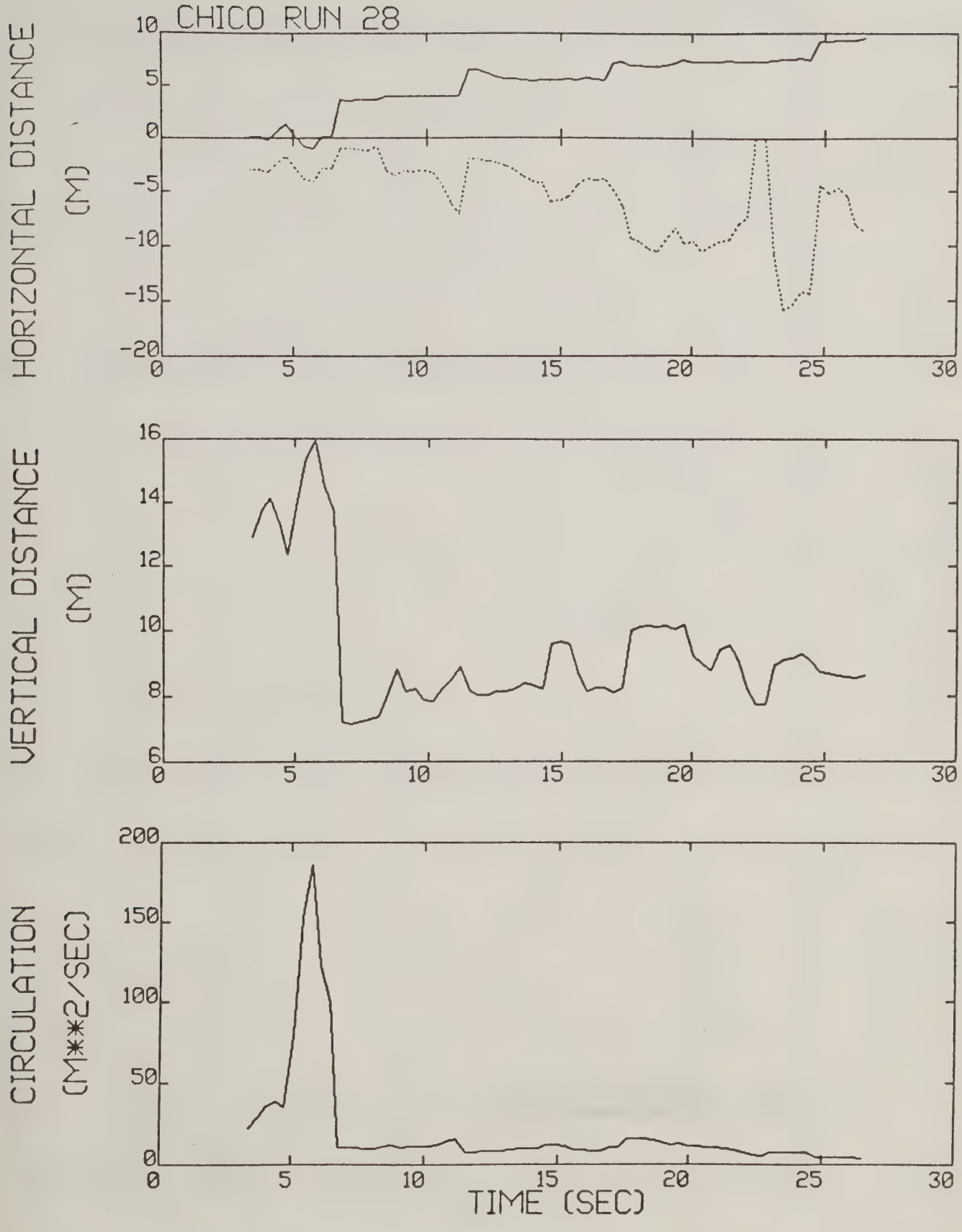

Figure B-12. Chico test run 28 generalized algorithm results.

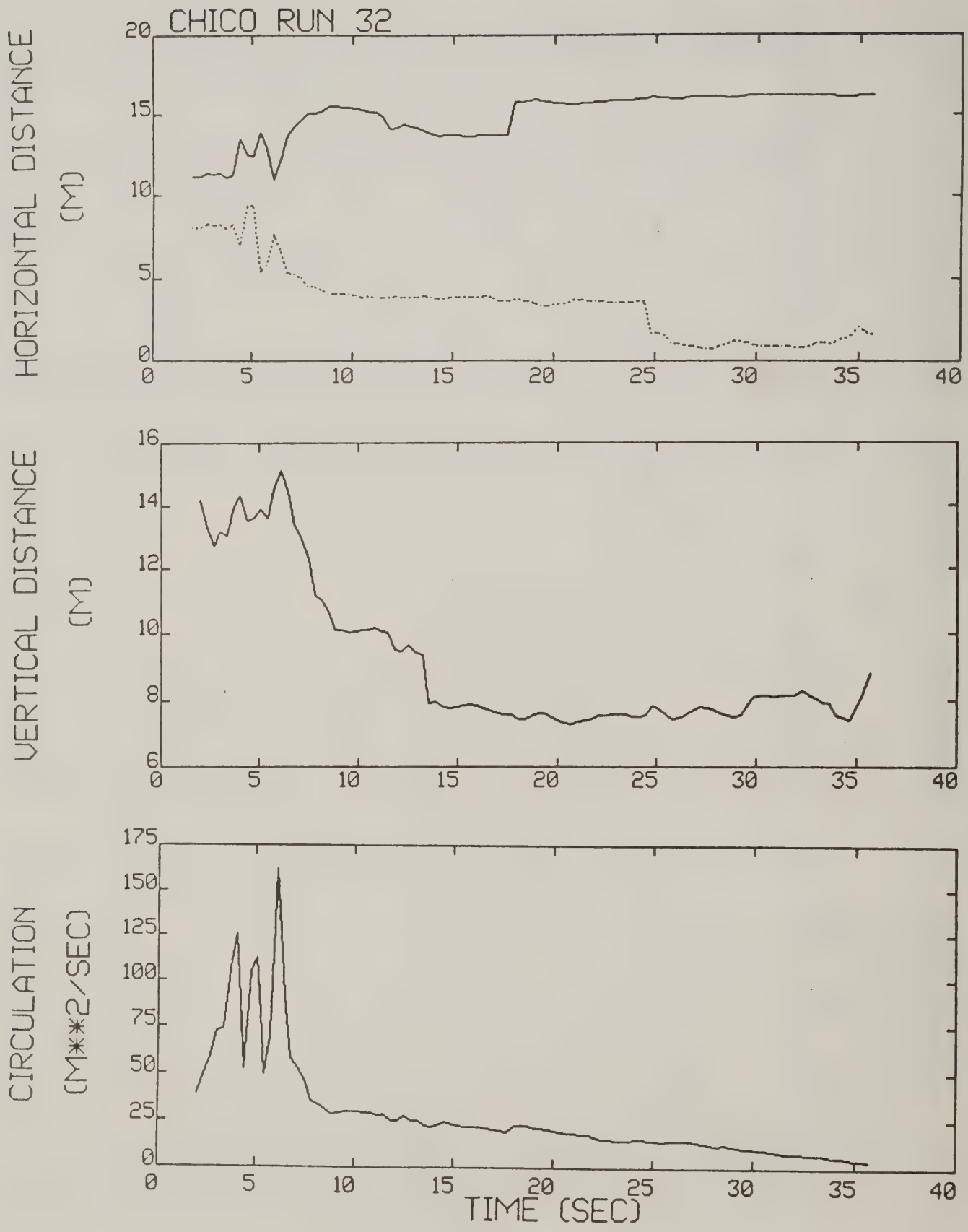

Figure B-13. Chico test run 32 generalized algorithm results (*).

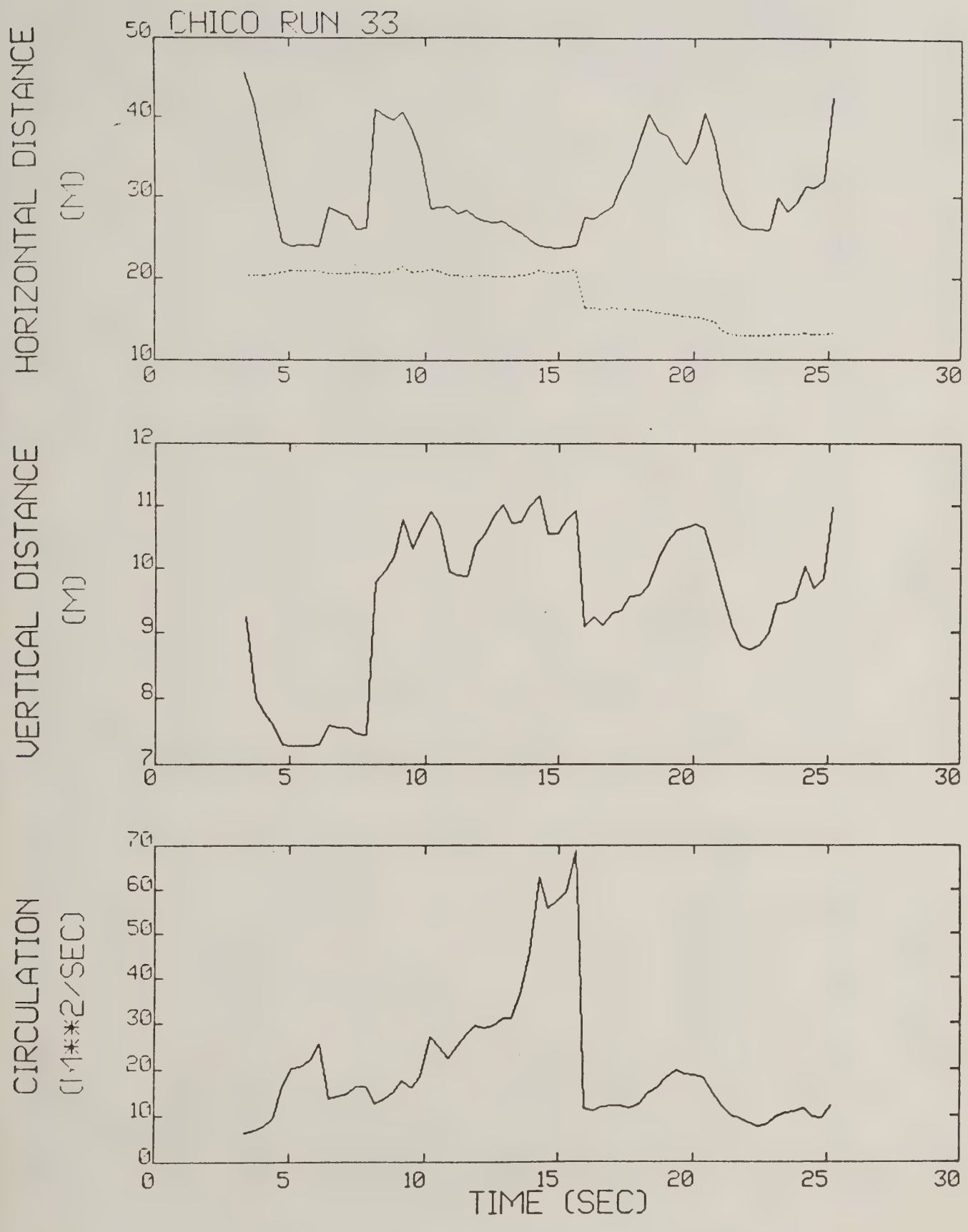

Figure B-14. Chico test run 33 generalized algorithm results.

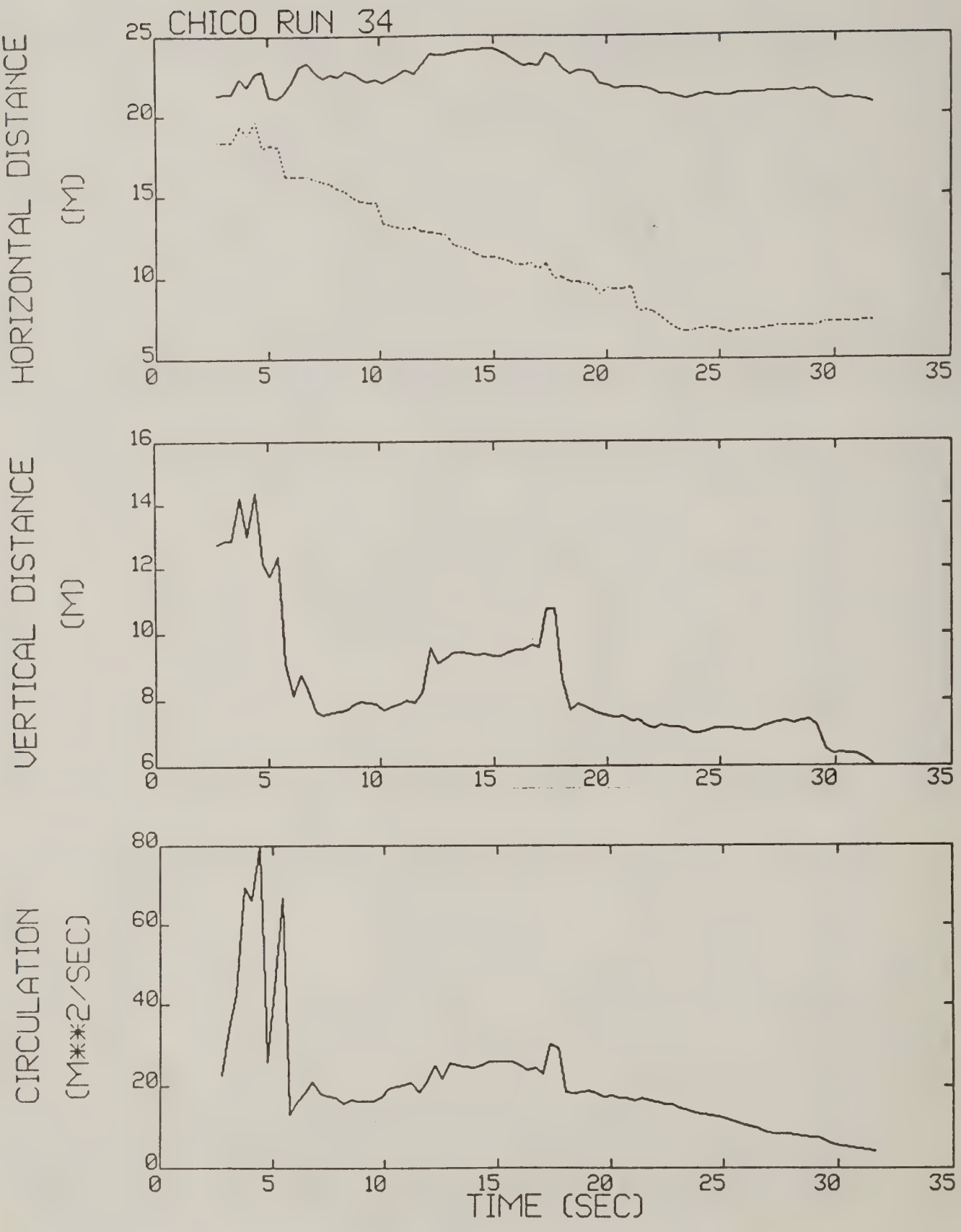

Figure B-15. Chico test run 34 generalized algorithm results (*).

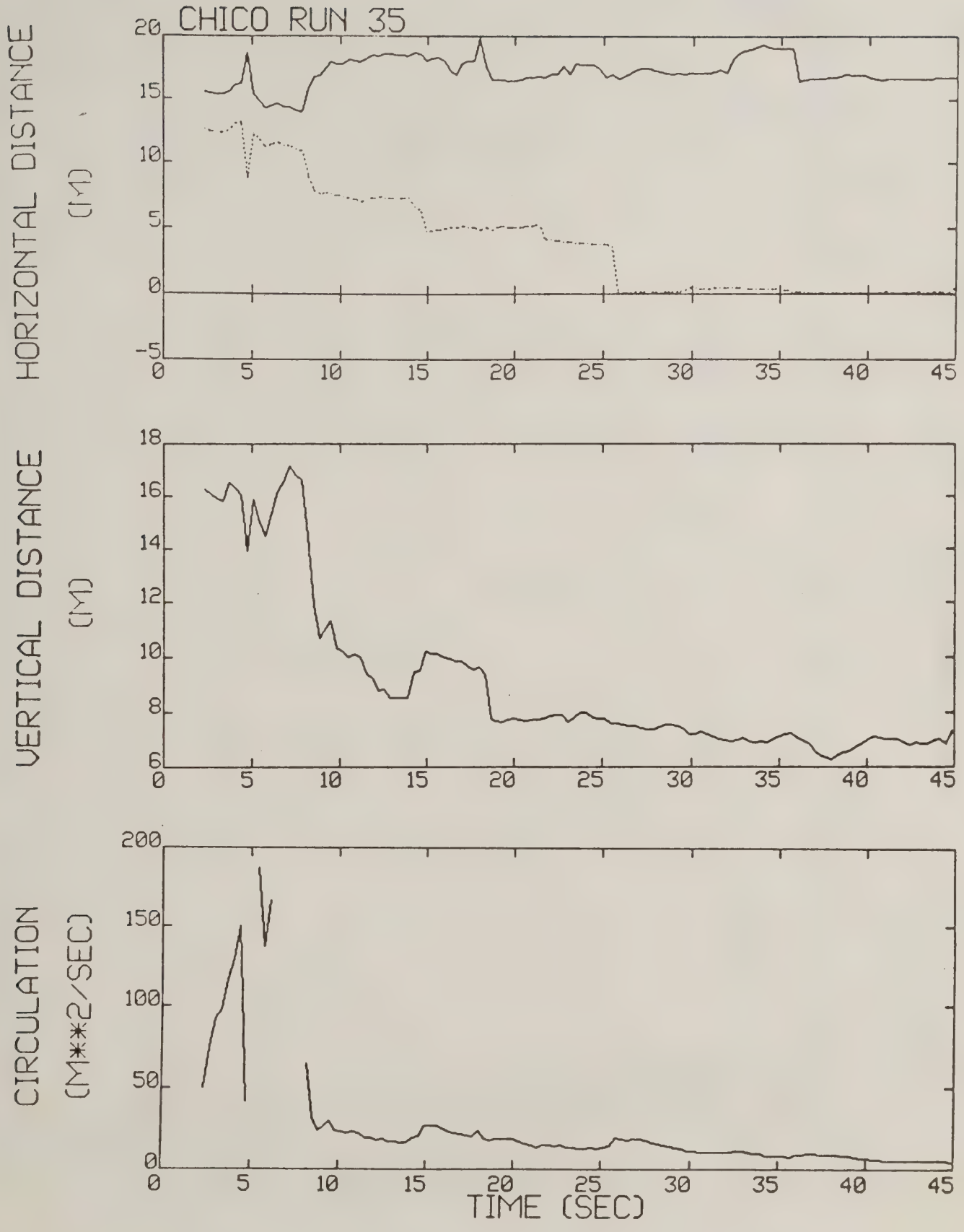

Figure B-16. Chico test run 35 generalized algorithm results (*).

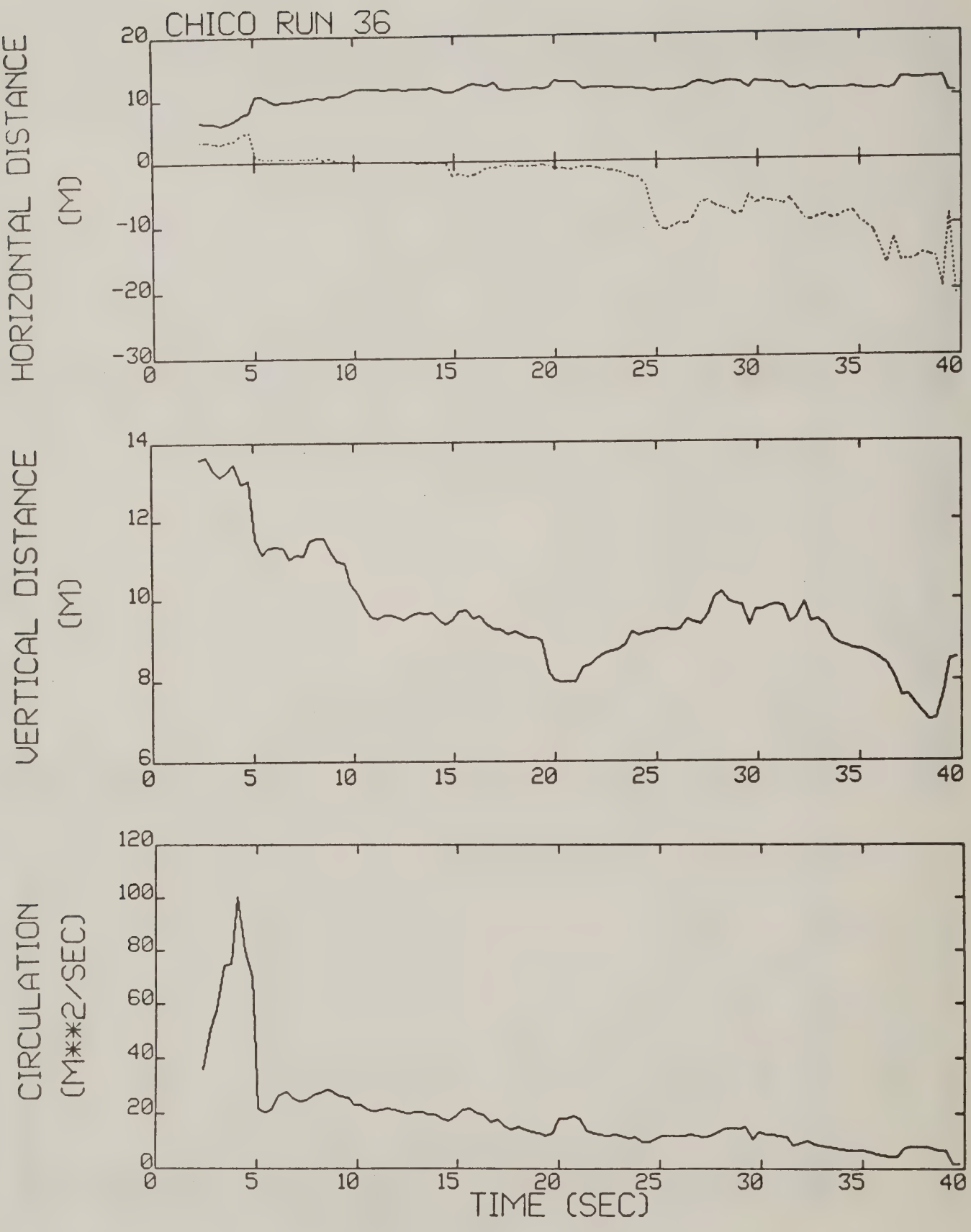

Figure B-17. Chico test run 36 generalized algorithm results (*).

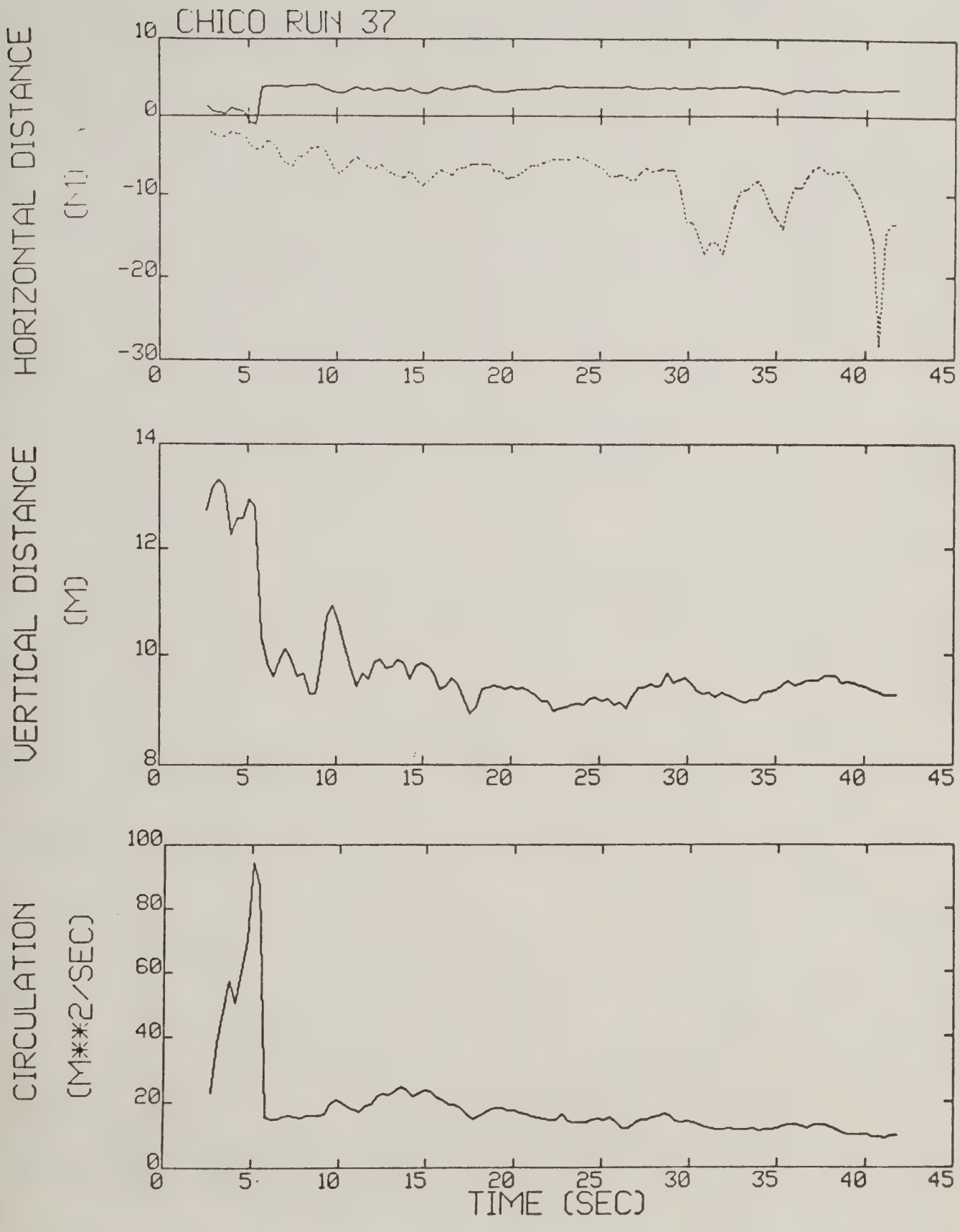

Figure B-18. Chico test run 37 generalized algorithm results.

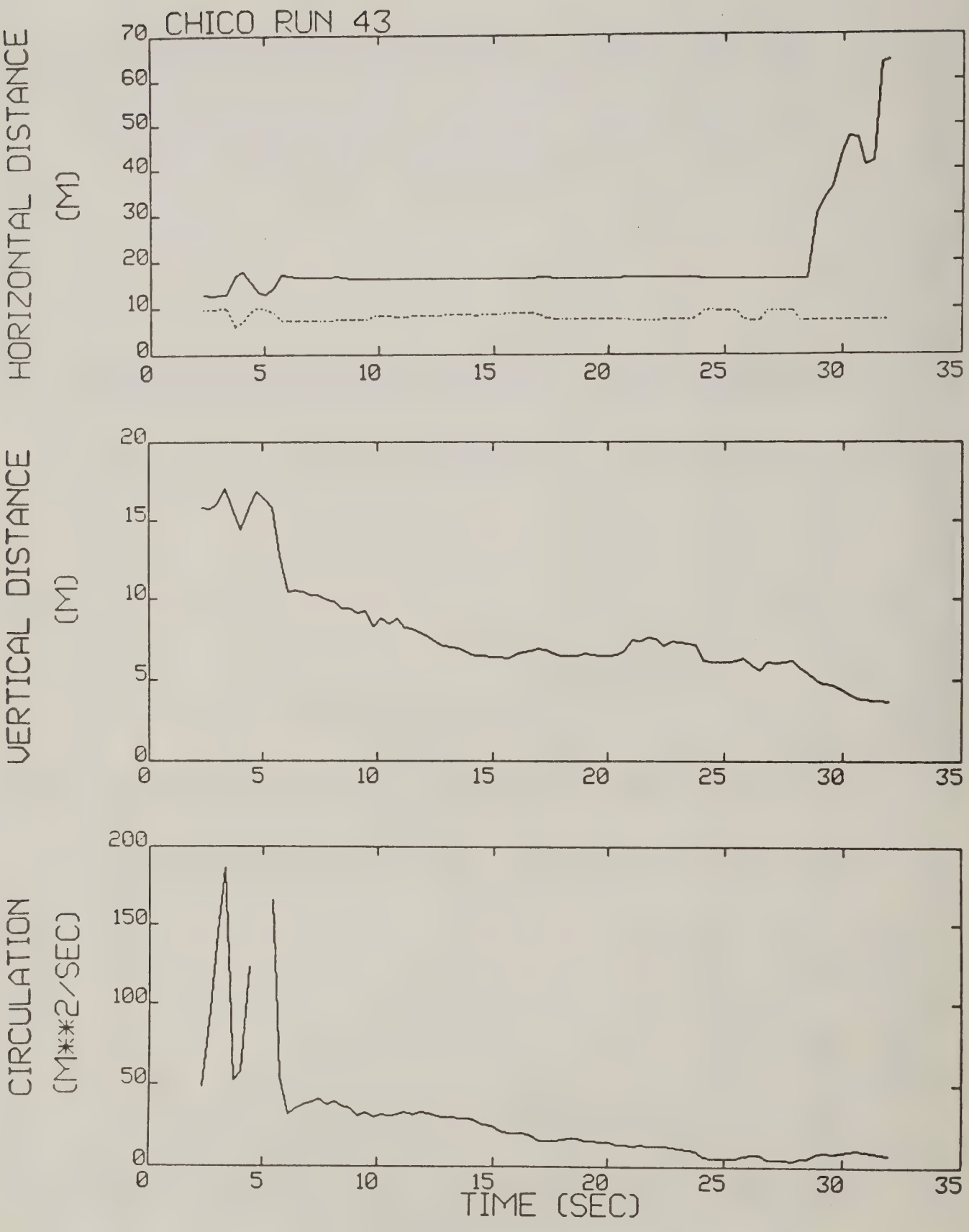

Figure B-19. Chico test run 43 generalized algorithm results (*).

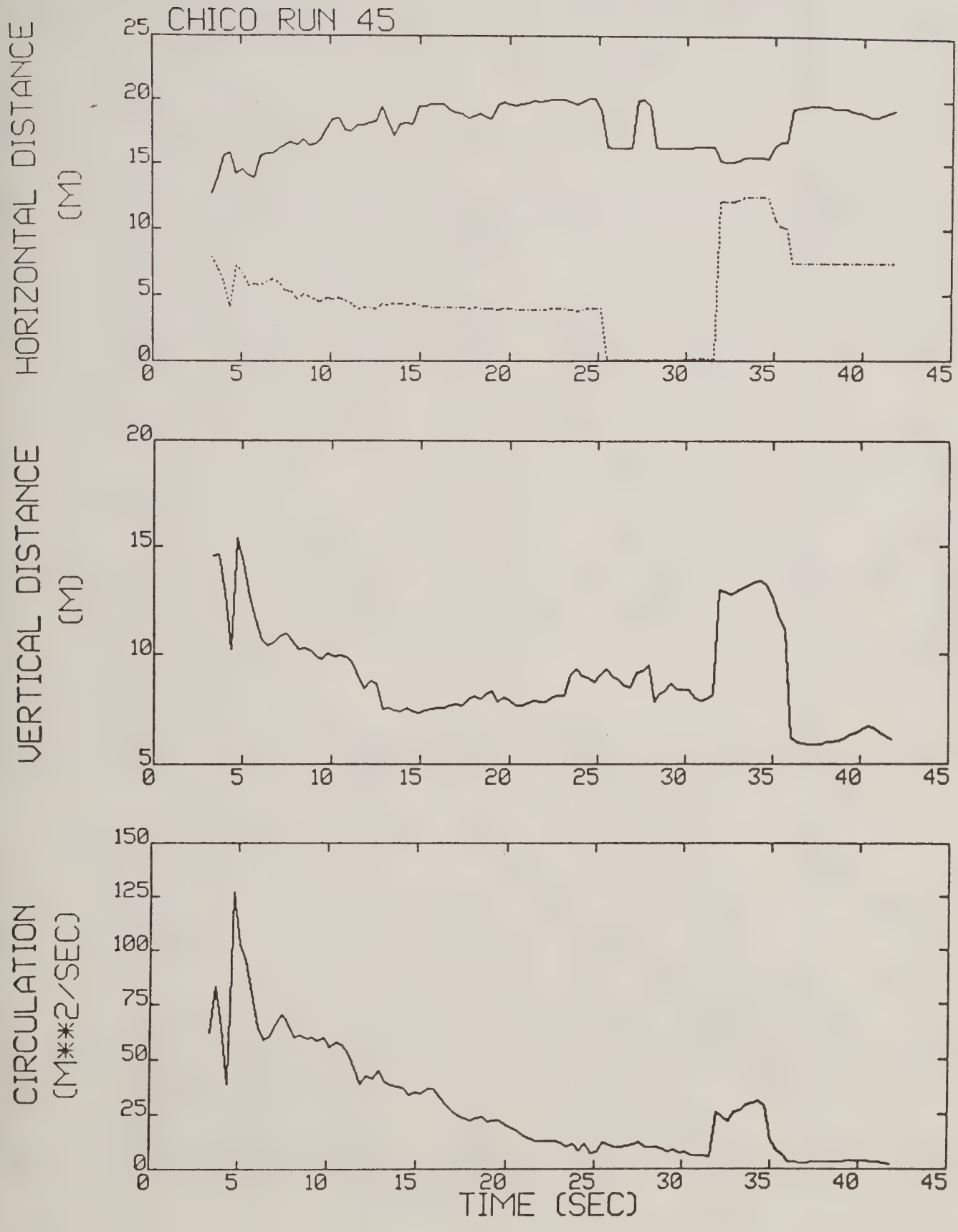

Figure B-20. Chico test run 45 generalized algorithm results (*).

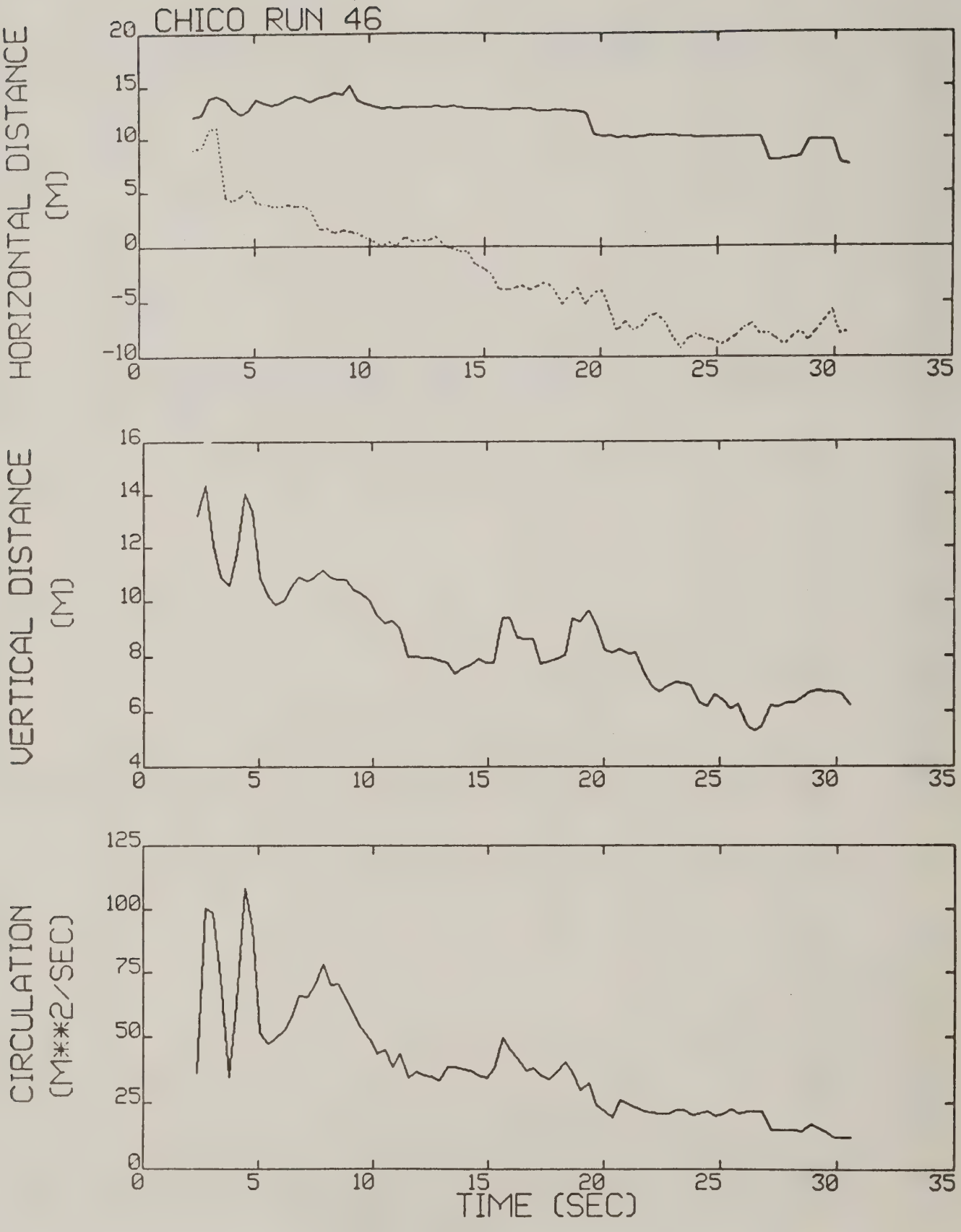

Figure B-21. Chico test run 46 generalized algorithm results (*).

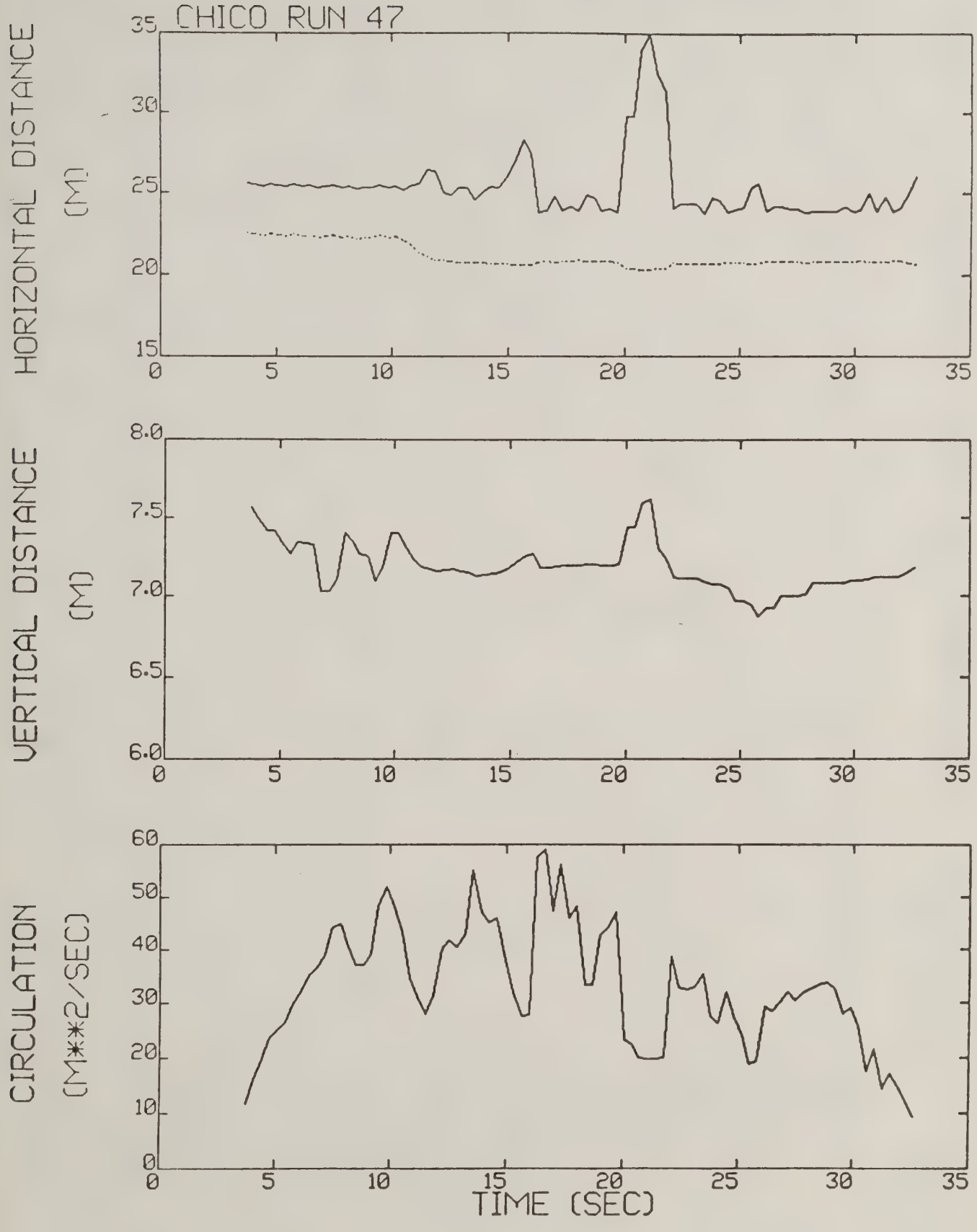

Figure B-22. Chico test run 47 generalized algorithm results (*).

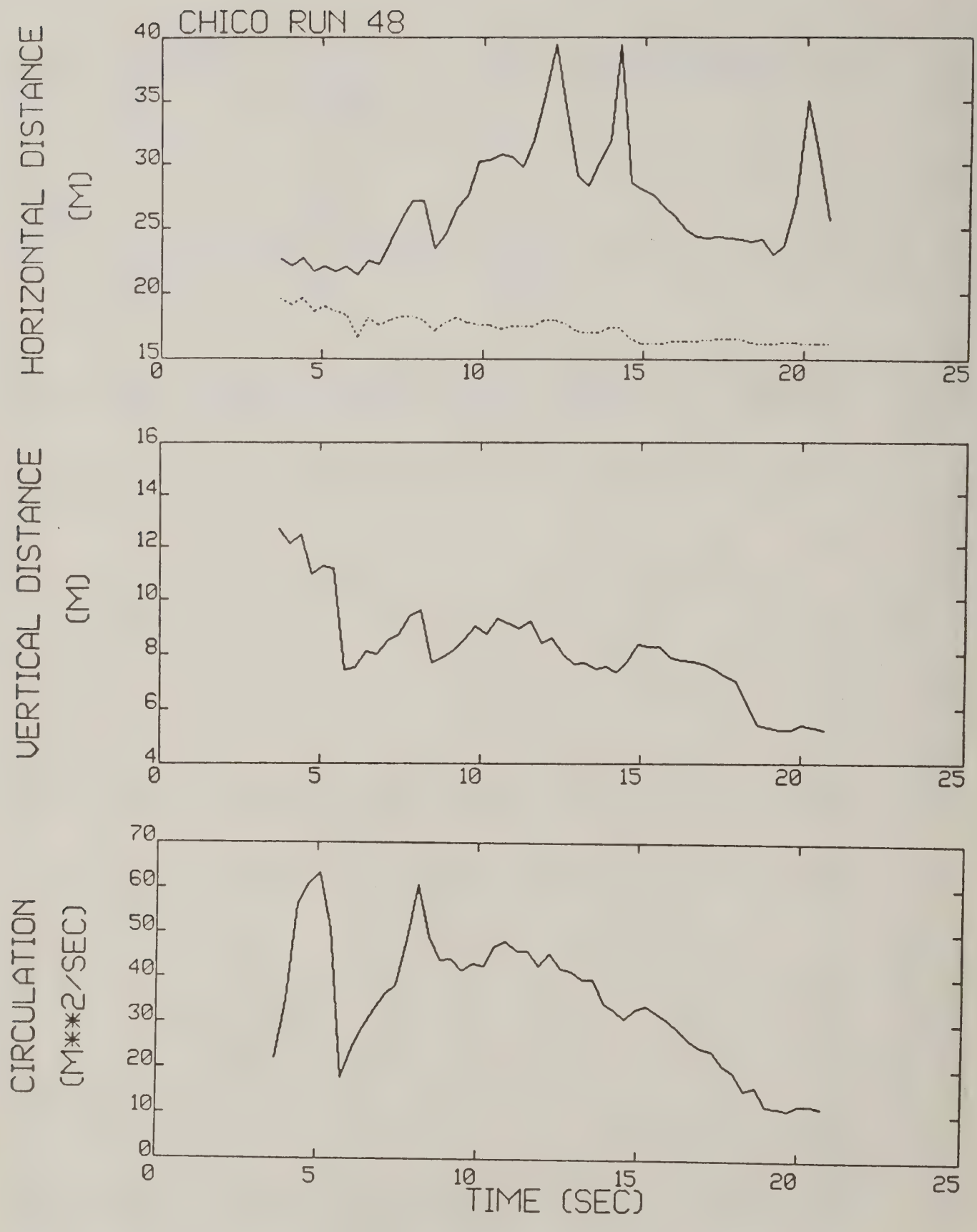

Figure B-23. Chico test run 48 generalized algorithm results.

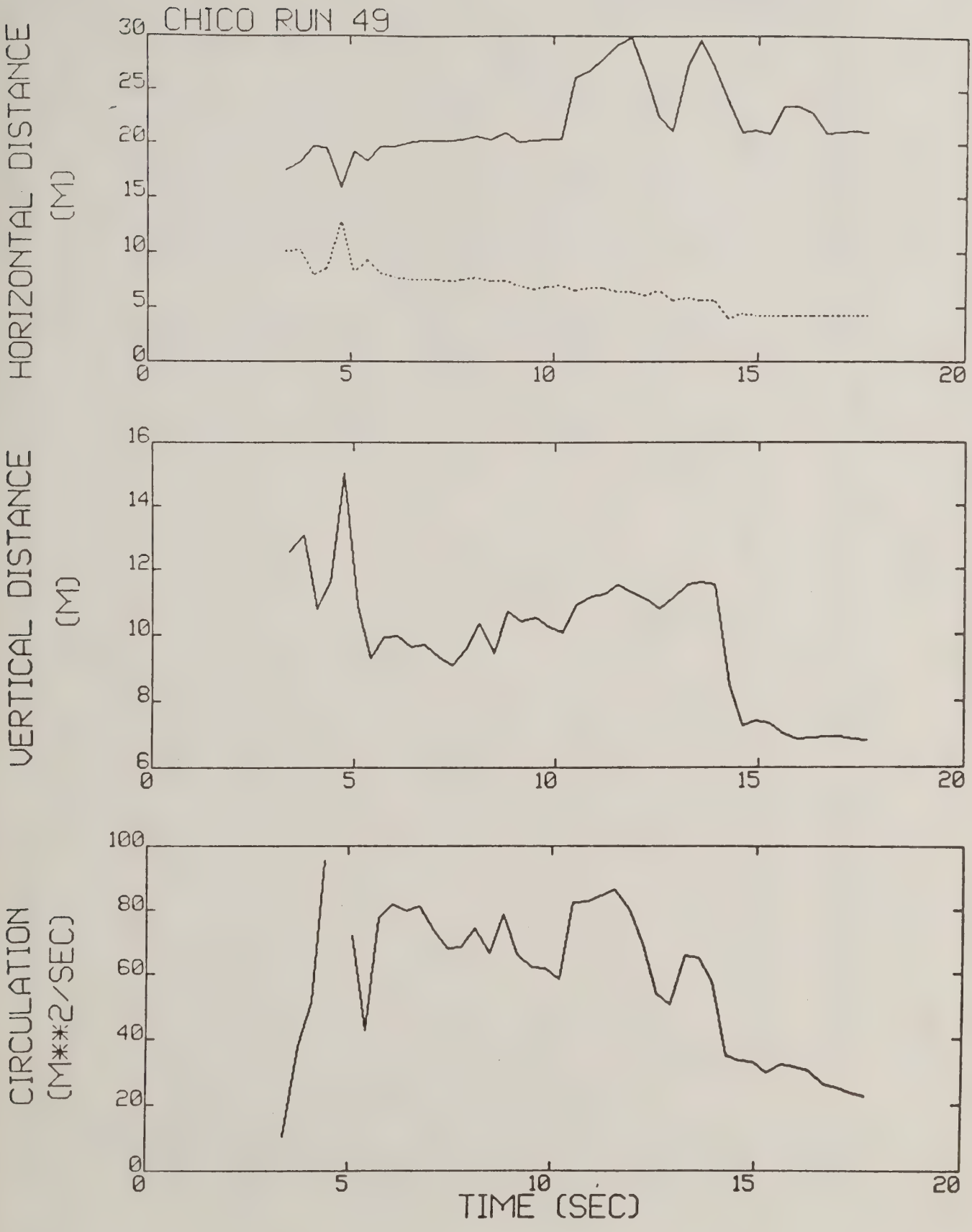

Figure B-24. Chico test run 49 generalized algorithm results (*).

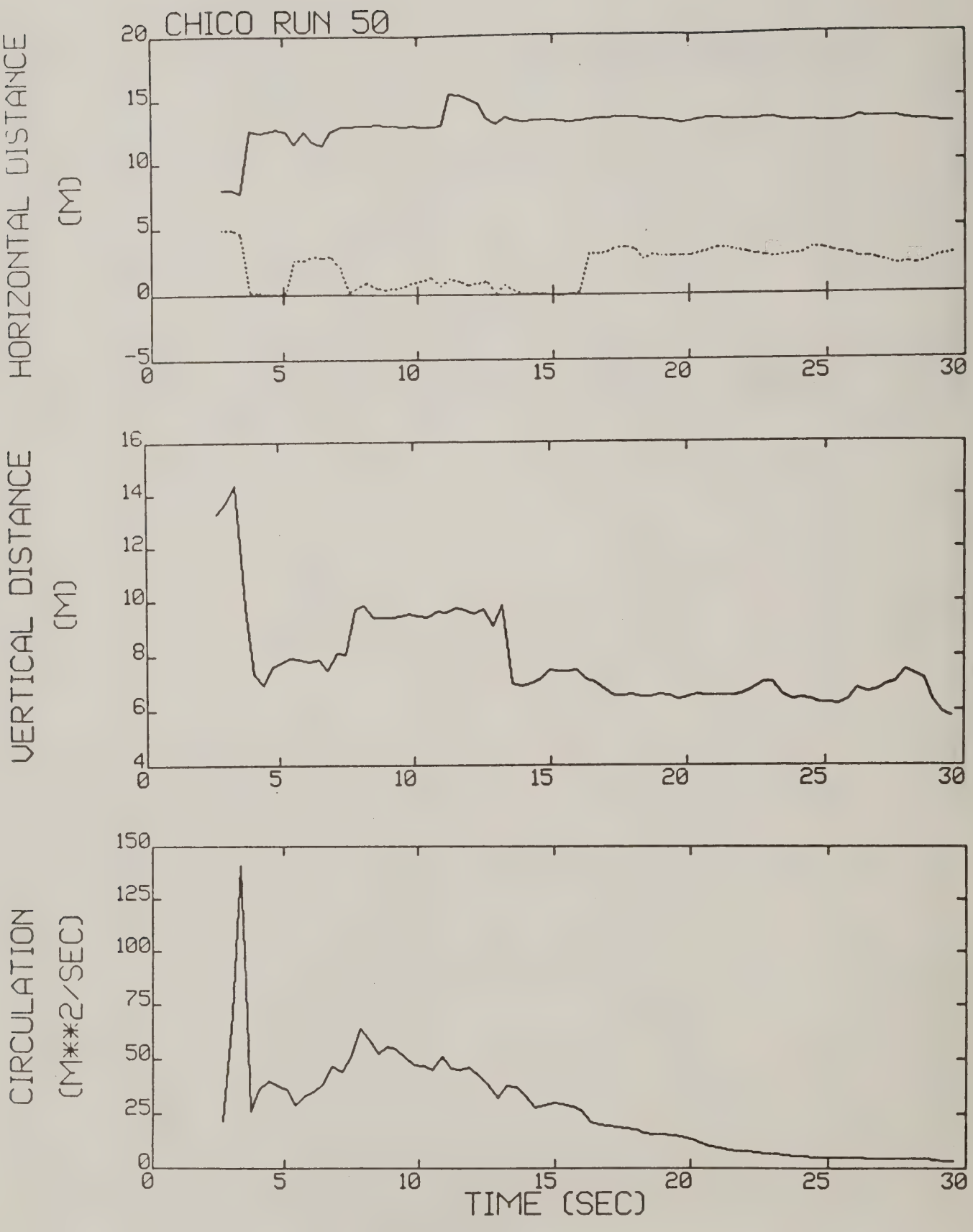

Figure B-25. Chico test run 50 generalized algorithm results (*).

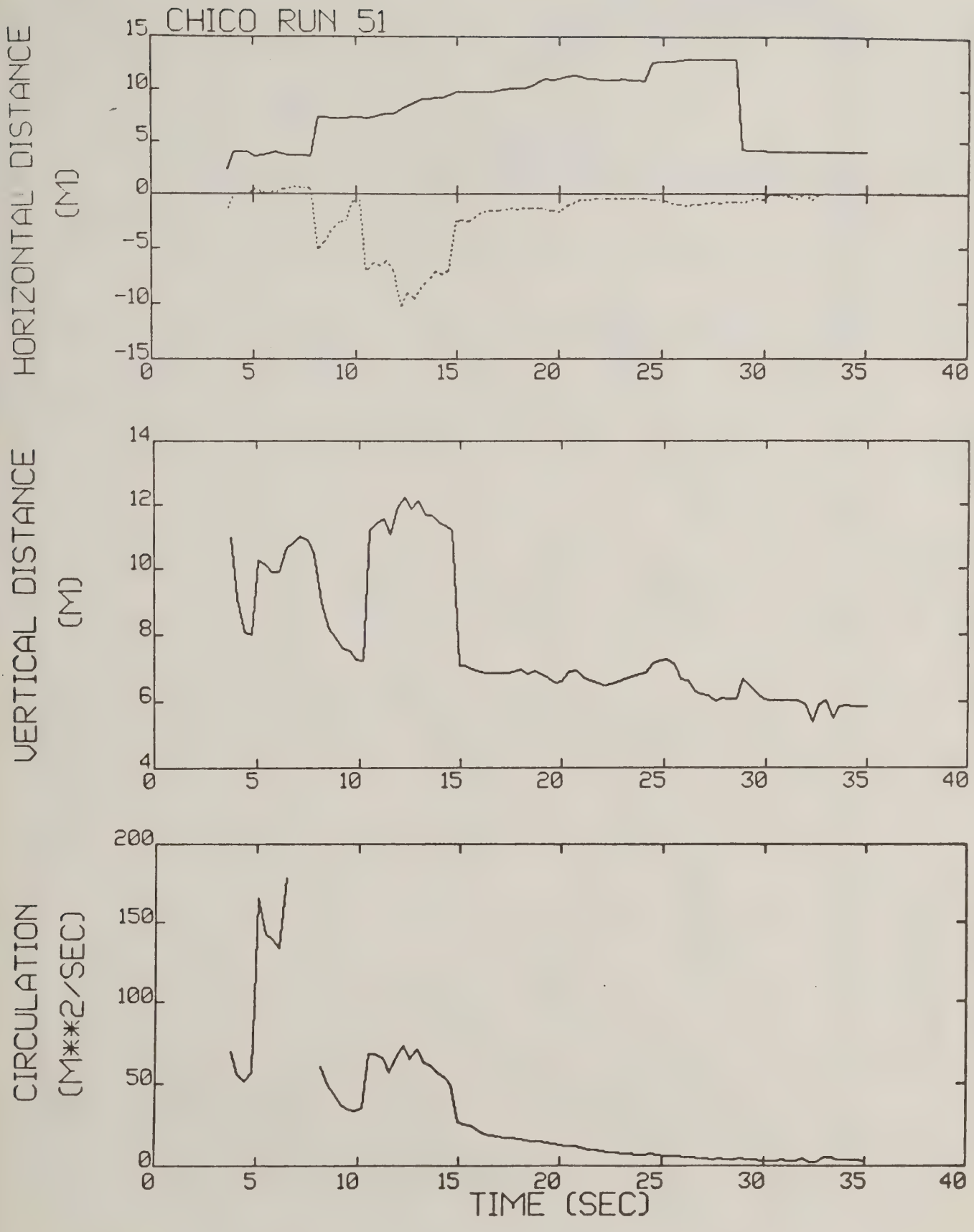

Figure B-26. Chico test run 51 generalized algorithm results (*).

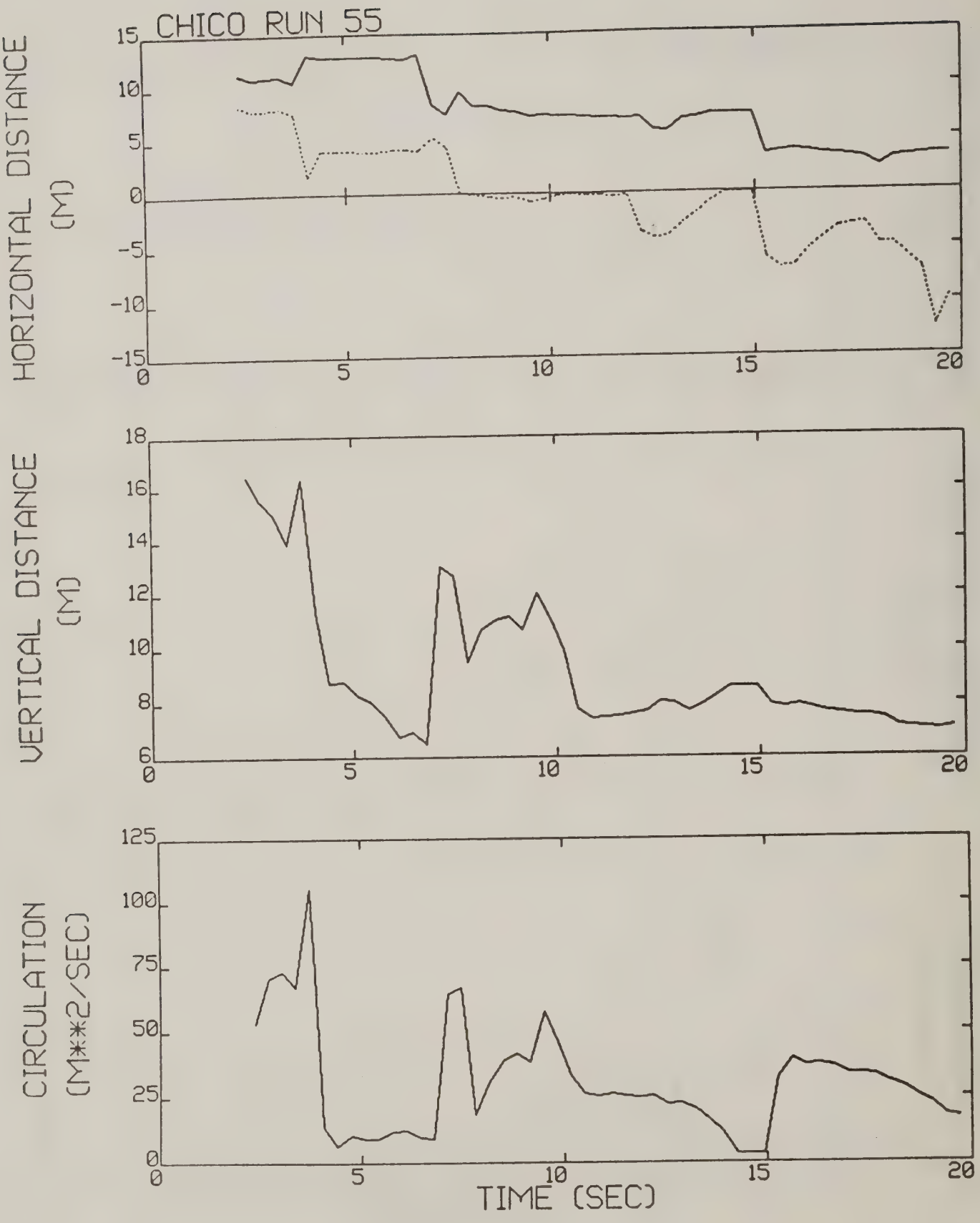

Figure B-27. Chico test run 55 generalized algorithm results.

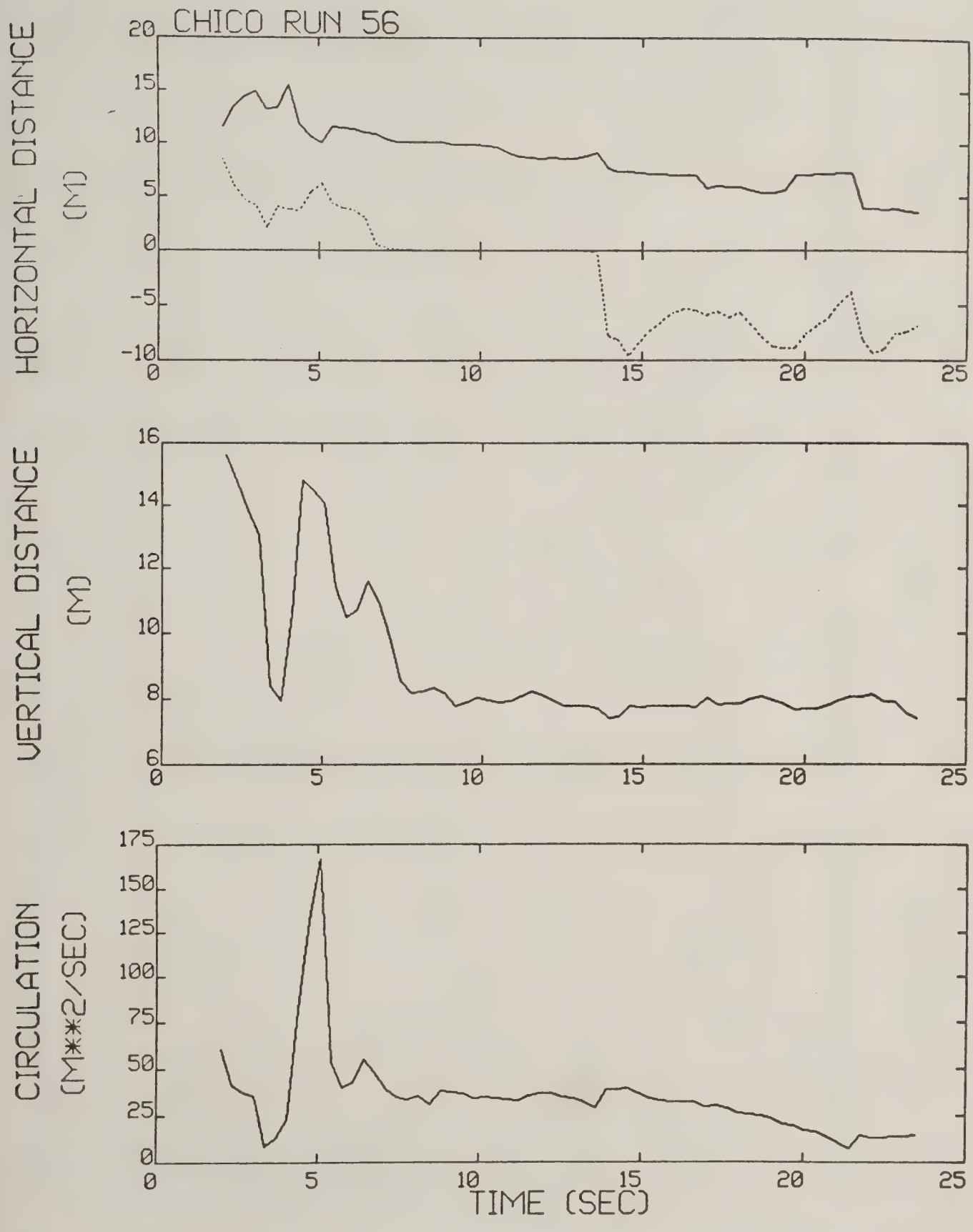

Figure B-28. Chico test run 56 generalized algorithm results.

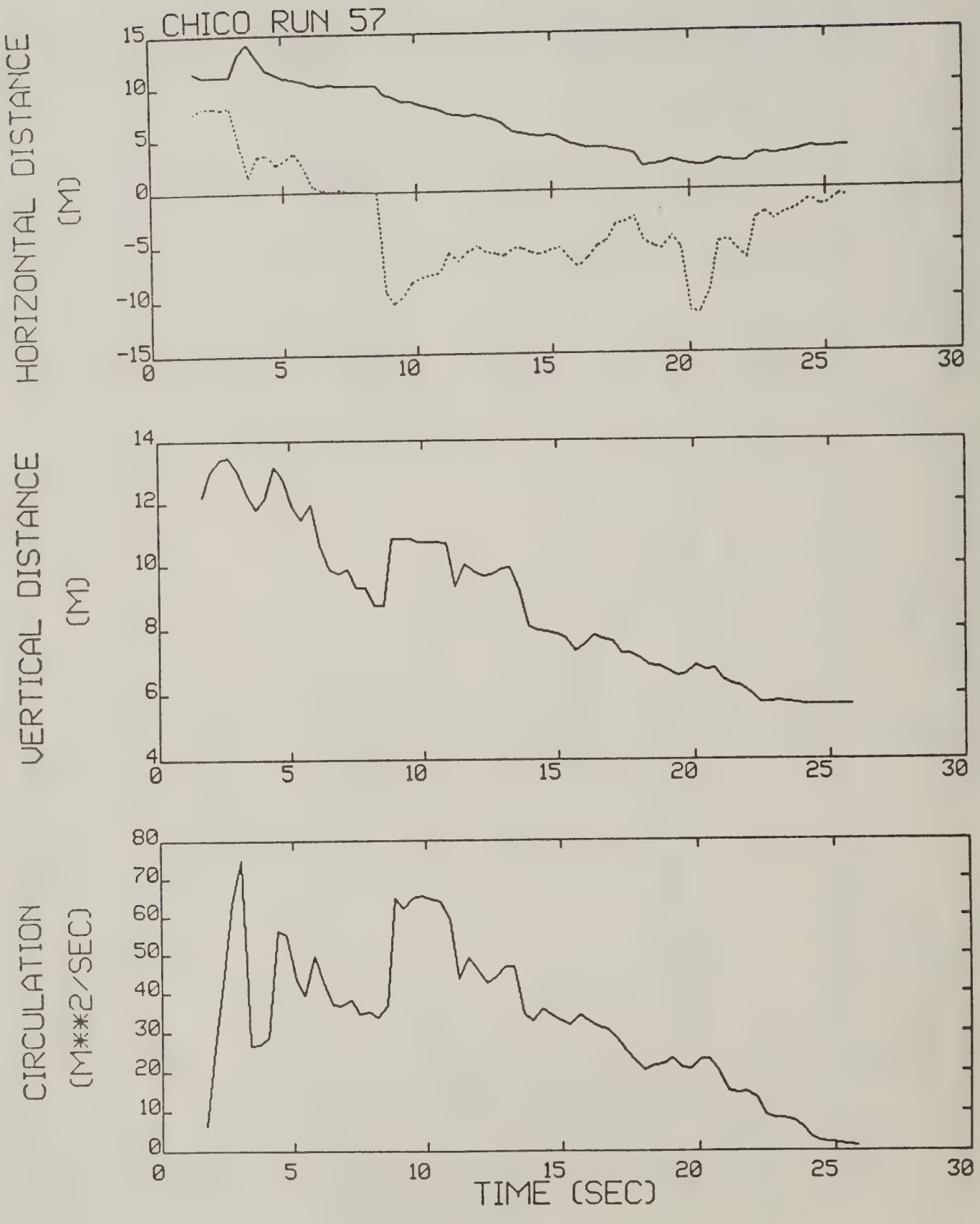

Figure B-29. Chico test run 57 generalized algorithm results (*).

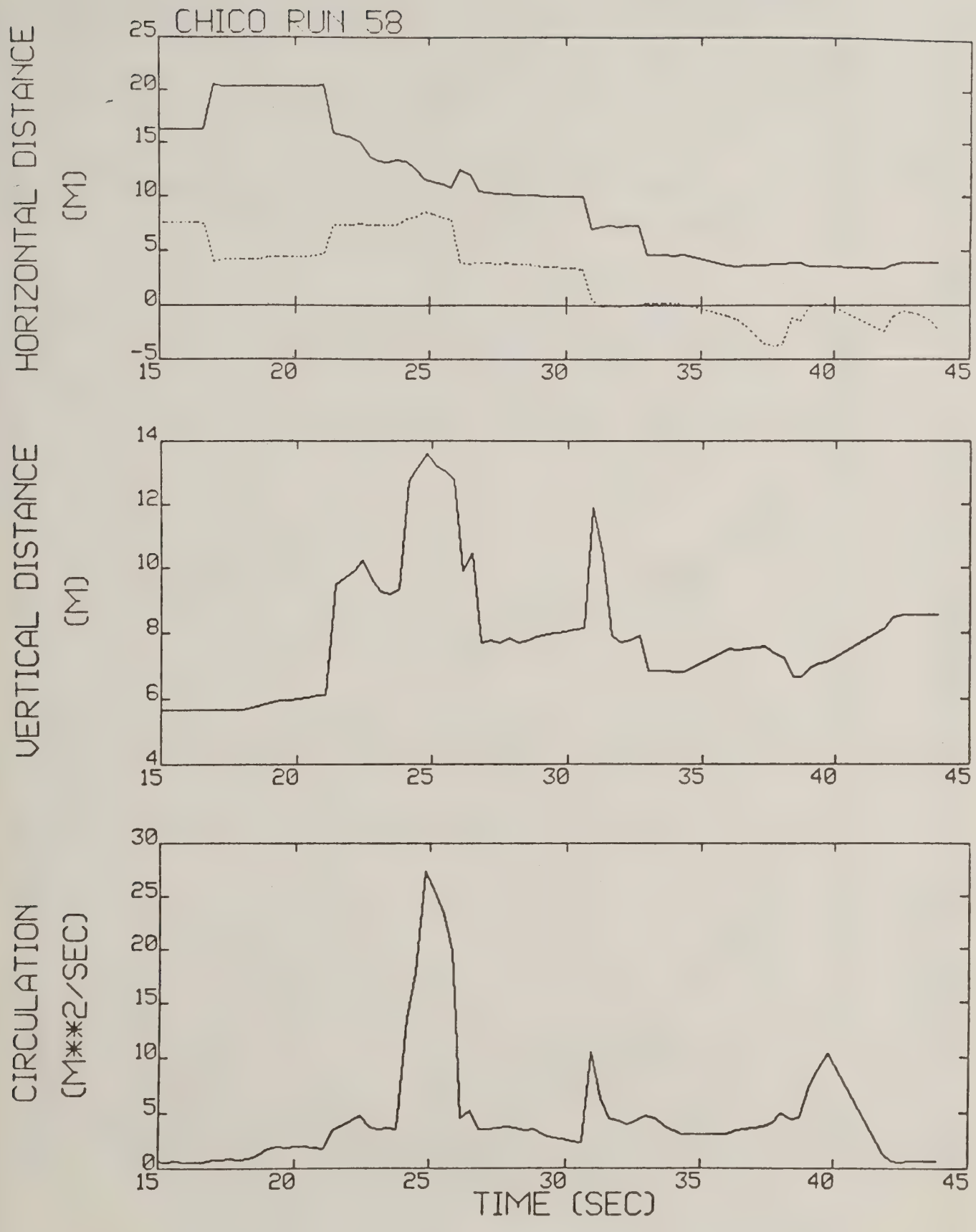

Figure B-30. Chico test run 58 generalized algorithm results.

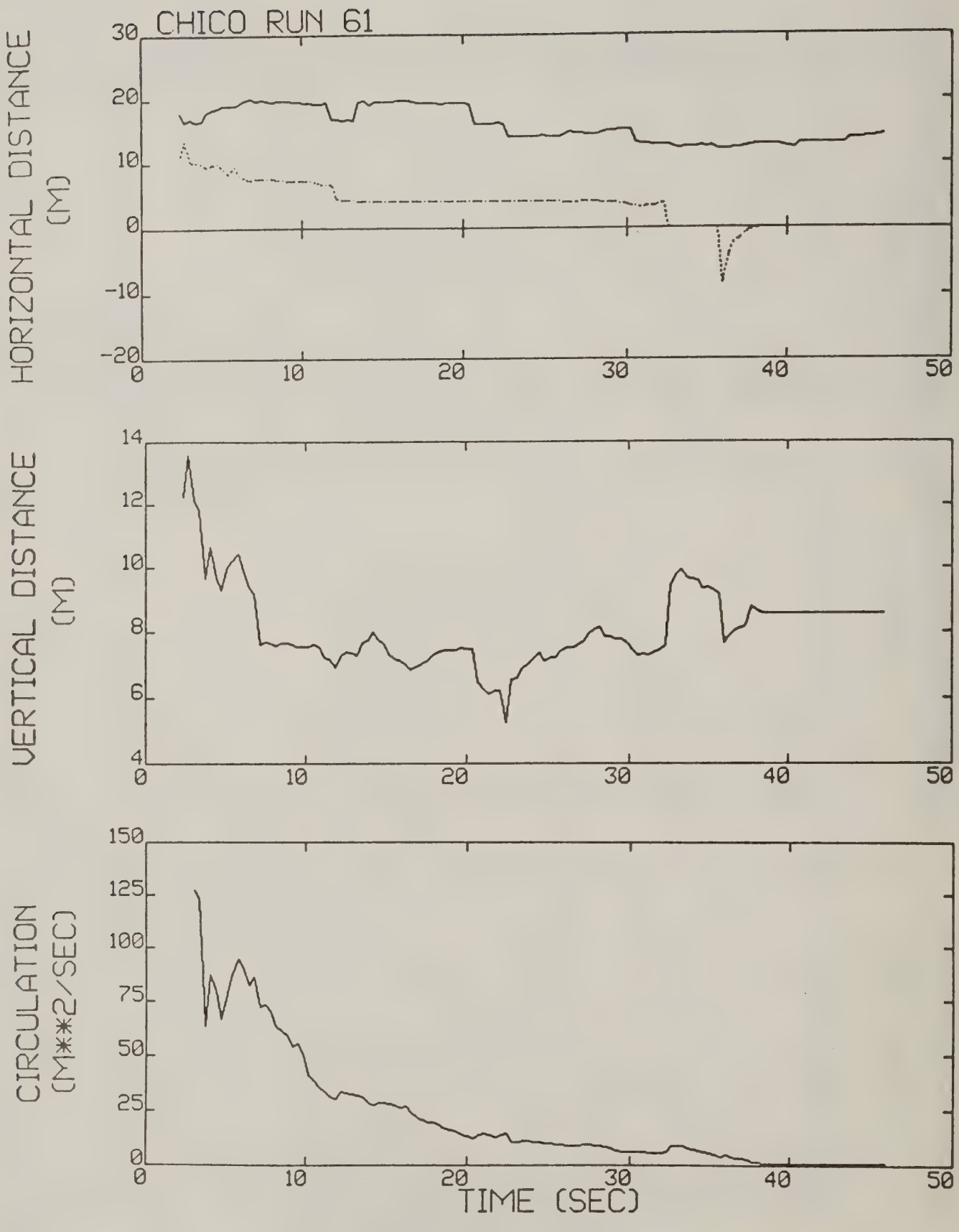

Figure B-31. Chico test run 61 generalized algorithm results (*).

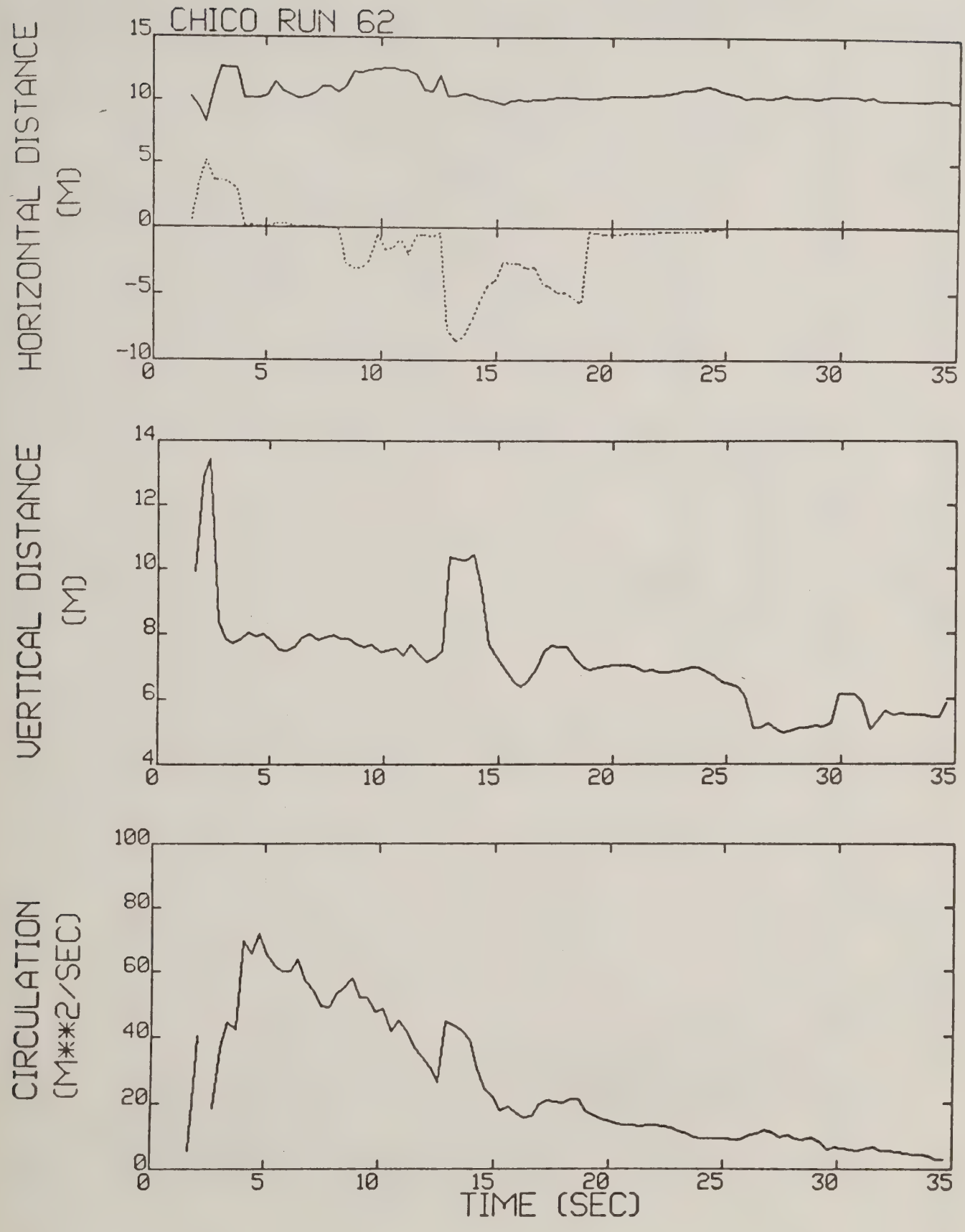

Figure B-32. Chico test run 62 generalized algorithm results (*).

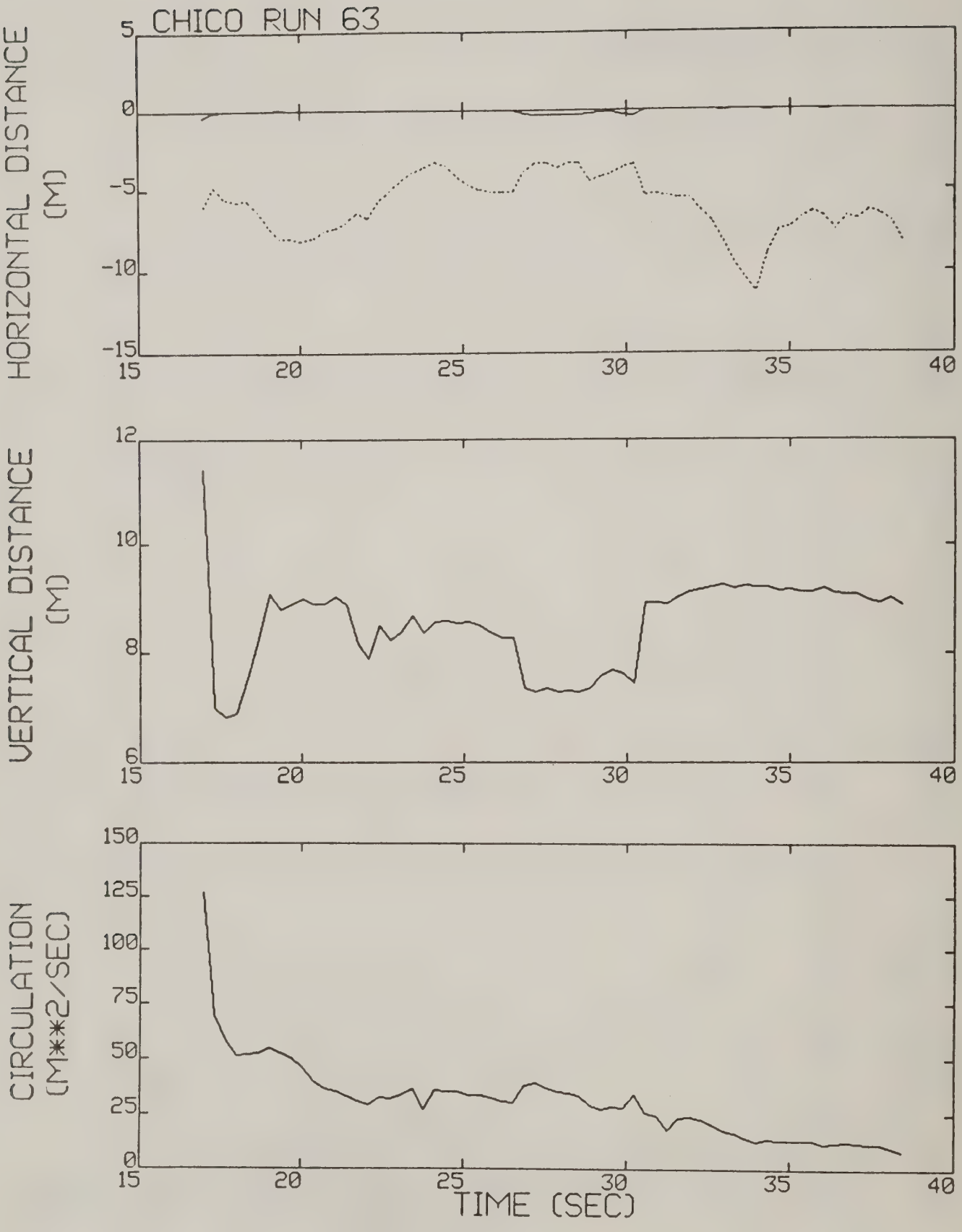

Figure B-33. Chico test run 63 generalized algorithm results (*).

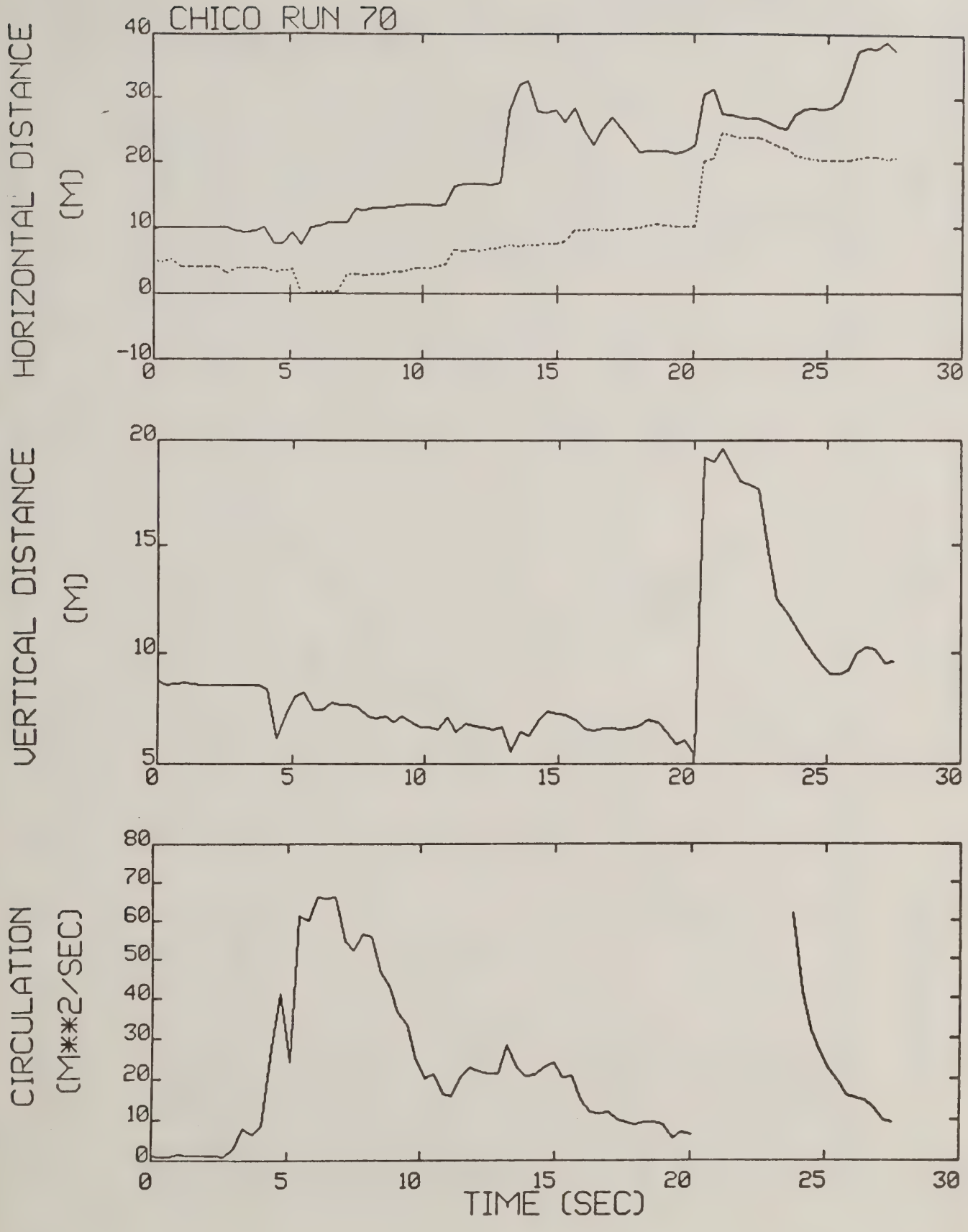

Figure B-34. Chico test run 70 generalized algorithm results (*).

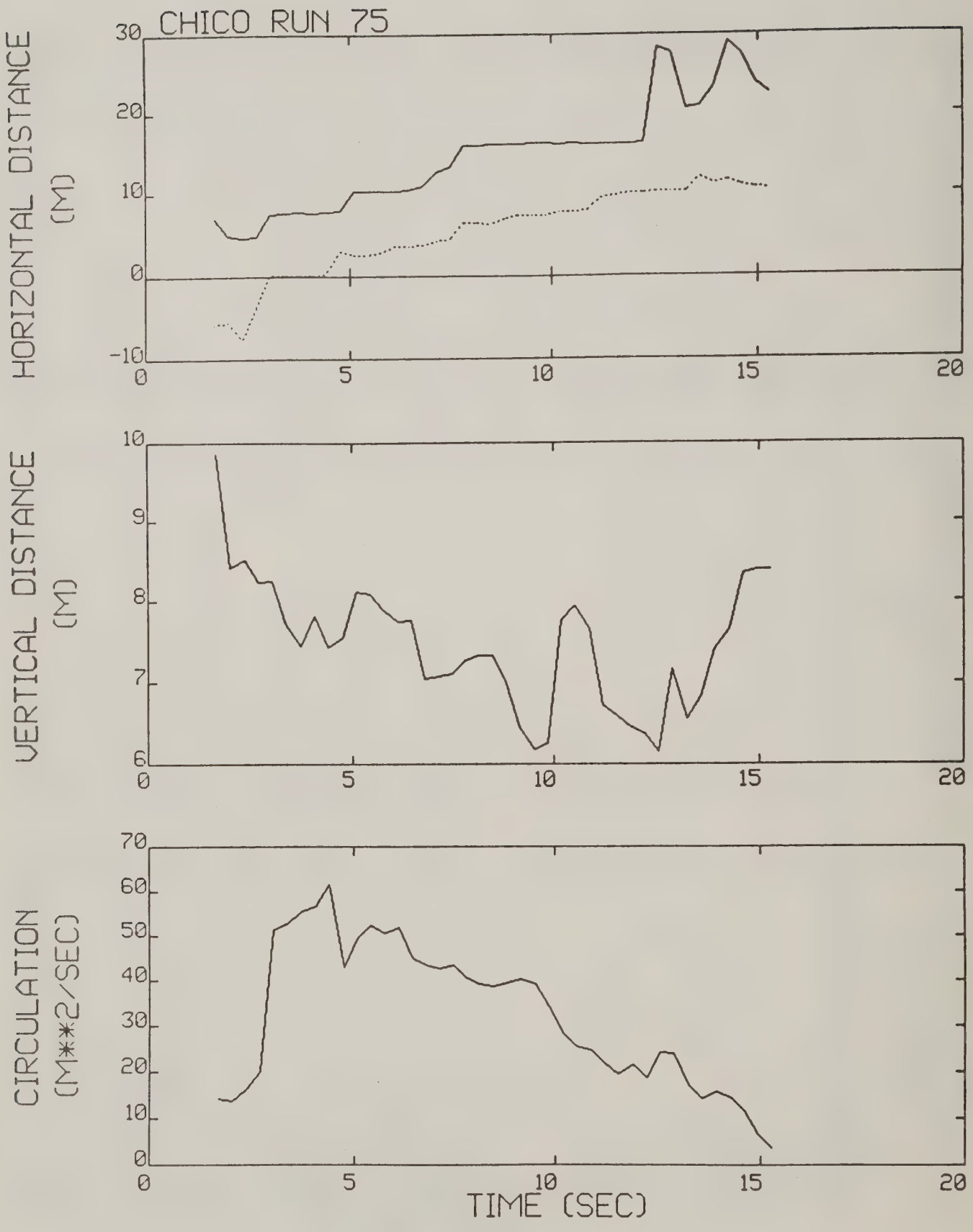

Figure B-35. Chico test run 75 generalized algorithm results (*).

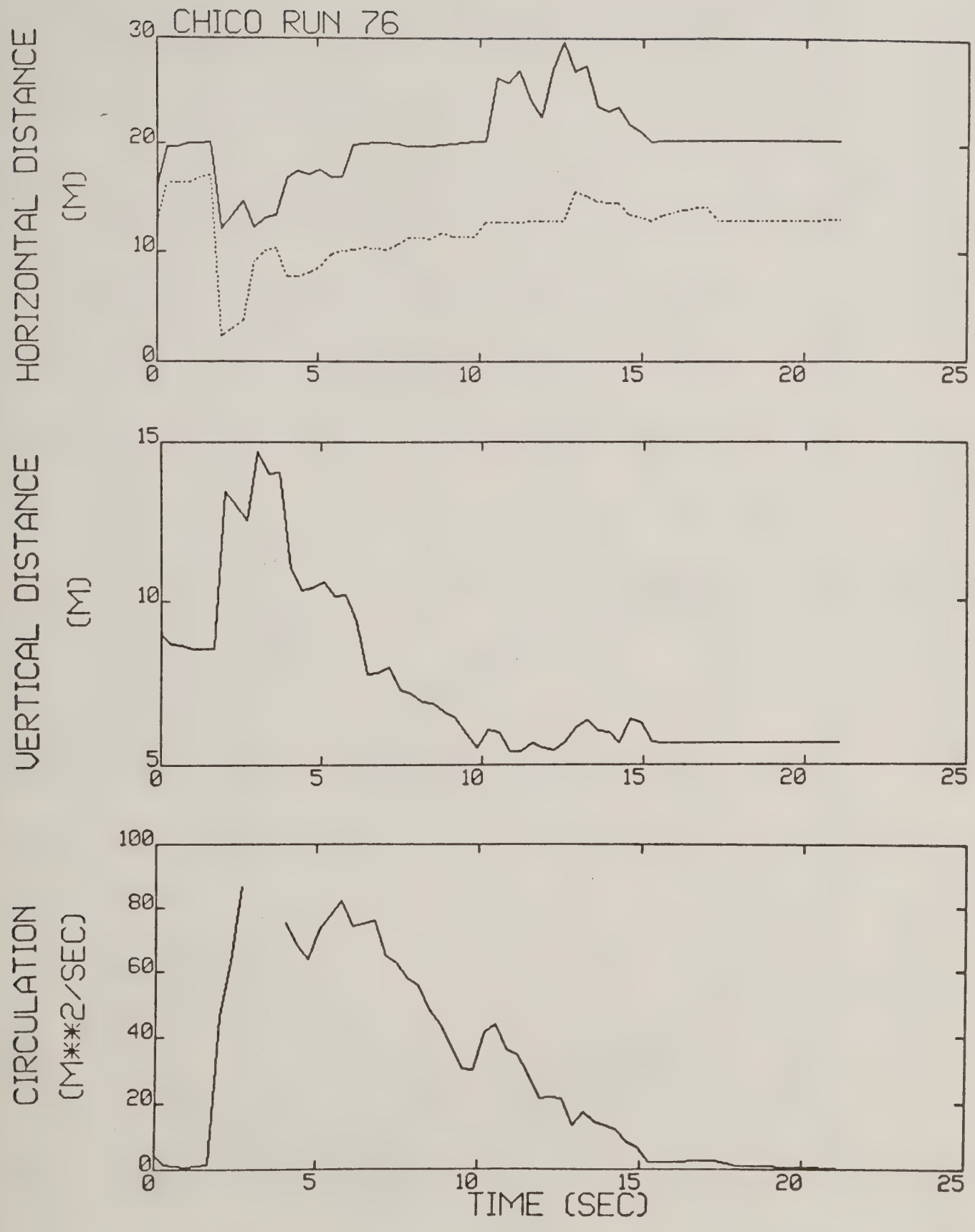

Figure B-36. Chico test run 76 generalized algorithm results (*).

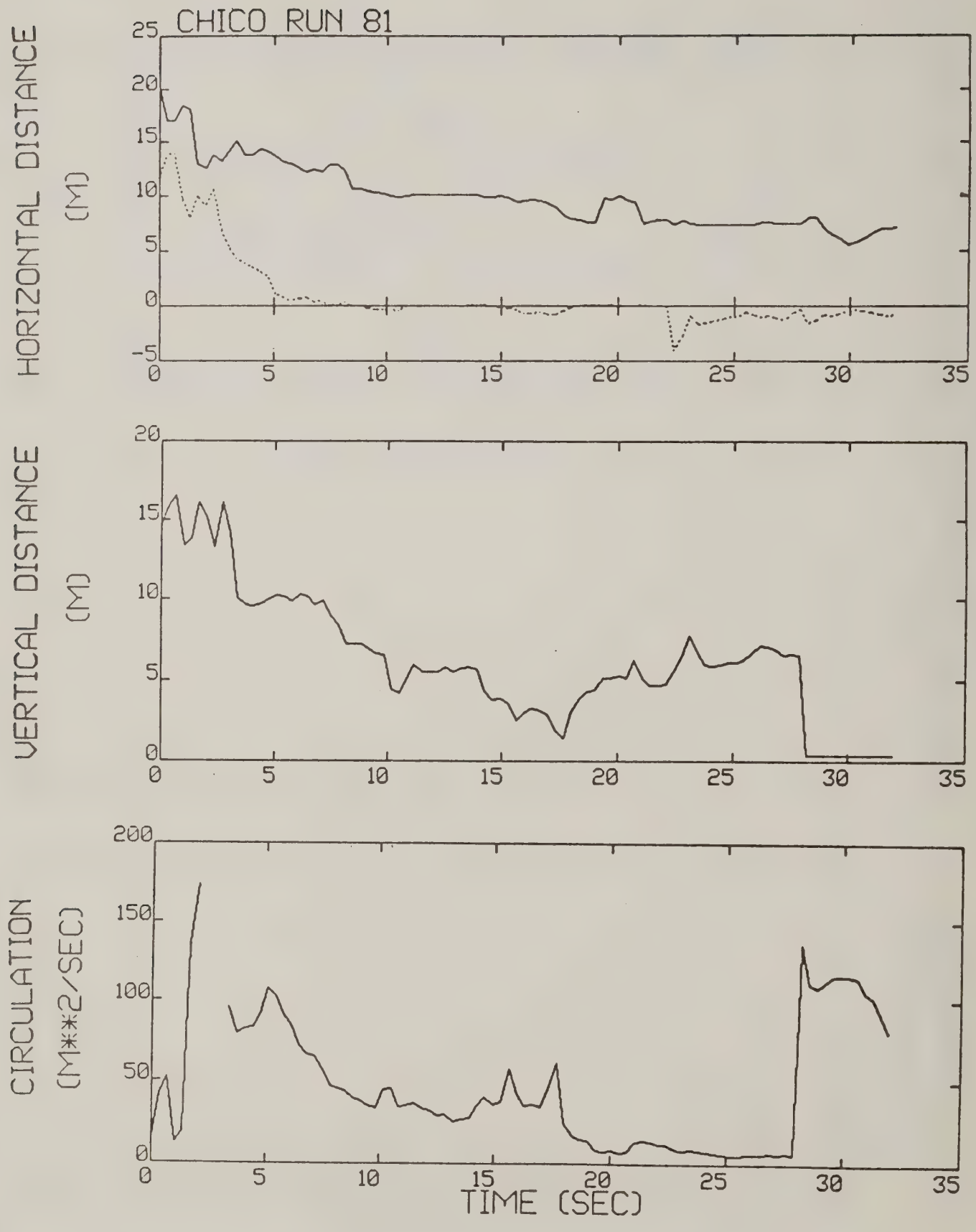

Figure B-37. Chico test run 81 generalized algorithm results (*).

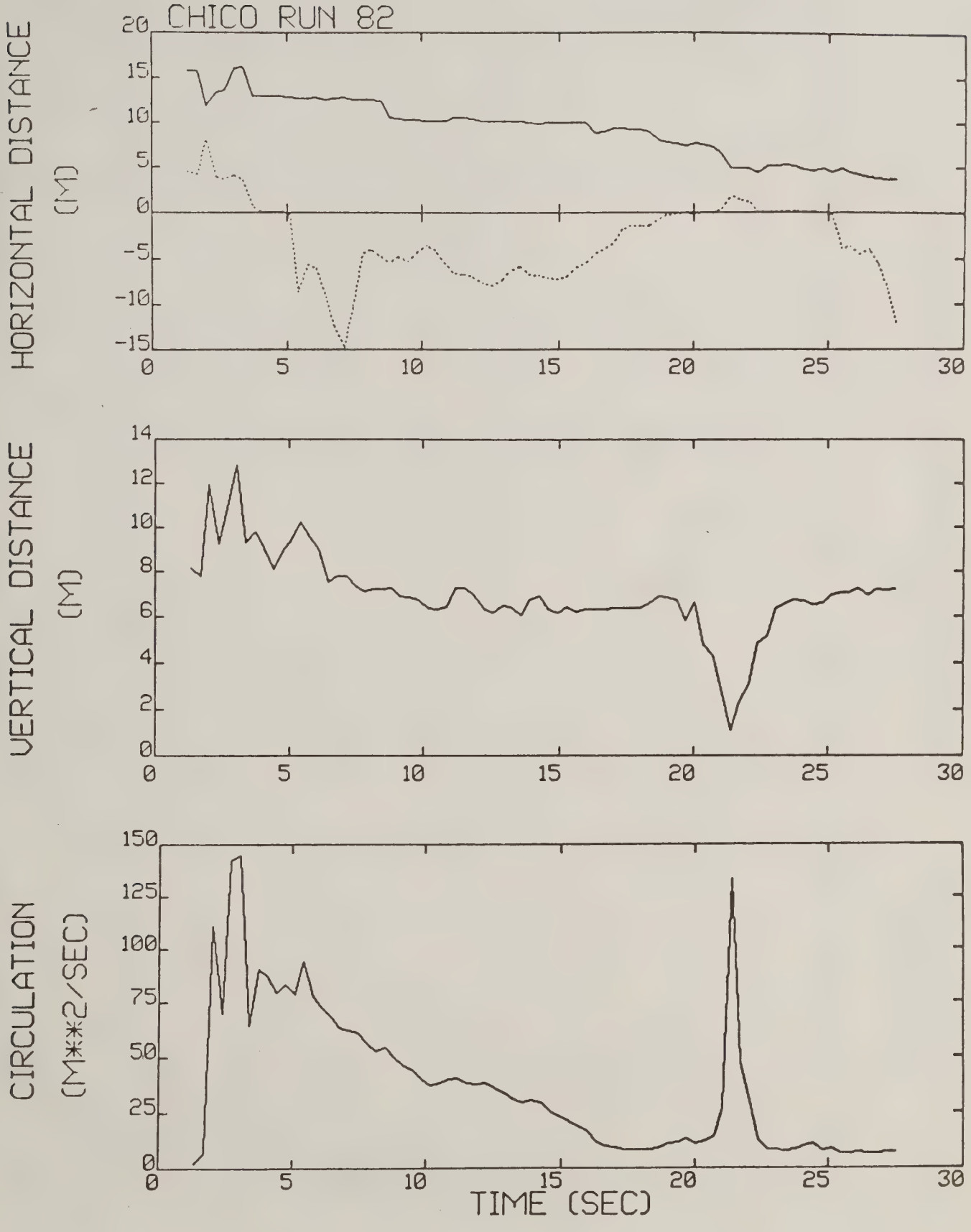

Figure B-38. Chico test run 82 generalized algorithm results (*).

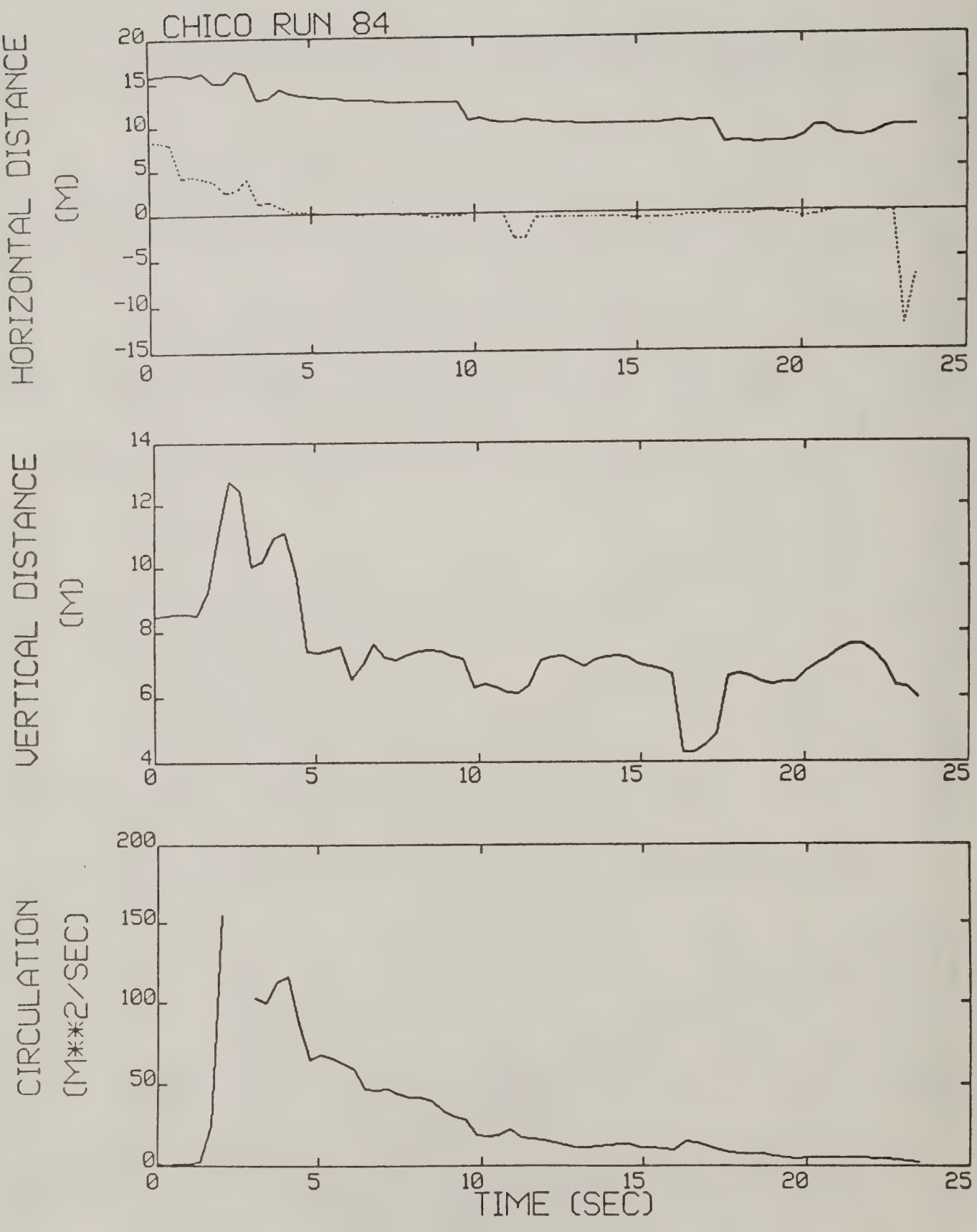

Figure B-39. Chico test run 84 generalized algorithm results (*).

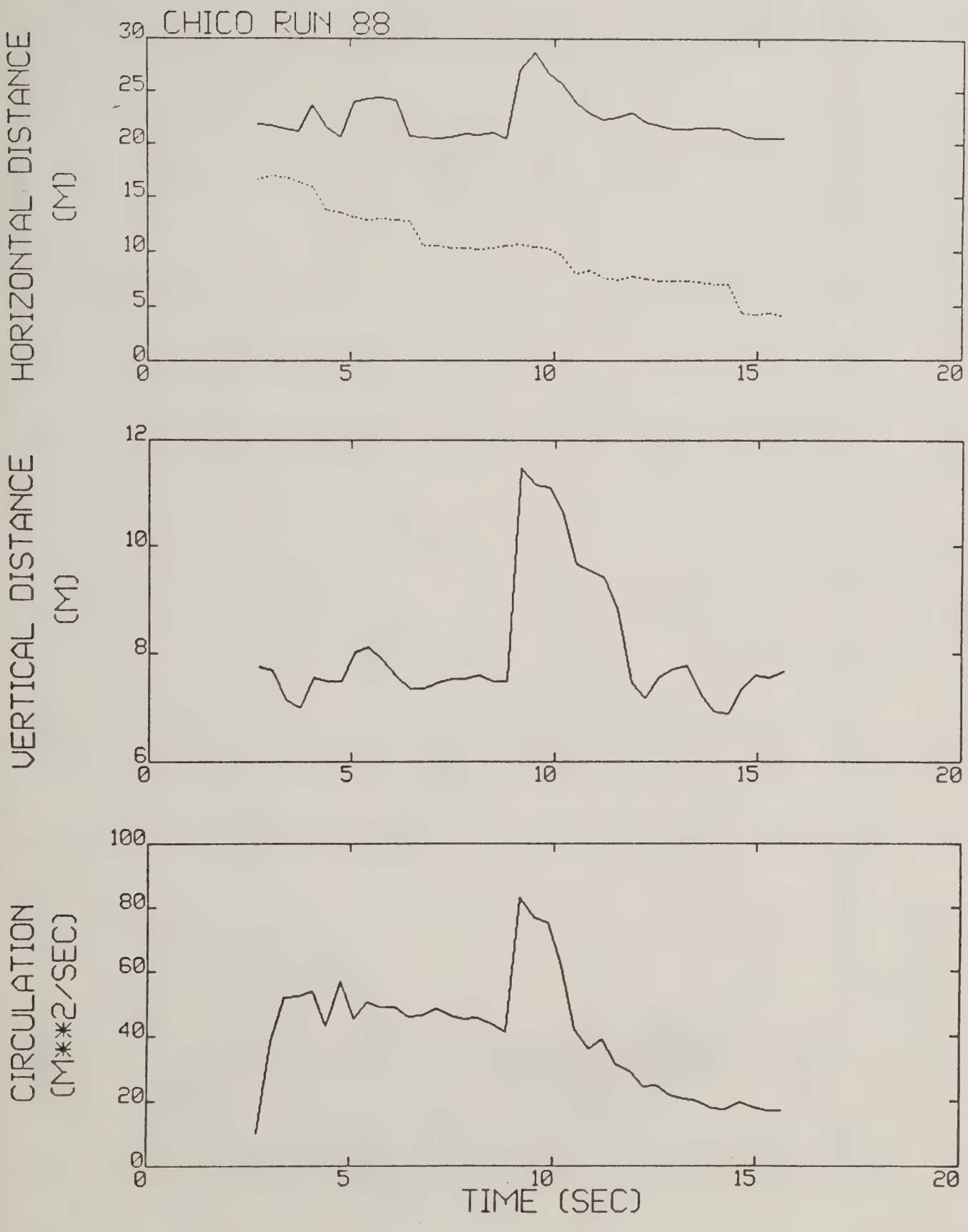

Figure B-40. Chico test run 88 generalized algorithm results.

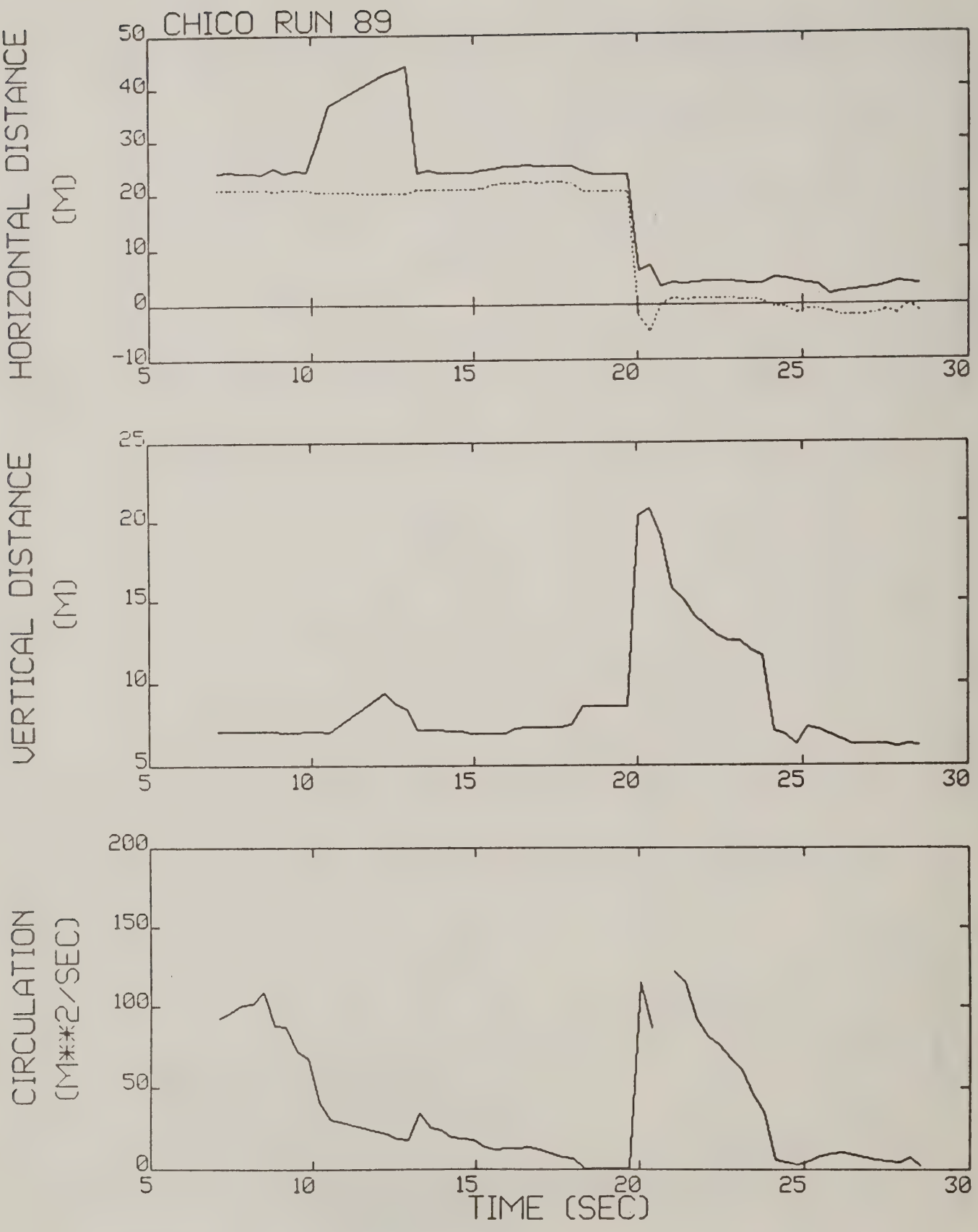

Figure B-41. Chico test run 89 generalized algorithm results.

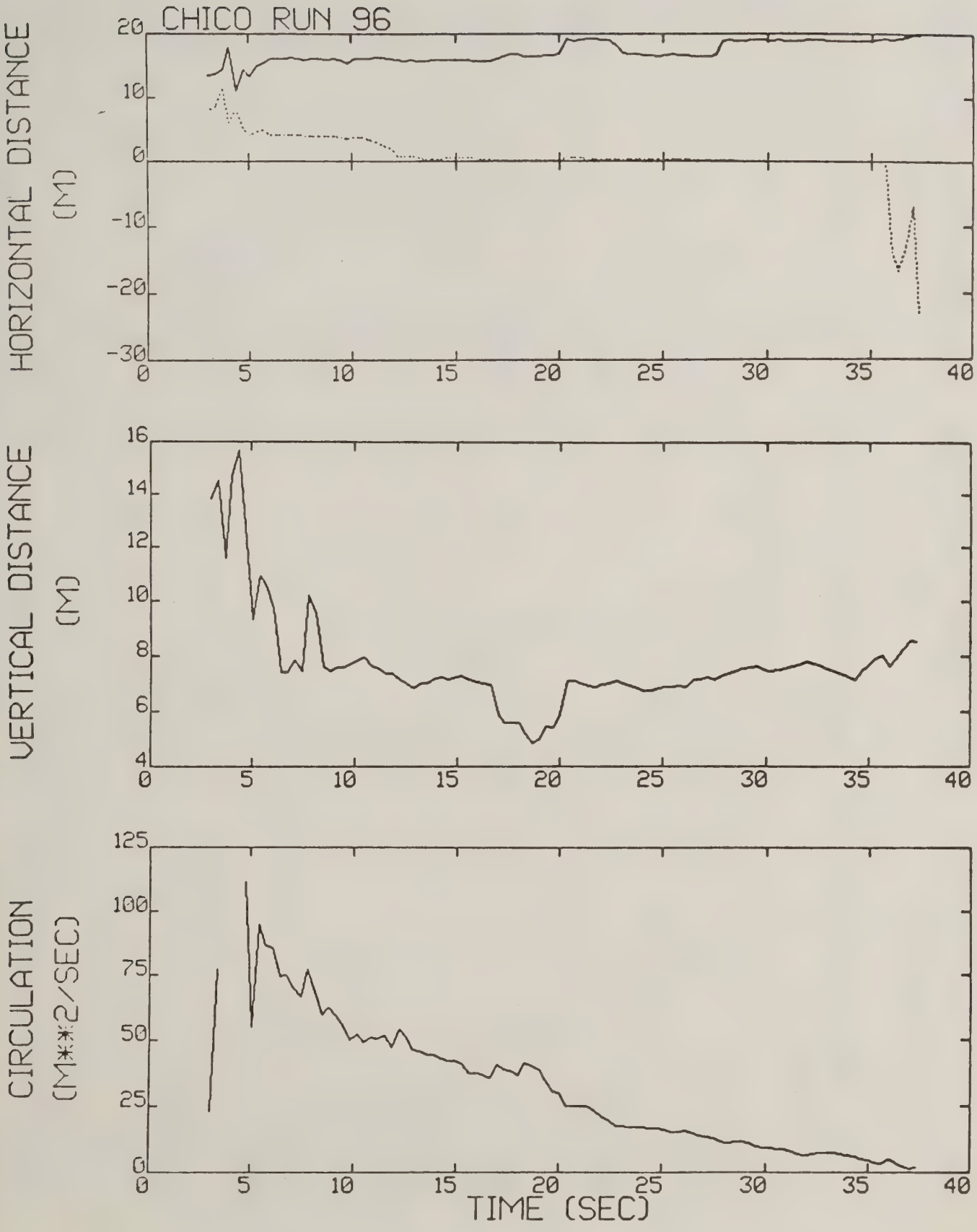

Figure B-42. Chico test run 96 generalized algorithm results (*).

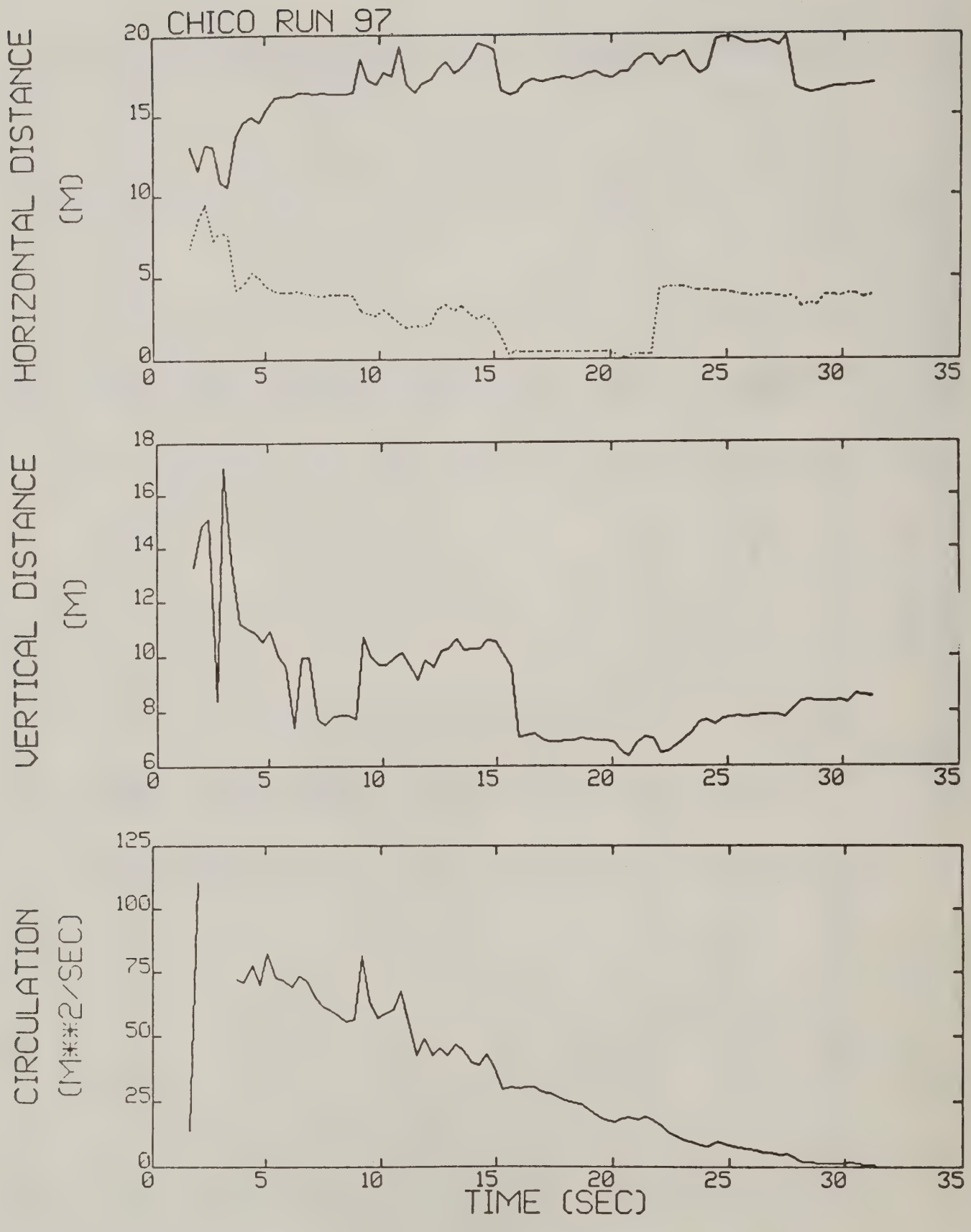

Figure B-43. Chico test run 97 generalized algorithm results (*).

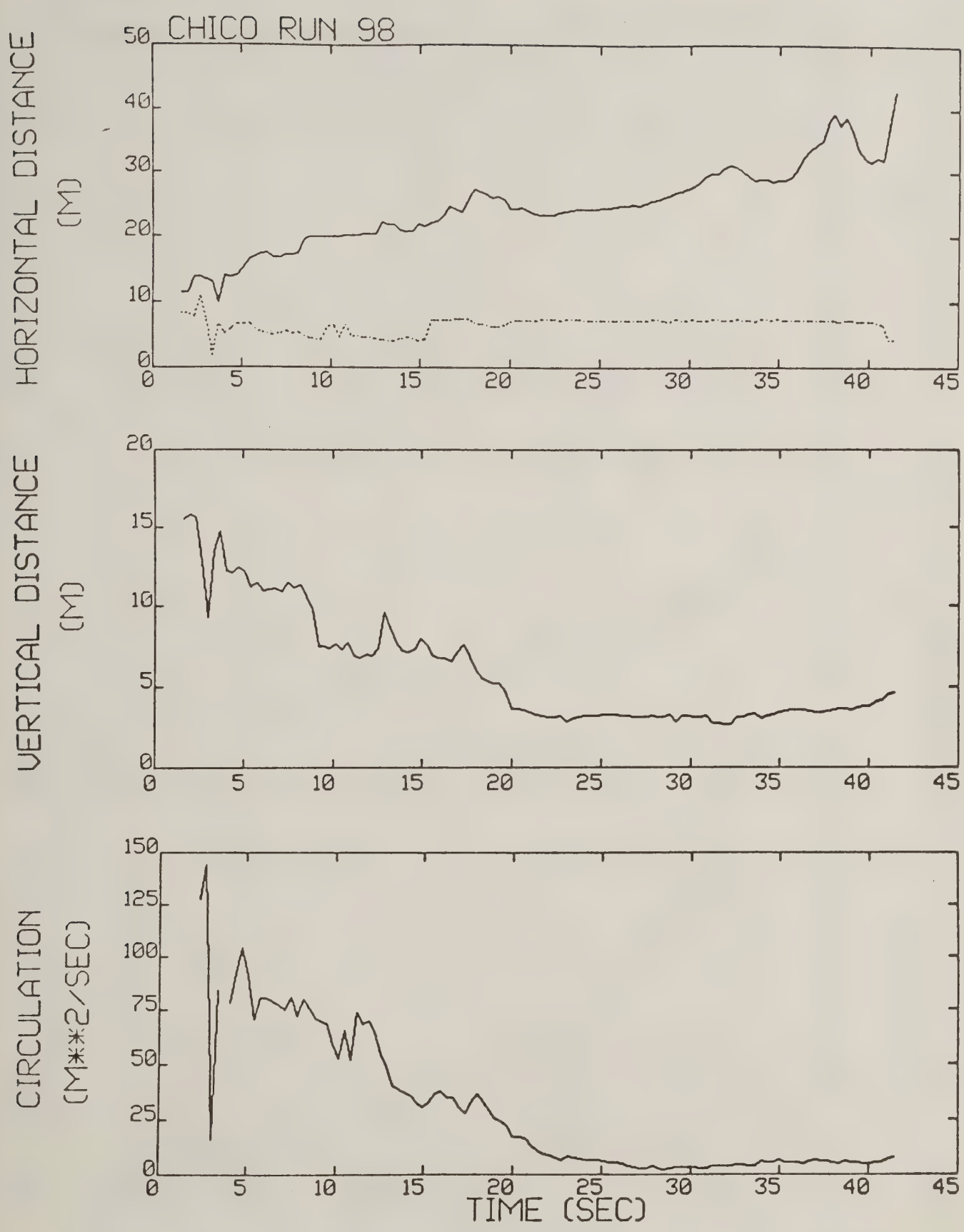

Figure B-44. Chico test run 98 generalized algorithm results (*).

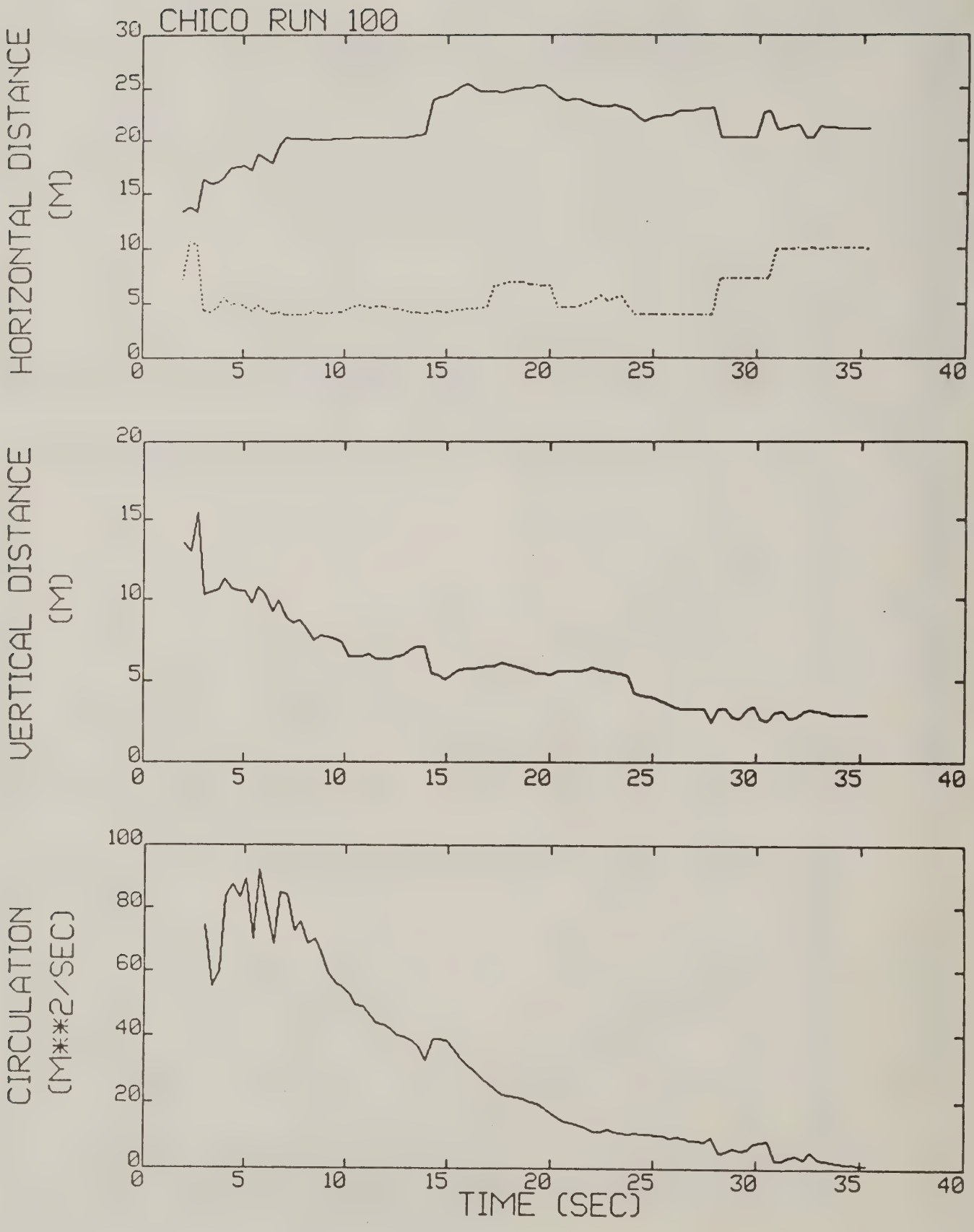

Figure B-45. Chico test run 100 generalized algorithm results (*).

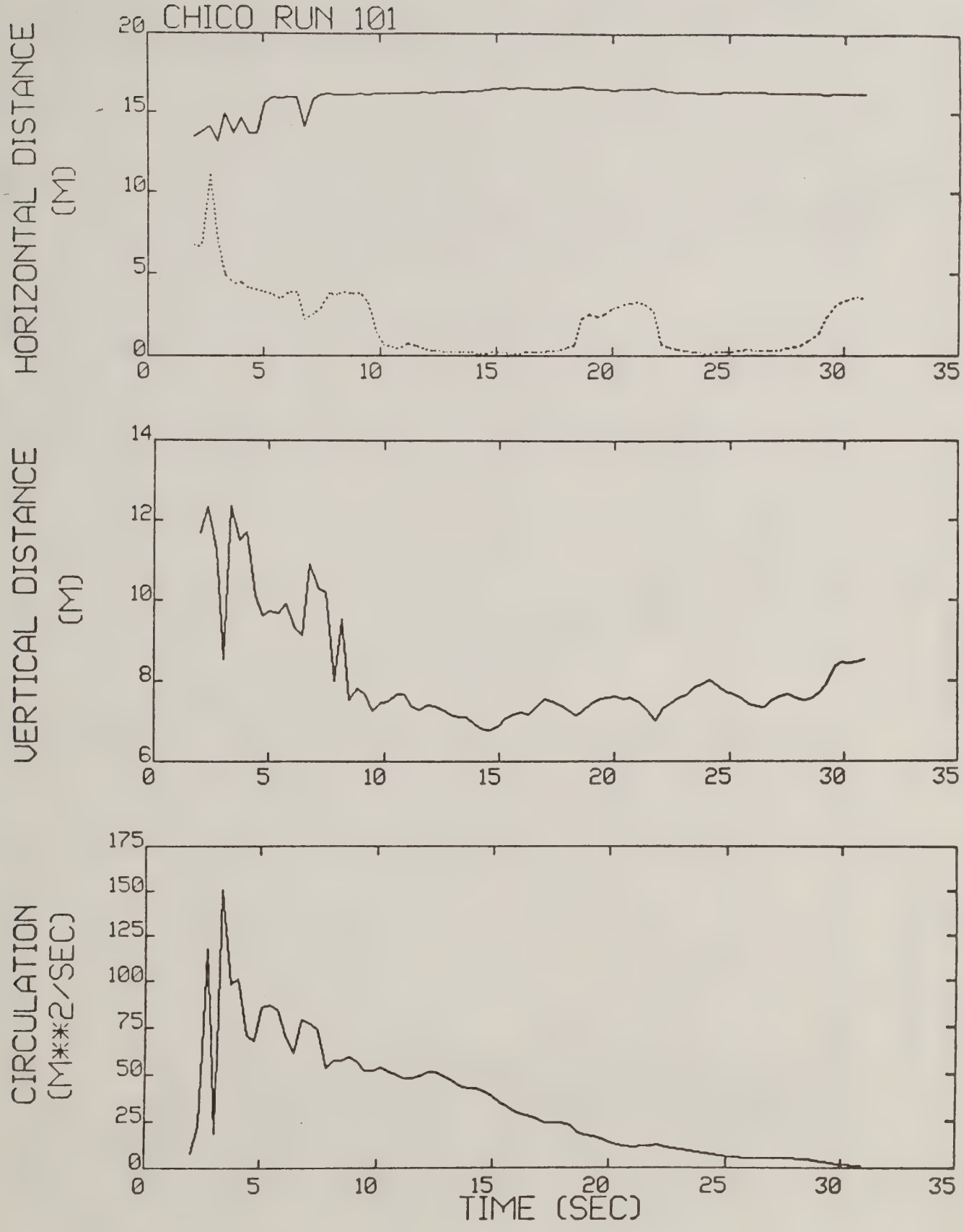

Figure B-46. Chico test run 101 generalized algorithm results (*).

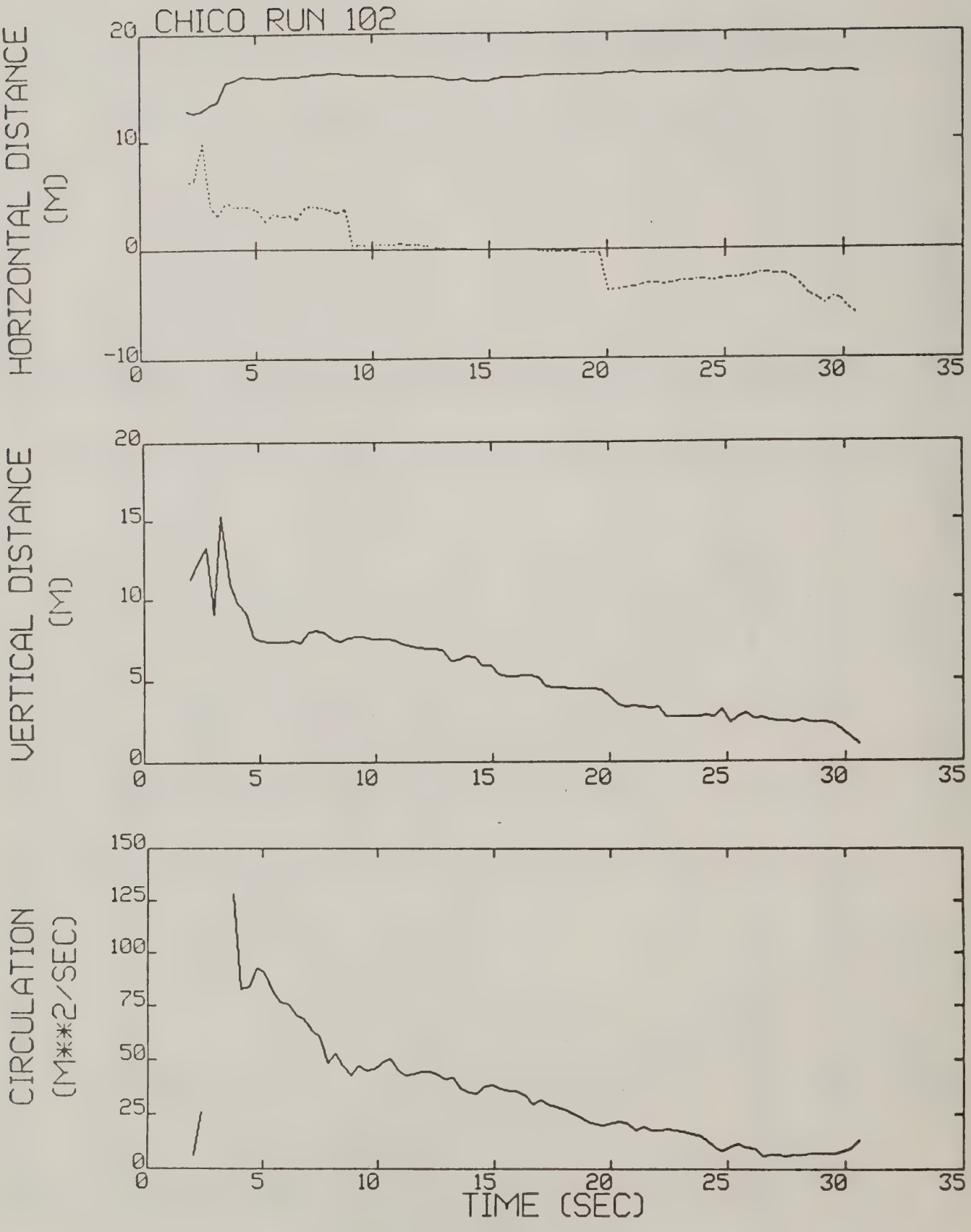

Figure B-47. Chico test run 102 generalized algorithm results (*).

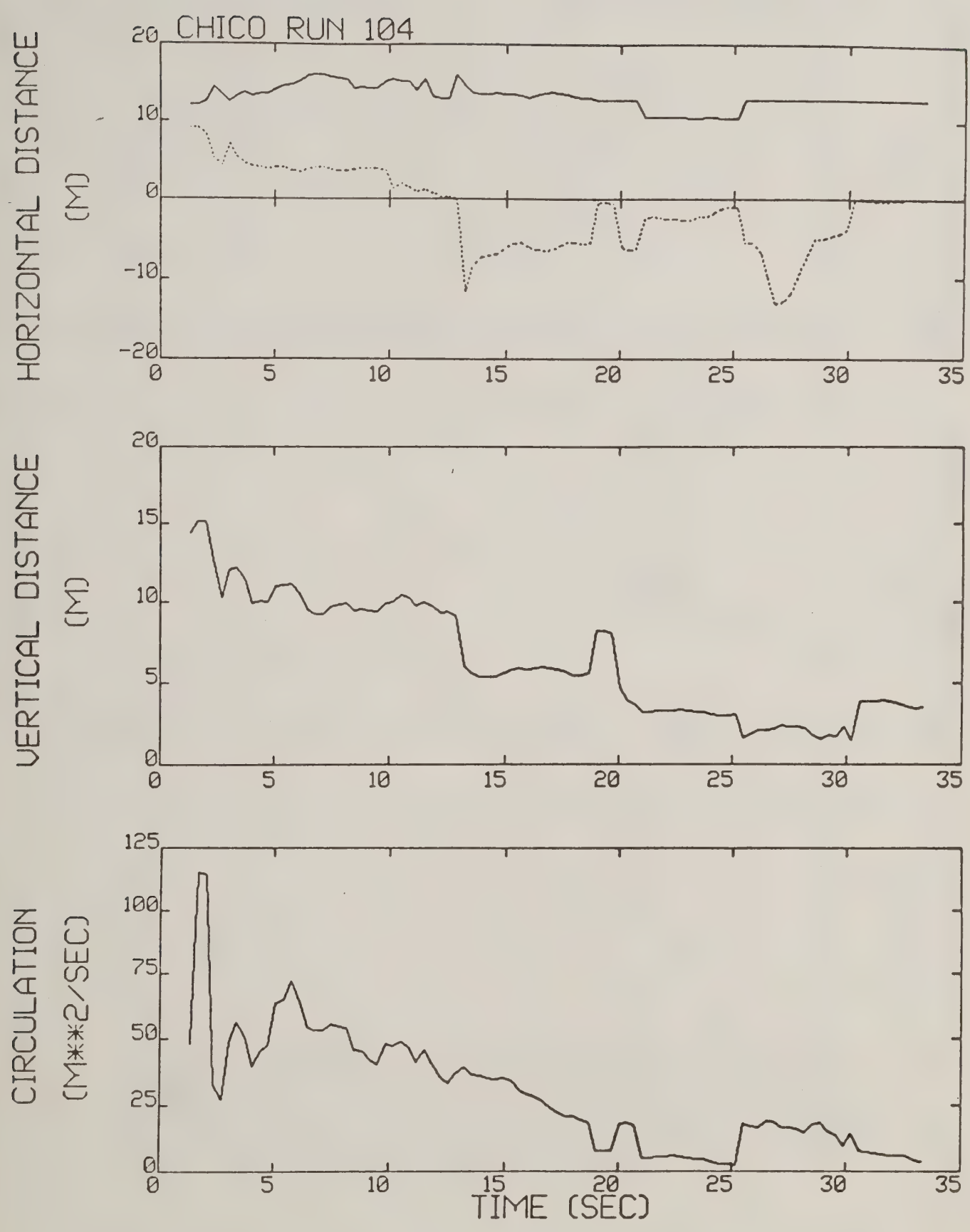

Figure B-48. Chico test run 104 generalized algorithm results (*).

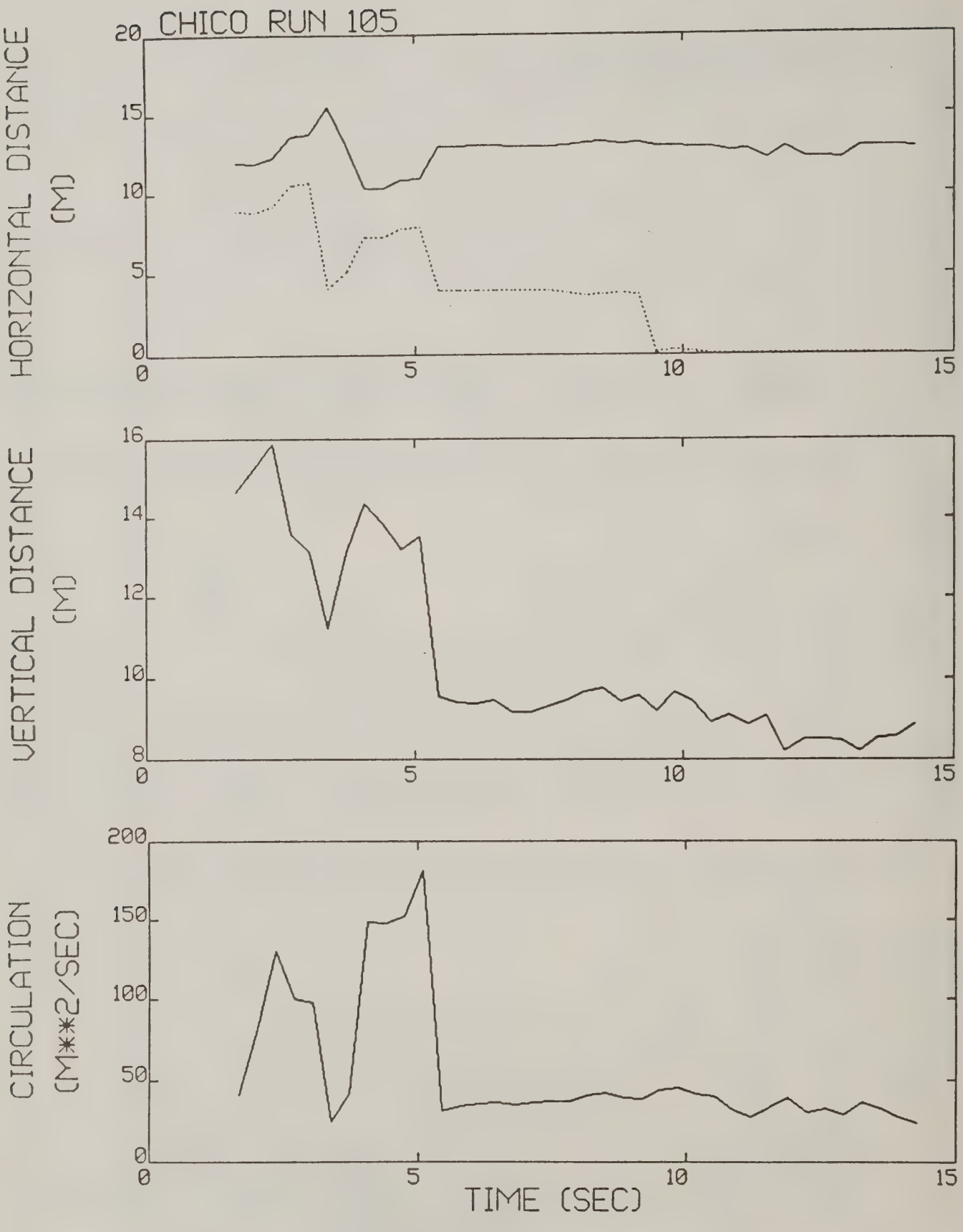

Figure B-49. Chico test run 105 generalized algorithm results.

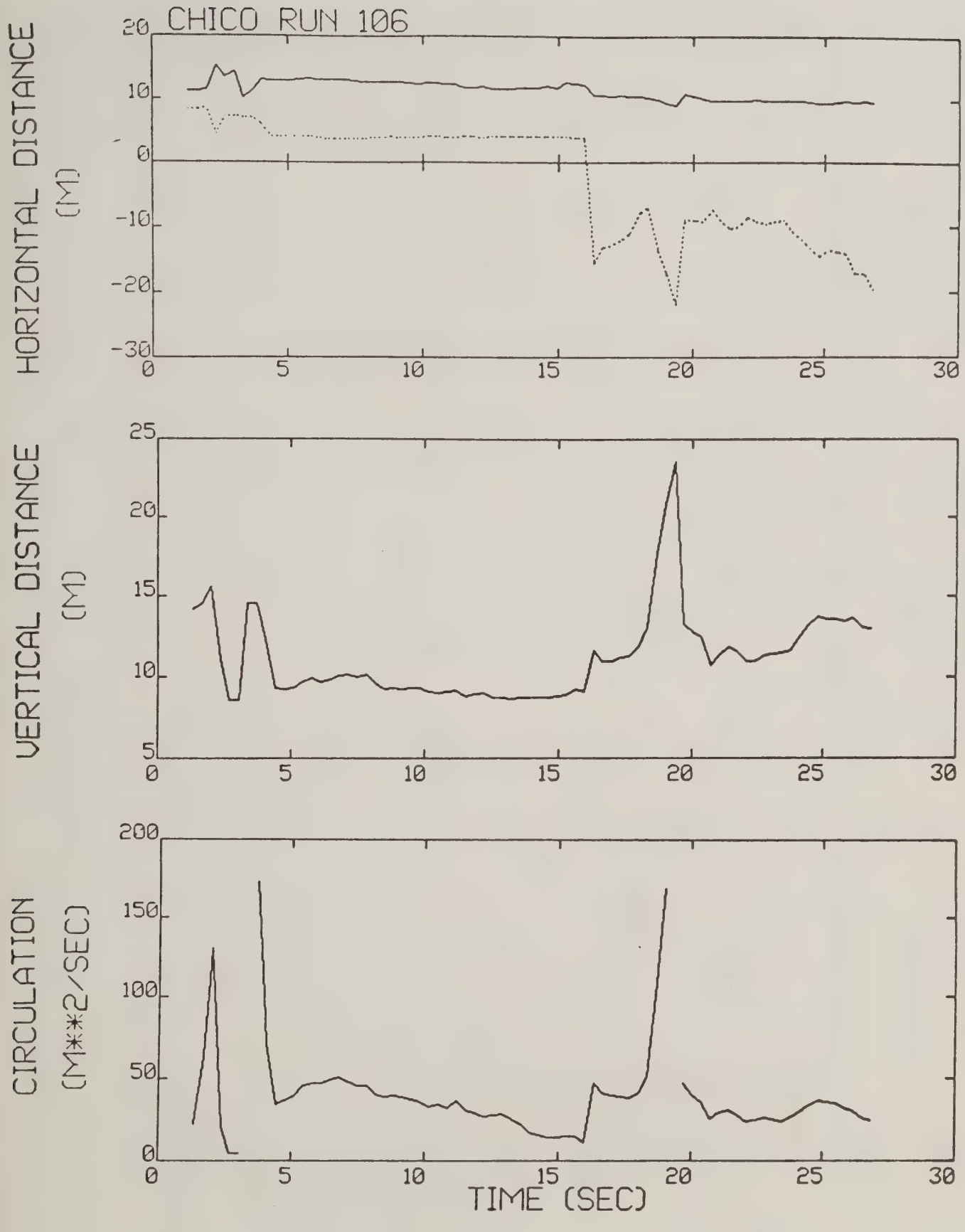

Figure B-50. Chico test run 106 generalized algorithm results.

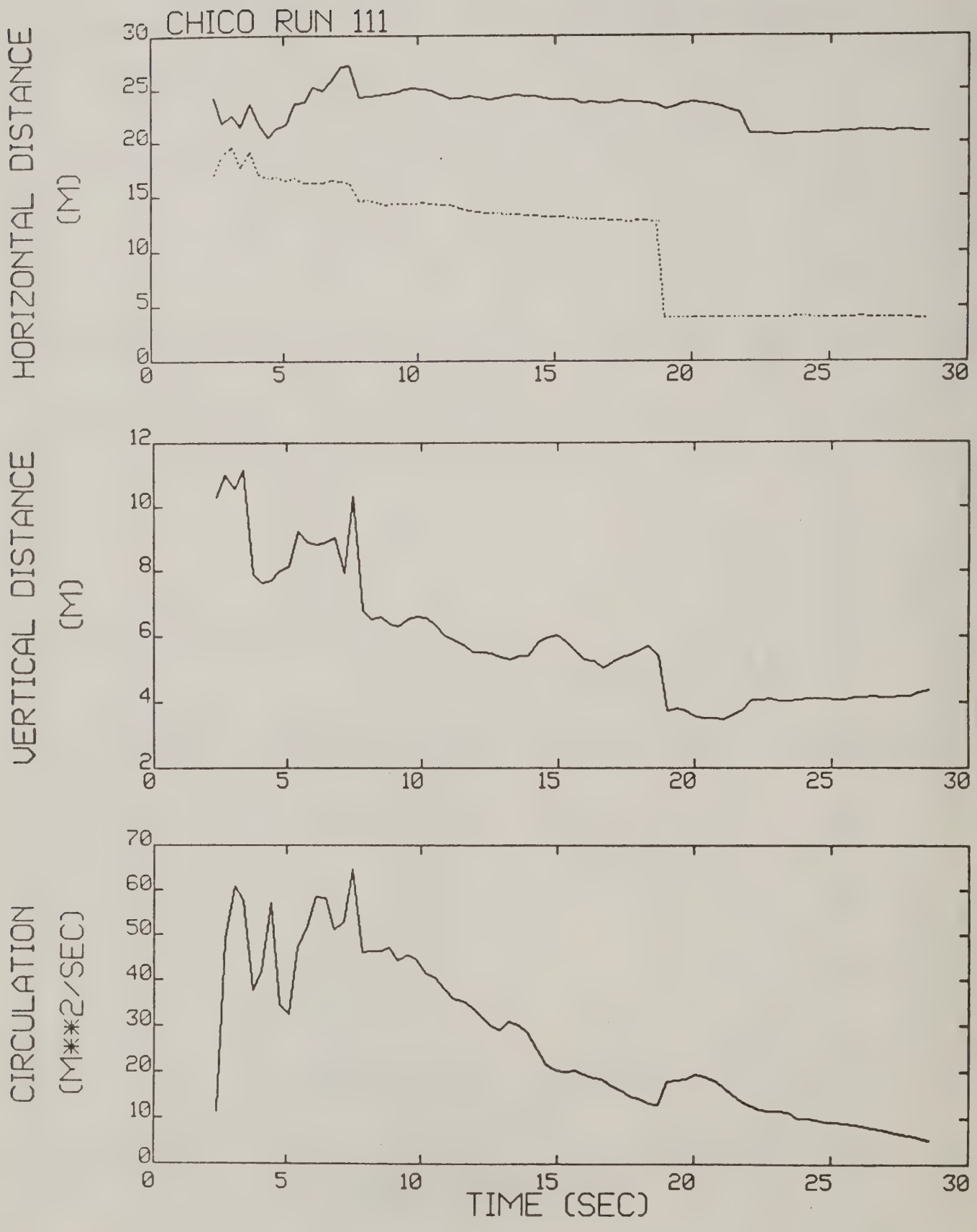

Figure B-51. Chico test run 111 generalized algorithm results (*).

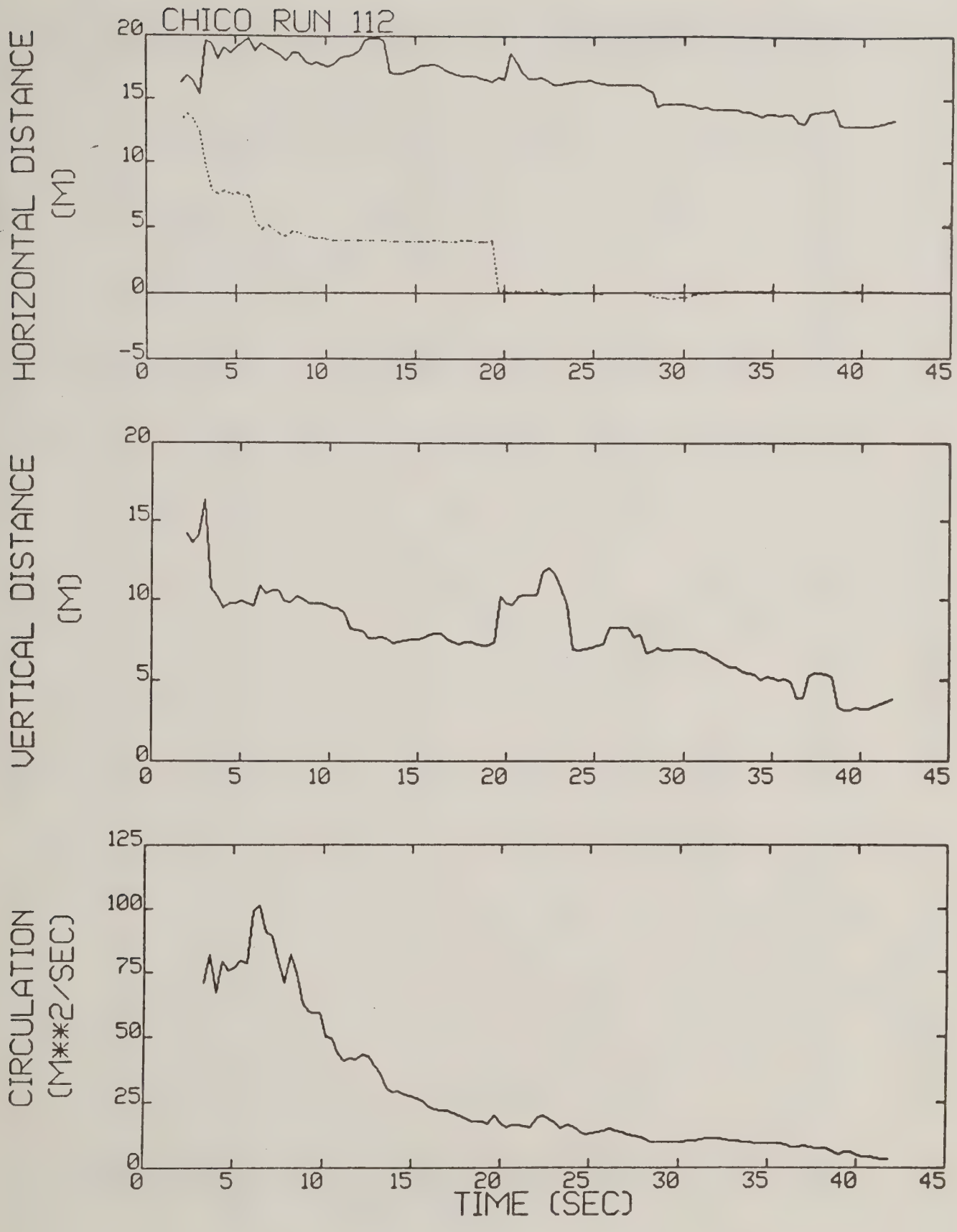

Figure B-52. Chico test run 112 generalized algorithm results (*).

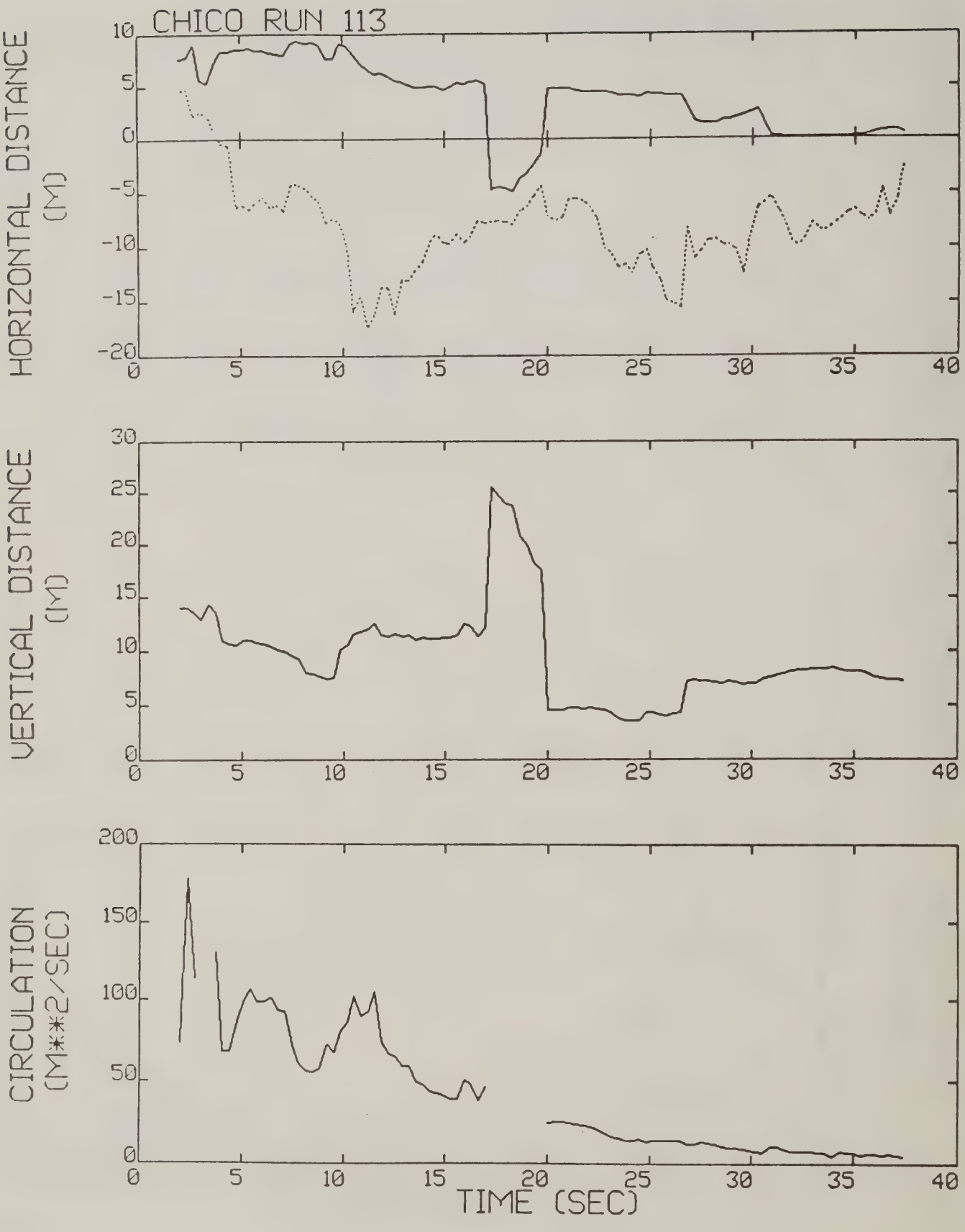

Figure B-53. Chico test run 113 generalized algorithm results (*).

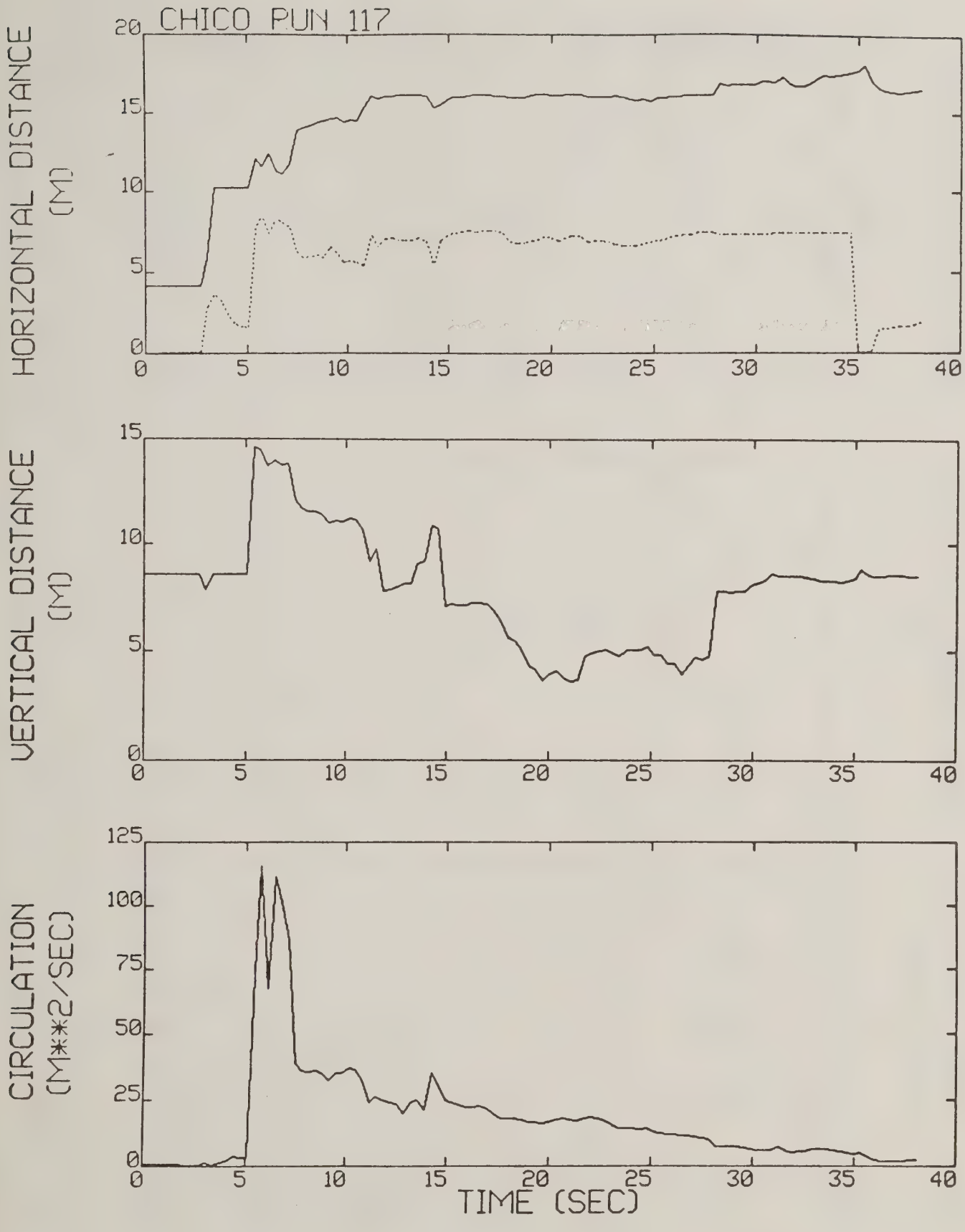

Figure B-54. Chico test run 117 generalized algorithm results (*).

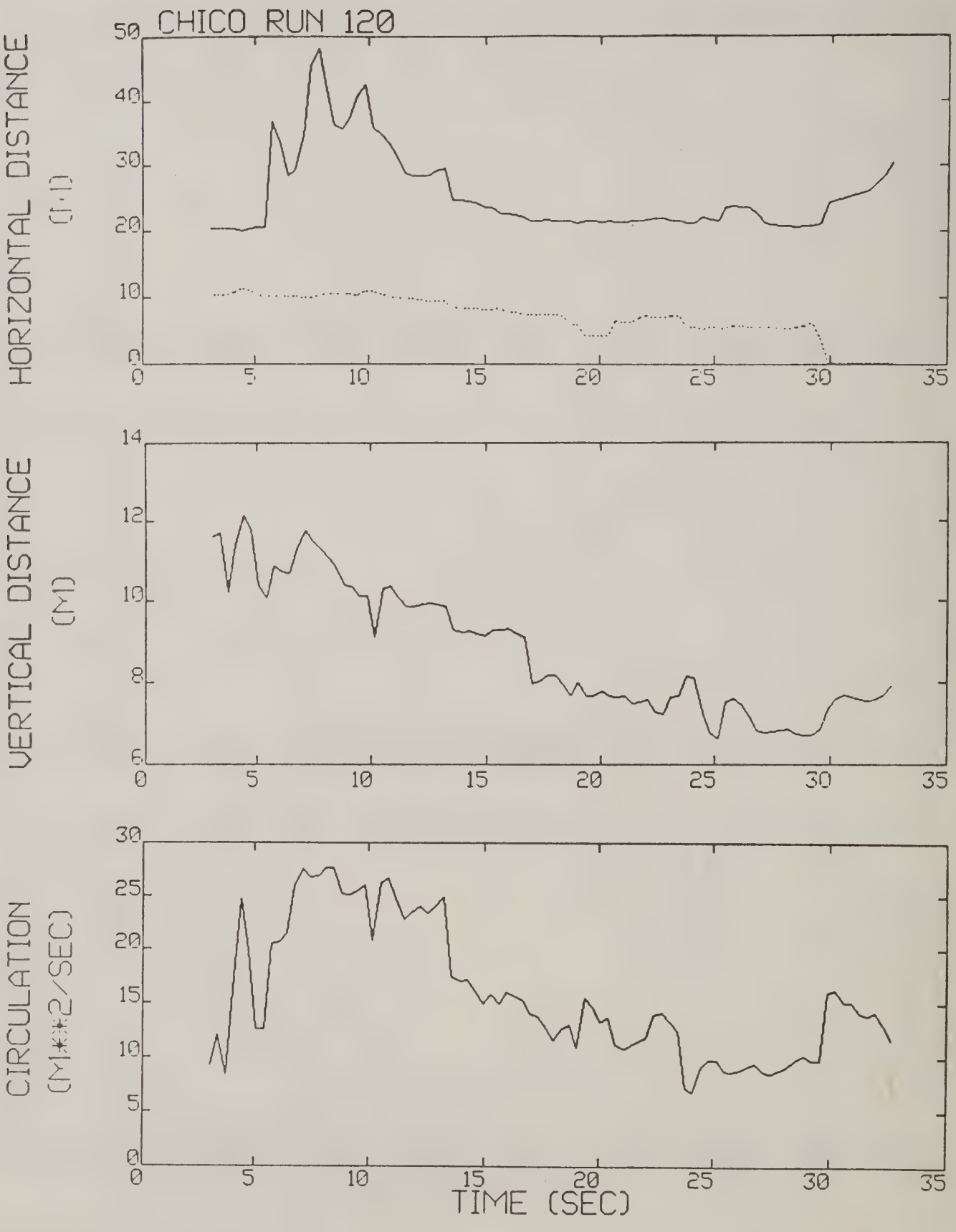

Figure B-55. Chico test run 120 generalized algorithm results (*).

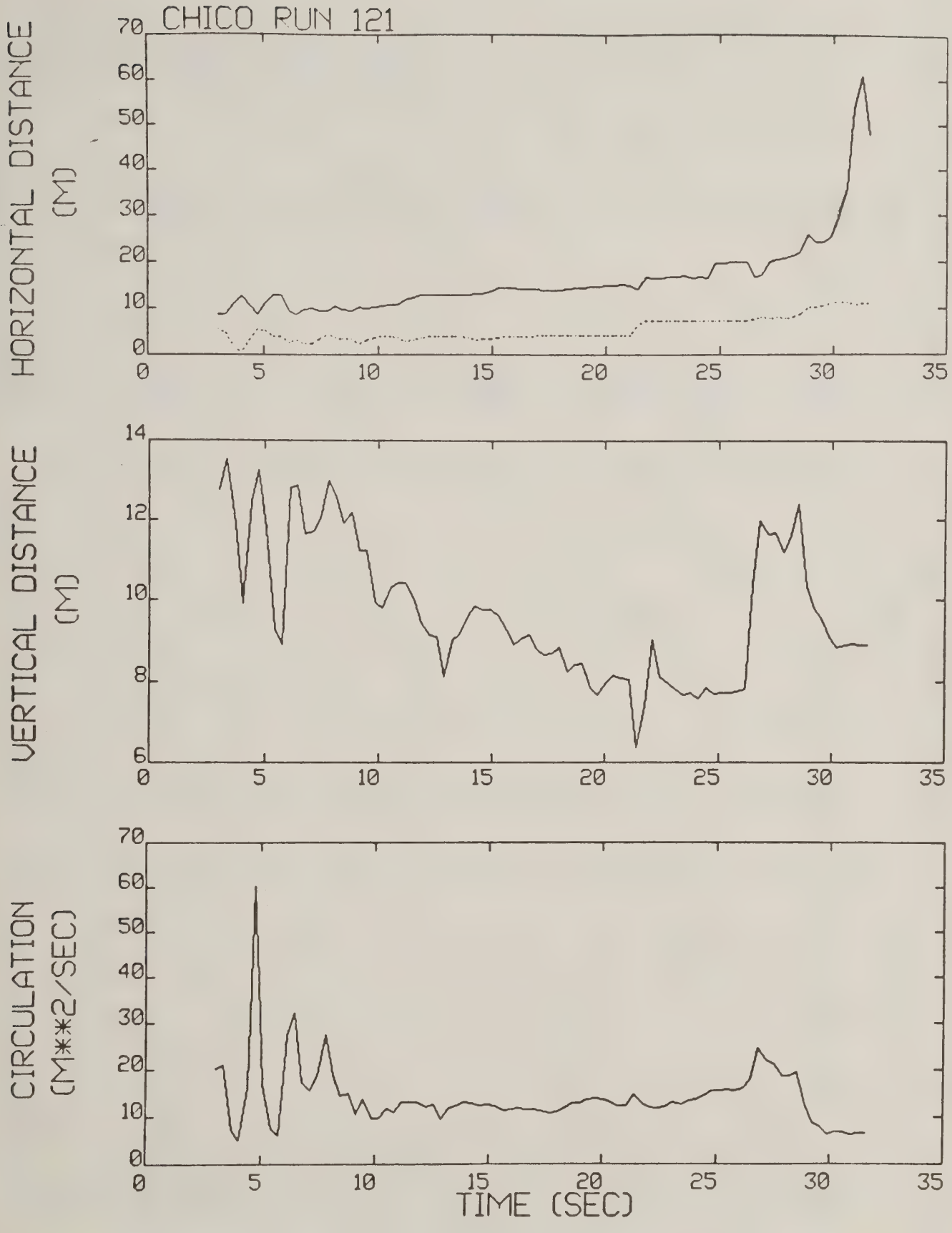

Figure B-56. Chico test run 121 generalized algorithm results.

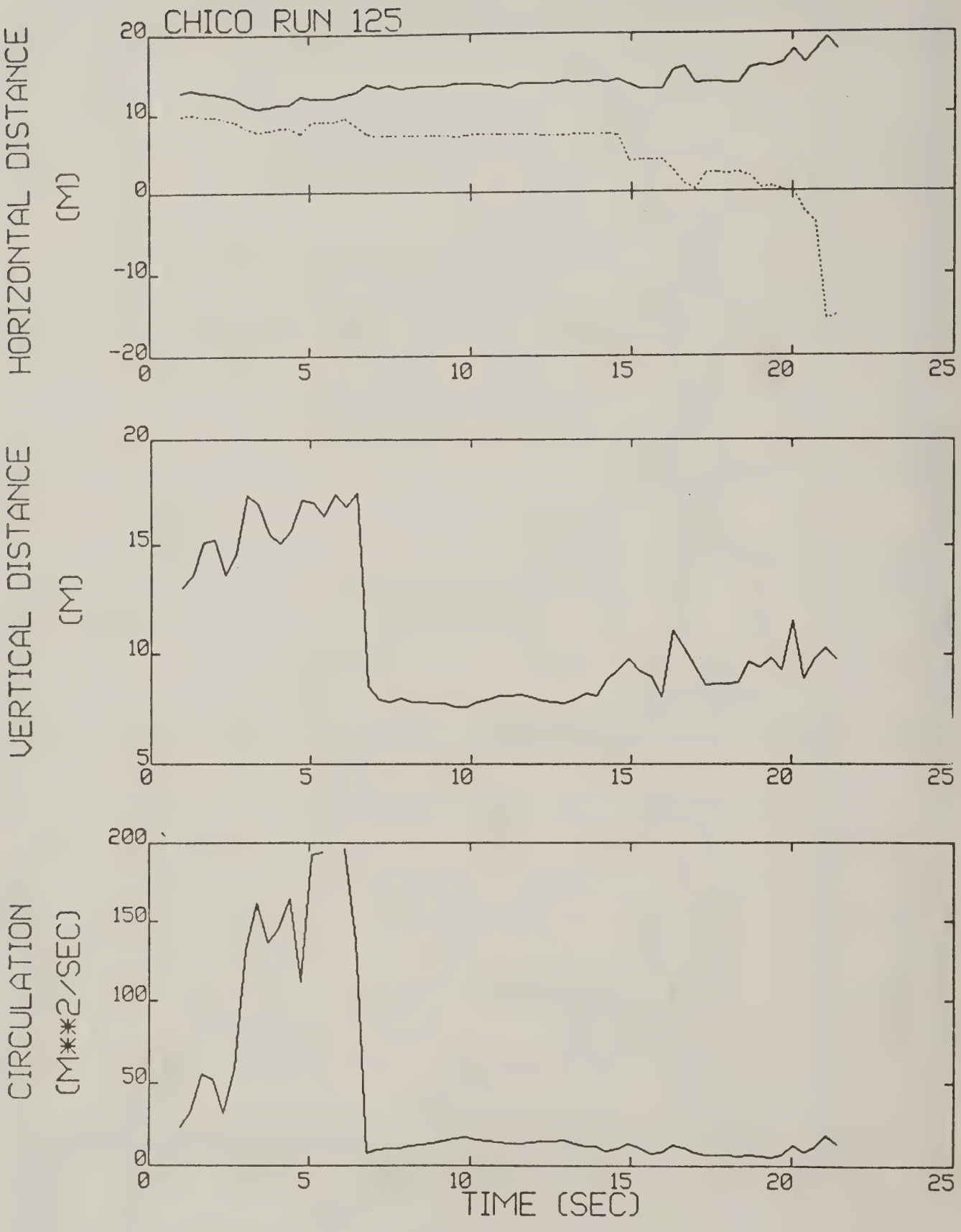

Figure B-57. Chico test run 125 generalized algorithm results.

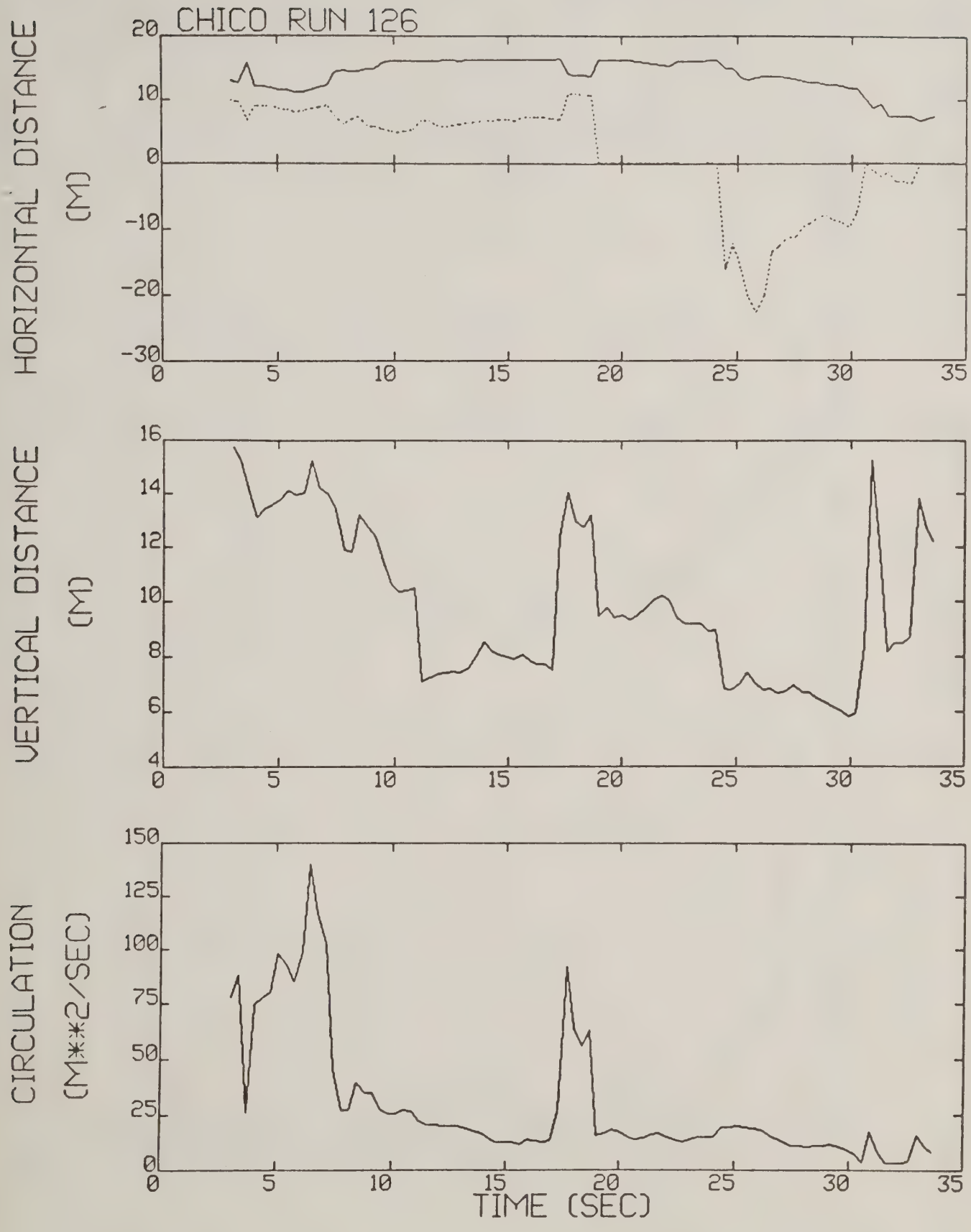

Figure B-58. Chico test run 126 generalized algorithm results (*).

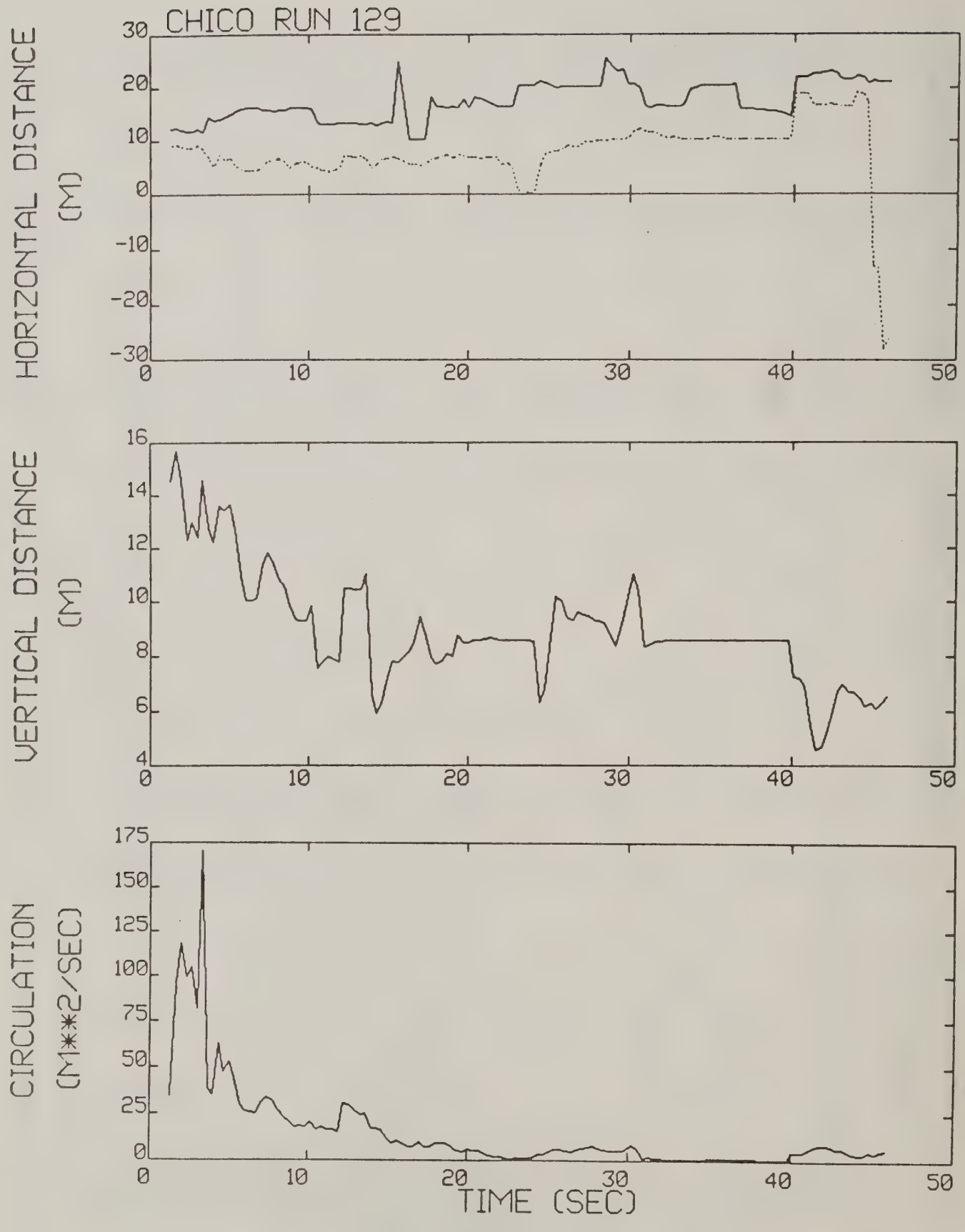

Figure B-59. Chico test run 129 generalized algorithm results (*).

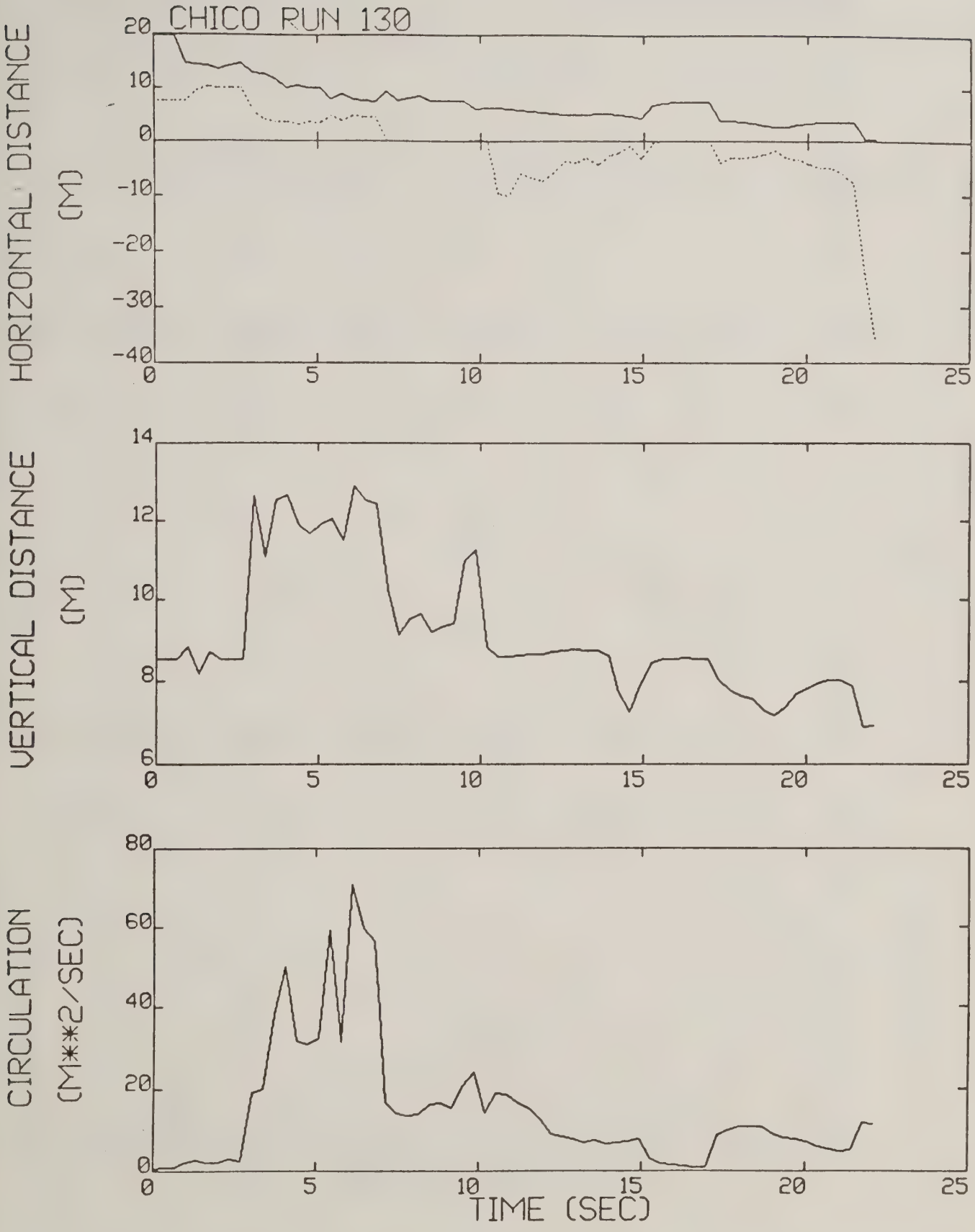

Figure B-60. Chico test run 130 generalized algorithm results (*).

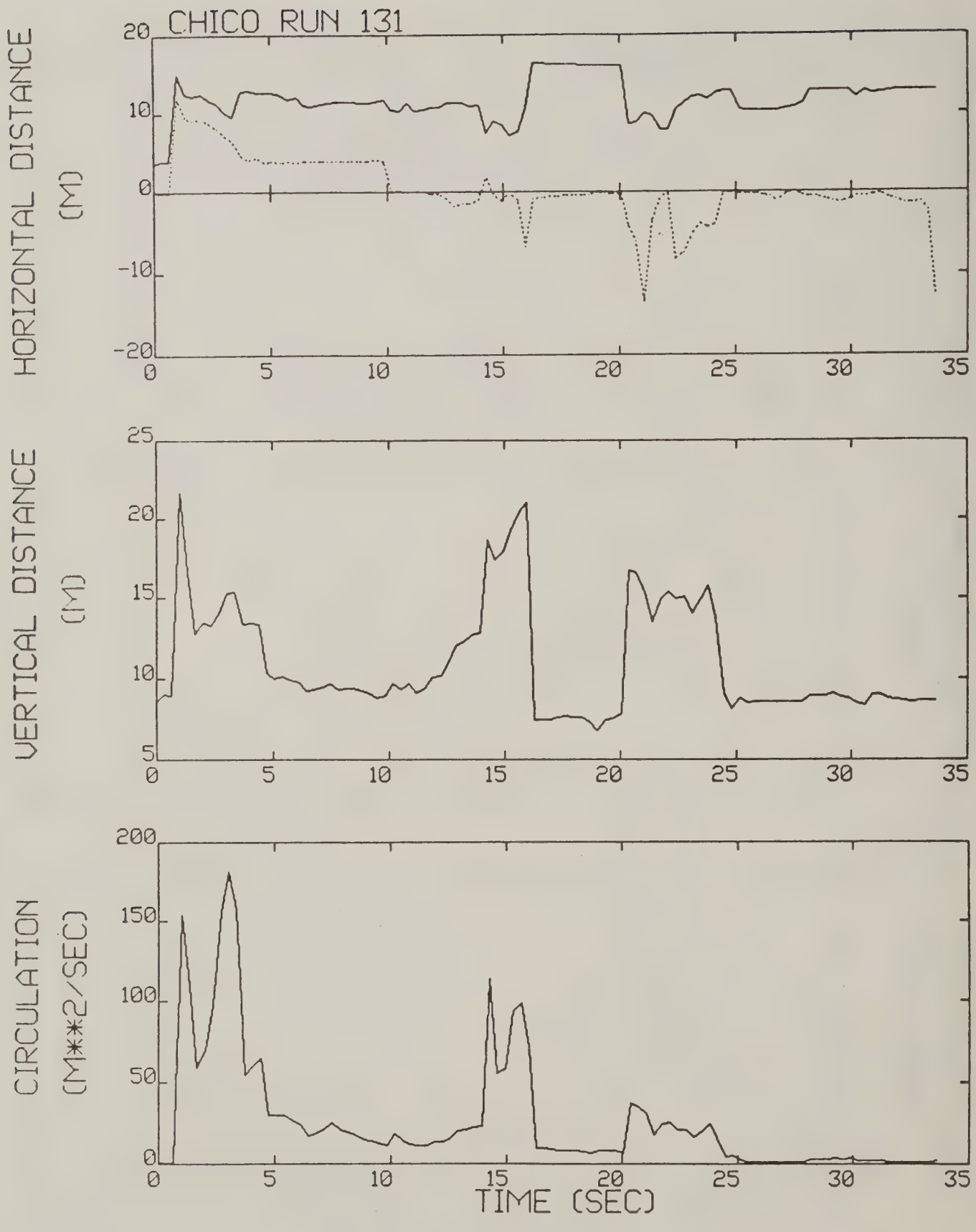

Figure B-61. Chico test run 131 generalized algorithm results (*).

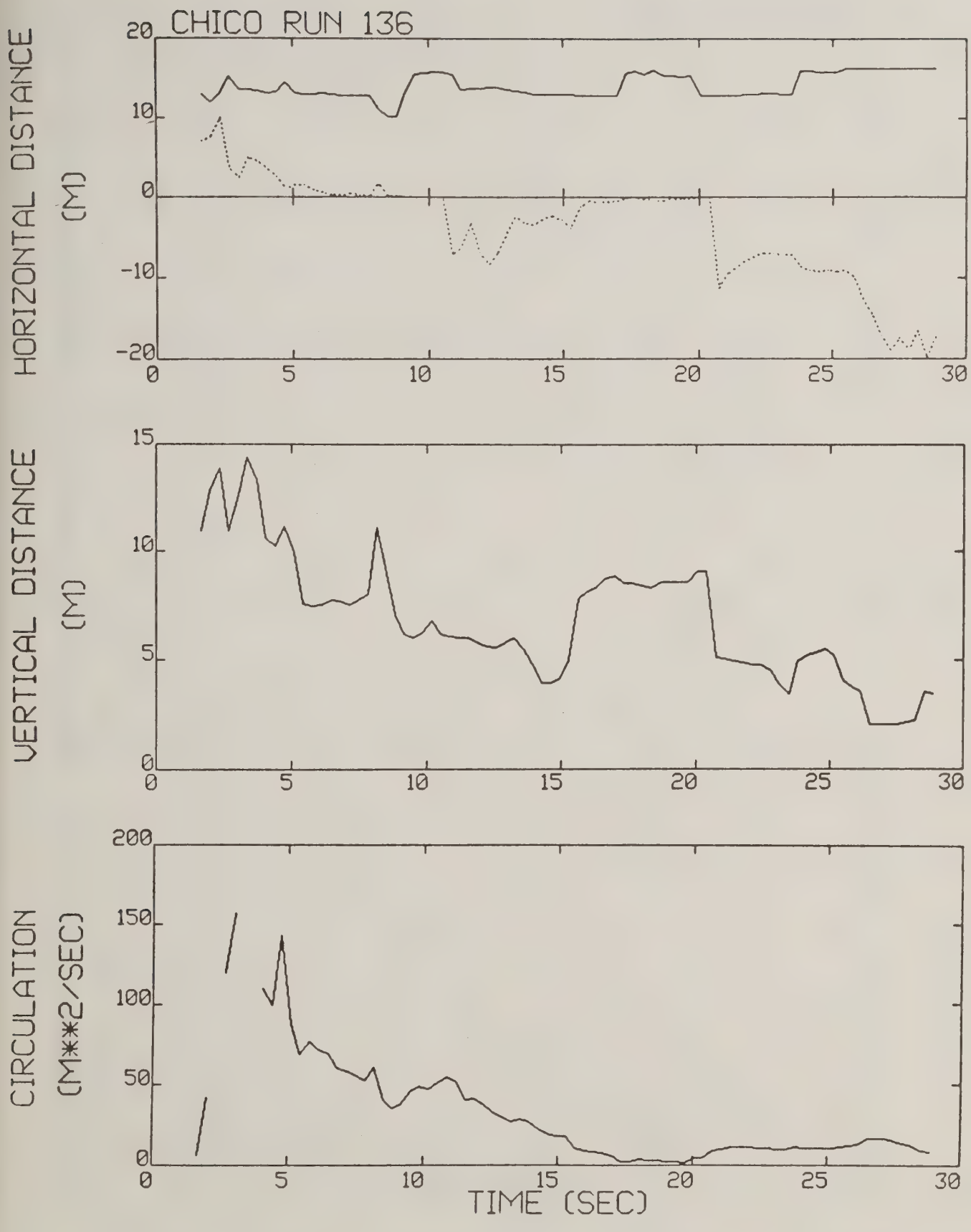

Figure B-62. Chico test run 136 generalized algorithm results (*).

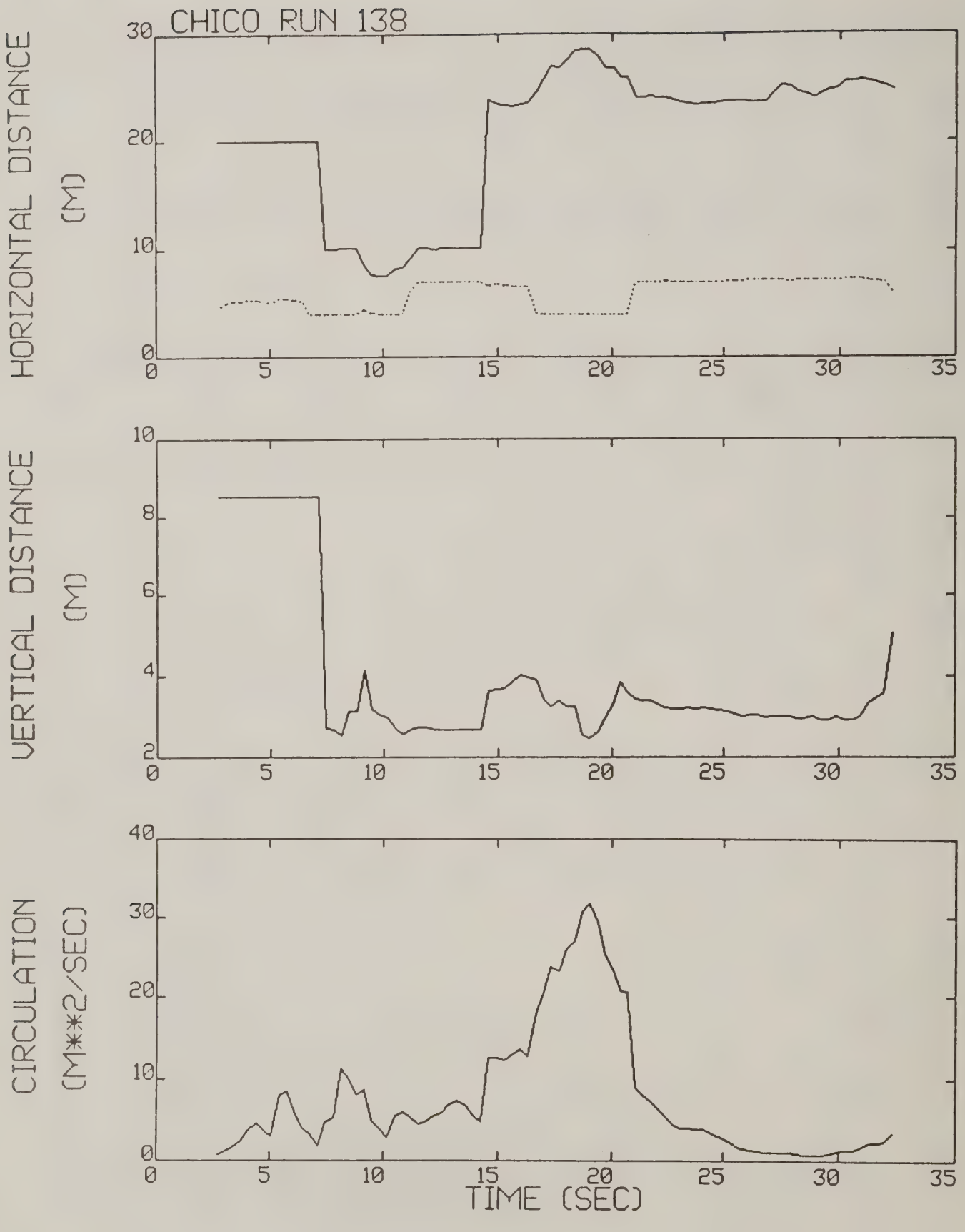

Figure B-63. Chico test run 138 generalized algorithm results.

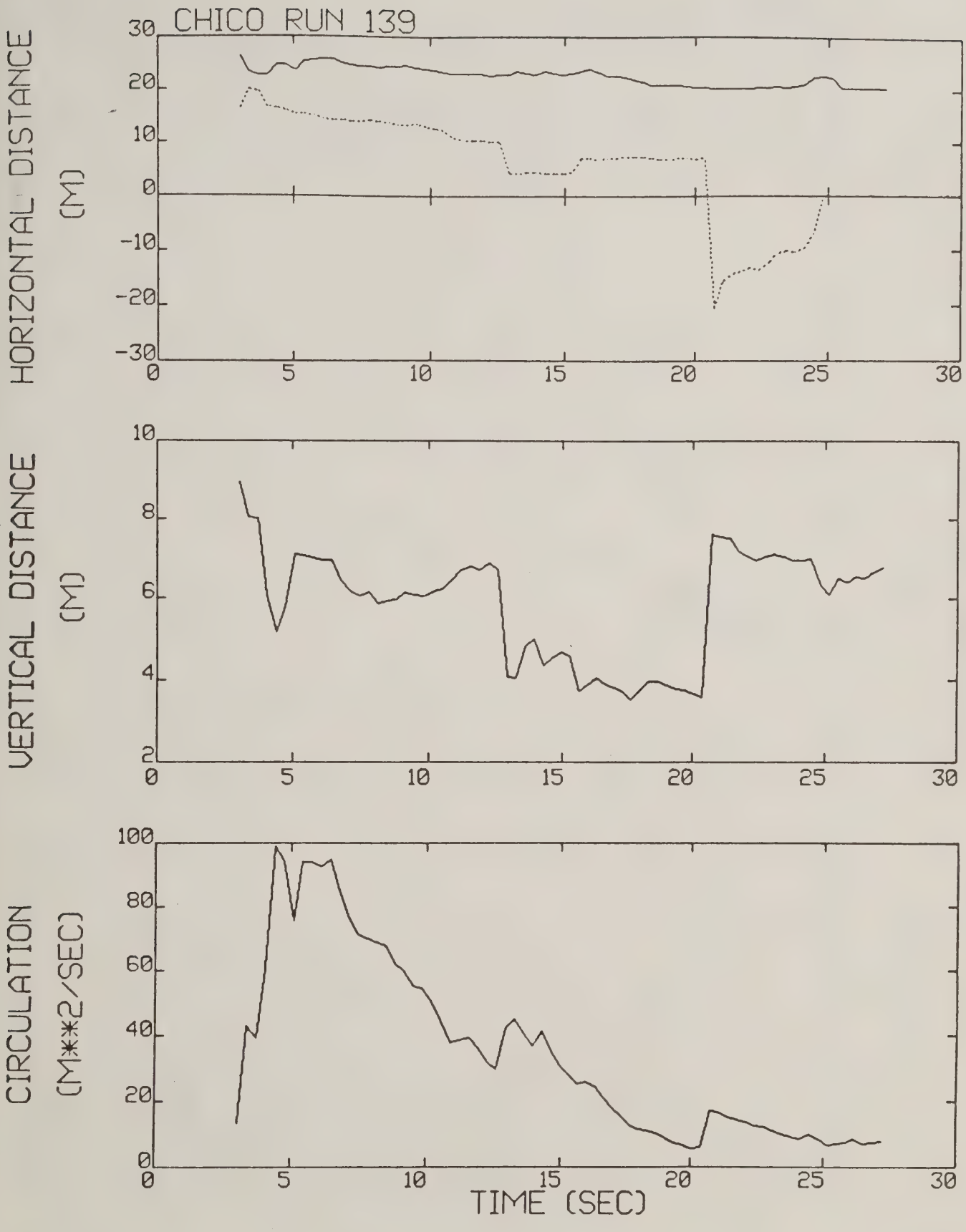

Figure B-64. Chico test run 139 generalized algorithm results (*).

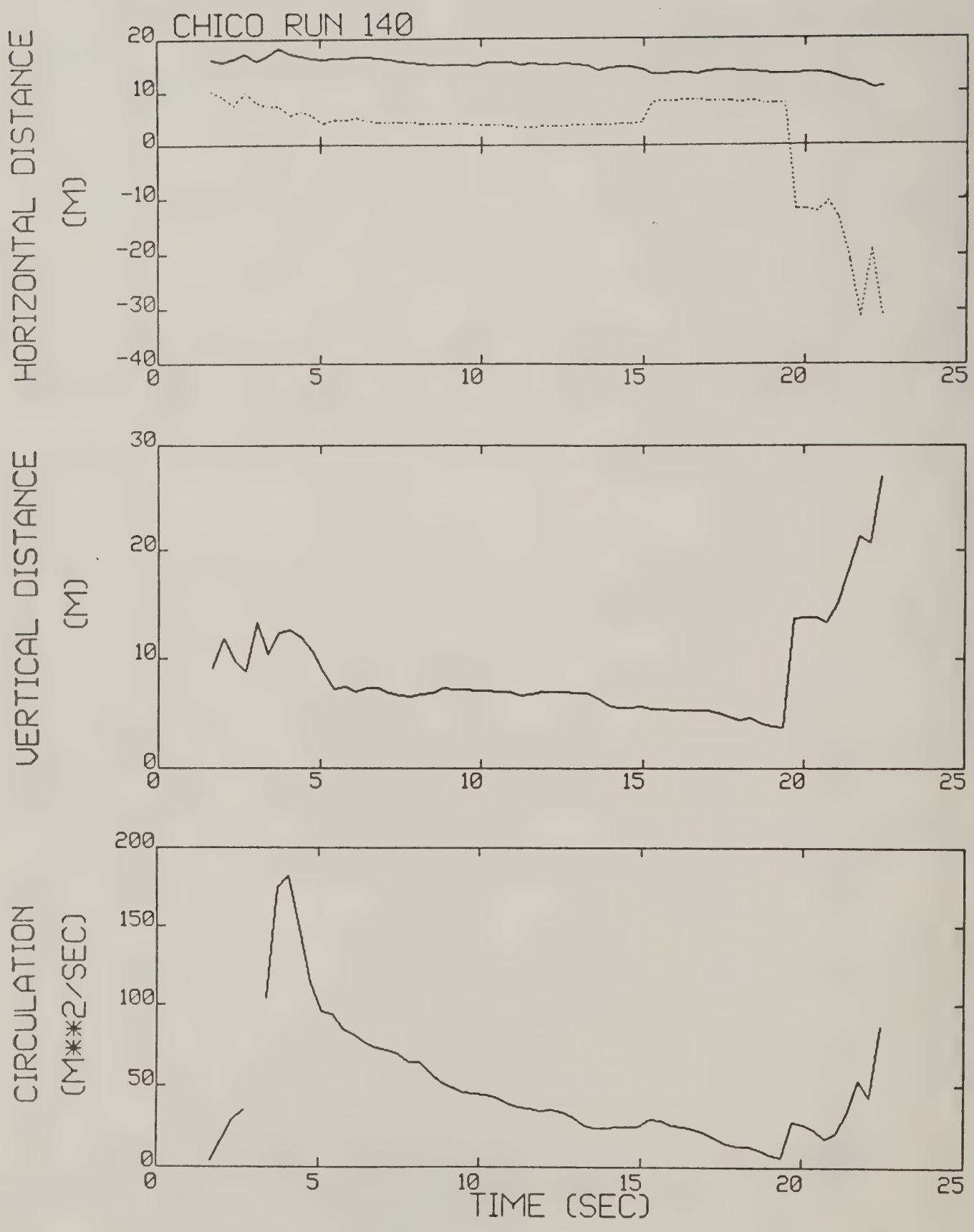

Figure B-65. Chico test run 140 generalized algorithm results (*).

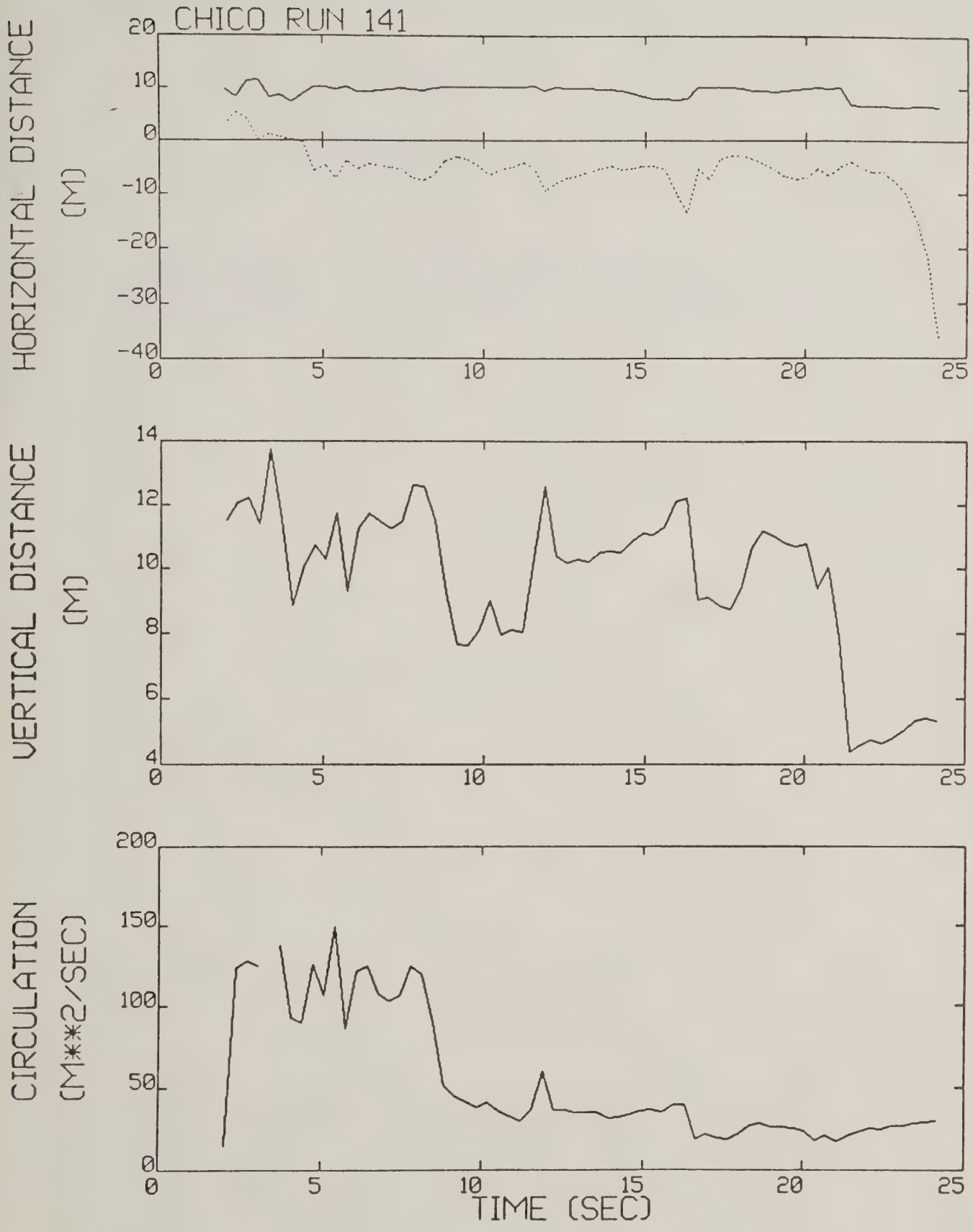

Figure B-66. Chico test run 141 generalized algorithm results (*).

APPENDIX C

Red Bluff Reduced Plots

Generalized algorithm results for Program WIND Phase III at Red Bluff are plotted on the following pages in the same format as discussed in Appendix A.

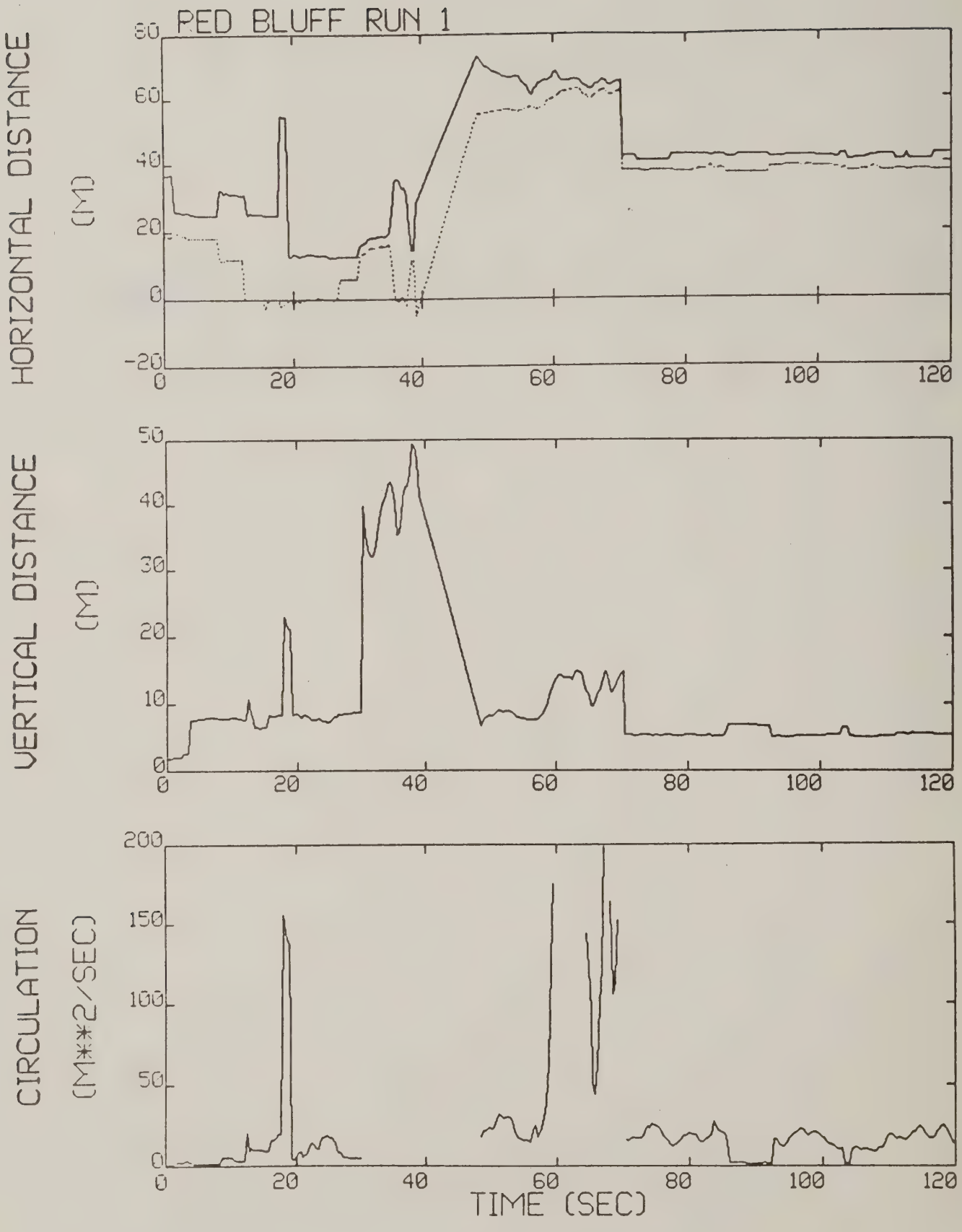

Figure C-1. Red Bluff test run 1 generalized algorithm results.

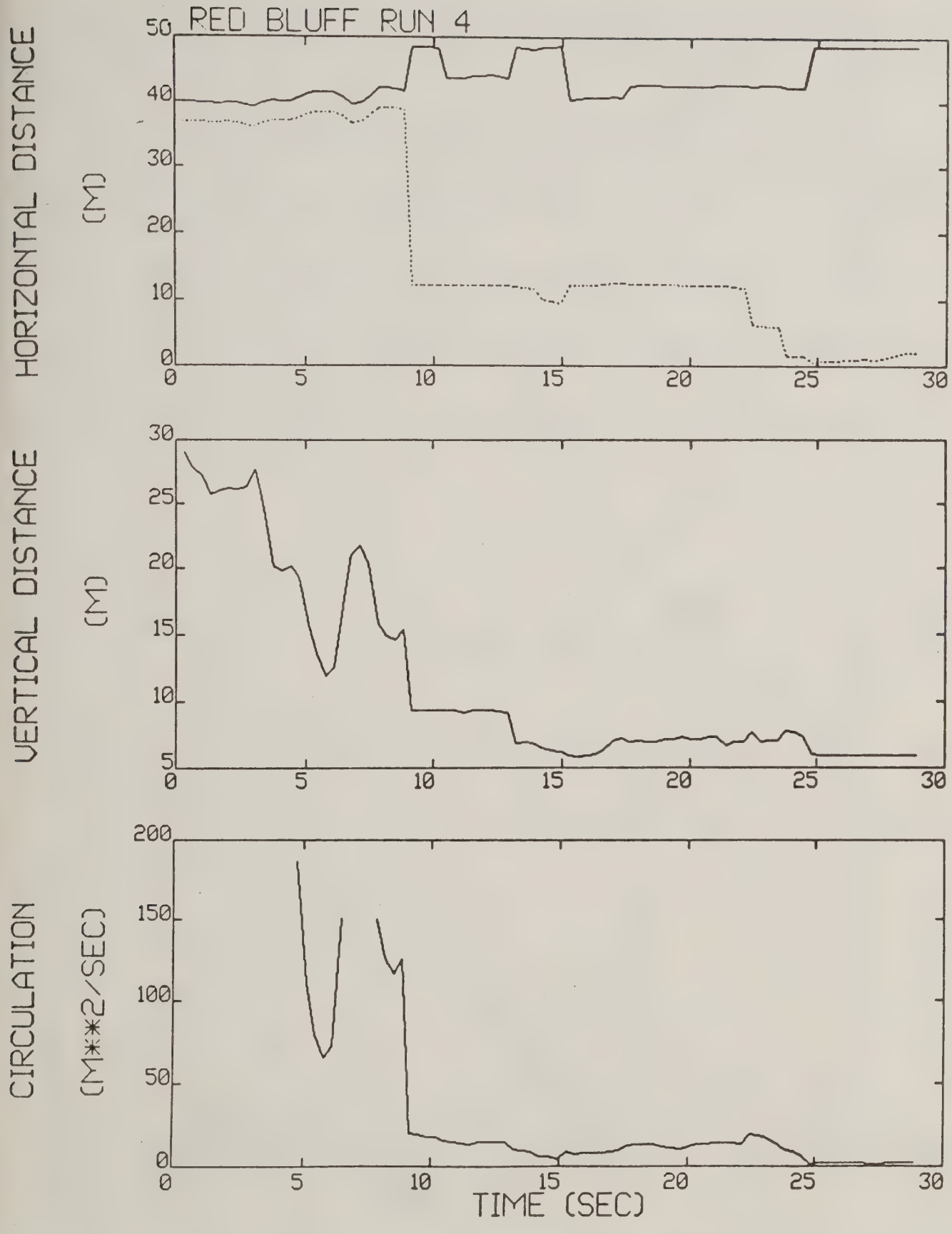

Figure C-2. Red Bluff test run 4 generalized algorithm results.

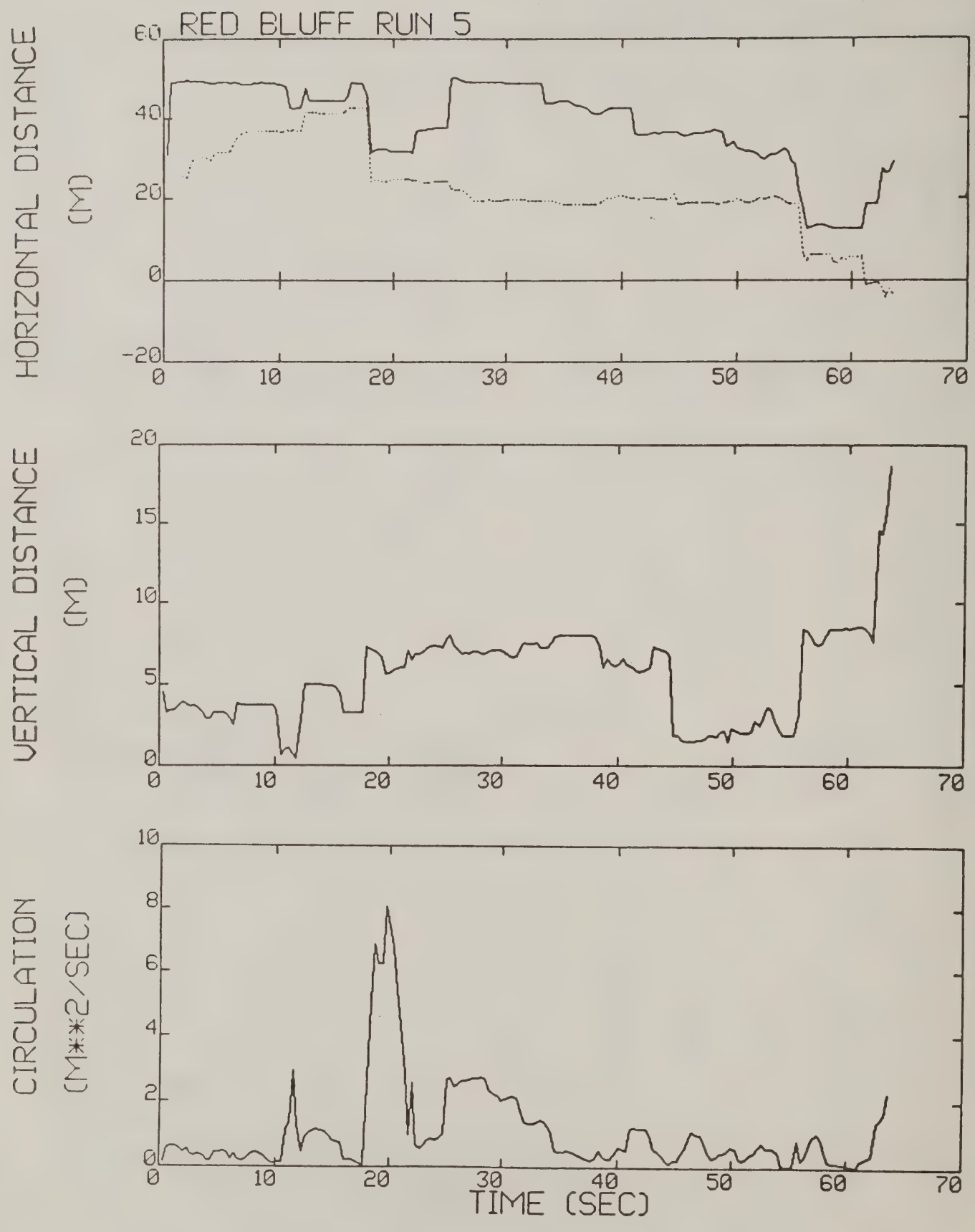

Figure C-3. Red Bluff test run 5 generalized algorithm results (*).

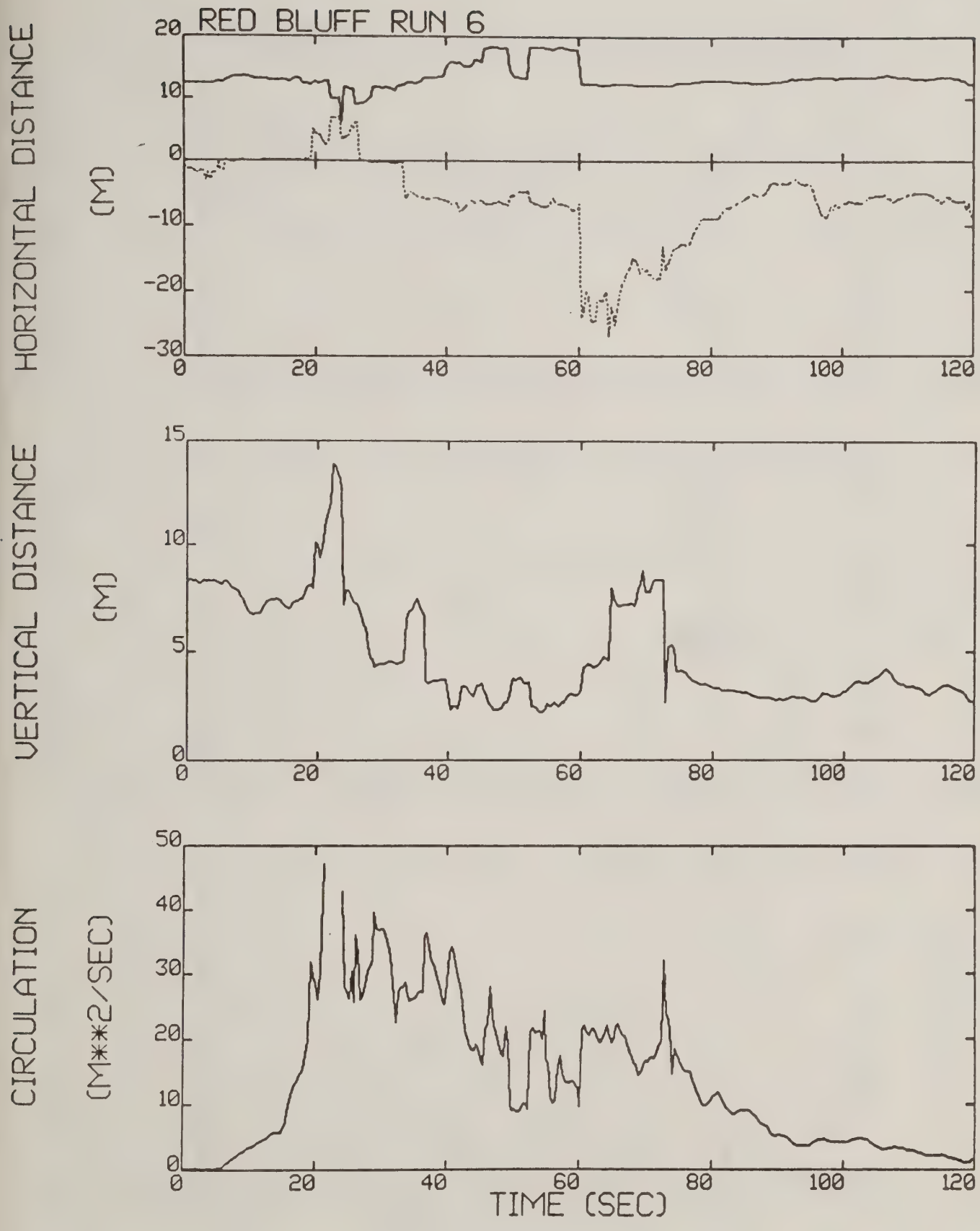

Figure C-4. Red Bluff test run 6 generalized algorithm results (*).

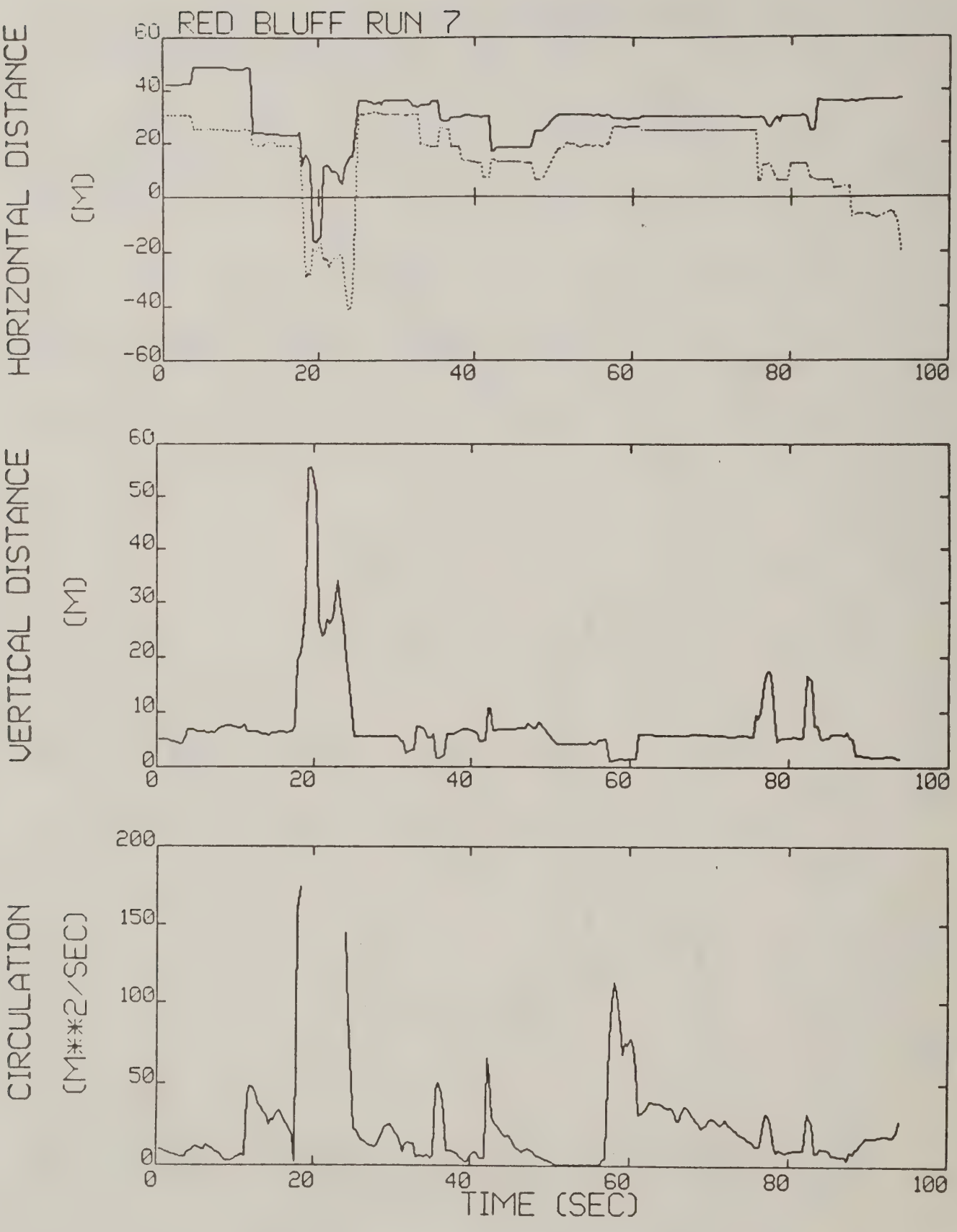

Figure C-5. Red Bluff test run 7 generalized algorithm results.

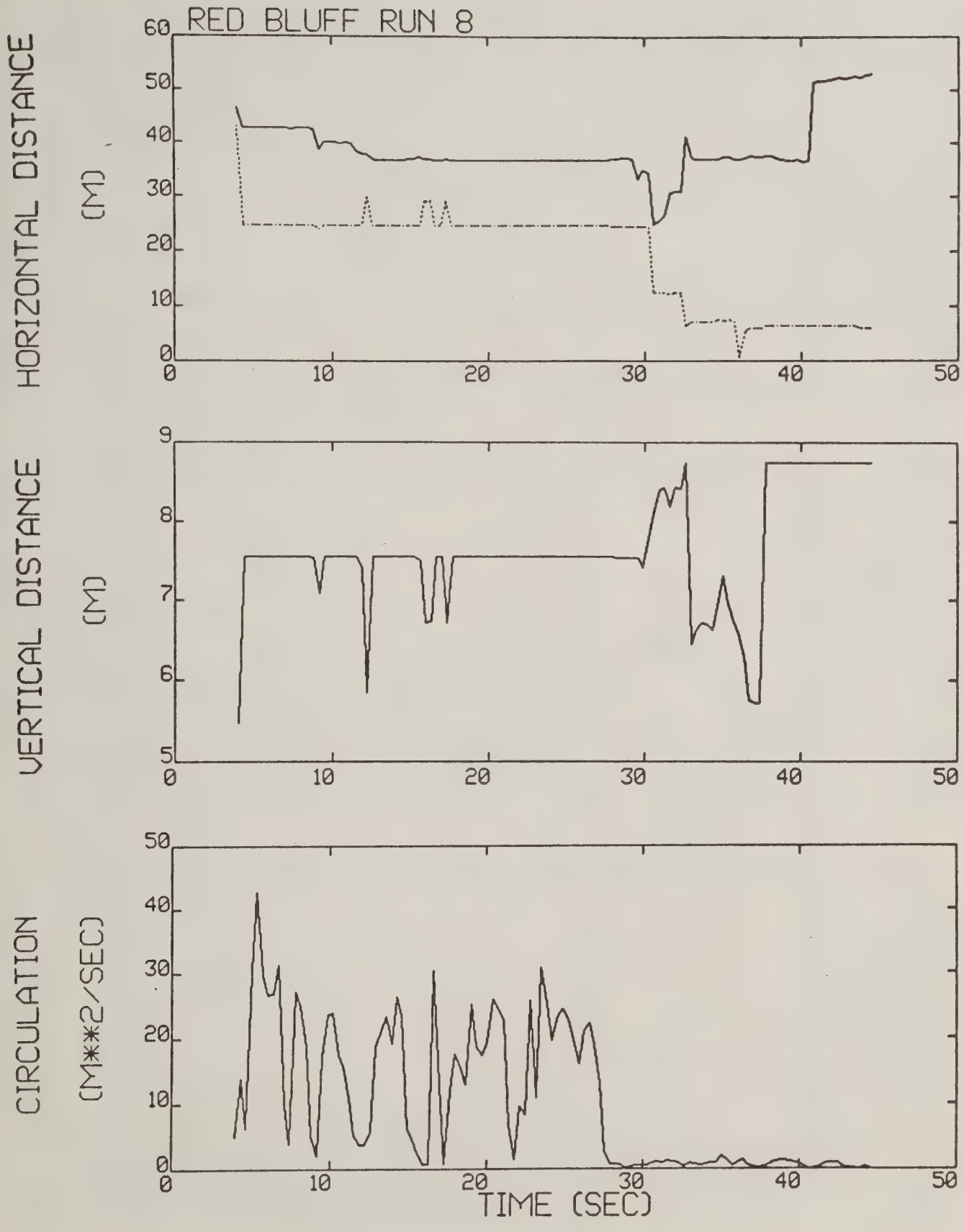

Figure C-6. Red Bluff test run 8 generalized algorithm results.

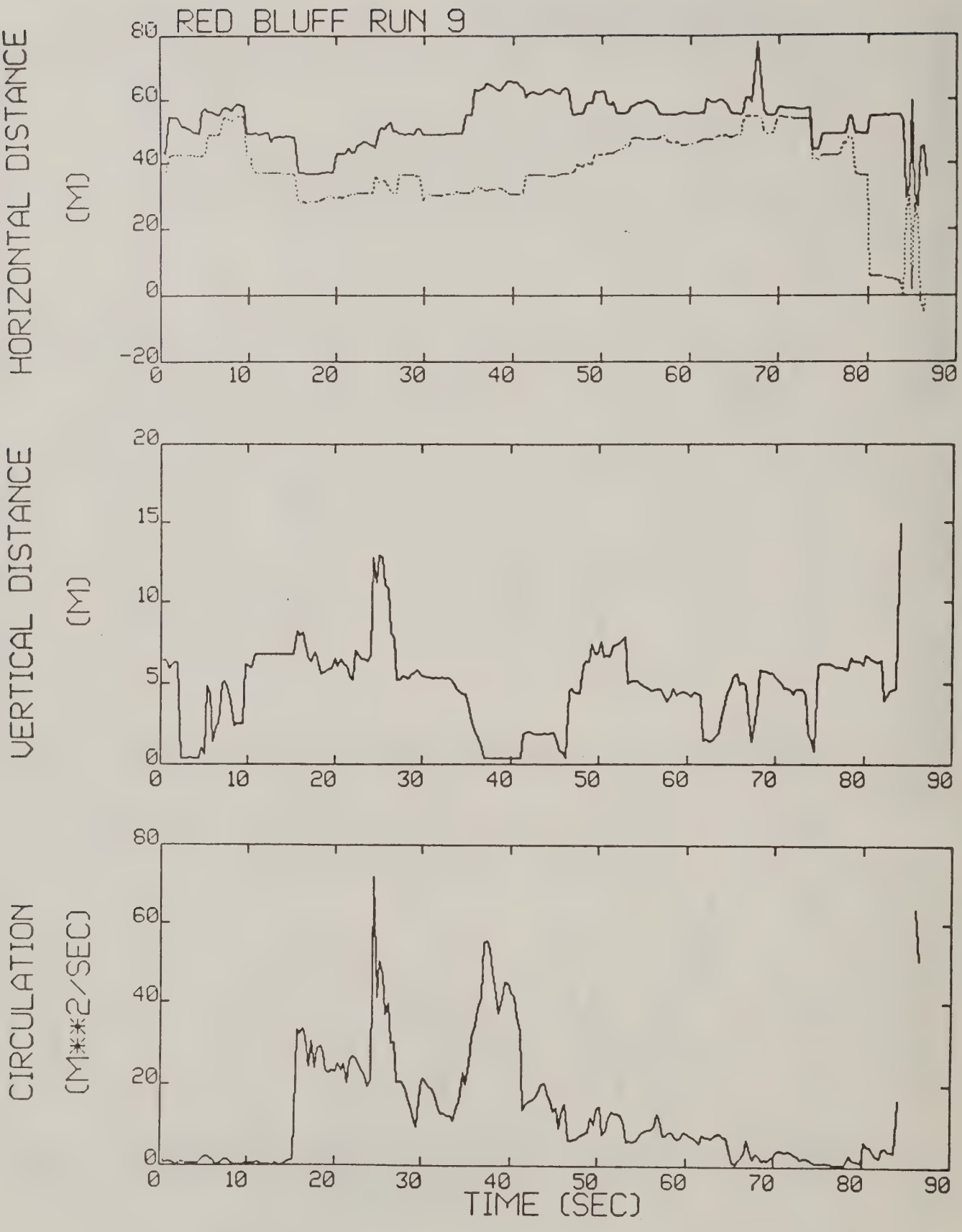

Figure C-7. Red Bluff test run 9 generalized algorithm results (*).

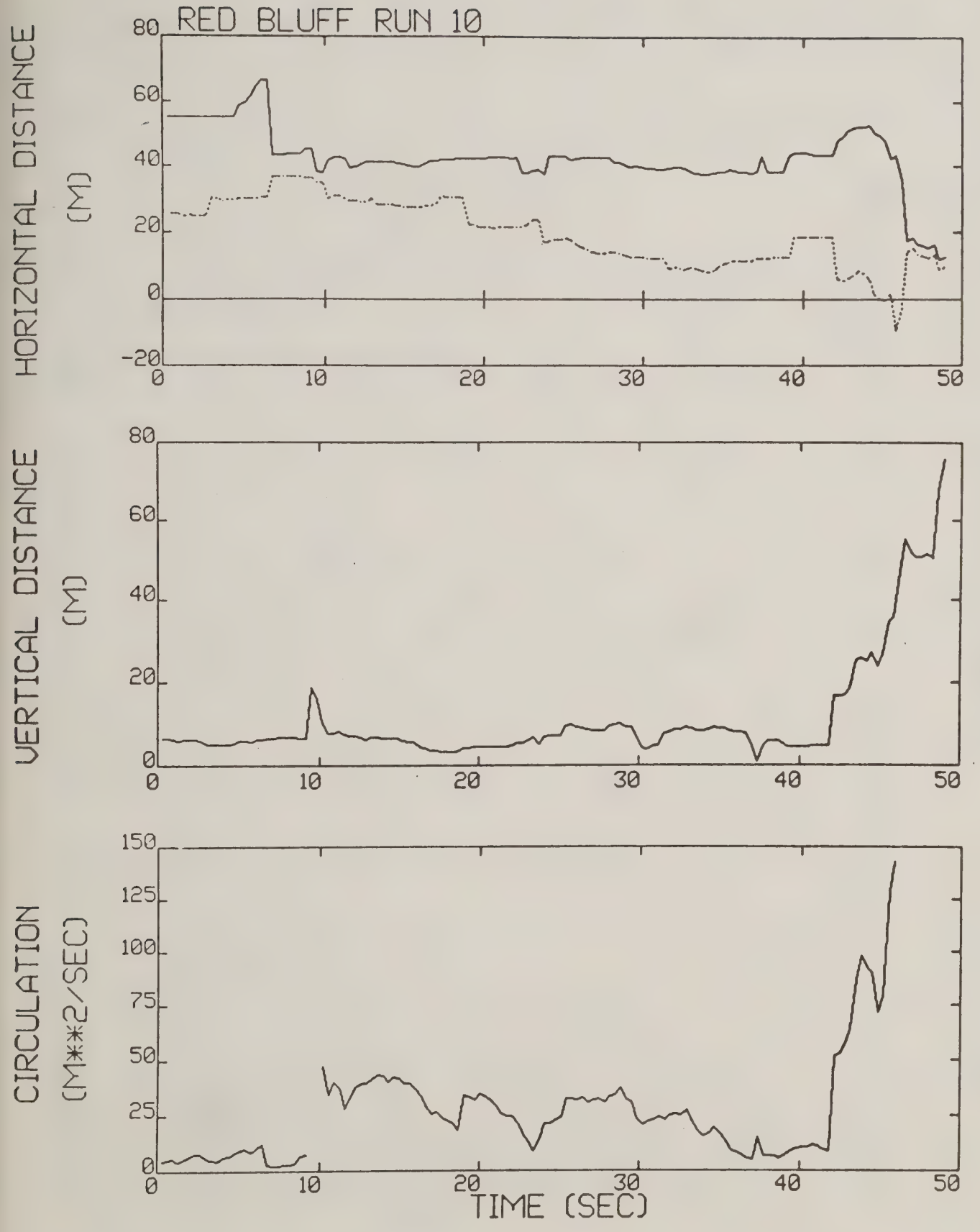

Figure C-8. Red Bluff test run 10 generalized algorithm results (*).

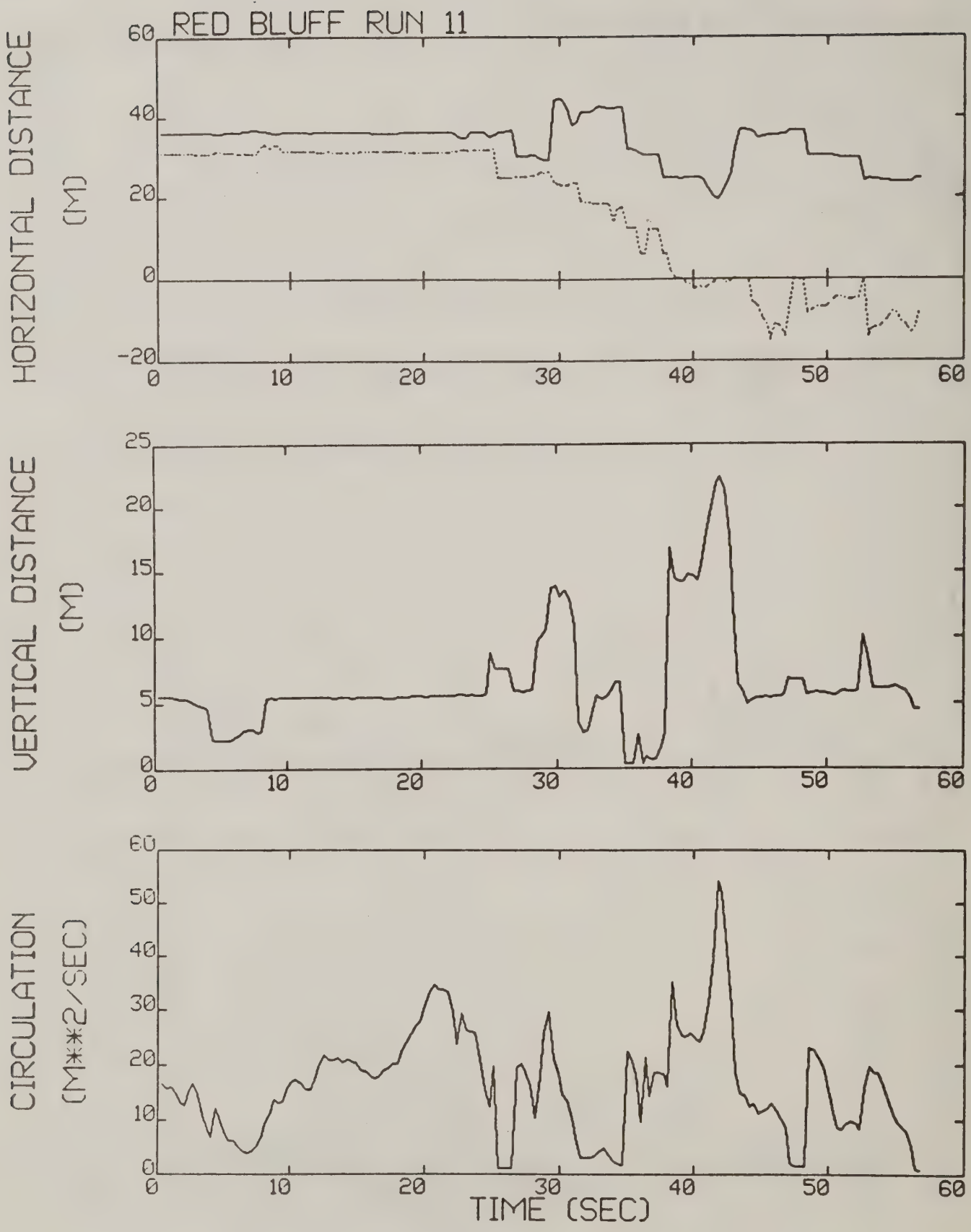

Figure C-9. Red Bluff test run 11 generalized algorithm results.

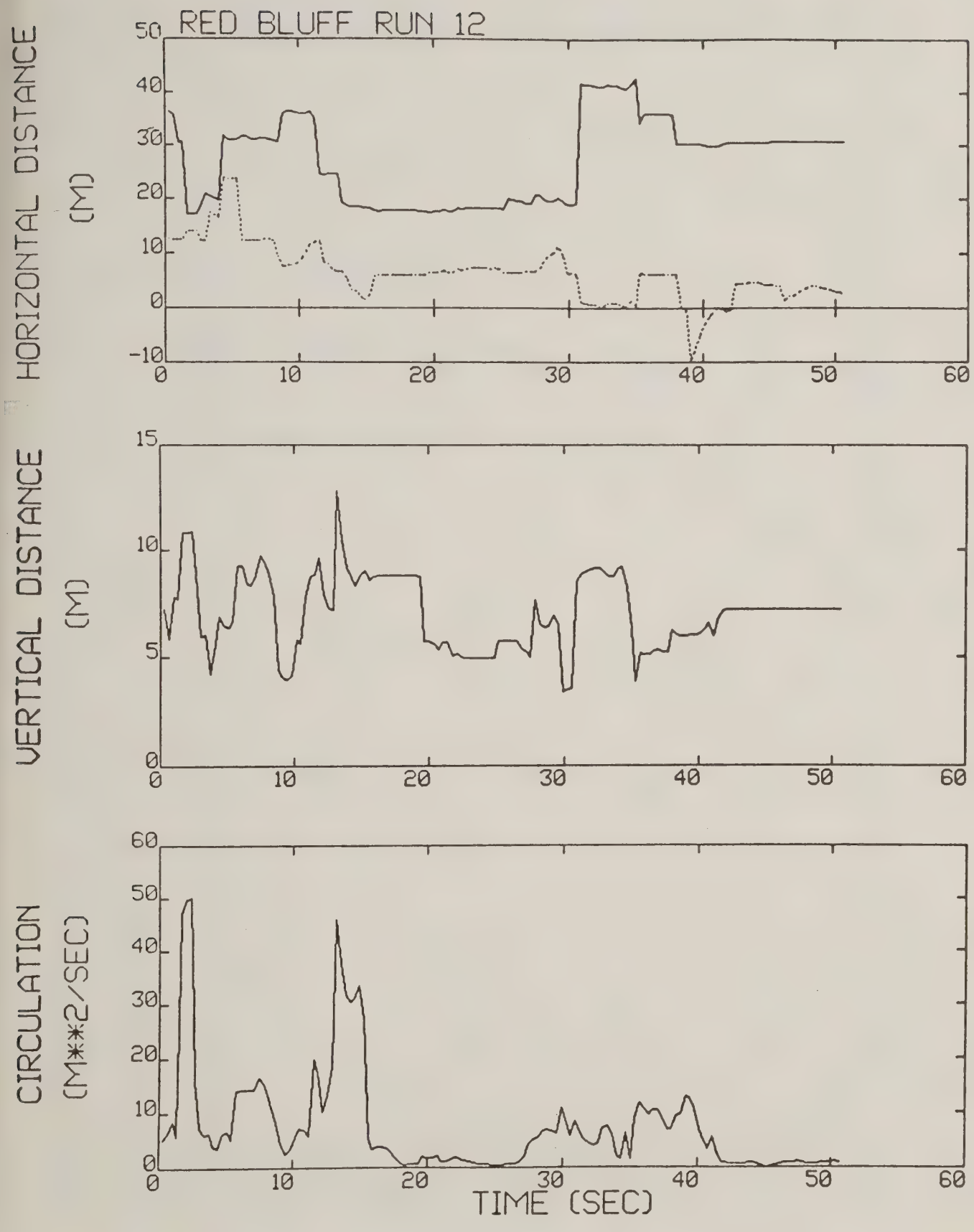

Figure C-10. Red Bluff test run 12 generalized algorithm results.

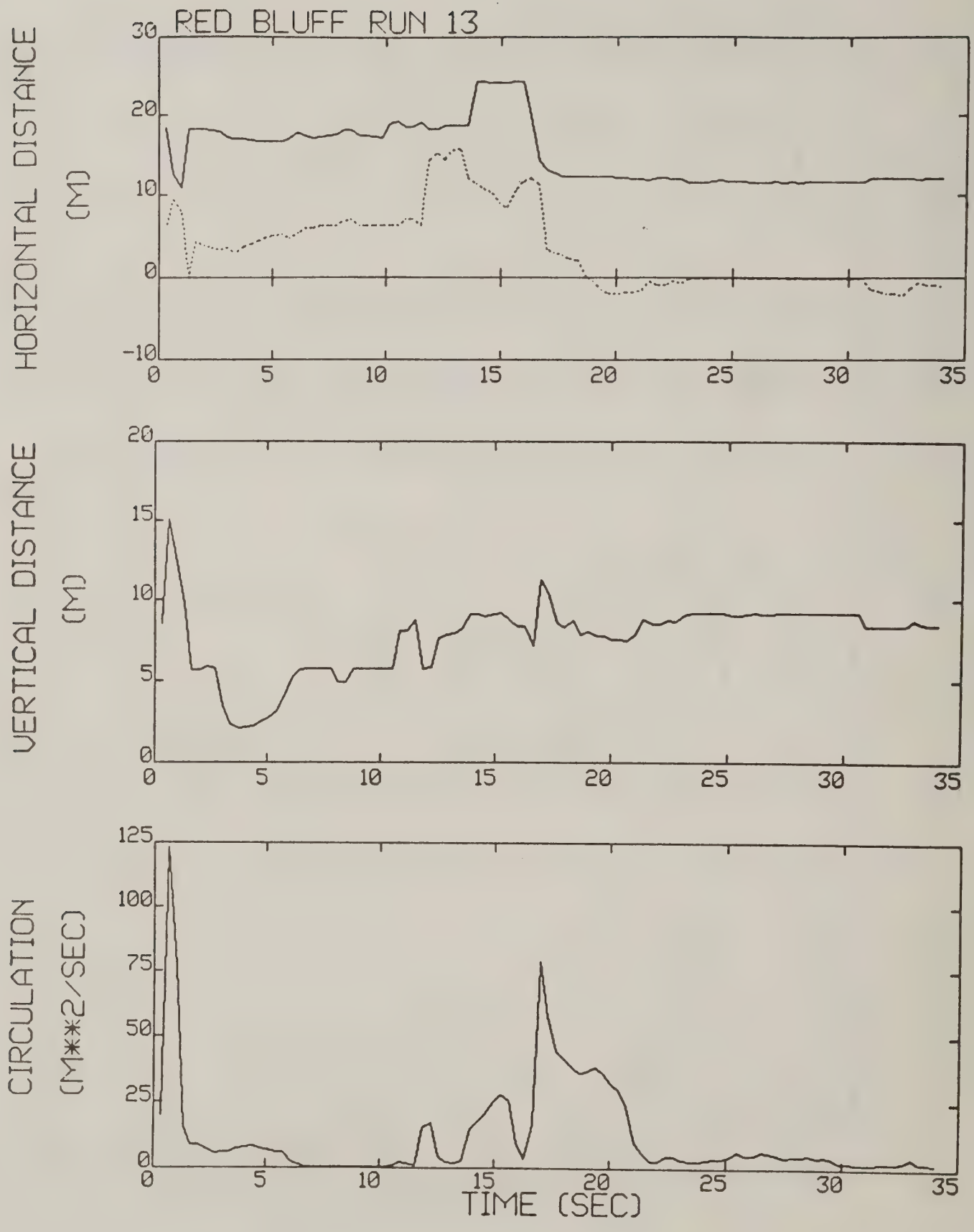

Figure C-11. Red Bluff test run 13 generalized algorithm results.

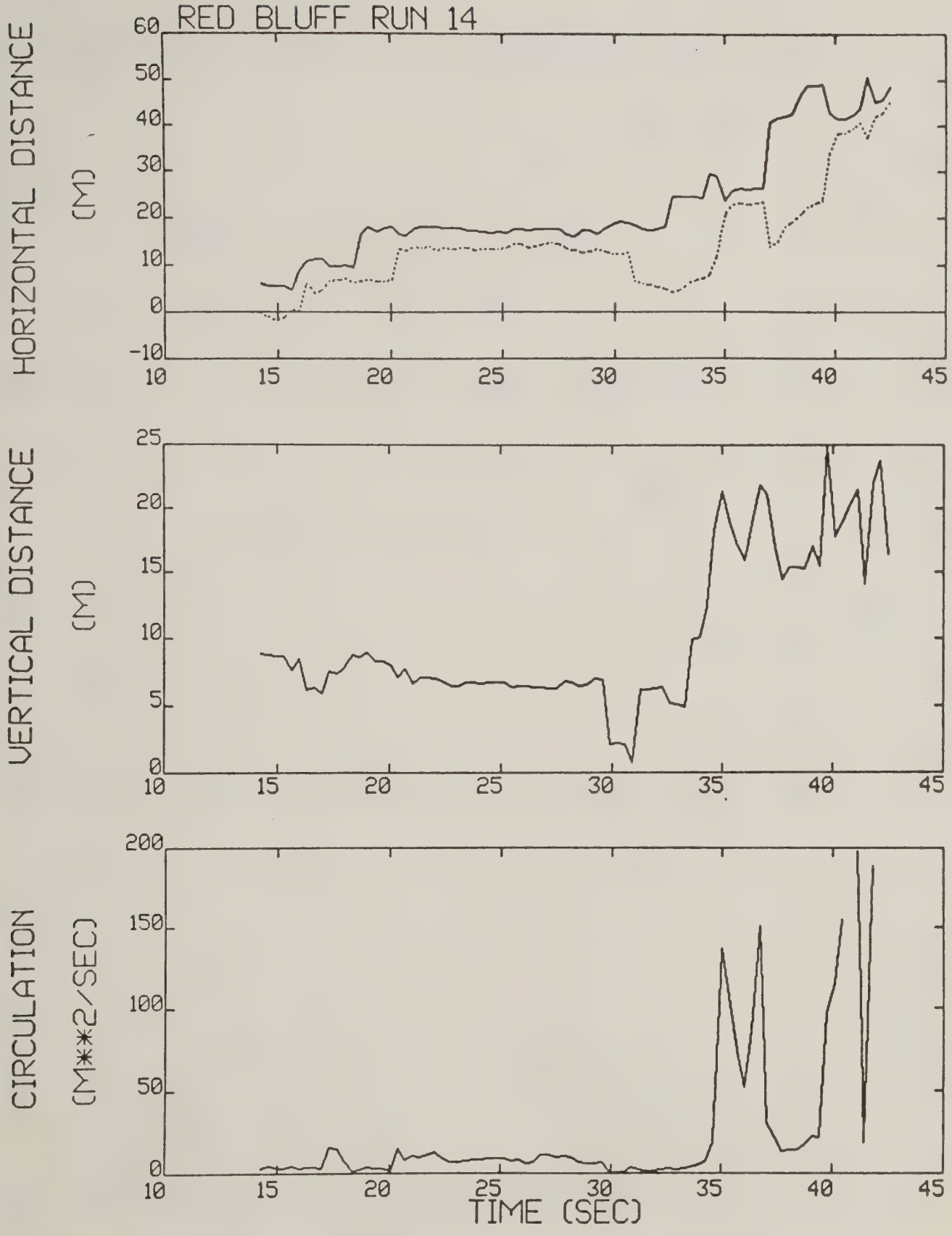

Figure C-12. Red Bluff test run 14 generalized algorithm results.

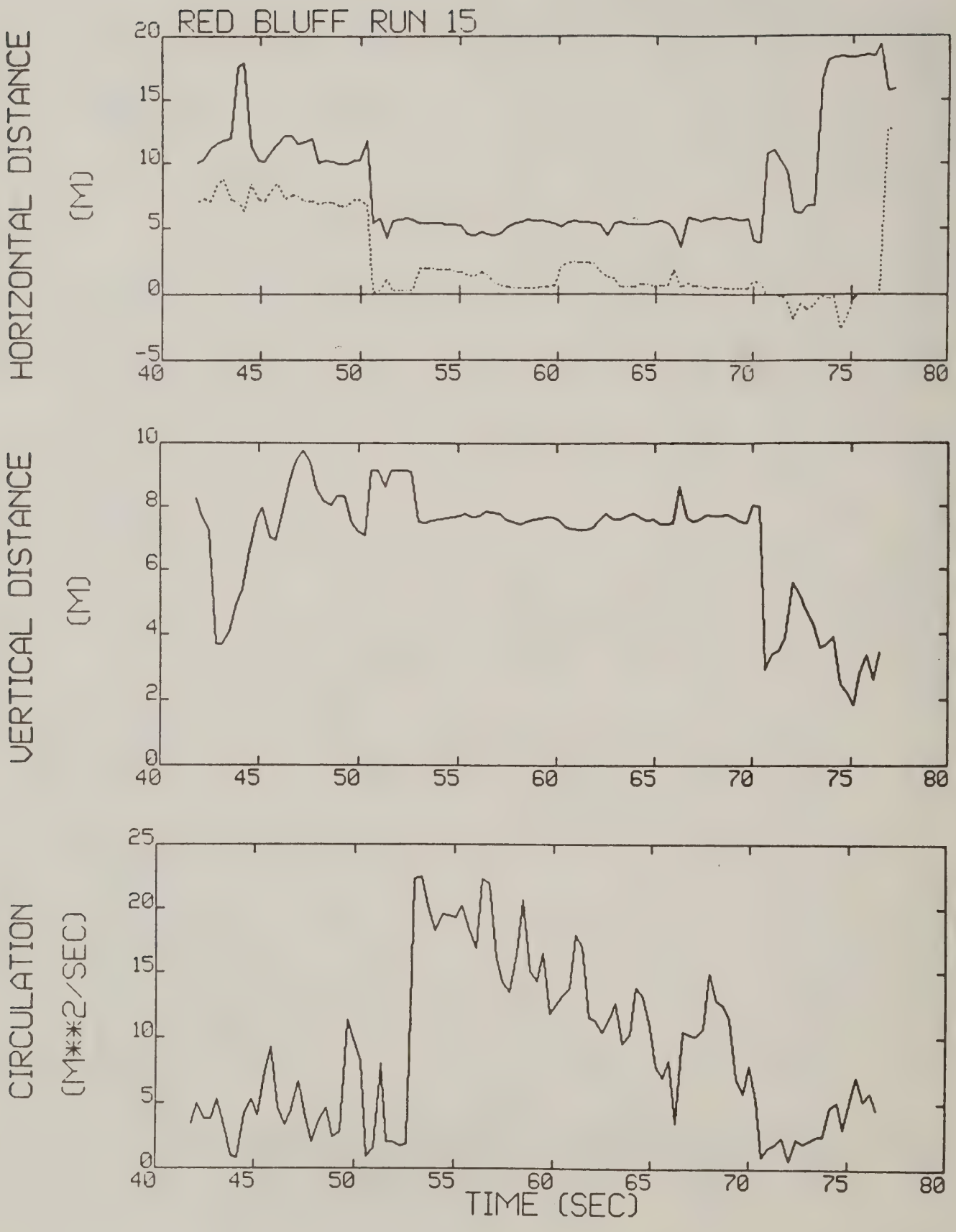

Figure C-13. Red Bluff test run 15 generalized algorithm results (*).

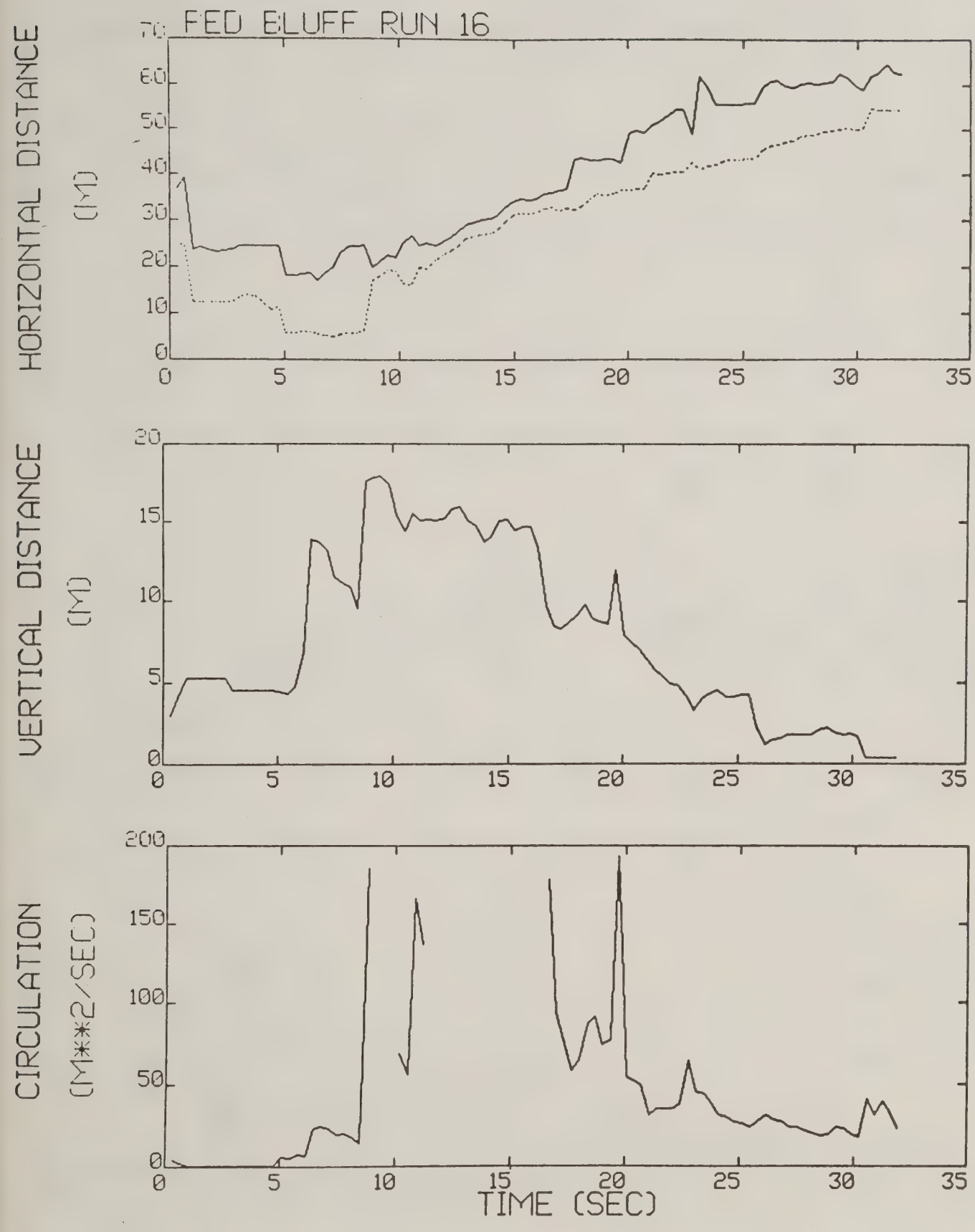

Figure C-14. Red Bluff test run 16 generalized algorithm results (*).

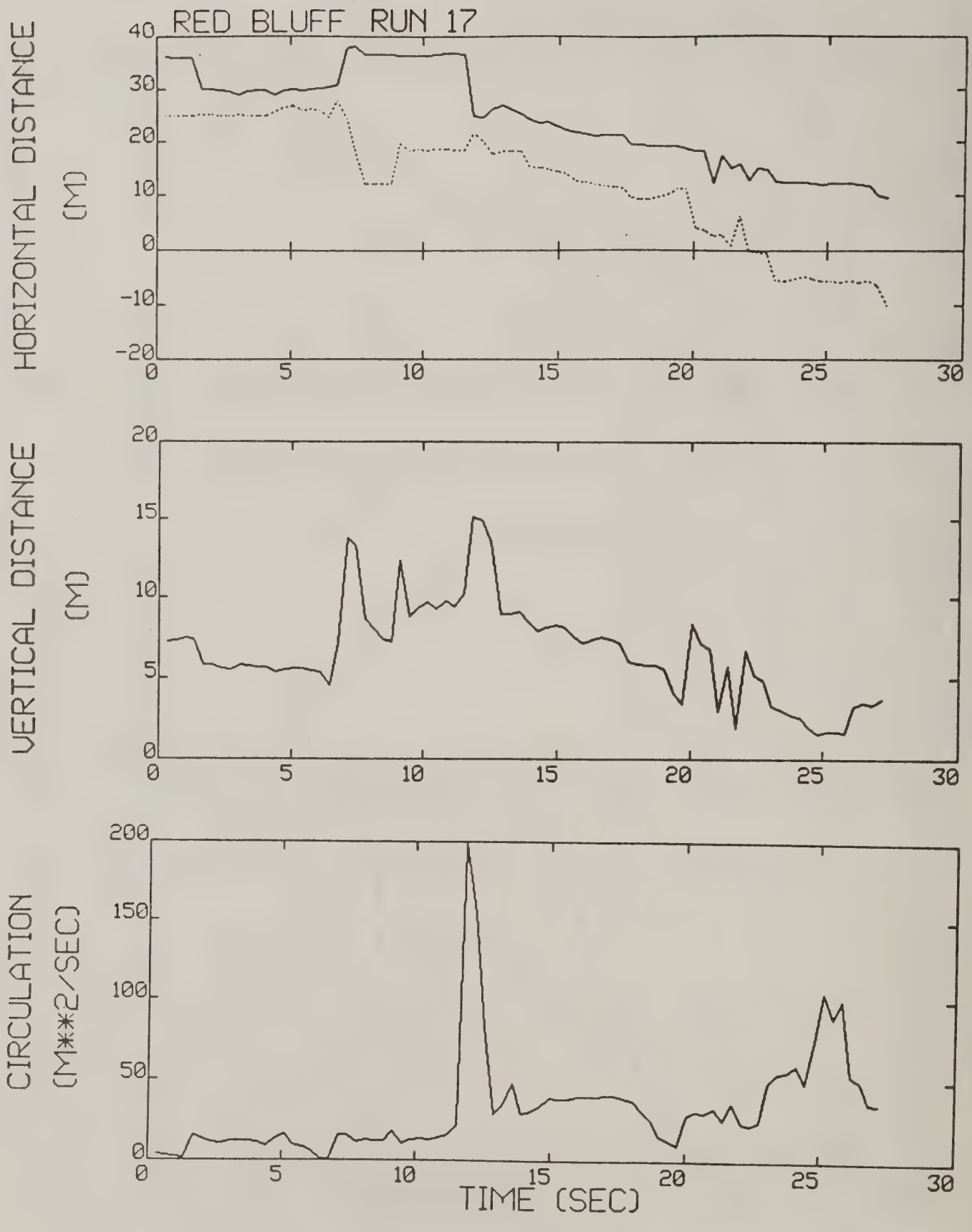

Figure C-15. Red Bluff test run 17 generalized algorithm results.

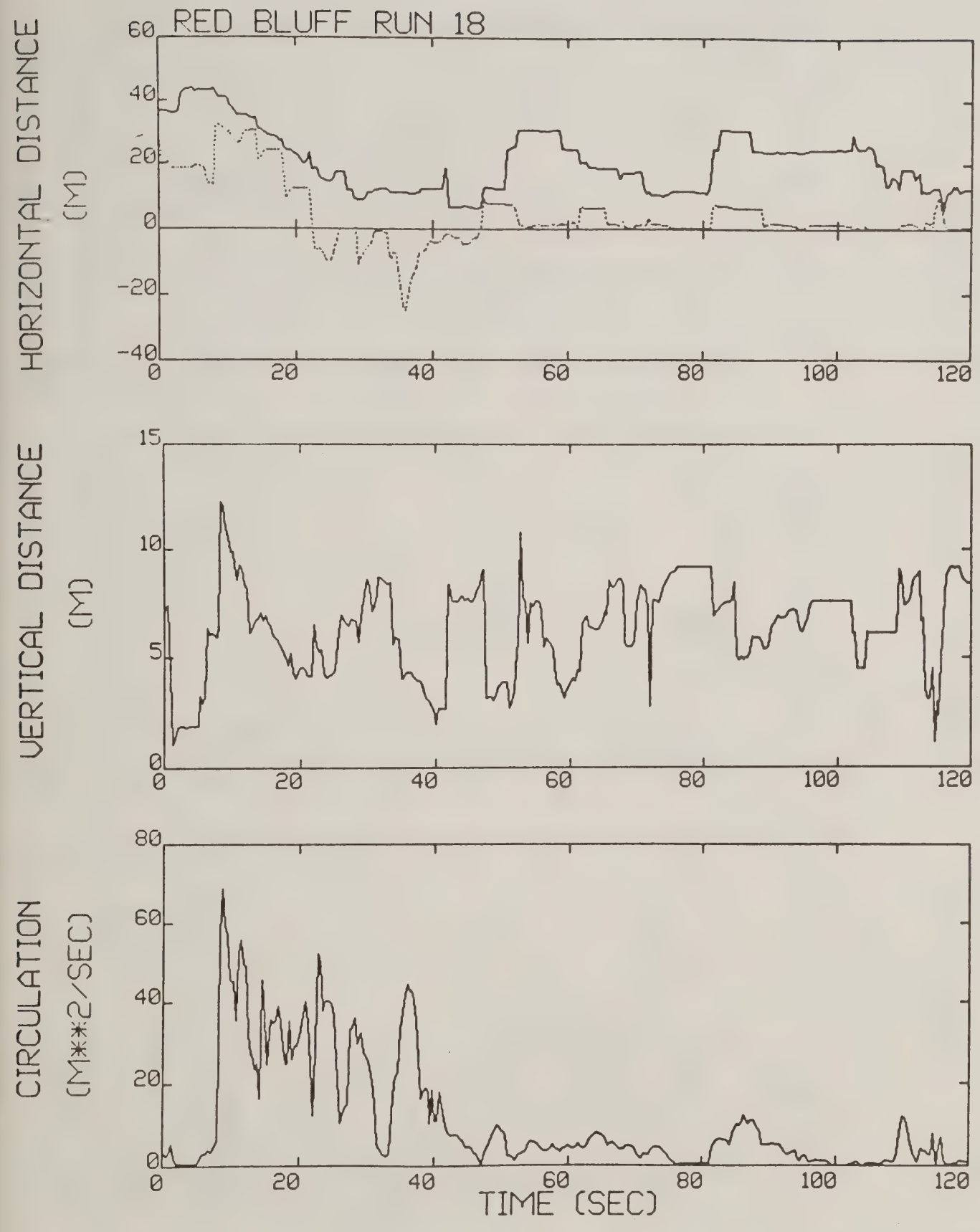

Figure C-16. Red Bluff test run 18 generalized algorithm results (*).

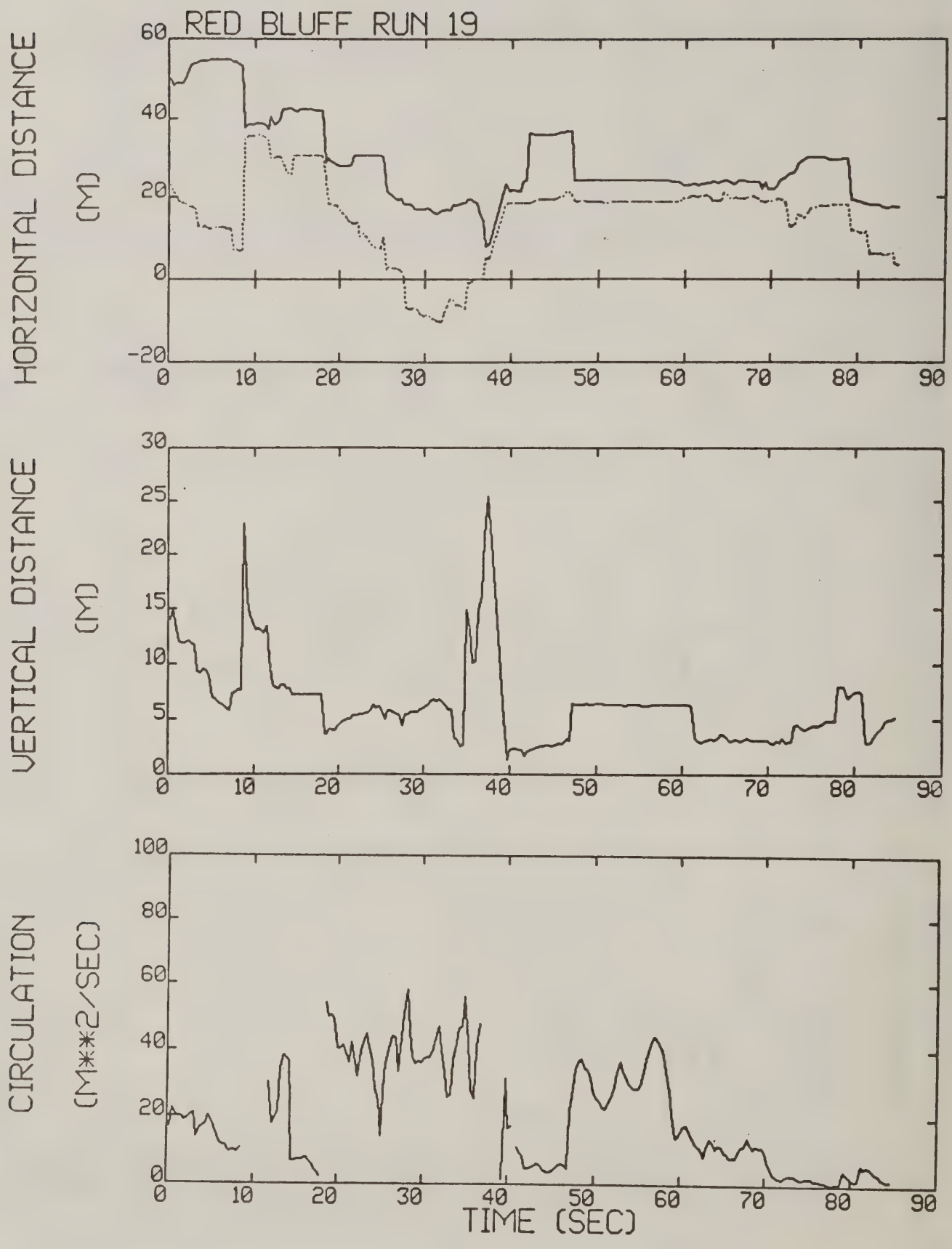

Figure C-17. Red Bluff test run 19 generalized algorithm results (*).

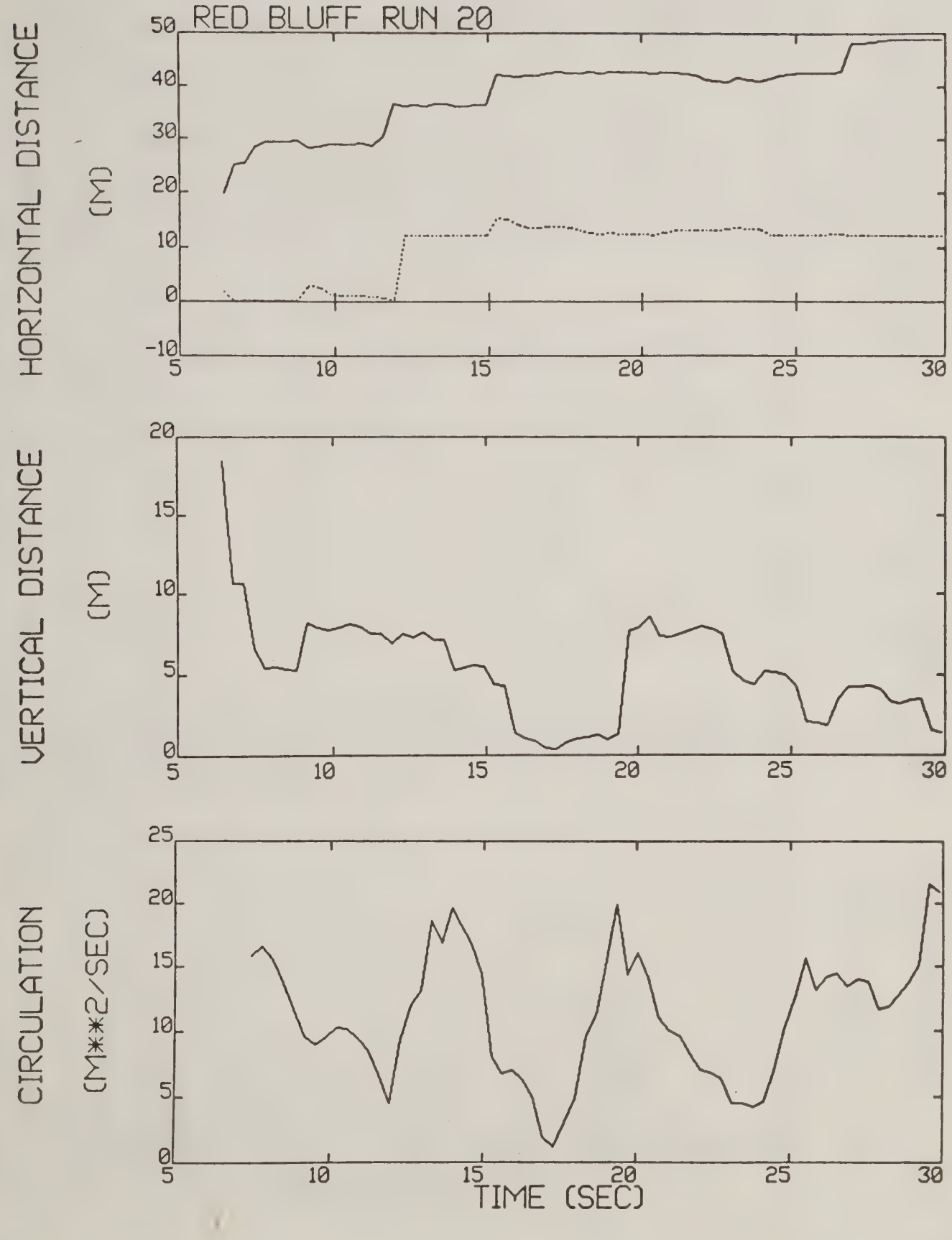

Figure C-18. Red Bluff test run 20 generalized algorithm results.

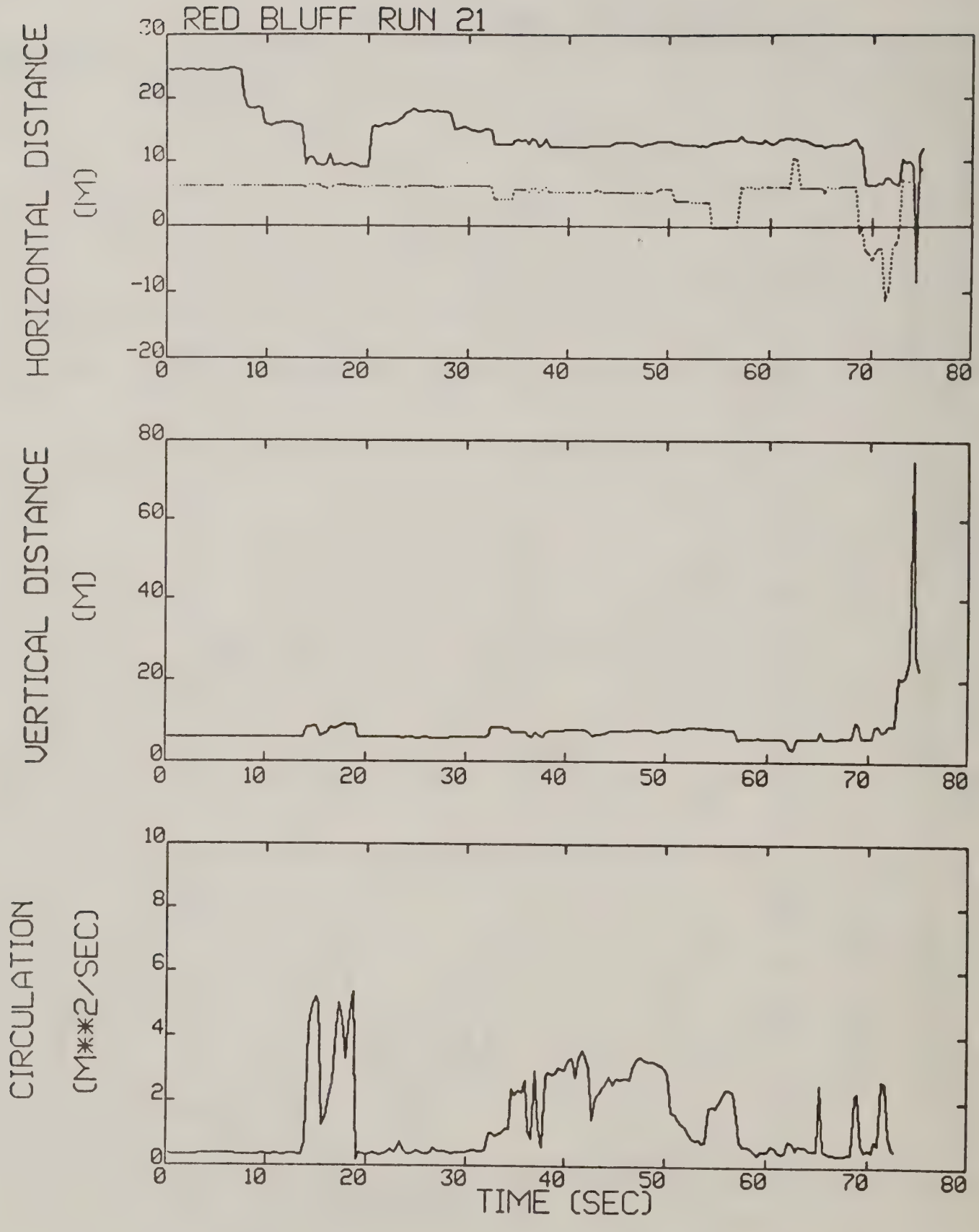

Figure C-19. Red Bluff test run 21 generalized algorithm results (*).

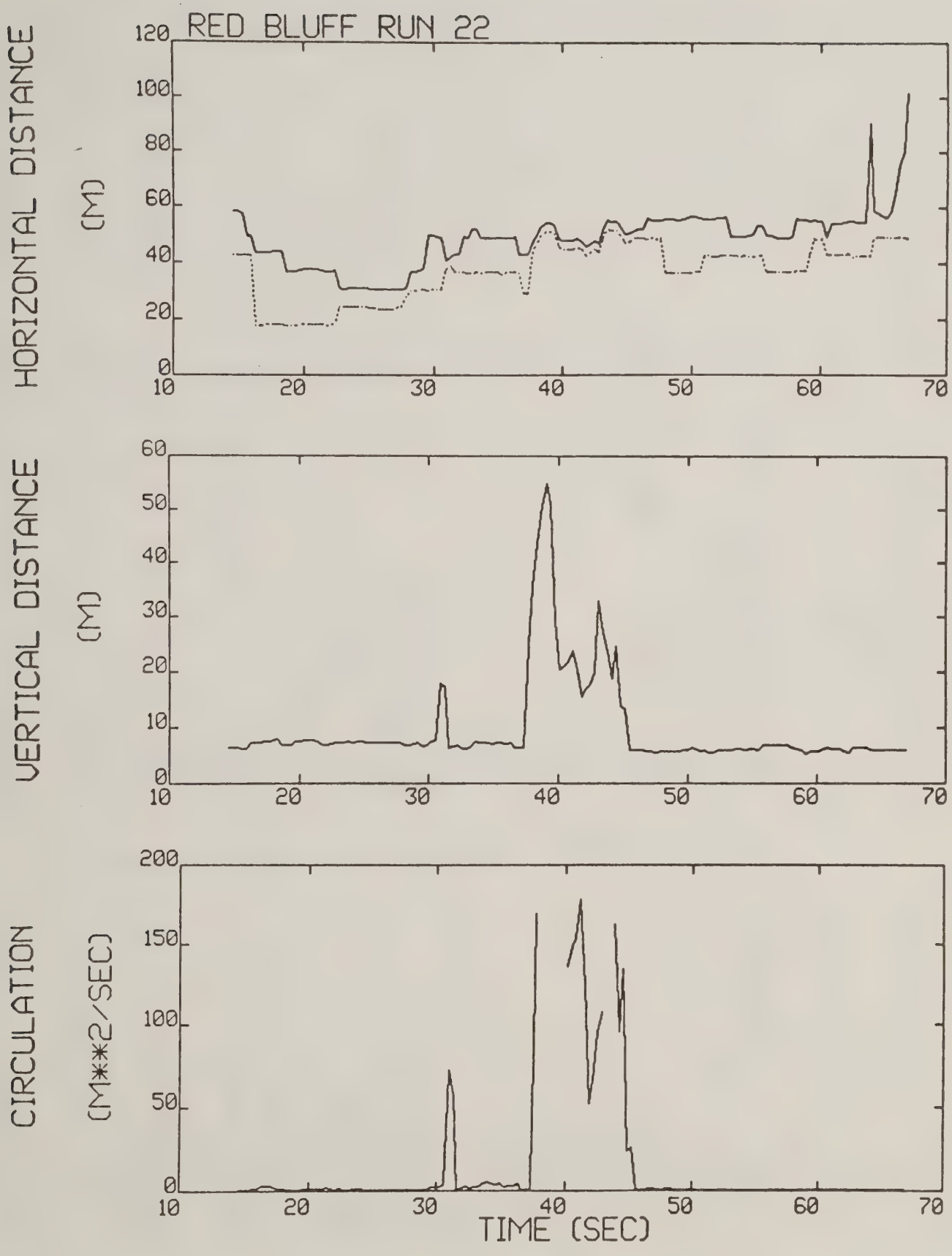

Figure C-20. Red Bluff test run 22 generalized algorithm results.

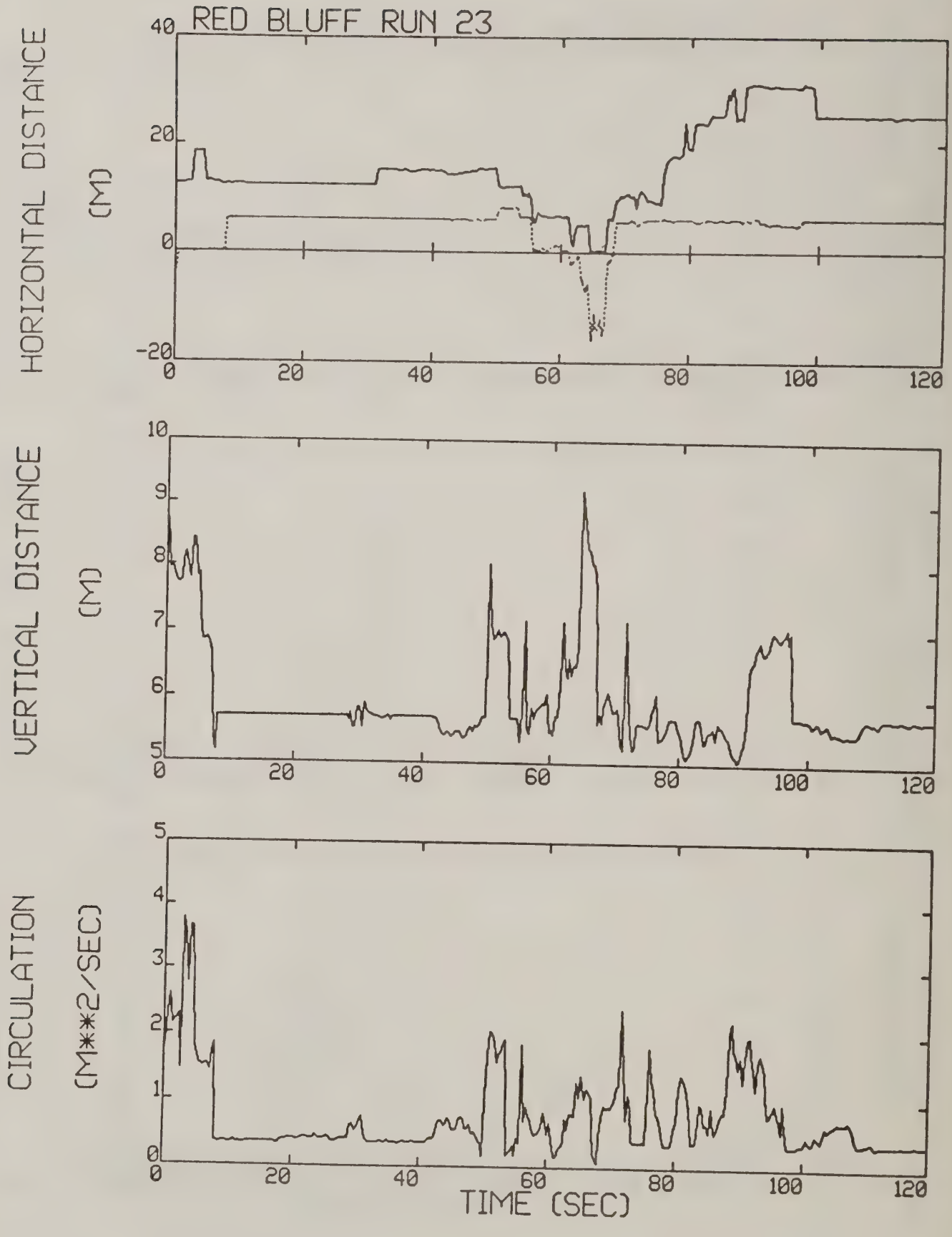

Figure C-21. Red Bluff test run 23 generalized algorithm results.

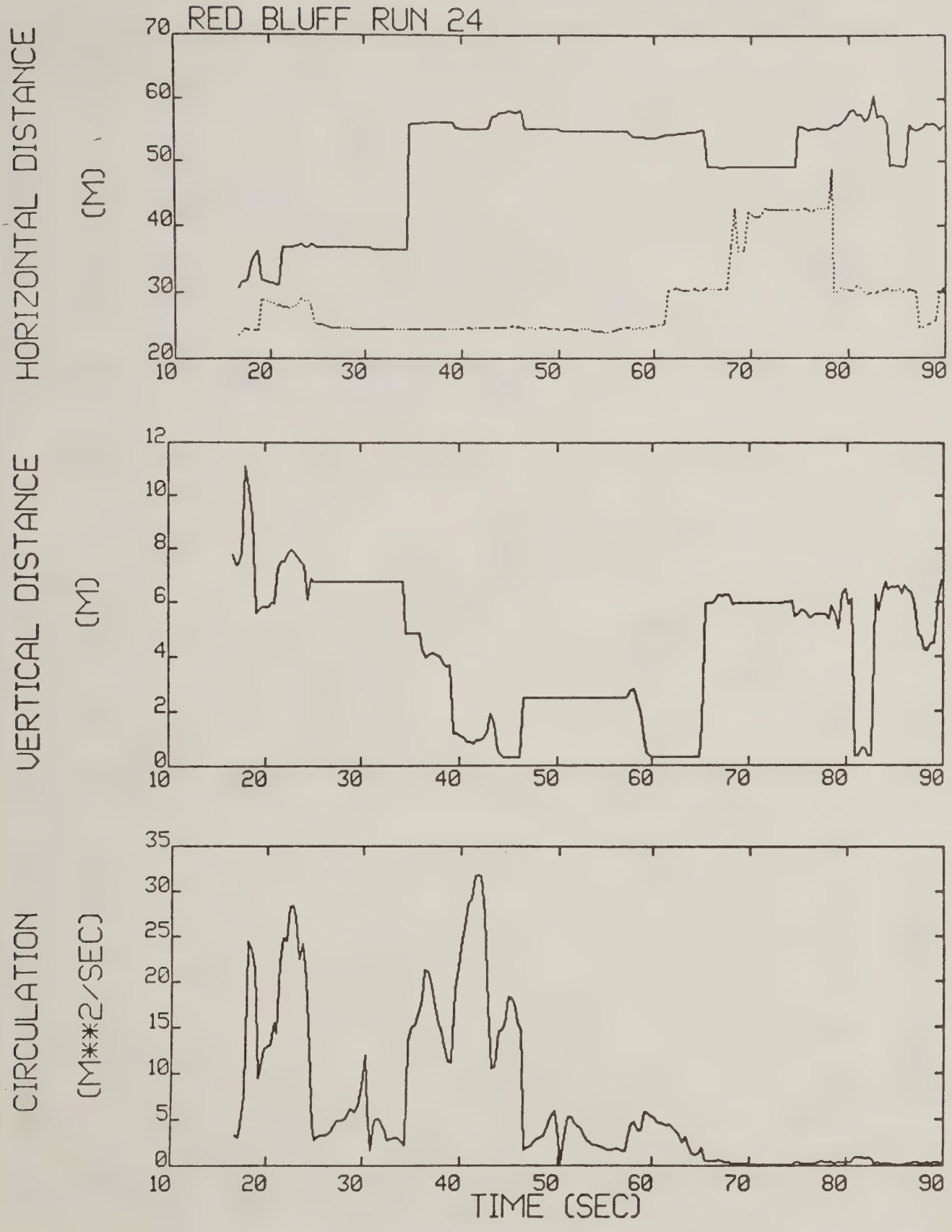

Figure C-22. Red Bluff test run 24 generalized algorithm results.

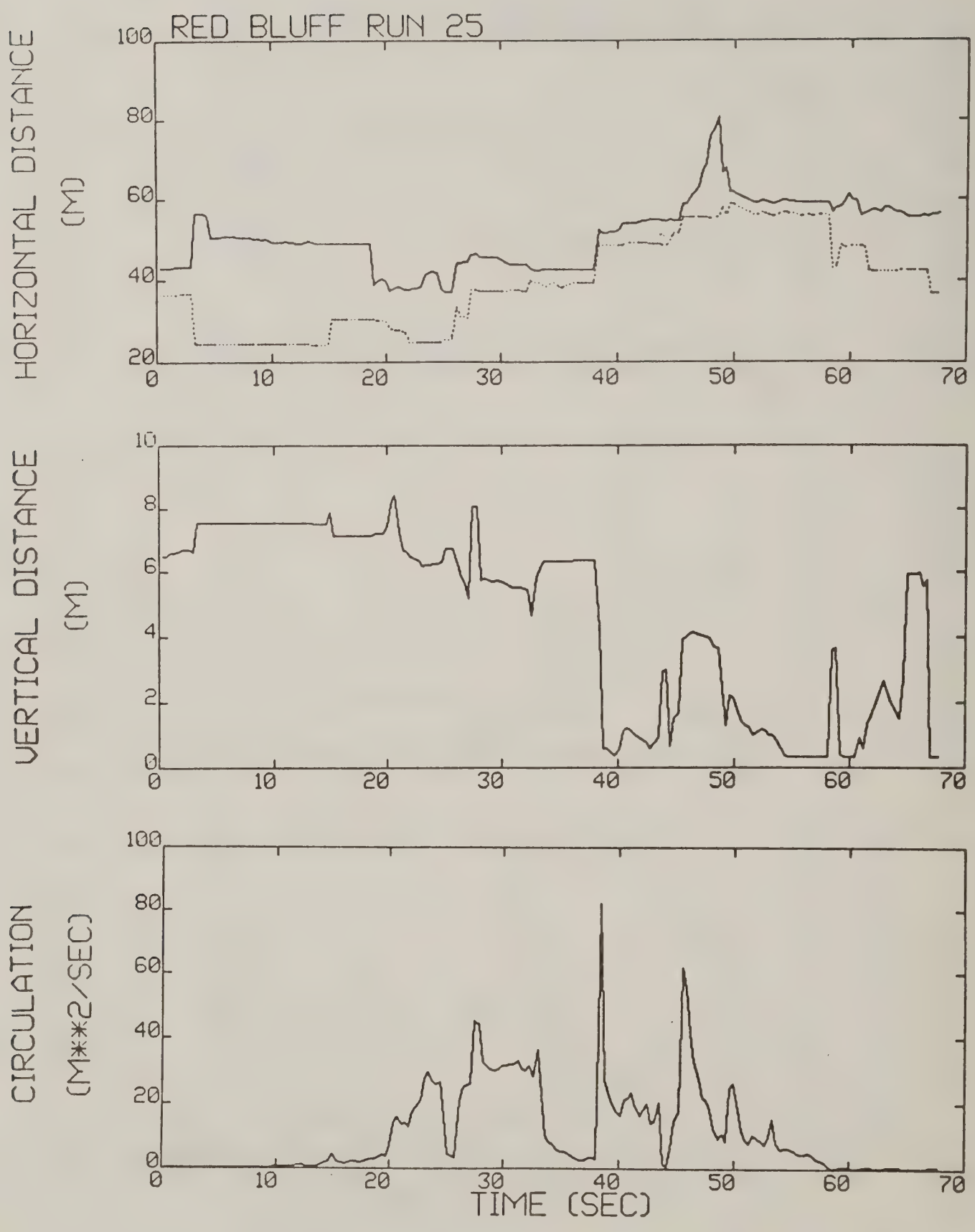

Figure C-23. Red Bluff test run 25 generalized algorithm results (*).

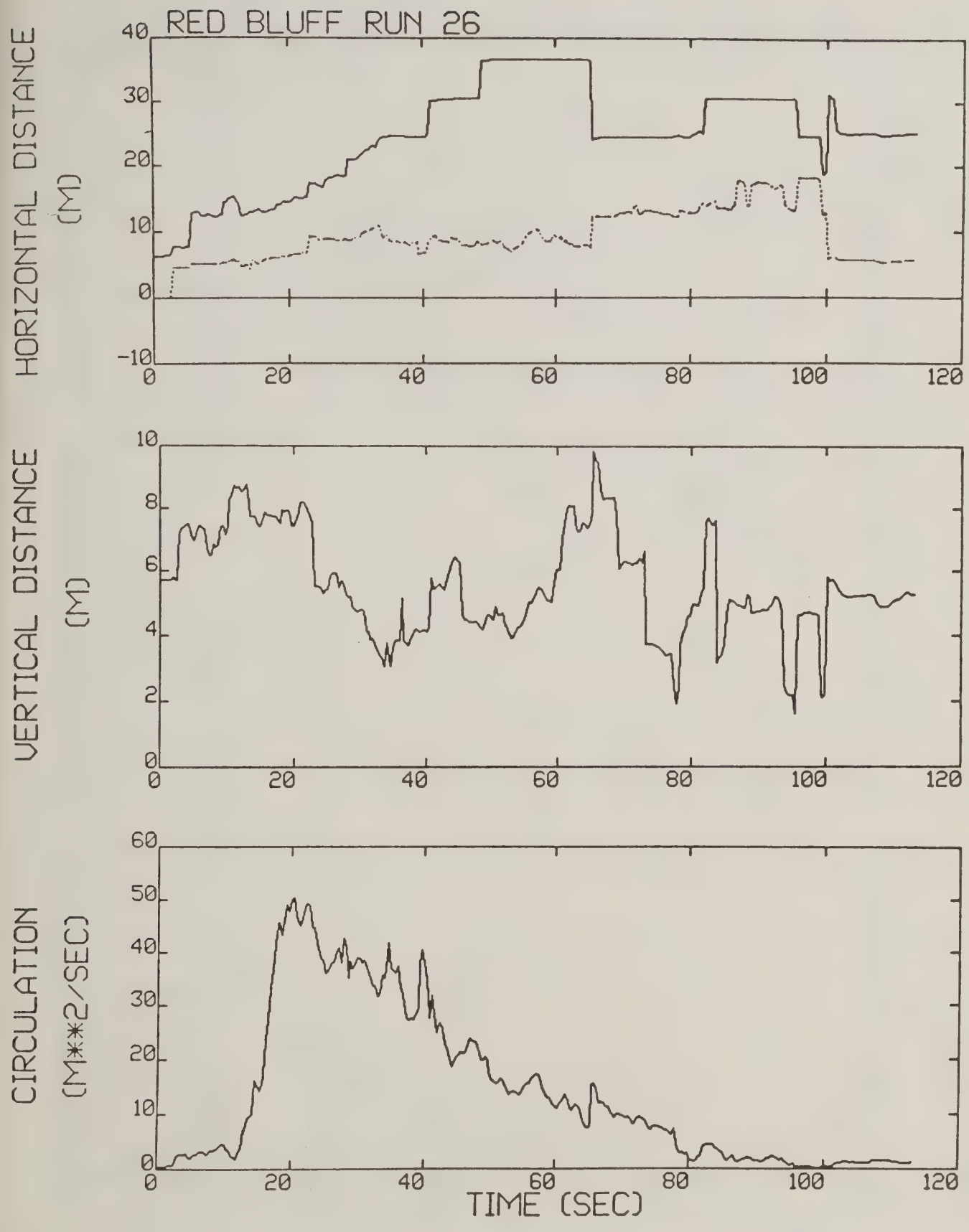

Figure C-24. Red Bluff test run 26 generalized algorithm results (*).

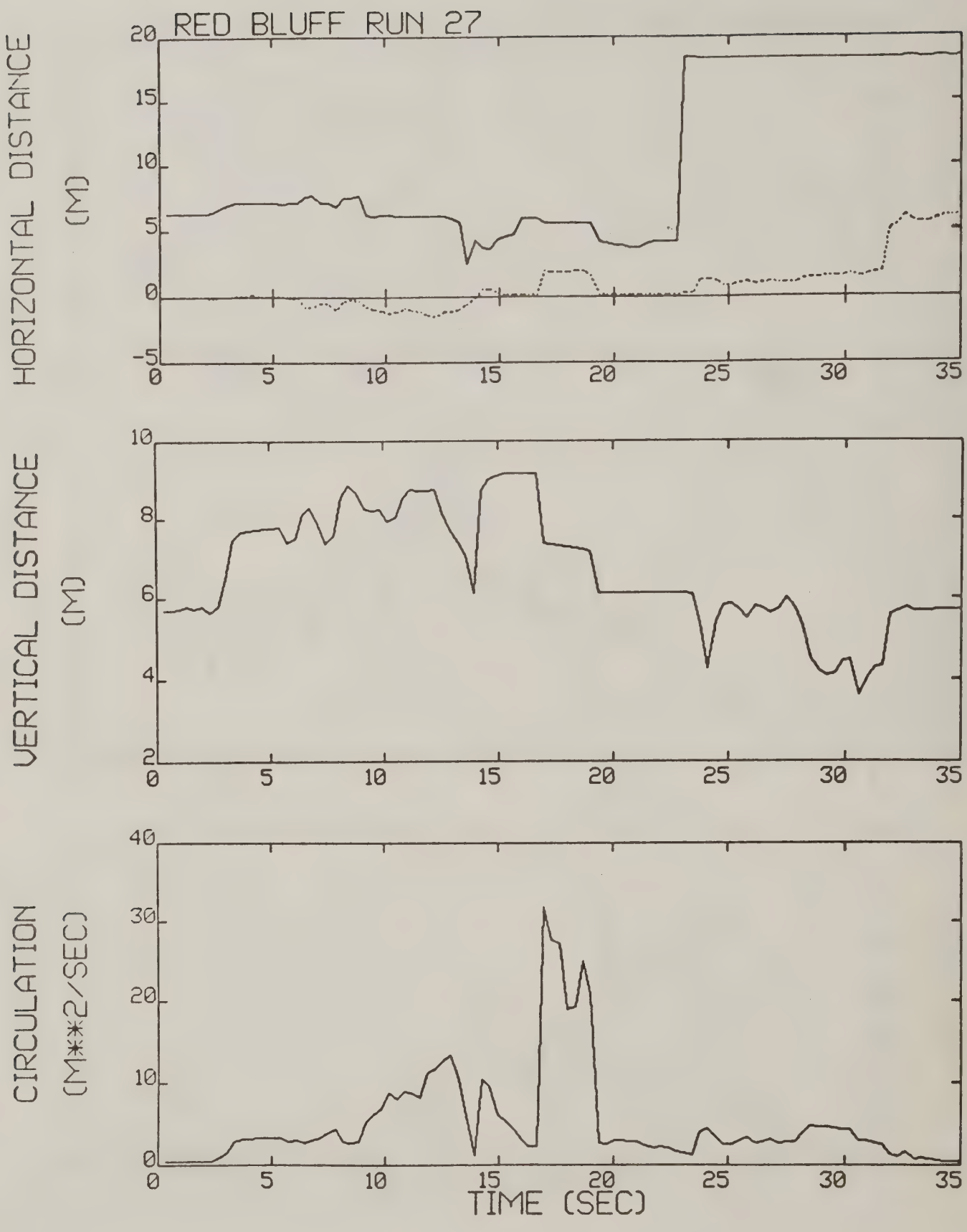

Figure C-25. Red Bluff test run 27 generalized algorithm results.

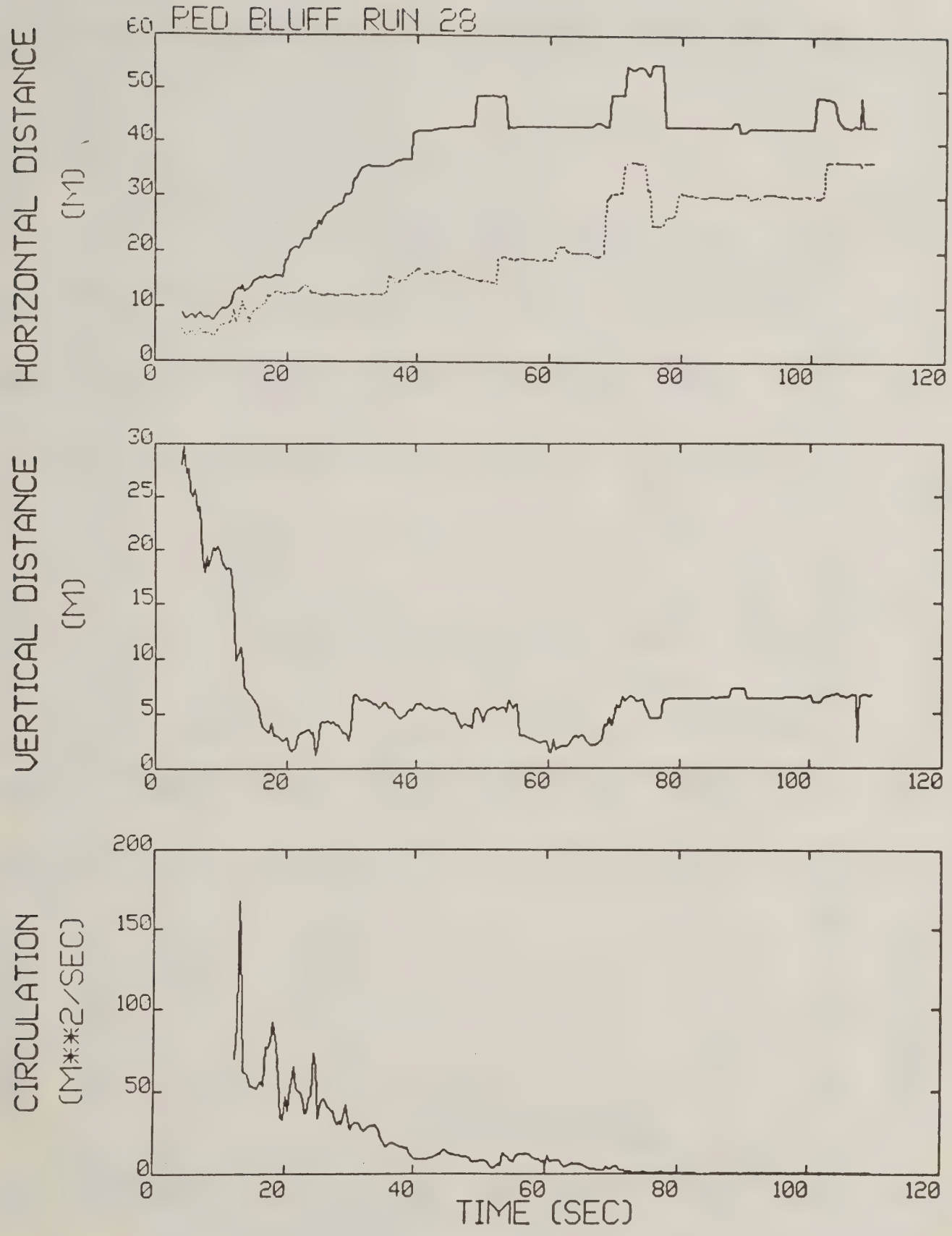

Figure C-26. Red Bluff test run 28 generalized algorithm results (*).

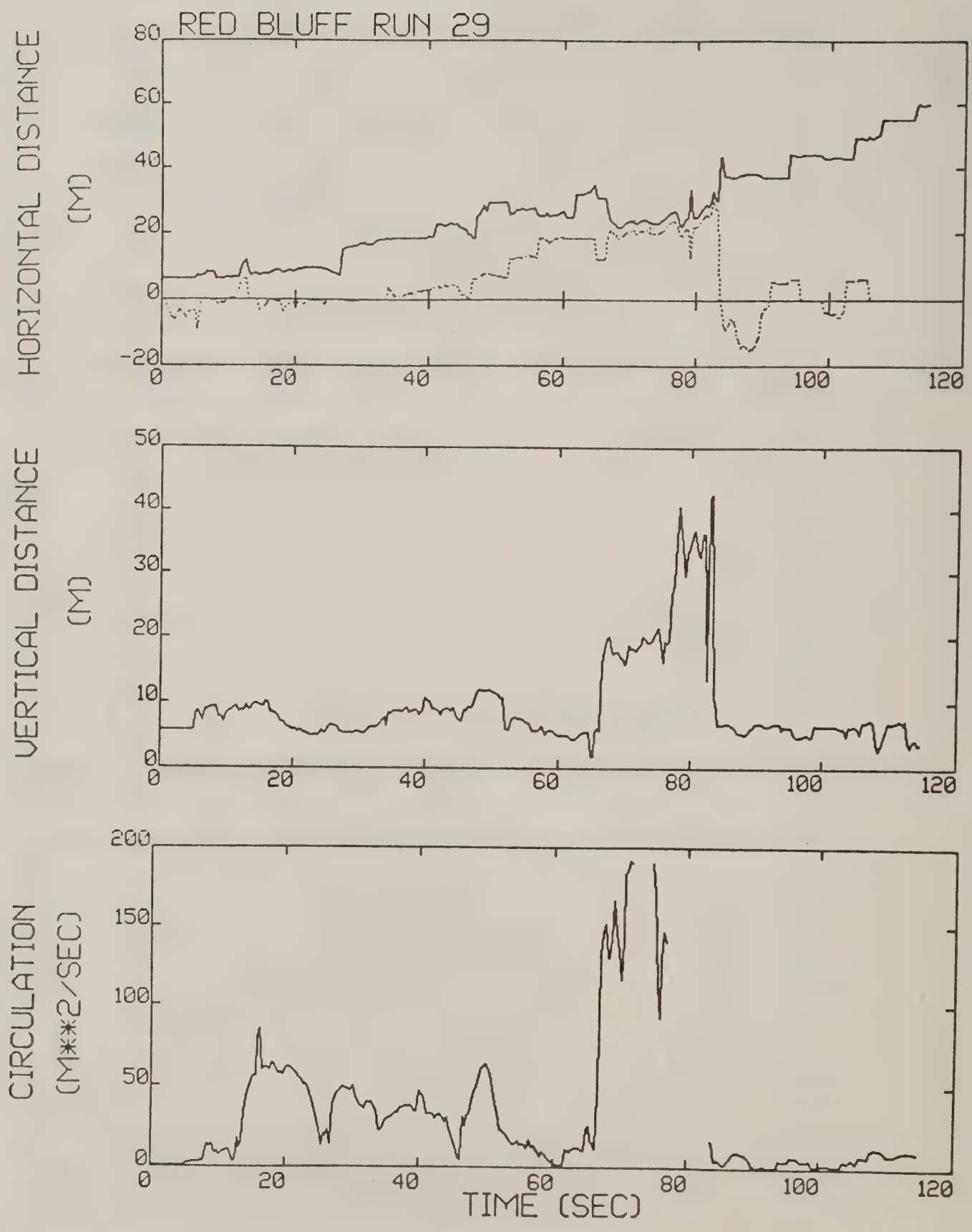

Figure C-27. Red Bluff test run 29 generalized algorithm results (*).

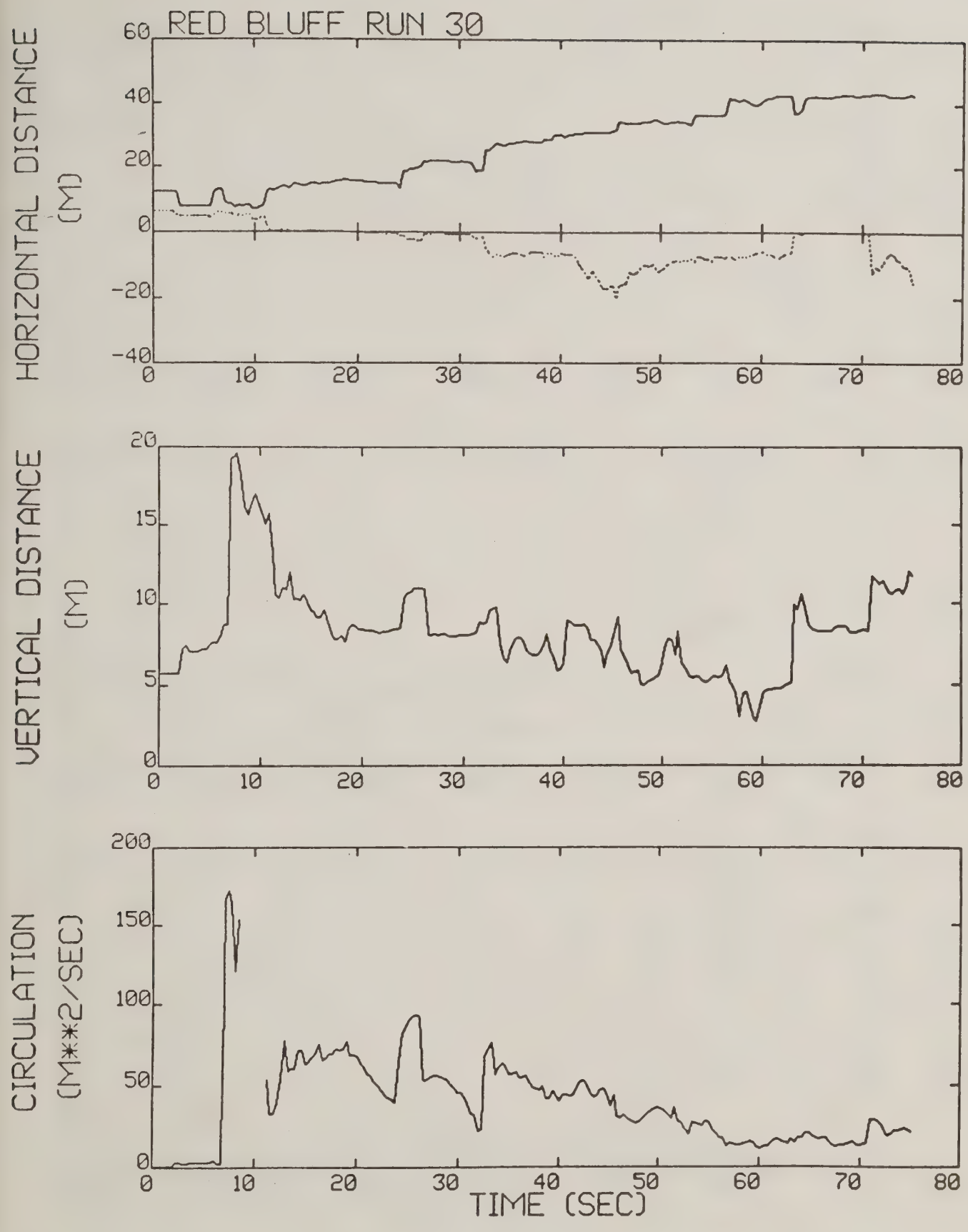

Figure C-28. Red Bluff test run 30 generalized algorithm results (*).

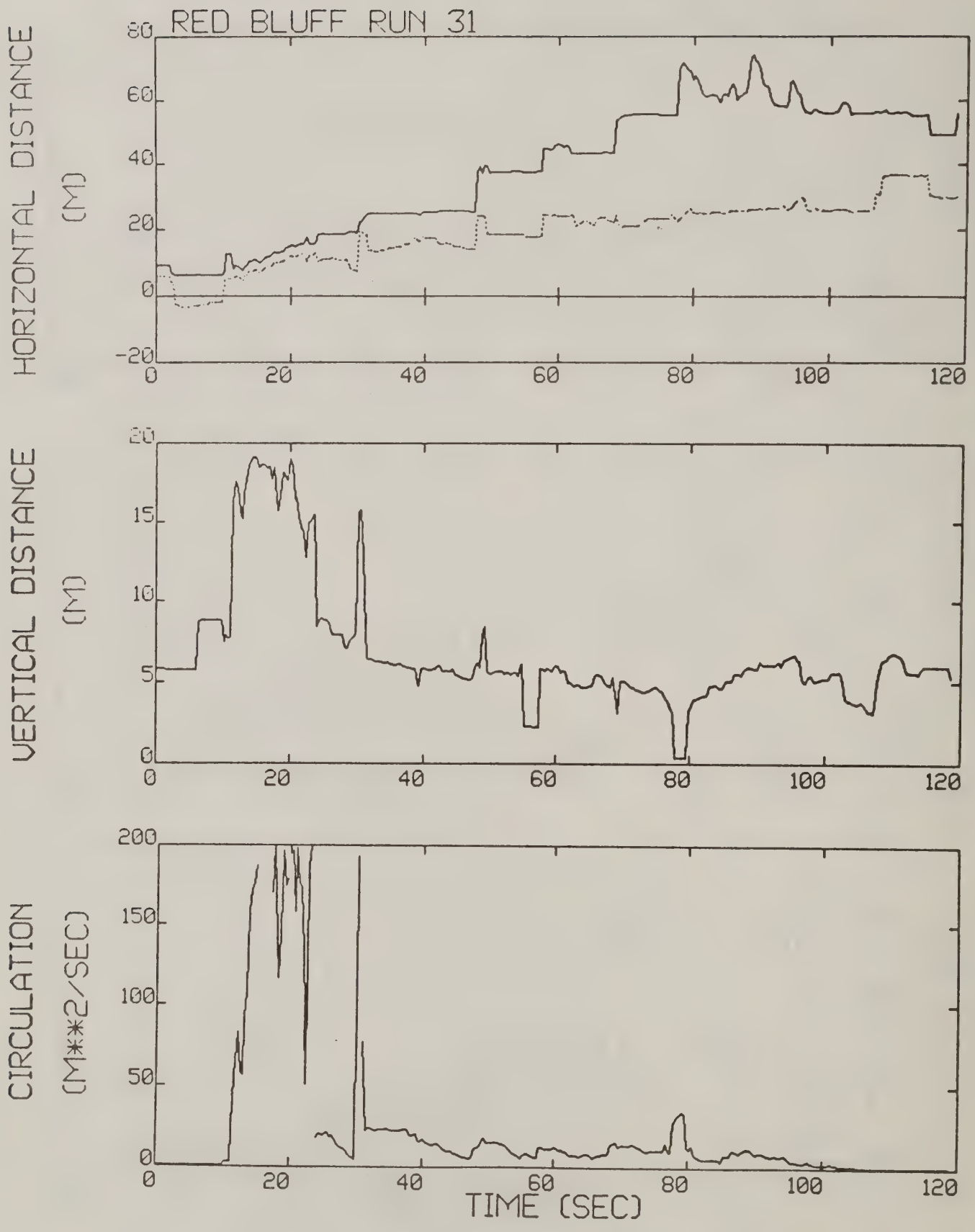

Figure C-29. Red Bluff test run 31 generalized algorithm results (*).

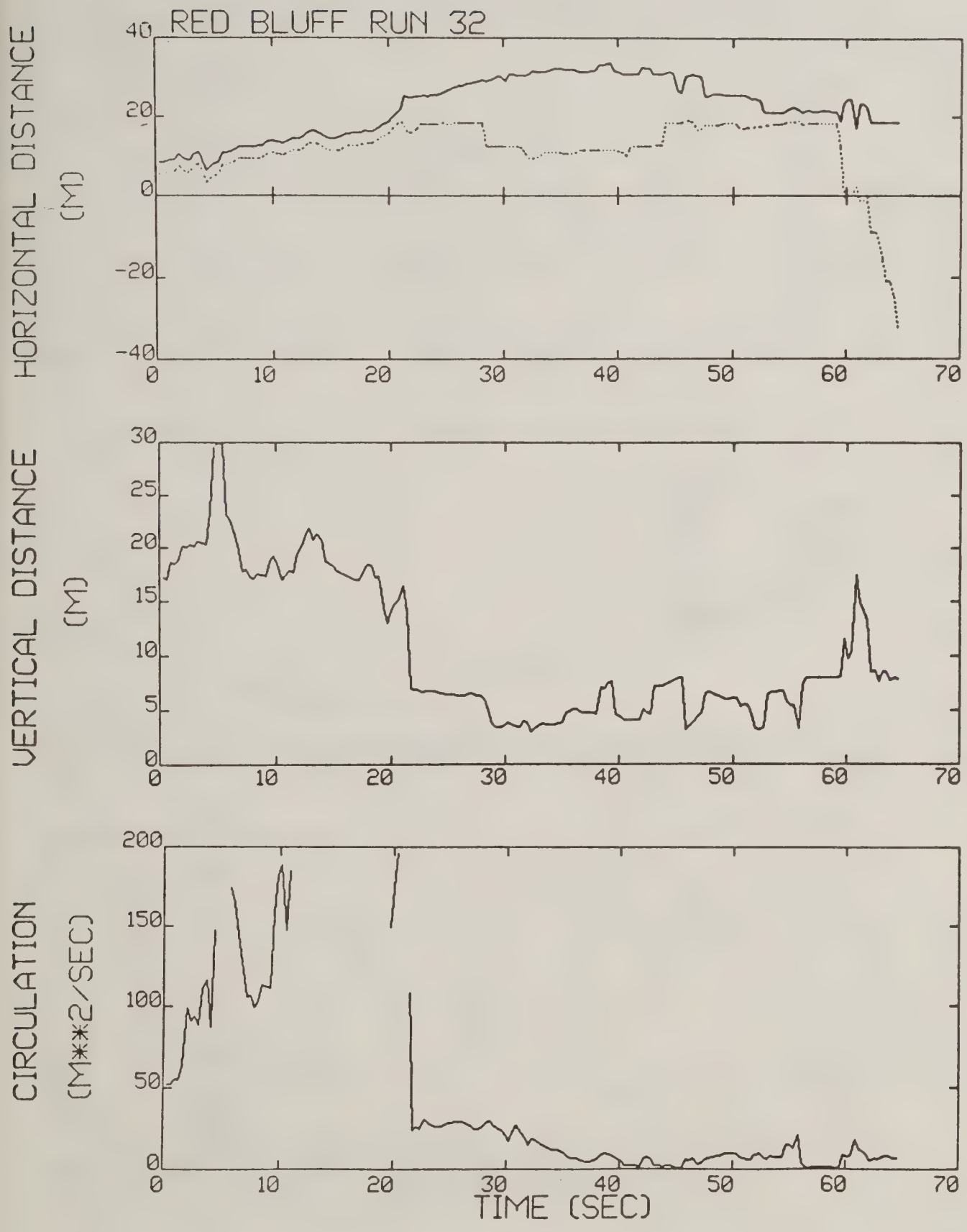

Figure C-30. Red Bluff test run 32 generalized algorithm results (*).

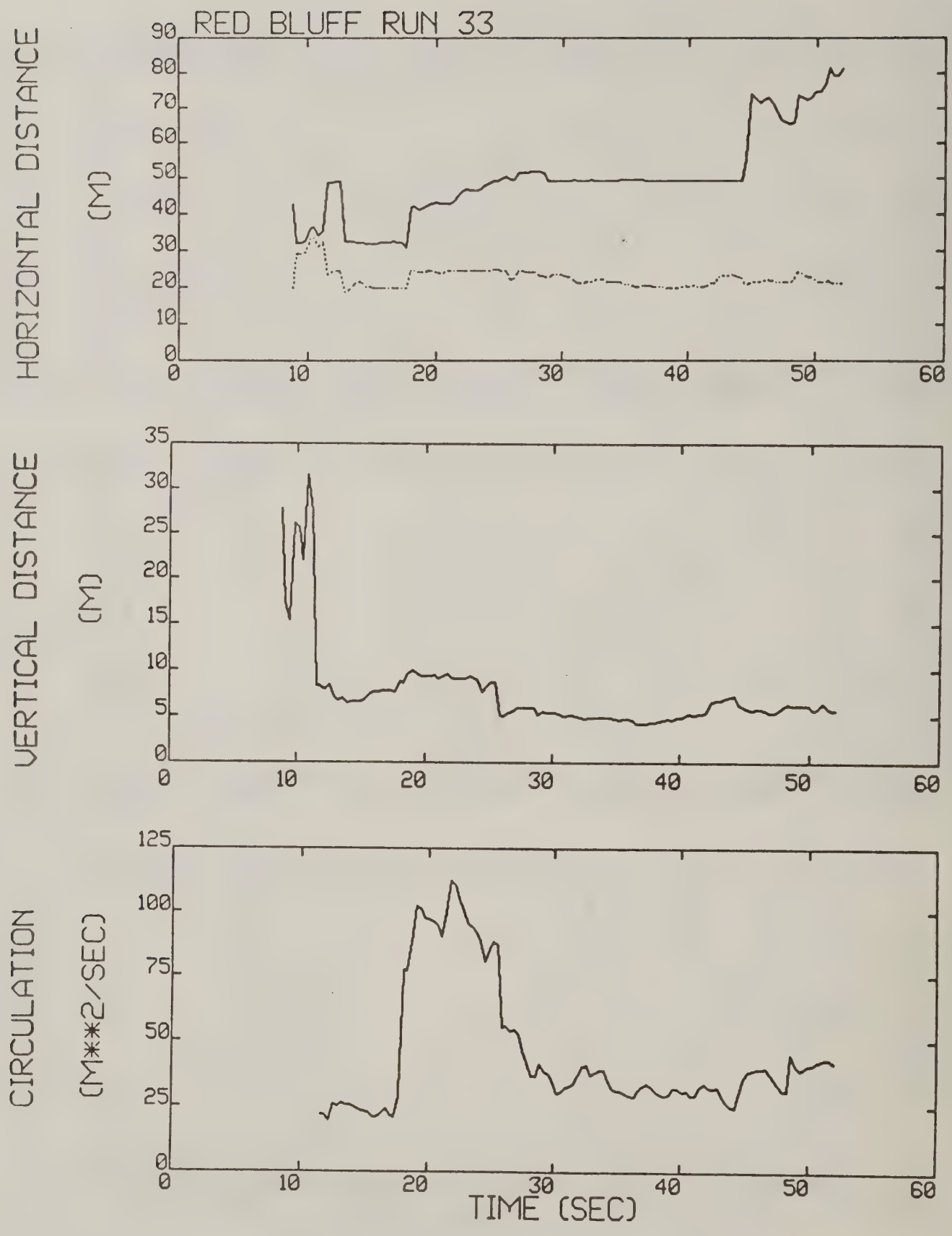

Figure C-31. Red Bluff test run 33 generalized algorithm results (*).

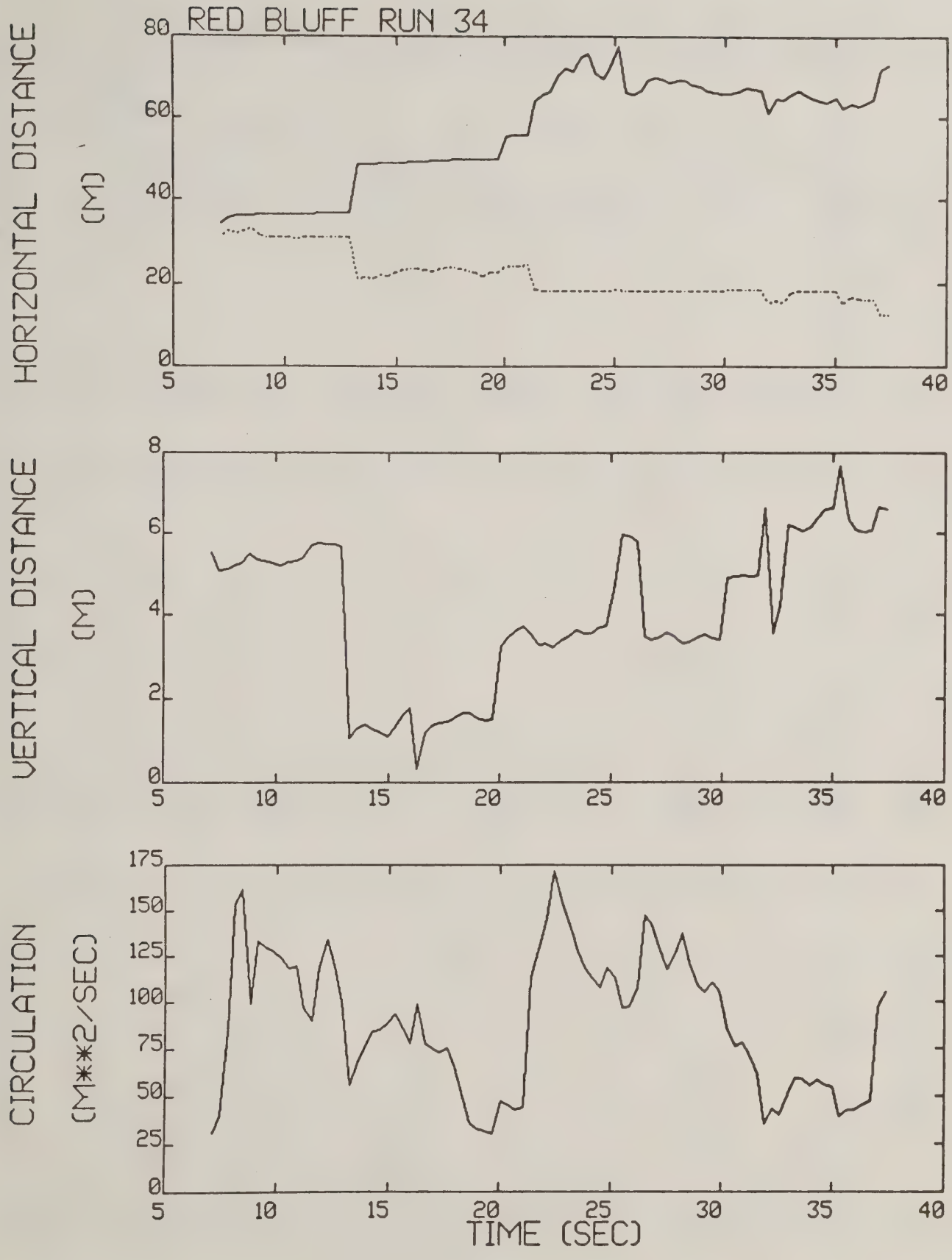

Figure C-32. Red Bluff test run 34 generalized algorithm results.

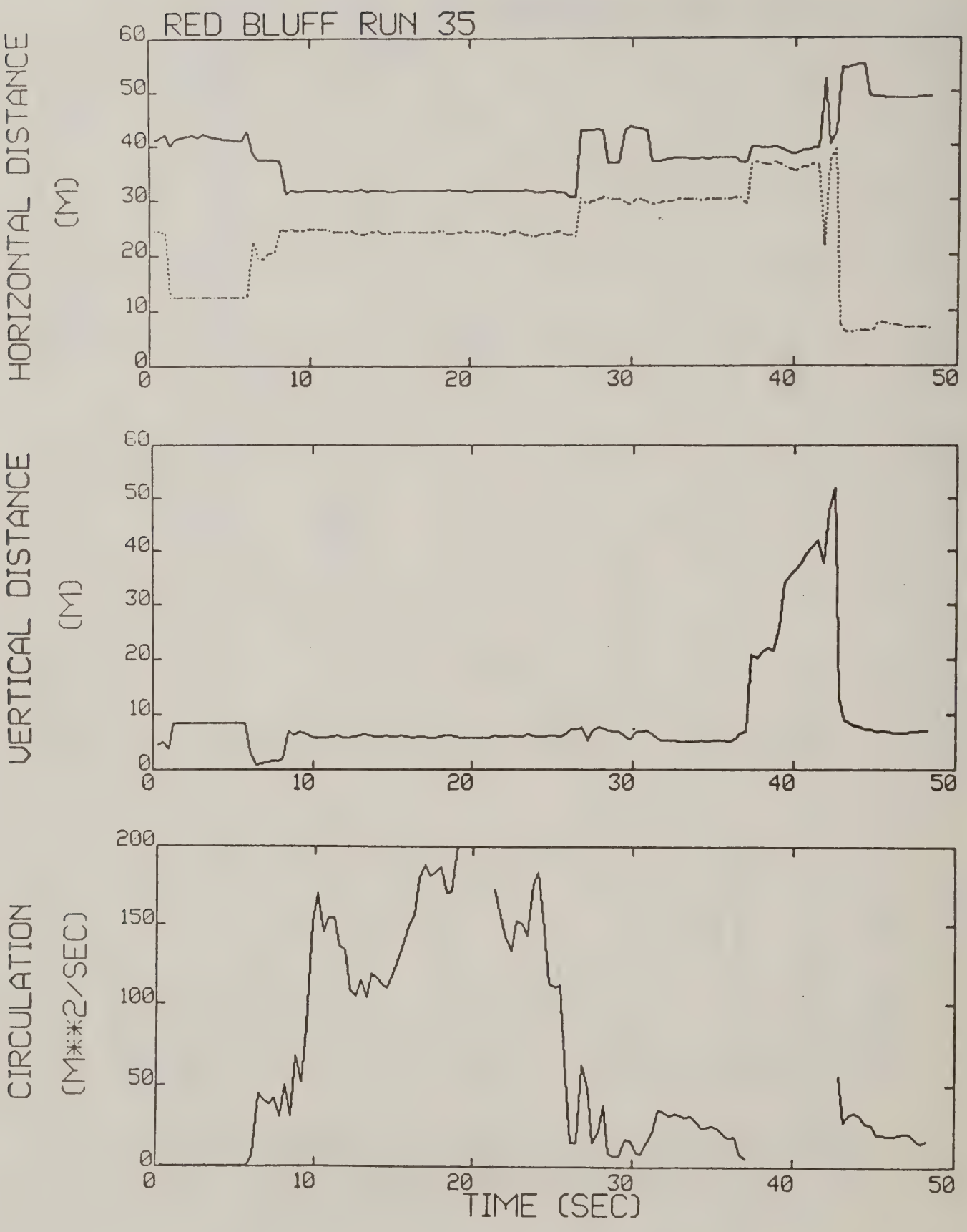

Figure C-33. Red Bluff test run 35 generalized algorithm results (*).

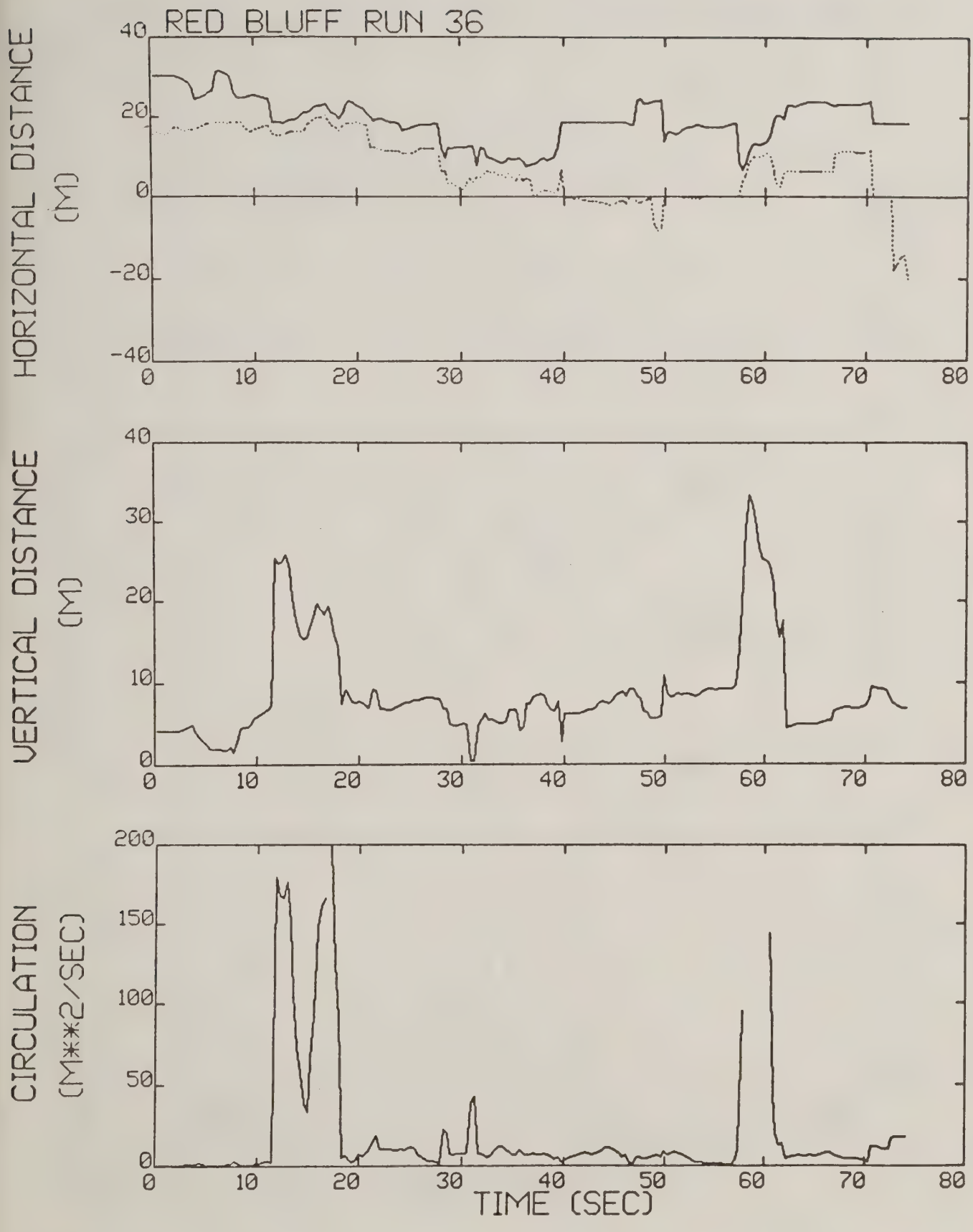

Figure C-34. Red Bluff test run 36 generalized algorithm results.

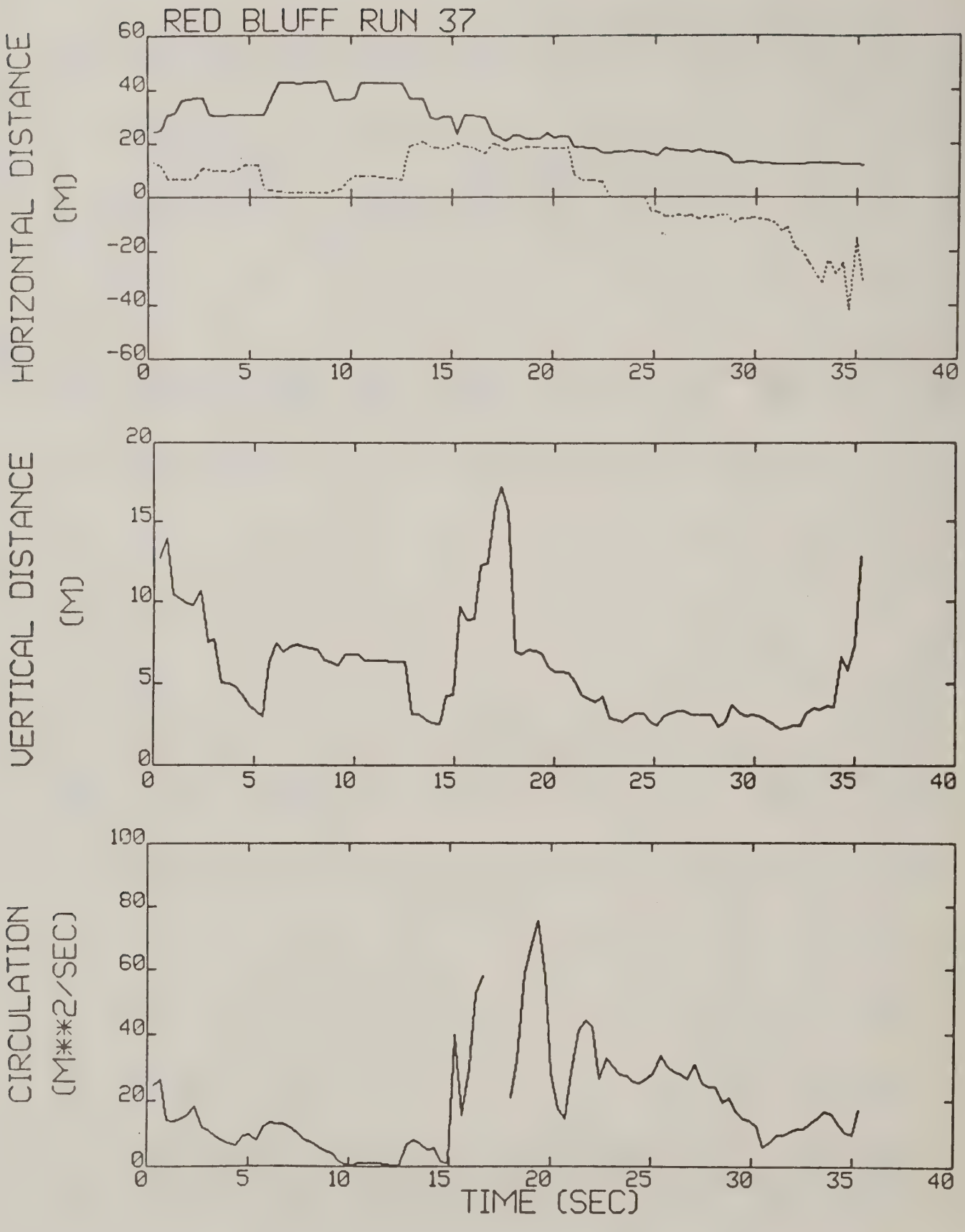

Figure C-35. Red Bluff test run 37 generalized algorithm results (*).

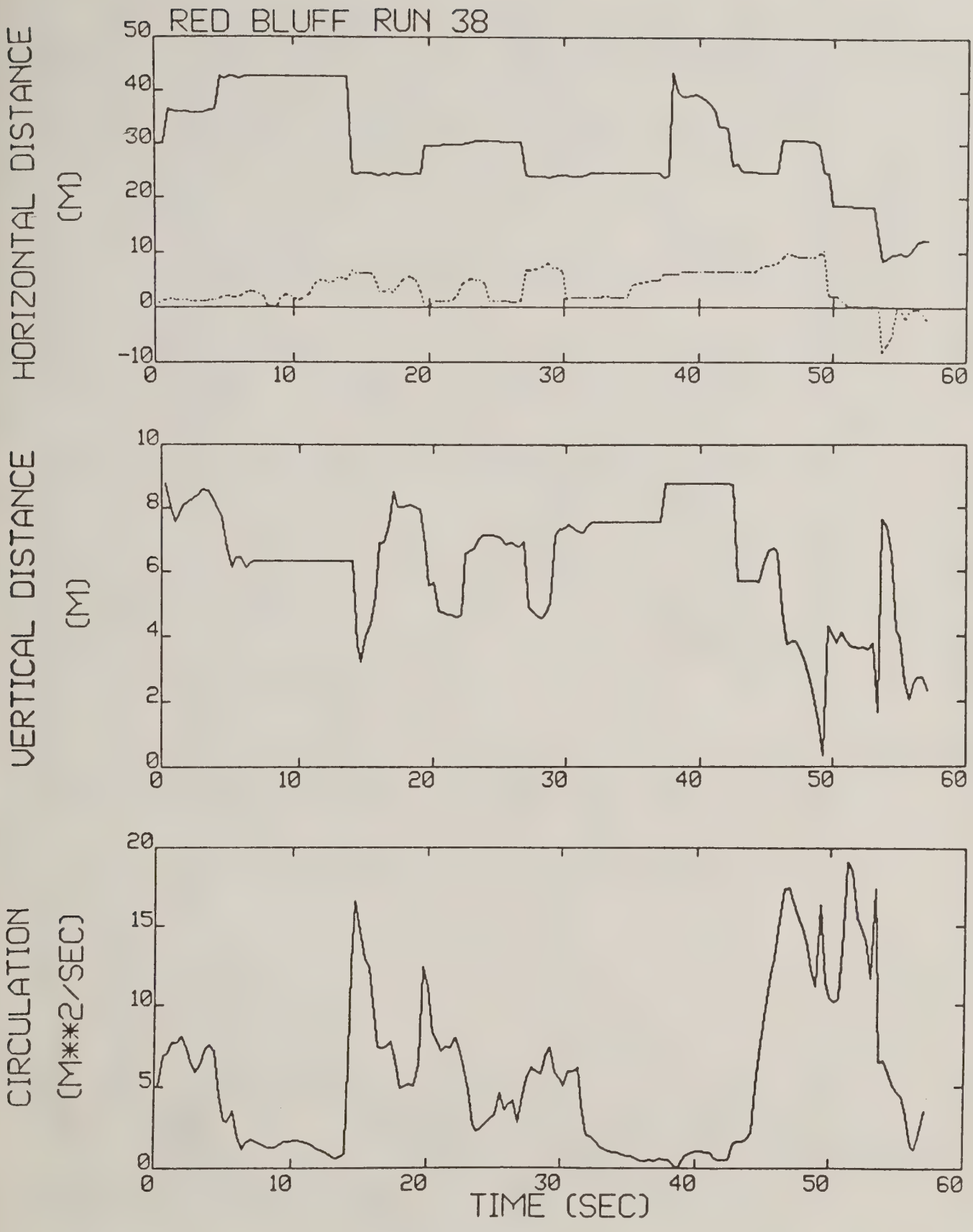

Figure C-36. Red Bluff test run 38 generalized algorithm results (*).

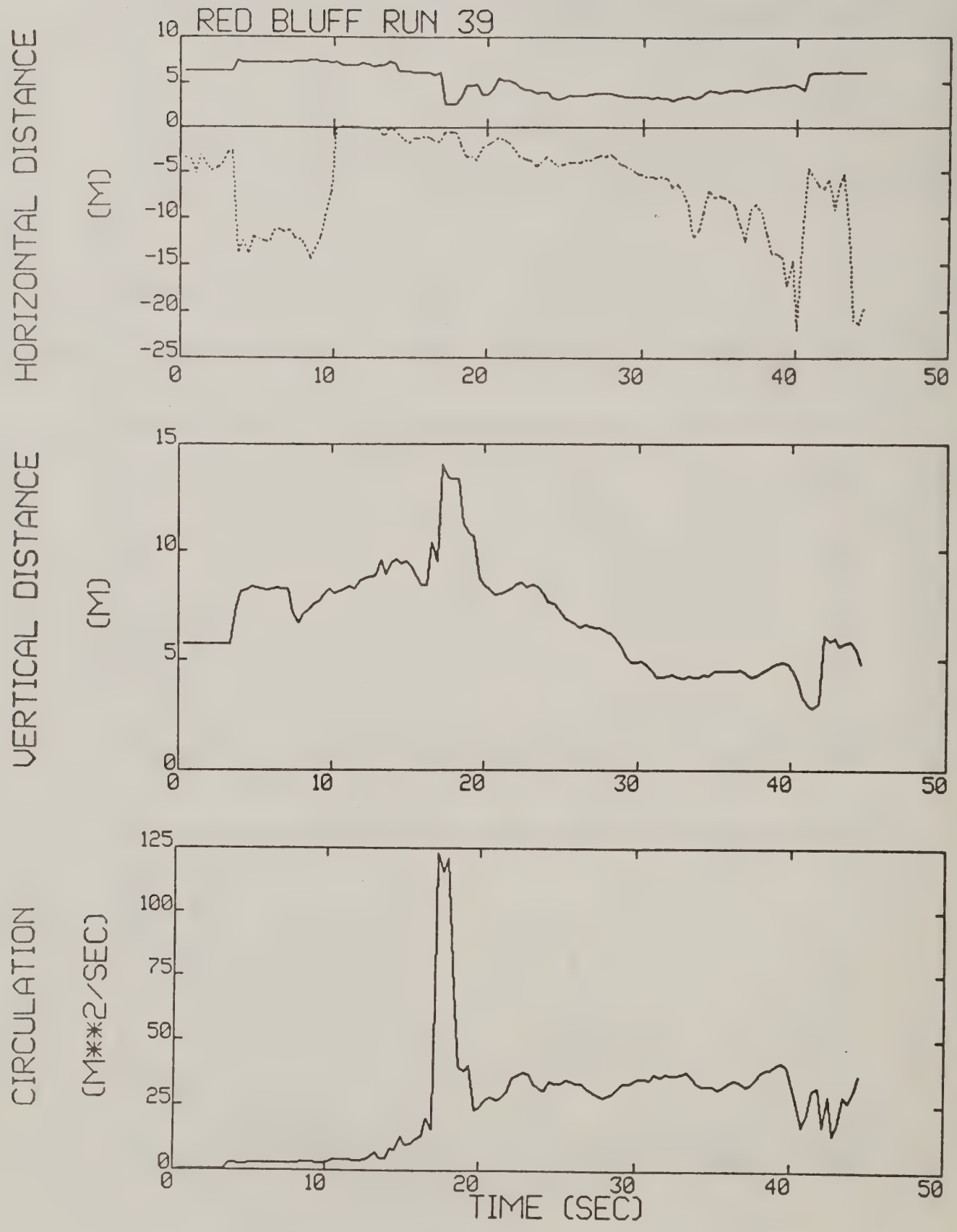

Figure C-37. Red Bluff test run 39 generalized algorithm results.

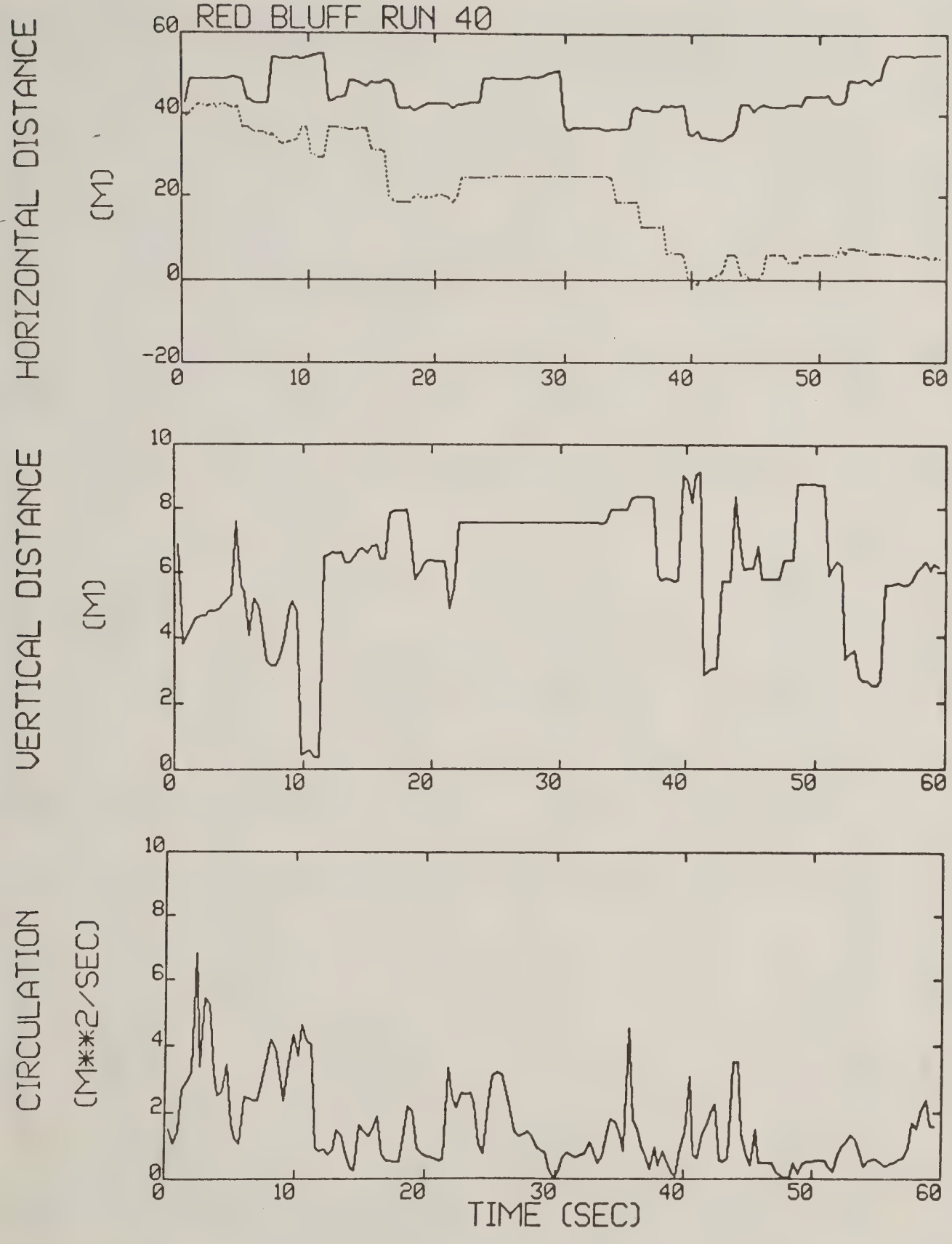

Figure C-38. Red Bluff test run 40 generalized algorithm results (*).

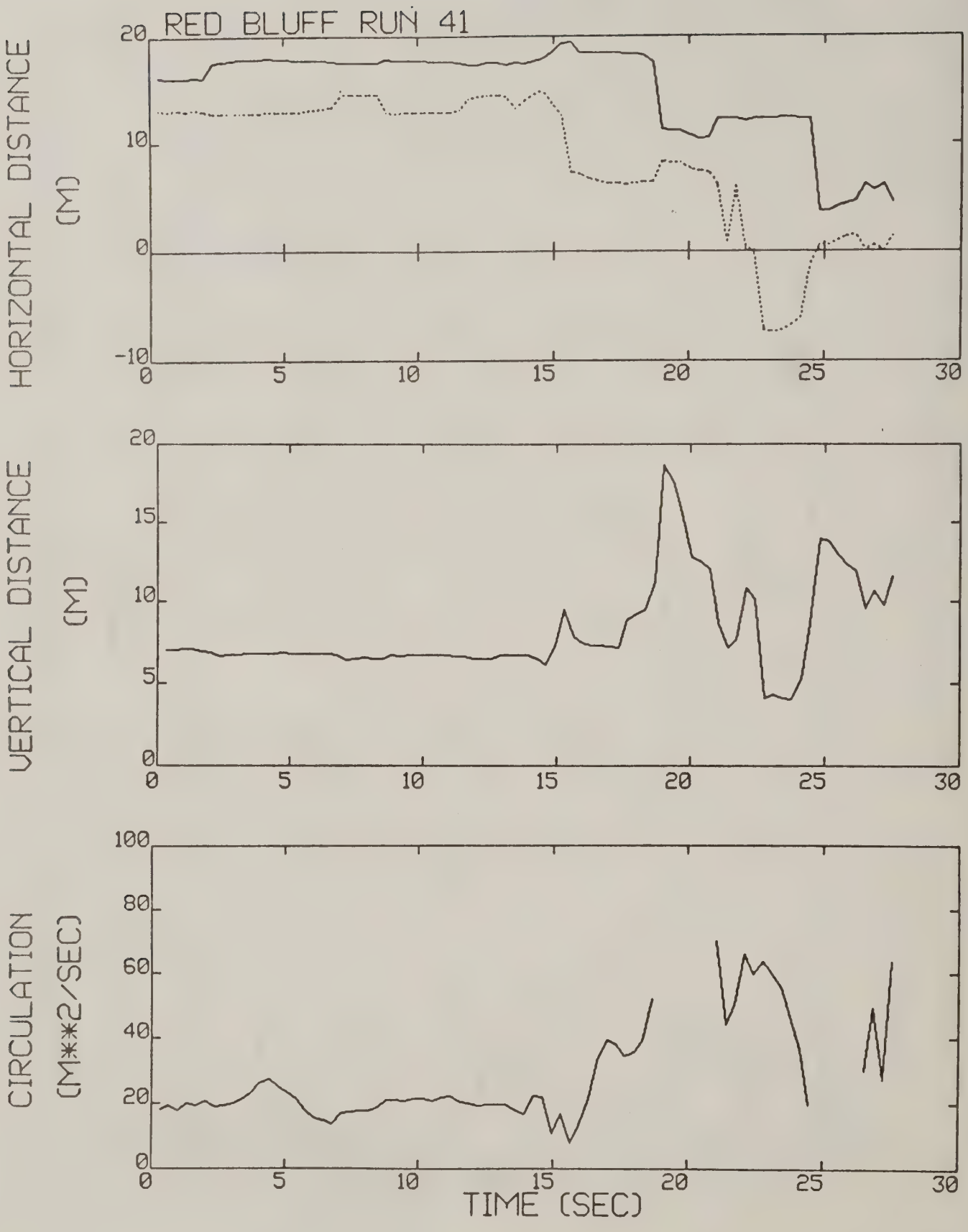

Figure C-39. Red Bluff test run 41 generalized algorithm results.

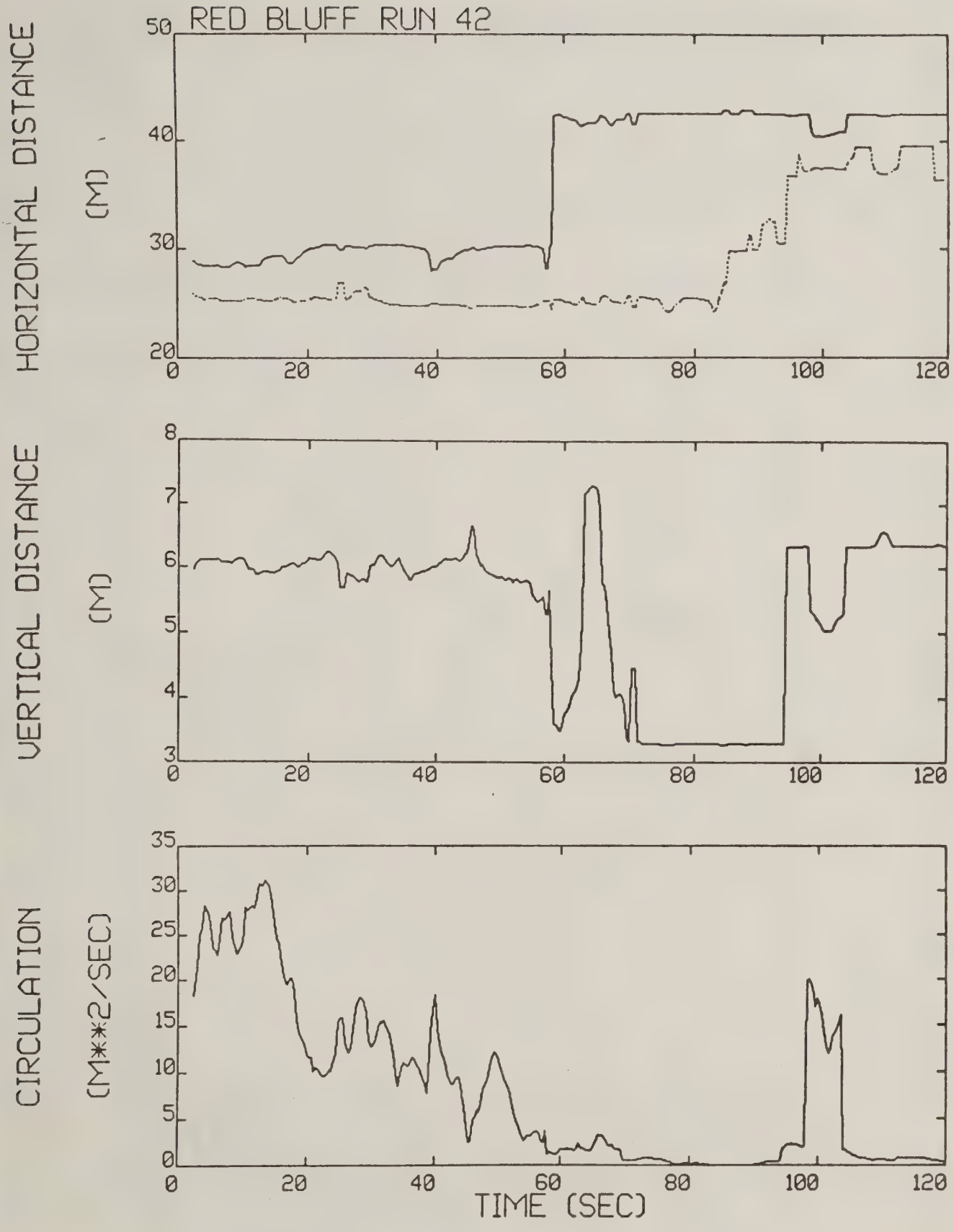

Figure C-40. Red Bluff test run 42 generalized algorithm results (*).

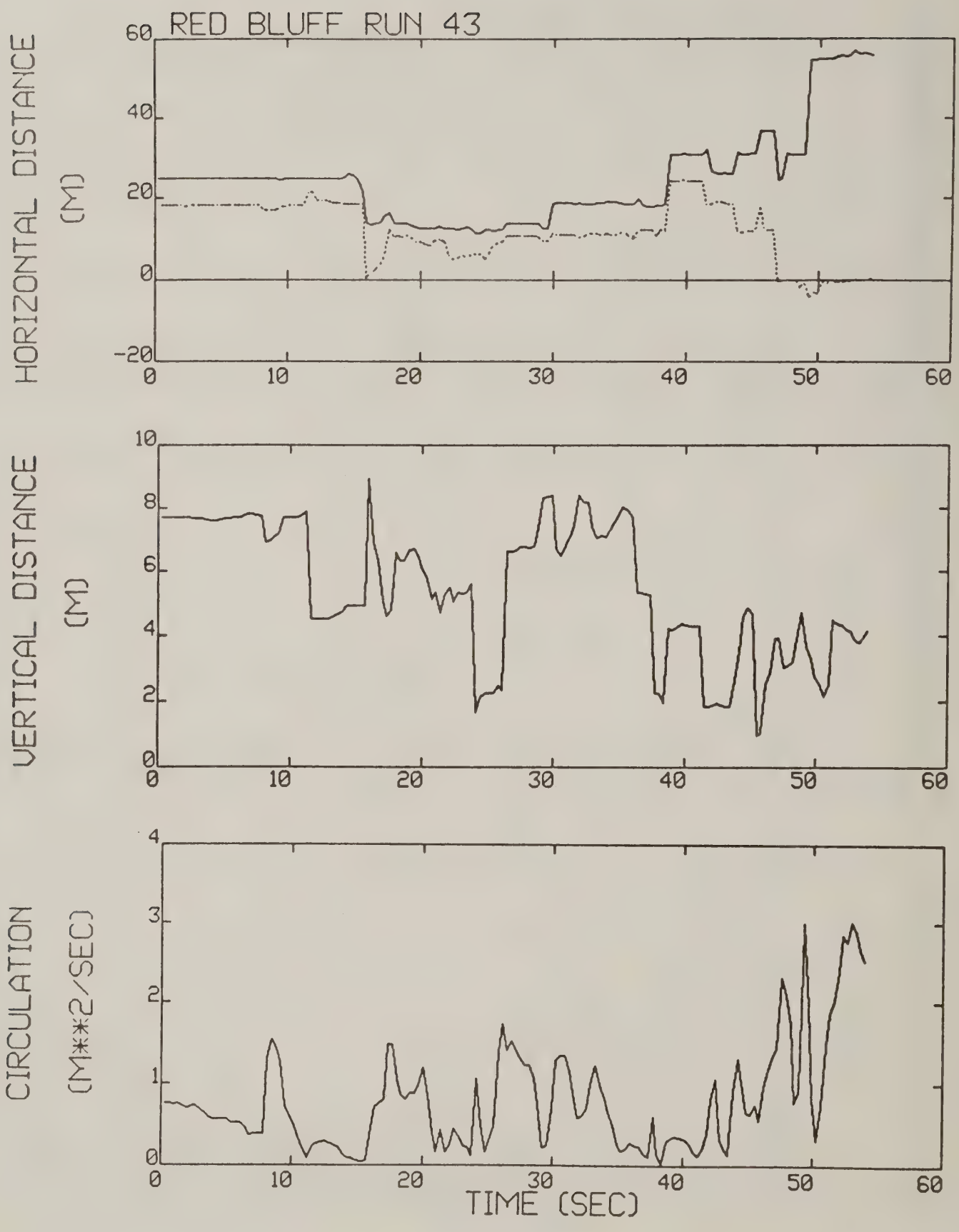

Figure C-41. Red Bluff test run 43 generalized algorithm results.

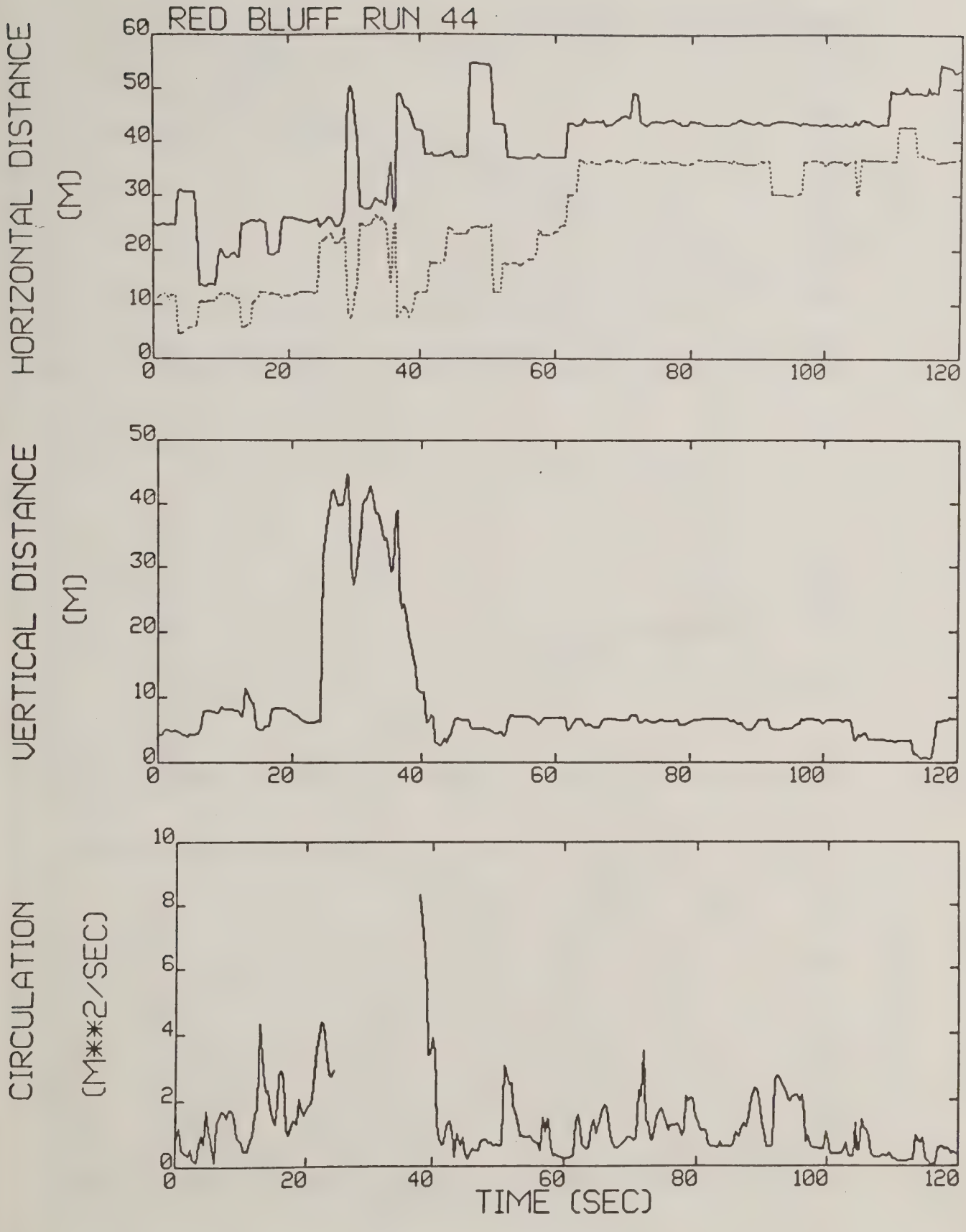

Figure C-42. Red Bluff test run 44 generalized algorithm results.

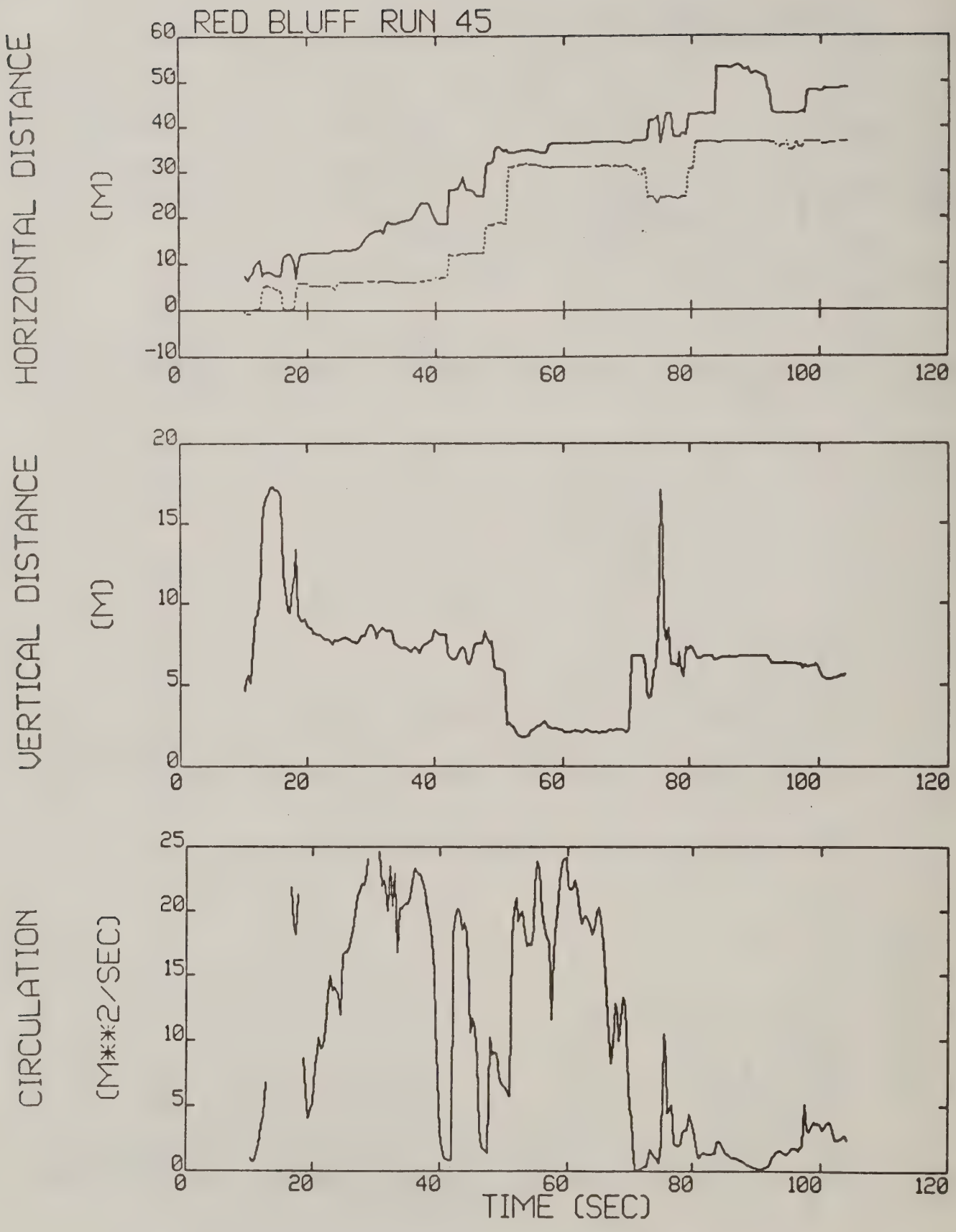

Figure C-43. Red Bluff test run 45 generalized algorithm results.

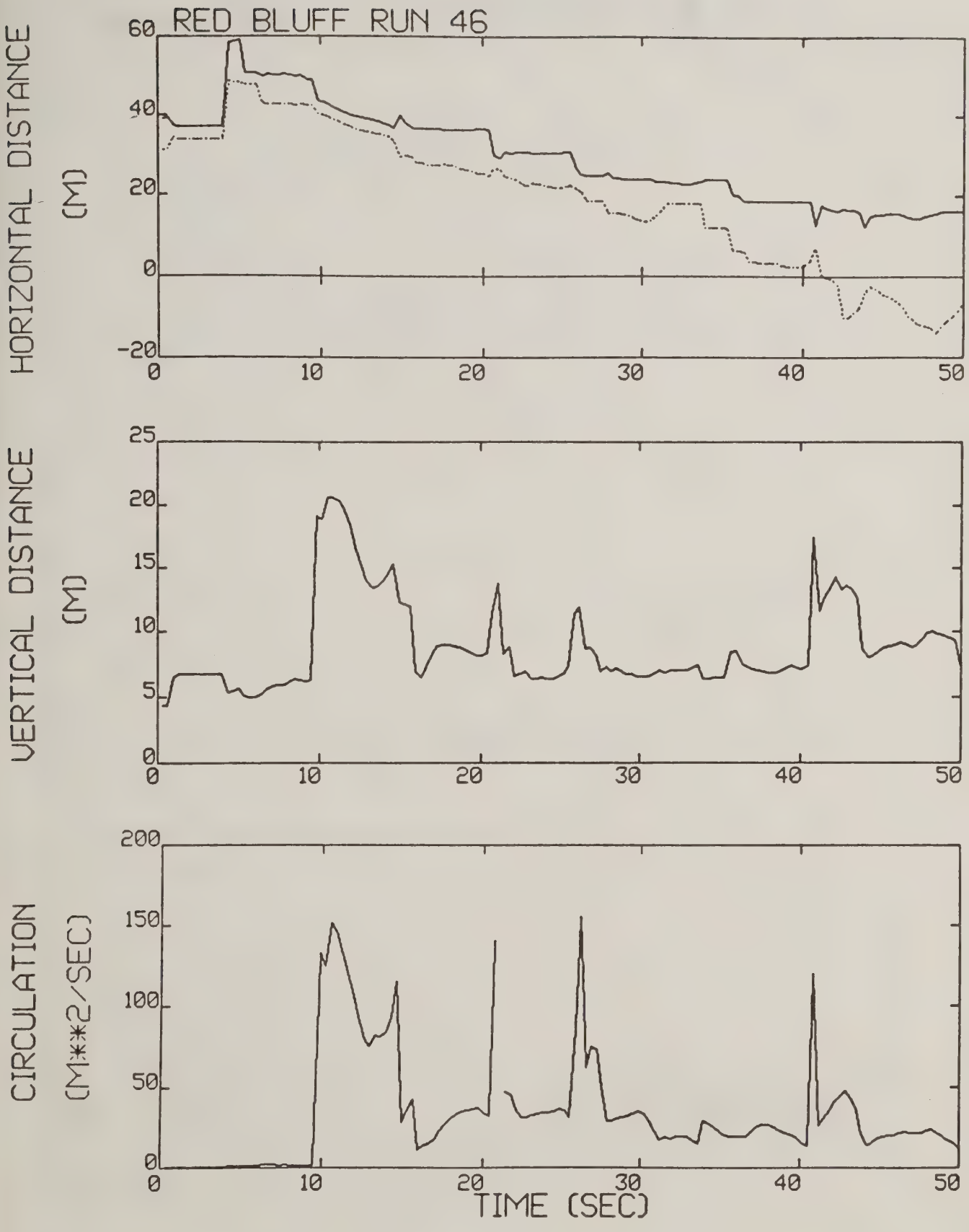

Figure C-44. Red Bluff test run 46 generalized algorithm results (*).

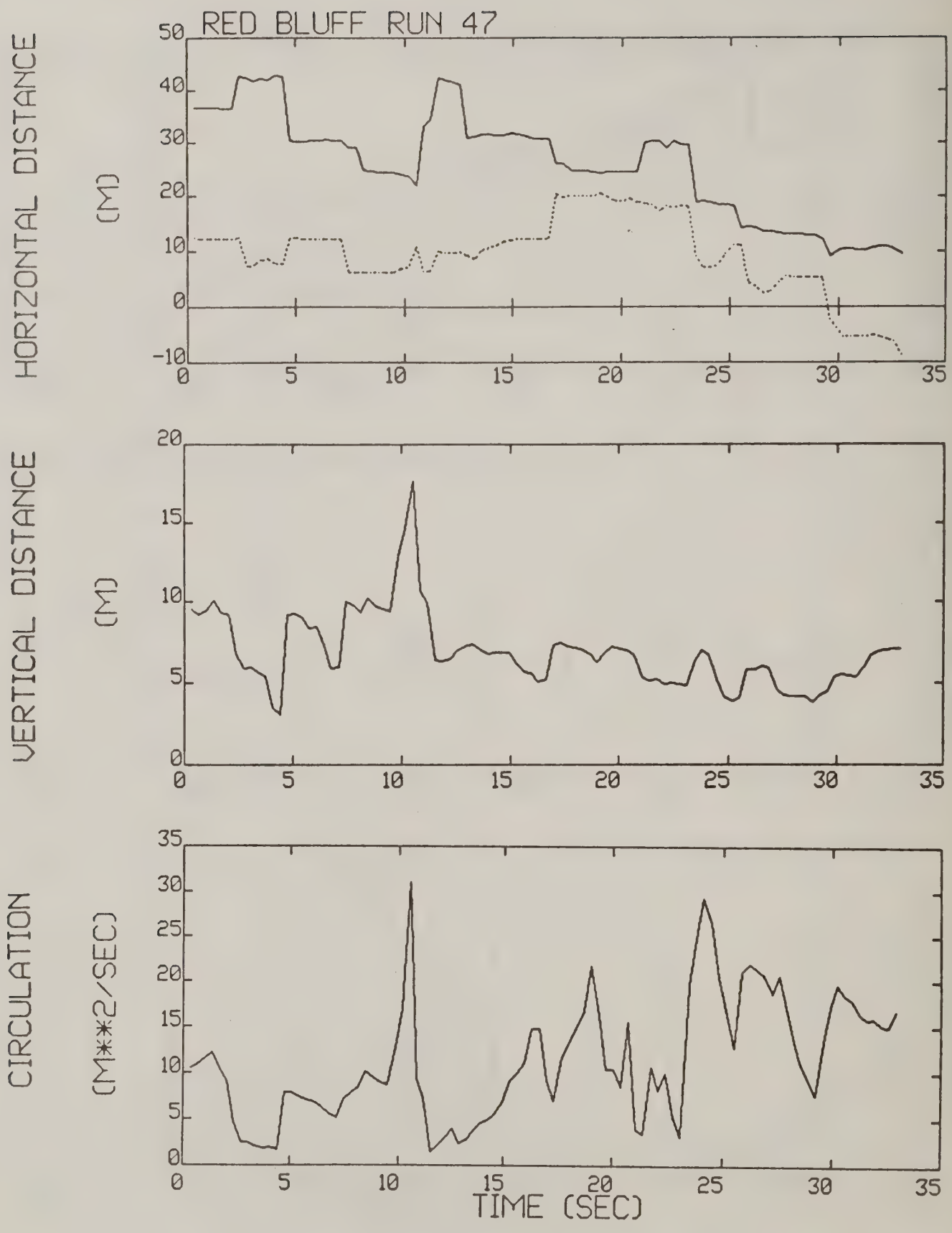

Figure C-45. Red Bluff test run 47 generalized algorithm results.

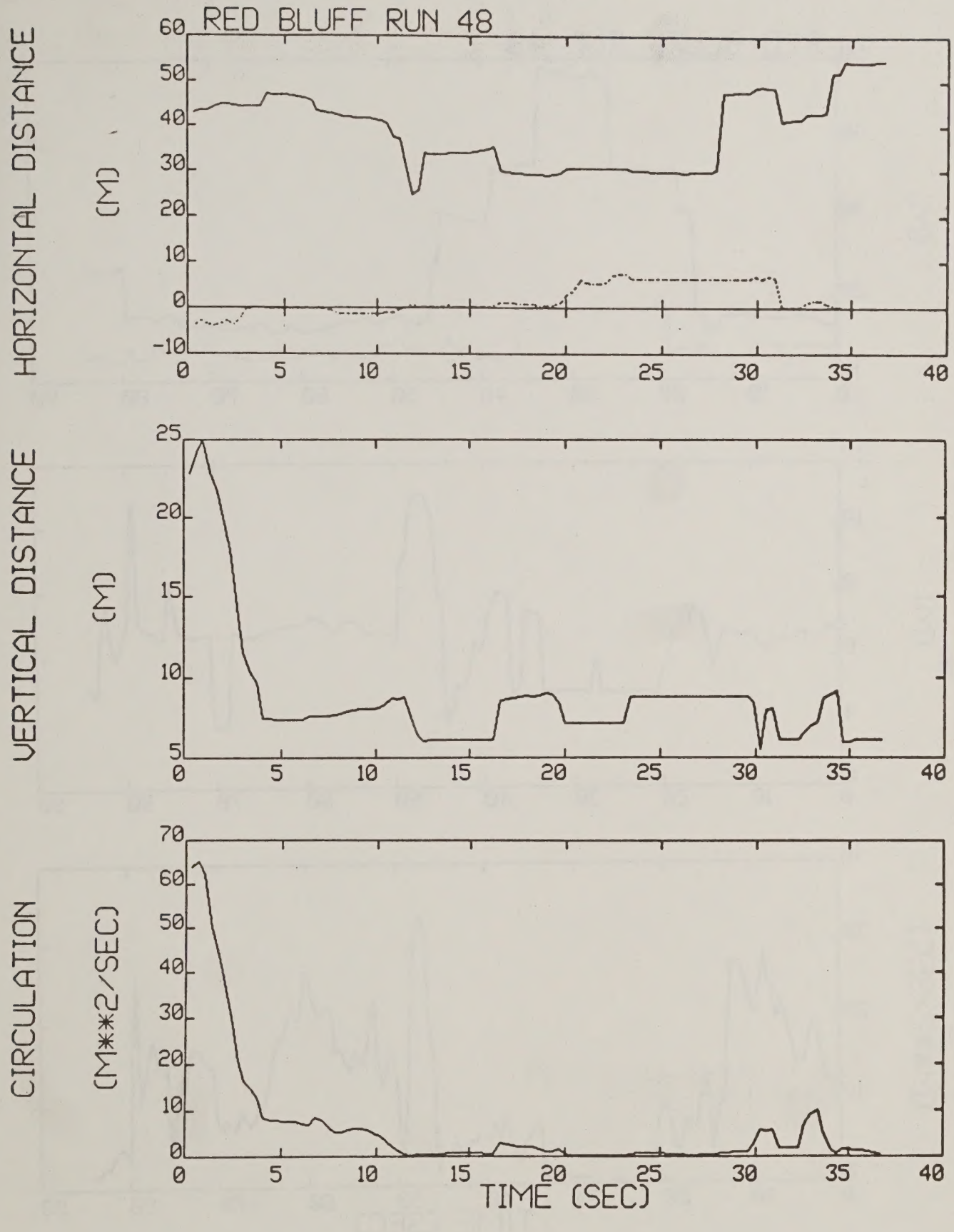

Figure C-46. Red Bluff test run 48 generalized algorithm results.

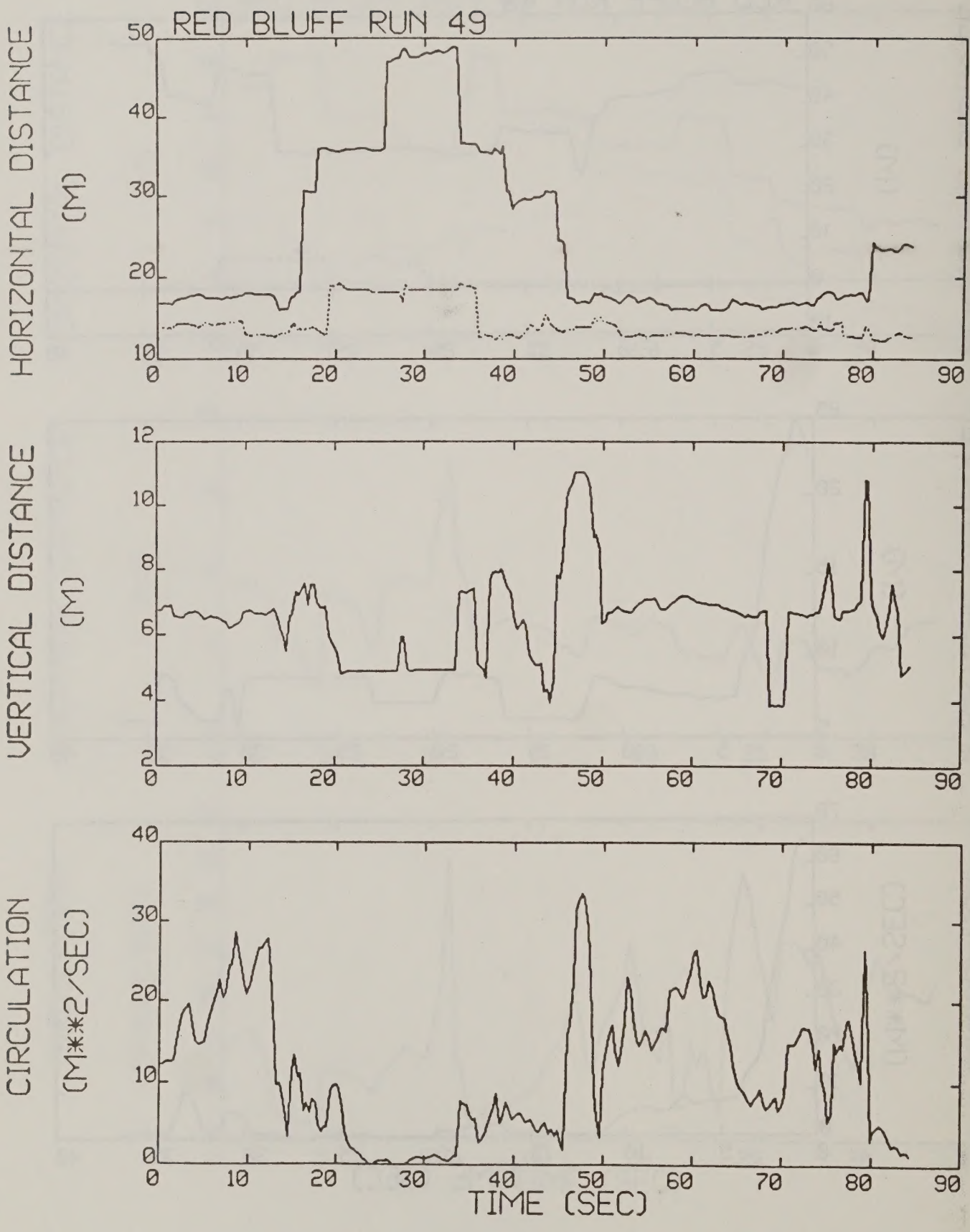

Figure C-47. Red Bluff test run 49 generalized algorithm results (*).